



NUREG/CR-7028
Volume 1

Engineered Covers for Waste Containment: Changes in Engineering Properties and Implications for Long-Term Performance Assessment

Office of Nuclear Regulatory Research

**AVAILABILITY OF REFERENCE MATERIALS
IN NRC PUBLICATIONS**

NRC Reference Material

As of November 1999, you may electronically access NUREG-series publications and other NRC records at NRC's Public Electronic Reading Room at <http://www.nrc.gov/reading-rm.html>. Publicly released records include, to name a few, NUREG-series publications; *Federal Register* notices; applicant, licensee, and vendor documents and correspondence; NRC correspondence and internal memoranda; bulletins and information notices; inspection and investigative reports; licensee event reports; and Commission papers and their attachments.

NRC publications in the NUREG series, NRC regulations, and *Title 10, Energy*, in the Code of *Federal Regulations* may also be purchased from one of these two sources.

1. The Superintendent of Documents
U.S. Government Printing Office
Mail Stop SSOP
Washington, DC 20402-0001
Internet: bookstore.gpo.gov
Telephone: 202-512-1800
Fax: 202-512-2250
2. The National Technical Information Service
Springfield, VA 22161-0002
www.ntis.gov
1-800-553-6847 or, locally, 703-605-6000

A single copy of each NRC draft report for comment is available free, to the extent of supply, upon written request as follows:

Address: U.S. Nuclear Regulatory Commission
Office of Administration
Publications Branch
Washington, DC 20555-0001
E-mail: DISTRIBUTION.RESOURCE@NRC.GOV
Facsimile: 301-415-2289

Some publications in the NUREG series that are posted at NRC's Web site address <http://www.nrc.gov/reading-rm/doc-collections/nuregs> are updated periodically and may differ from the last printed version. Although references to material found on a Web site bear the date the material was accessed, the material available on the date cited may subsequently be removed from the site.

Non-NRC Reference Material

Documents available from public and special technical libraries include all open literature items, such as books, journal articles, and transactions, *Federal Register* notices, Federal and State legislation, and congressional reports. Such documents as theses, dissertations, foreign reports and translations, and non-NRC conference proceedings may be purchased from their sponsoring organization.

Copies of industry codes and standards used in a substantive manner in the NRC regulatory process are maintained at—

The NRC Technical Library
Two White Flint North
11545 Rockville Pike
Rockville, MD 20852-2738

These standards are available in the library for reference use by the public. Codes and standards are usually copyrighted and may be purchased from the originating organization or, if they are American National Standards, from—

American National Standards Institute
11 West 42nd Street
New York, NY 10036-8002
www.ansi.org
212-642-4900

Legally binding regulatory requirements are stated only in laws; NRC regulations; licenses, including technical specifications; or orders, not in NUREG-series publications. The views expressed in contractor-prepared publications in this series are not necessarily those of the NRC.

The NUREG series comprises (1) technical and administrative reports and books prepared by the staff (NUREG-XXXX) or agency contractors (NUREG/CR-XXXX), (2) proceedings of conferences (NUREG/CP-XXXX), (3) reports resulting from international agreements (NUREG/IA-XXXX), (4) brochures (NUREG/BR-XXXX), and (5) compilations of legal decisions and orders of the Commission and Atomic and Safety Licensing Boards and of Directors' decisions under Section 2.206 of NRC's regulations (NUREG-0750).

DISCLAIMER: This report was prepared as an account of work sponsored by an agency of the U.S. Government. Neither the U.S. Government nor any agency thereof, nor any employee, makes any warranty, expressed or implied, or assumes any legal liability or responsibility for any third party's use, or the results of such use, of any information, apparatus, product, or process disclosed in this publication, or represents that its use by such third party would not infringe privately owned rights.

Engineered Covers for Waste Containment: Changes in Engineering Properties and Implications for Long-Term Performance Assessment

Prepared by:

C.H.Benson¹, W.H. Albright², D.O. Fratta¹, J.M. Tinjum¹,
E. Kucukkirca¹, S.H. Lee¹, J. Scalia¹, P.D. Schlicht¹, and X. Wang¹,

¹Geological Engineering
University of Wisconsin-Madison
1415 Engineering Drive
Madison, WI 53706

²Desert Research Institute
2215 Raggio Parkway
Reno, NV 89512

Manuscript Completed: July 2010
Date Published: December 2011

Jacob Philip, NRC Project Manager

NRC Job Code N6366

Office of Nuclear Regulatory Research

ABSTRACT

This peer-reviewed study demonstrates that engineering properties of cover soils change while in service and that long-term engineering properties should be used as input to models employed for performance assessments. Recommendations for appropriate input are made based on the data that were collected. Increases in the saturated hydraulic conductivity, saturated volumetric water content, and the air entry suction (as characterized by van Genuchten's α parameter) occurred due to formation of soil structure, regardless of climate, cover design, or service life. Substantial changes in hydraulic conductivity were observed in some geosynthetic clay liners (GCLs) that did not hydrate completely and underwent cation exchange. Changes in geomembranes and geosynthetic drainage layers were modest or small, and computations based on antioxidant depletion rates suggest that the minimum service life of geomembranes is on the order of 50-125 yrs (the actual service life will be longer). The findings indicate that covers should be monitored to ensure that they are functioning as intended. Monitoring using pan lysimeters combined with secondary measurements collected for interpretive purposes is recommended. Future research investments should include an evaluation of remote sensing technologies for cover monitoring and analog studies to estimate properties of earthen and geosynthetic cover materials corresponding to service lives of 100s to 1000s of years.

CONTENTS

Abstract.....	iii
Executive Summary	xv
Acknowledgement.....	xvii
Abbreviations	xix
1. Introduction	1-1
2. Background: ACAP Test Sections	2-1
2.1 ACAP Lysimeters.....	2-6
2.2 Data Collection.....	2-6
2.3 Calibration and Data Quality Control.....	2-8
2.4 Cover Soils.....	2-8
2.5 Geosynthetics	2-8
3. Exhumations	3-1
3.1 Soil Sampling and Field Testing.....	3-1
3.2 Sampling of Geosynthetics	3-6
3.3 Geomorphological Surveys	3-6
3.4 Geophysical Surveys	3-6
4. Field Test Methods	4-1
4.1 Sealed Double-Ring Infiltrometer Tests	4-1
4.2 Borehole Tests.....	4-1
4.3 Hydraulic Conductivity from Peak Lysimeter Flow Rates.....	4-2
5. Laboratory Test Methods	5-1
5.1 Hydraulic Properties of Earthen Materials.....	5-1
5.2 Properties of Geosynthetic Clay Liners.....	5-1
5.2.1 Saturated Hydraulic Conductivity	5-1
5.2.2 Swell Index.....	5-2
5.2.3 Soluble Cations, Bound Cations, and Cation Exchange Capacity	5-2
5.2.4 Subgrade Soils	5-3
5.3 Properties of Geomembranes and Geosynthetic Drainage Layers.....	5-3
5.3.1 Tensile Strength of Geomembranes	5-3
5.3.2 Ply Adhesion of Geosynthetic Drainage Layers	5-3
5.3.3 Interface Shear Strength	5-3
5.3.4 Hydraulic Properties	5-4
5.3.5 Melt Flow Index and Oxidation Induction Time	5-4
6. Earthen Barrier and Storage Layers	6-1
6.1 Soil Characteristics	6-1
6.2 Field Hydraulic Conductivity.....	6-6
6.3 Laboratory Hydraulic Conductivity	6-10
6.4 Comparison of In-Service and As-Built Hydraulic Conductivity.....	6-12
6.5 Factors Affecting Changes in Hydraulic Conductivity	6-18

6.5.1 Service Life.....	6-18
6.5.2 Climate	6-18
6.5.3 Soil Composition	6-22
6.5.4 Compaction Conditions	6-22
6.5.5 Effect of Freeze-Thaw and Wet-Dry Cycles	6-28
6.6 Soil Water Characteristic Curves	6-31
6.7 Summary of Findings for Earthen Storage and Barrier Layers	6-38
7. Geosynthetic Clay Liners	7-1
7.1 Background on GCLs.....	7-3
7.2 Properties of Exhumed GCLs	7-4
7.2.1 GCL Water Content and Cation Exchange	7-4
7.2.2 Hydraulic Conductivity.....	7-8
7.2.3 Effect of Subgrade Condition	7-11
7.2.4 Service Life and Cover Soil Thickness.....	7-15
7.3 Key Factors to Successful GCL Performance.....	7-15
7.4 Summary of Findings for GCLs.....	7-22
8. Geomembranes and Geosynthetic Drainage Layers.....	8-1
8.1 Properties of Geomembranes	8-1
8.1.1 Tensile Strength.....	8-1
8.1.2 OIT and MFI	8-6
8.2 Properties of Geocomposite Drainage Layer	8-11
8.2.1 Transmissivity	8-11
8.2.2 Permittivity.....	8-16
8.2.3 Ply Adhesion.....	8-16
8.3 Interface Shear Strength.....	8-21
8.4 Reduction Factors for Design	8-21
8.5 Summary of Findings for Geomembranes and Drainage Layers	8-26
9. Geophysical Evaluation	9-1
9.1 Electrical Resistivity Surveys	9-1
9.2 Ground Penetrating Radar Surveys.....	9-8
9.3 Summary of Findings from Geophysical Surveys	9-15
10. Practical Implications for Design, Performance Assessment, and Monitoring.....	10-1
10.1 Design Conditions	10-2
10.2 Parameters for Performance Assessments	10-3
10.3 Monitoring	10-4
10.3.1 Performance Monitoring	10-5
10.3.2 Interpretive Monitoring	10-8
10.3.3 Recommended Practice for Final Cover Monitoring	10-11
11. Conclusions and Recommendations	11-1
12. References.....	12-1
Appendices (Volume 2)	
Appendix A Exhumation Photo Gallery	A-1
Appendix B Sealed Double-Ring Infiltrometer (SDRI) Data.....	B-1
Appendix C TSB Data	C-1

Appendix D	Laboratory Hydraulic Conductivity Data.....	D-1
Appendix E	Soil Water Characteristic Curve Test Data.....	E-1
Appendix F	Statistical Analyses of Hydraulic Conductivity Data	F-1
Appendix G	Methods Used in Chemical Analyses of Geosynthetic Clay Liners.....	G-1
Appendix H	Test Methods for Measuring Soluble Cations, Bound Cations, and Cation Exchange Capacity.....	H-1
Appendix I	Schematic and Photograph of Hydraulic Conductivity Test Set-Up for Geosynthetic Clay Liners (GCLs)	I-1
Appendix J	Exhumed Subgrade Porewater Chemistries.....	J-1
Appendix K	Exhumed GCLs Water Content, Bound Cations, and Soluble Cations.....	K-1
Appendix L	Hydraulic Conductivity Records for Exhumed GCLs	L-1
Appendix M	Field Exhumation Photographs and Observations	M-1
Appendix N	Laboratory Testing Photography and Observations.....	N-1
Appendix O	Exploration of GCL Laboratory Testing Methods.....	O-1
Appendix P	Supplemental Graphs and Tables from Geosynthetic Membrane (GM) and Geosynthetic Drainage Layer (GDL) Tests.....	P-1
Appendix Q	Photographs of GM and GDL Testing Data	Q-1
Appendix R	GM Test Data.....	R-1
Appendix S	GDL Test Data	S-1

List of Figures

Fig. 2.1.	Locations of ACAP field sites. Sites exhumed in this study marked with a star.	2-2
Fig. 2.2.	Profiles of conventional covers evaluated by ACAP.	2-3
Fig. 2.3.	Profiles of store-and-release covers evaluated by ACAP.	2-4
Fig. 2.4.	Schematic of ACAP lysimeter (not to scale).	2-7
Fig. 3.1.	Profiles of the final covers at full-scale MSW landfills in Wisconsin (Site E) and Michigan (Site F). GDL = geosynthetic drainage layer, GM = geomembrane, and GCL = geosynthetic clay liner. Service life of Wisconsin site is 4.7-5.8 yr (depending on test pit). Service life of Michigan site is 3.1 yr.	3-2
Fig. 3.2.	BH test conducted during exhumation of ACAP test section in Helena, MT.	3-3
Fig. 3.3.	SDRI test conducted at ACAP test facility in Polson, MT. Upper photograph shows inner and outer rings after installation. Lower photograph shows filled SDRI with Mariotte bottle in the rear.	3-4
Fig. 3.4.	Block sample being collected at ACAP test facility in Underwood, ND. Upper photograph shows sample partially trimmed into ring. Lower photograph shows sample in ring and ready for separation from subgrade.	3-5
Fig. 3.5.	Removing cover soils over a composite barrier layer (a) and removing a sample of geosynthetic drainage layer (b). Both photographs are from final cover at Wisconsin MSW landfill.	3-7
Fig. 3.6.	Exhumation of GCL samples: cutting around perimeter with razor knife (a) and delicately sliding sample onto rigid plastic plate (b).	3-8
Fig. 3.7.	Typical setup for evaluating punctures in geomembranes using electrical resistivity measurements (after Frangos 1997, Darilek and Miller 1998).	3-9
Fig. 3.8.	Typical voltage drop over a hole in a geomembrane hole: experimental measurements and theoretical response (from Parra 1988).	3-11
Fig. 3.9.	Common mid-point (a) and reflection survey (b) setup configuration for GPR.	3-12
Fig. 3.10.	Downhole setup for GPR.	3-13
Fig. 6.1.	Plasticity chart showing Atterberg limits of storage and barrier layers evaluated in this study.	6-3
Fig. 6.2.	Field hydraulic conductivity determined by SDRIs and BHs from each cover type (a) and hydraulic conductivity from SDRIs versus hydraulic conductivity from BHs for individual test sections (b).	6-8

Fig. 6.3.	Saturated hydraulic conductivity from SDRI and BH tests (a) and laboratory tests on 305, 150 and 75 mm diameter specimens for each cover type (b). The solid line within the box represents the median, the box encloses 50% of the data, and outliers are indicated with a circle.	6-9
Fig. 6.4.	Saturated hydraulic conductivity of large-scale (305 mm) laboratory specimens versus small-scale (150 and 75-mm-diameter) laboratory specimens.	6-13
Fig. 6.5.	Field hydraulic conductivity from SDRI and BH versus large-scale (305 mm) laboratory saturated hydraulic conductivity (a) and small scale (150 and 75-mm) laboratory saturated hydraulic conductivity (b).	6-14
Fig. 6.6.	Saturated hydraulic conductivity versus effective diameter for t Altamont store-and-release cover (a) and Apple Valley clay barrier (b). Trend lines drawn by hand.	6-15
Fig. 6.7.	In-service saturated hydraulic conductivity (K_{si}) versus as-built hydraulic conductivity (K_{sa}) by site (a) and cover type (b). “?” signifies apparent outliers.	6-17
Fig. 6.8.	Saturated hydraulic conductivity ratio (K_{si}/K_{sa}) versus as-built saturated hydraulic conductivity (K_{sa}). Trend lines drawn by hand. “?” signifies outliers.	6-19
Fig. 6.9.	Saturated hydraulic conductivity ratio versus service life of test section. Trend lines drawn by hand.	6-20
Fig. 6.10.	Saturated hydraulic conductivity ratio versus climate presented by cover type.	6-21
Fig. 6.11.	Saturated hydraulic conductivity ratio versus plasticity index (a), clay content ($< 2 \mu\text{m}$) (b), and activity (c). PI = 0 indicates soil is non plastic. .	6-23
Fig. 6.12.	Saturated hydraulic conductivity versus coarse fraction ($\% > 75 \mu\text{m}$) over clay content ($\% < 2 \mu\text{m}$) (a) and ratio of silt content ($\%$ between 2 and 75 μm) to fines content ($\% < 75 \mu\text{m}$) (b).	6-25
Fig. 6.13.	Saturated hydraulic conductivity ratio versus as-built compacted dry unit weight by site (a) and cover type (b).	6-27
Fig. 6.14.	Saturated hydraulic conductivity ratio versus water content relative to optimum water content.	6-29
Fig. 6.15.	Saturated hydraulic conductivity ratio versus number of freeze-thaw cycles (a) and number of wet-dry cycles (b).	6-30
Fig. 6.16.	In-service α parameter versus as-built α parameter (a) and in-service n parameter versus as-built n parameter (b).	6-35

Fig. 6.17.	In-service saturated volumetric water content versus as-built saturated volumetric water content.	6-36
Fig. 6.18.	The ratio of α (a) and n (b) from large-scale testing (254 or 150 mm) to small scale testing (75 mm).	6-37
Fig. 7.1.	Profiles of final covers evaluated by Meer and Benson (2007). The service life varied from 4.1 to 11.1 yr.	7-2
Fig. 7.2.	Swell index in DW (a) and mole fraction monovalent bound cations (b) for GCL-only and composite GCL covers. Data are from this study (open symbols) and Meer and Benson (2007) (closed symbols).	7-7
Fig. 7.3.	Water content of exhumed GCLs (a) and subgrades (b) for covers where GCLs were in composite barriers or the sole barrier layer. Data are from this study (open symbols) and Meer and Benson (2007) (closed symbols).	7-9
Fig. 7.4.	Hydraulic conductivity of exhumed GCLs from covers where GCLs were in composite barriers or the sole barrier layer. Data are from this study (open symbols) and Meer and Benson (2007) (closed symbols). Circles represent hydraulic conductivity to SW; shaded boxes represent hydraulic conductivity to DW. GCLs permeated with DW at Wisconsin site (W-02) are duplicates of GCLs that had high hydraulic conductivity to SW.	7-10
Fig. 7.5	Hydraulic conductivity versus (a) swell index in DW and (b) mole fraction bound sodium for exhumed GCLs from composite barriers. Data for new GCL are from Meer and Benson (2007).	7-12
Fig. 7.6.	Hydraulic conductivity of exhumed GCLs vs. water content (a) and water content of exhumed GCLs versus corresponding water content of subgrade (b). GCLs with lower K had hydraulic conductivities $< 5 \times 10^{-11}$ m/s, whereas GCLs with higher K had hydraulic conductivities $> 1 \times 10^{-9}$ m/s.	7-13
Fig. 7.7.	TCM (a) and X_m (b) of GCL versus water content of subgrade. GCLs with lower K had hydraulic conductivities $< 5 \times 10^{-11}$ m/s, whereas GCLs with higher K had hydraulic conductivities $> 1 \times 10^{-9}$ m/s.	7-14
Fig. 7.8.	TCM of GCL vs. TCM of subgrade (a) and MDR of GCL vs. MDR of subgrade (b). GCLs with lower K had hydraulic conductivities $< 5 \times 10^{-11}$ m/s, whereas GCLs with higher K had hydraulic conductivities $> 1 \times 10^{-9}$ m/s.	7-16
Fig. 7.9.	Hydraulic conductivities of GCLs exhumed in this study as a function of USCS classification of subgrade. Compilation of data from Meer and Benson (2007) Site S and from this study.	7-17
Fig. 7.10.	Hydraulic conductivity of exhumed GCLs permeated with SW and DW vs. service life (a) and thickness of overlying soil (b). Data are from this study and Site S in Meer and Benson (2007).	7-18

Fig. 7.11.	Cross-sections of exhumed GCLs from Site E-02 (a) and Site B (b). Vertical scale in mm.	7-20
Fig. 7.12.	Cross-sections of exhumed GCLs from Site S (a) and Site F-03 (b). Photo of GCL from Site S is from Meer (2004). Photo of GCL from Site F-03 is from after permeation with rhodamine WT dye. Vertical scale in mm.	7-21
Fig. 8.1.	Profiles of covers at sites where geosynthetics were exhumed. GCL = geosynthetic clay liner, GDL = geosynthetic drainage layer, GM = geomembrane, GX = geotextile, RB = root barrier.	8-2
Fig. 8.2.	Narrow strip break strengths for the geomembrane samples. Horizontal bars in each column represent the average for the data in the column. Polymer types are noted at the top of each column. Two headed arrows represent manufacturer's MARV.	8-4
Fig. 8.3.	Strains at narrow strip yield strength (a) and break strength (b). Horizontal bars in each column represent the average for the data in the column. Two headed arrows represent manufacturers' MARV.	8-5
Fig. 8.4	Comparison between narrow-strip and wide-strip yield strengths (a) and narrow strip break and narrow strip yield strengths (b).	8-7
Fig. 8.5.	Oxidation induction time (OIT) (a) and melt flow index (MFI) (b) for the geomembrane. OIT and MFI were measured by TRI Environmental, Inc. of Austin, Texas. Horizontal bars in each column represent the average for the data in the column. Solid line at 130 min in OIT graph represents the manufacturers' MARV. Two headed arrows represent the OIT estimates of the exhumed samples calculated by the Arrhenius equation.	8-9
Fig. 8.6.	OIT of exhumed geomembranes normalized by MARV and OIT as a function of time. OIT_e = exhumed OIT. OIT_o = MARV OIT.	8-10
Fig. 8.7.	Transmissivity of GDL under normal stress of 24 kPa (a) and 480 kPa (b). Horizontal bars in each column represent the average for data in the column.....	8-13
Fig. 8.8	Transmissivity of exhumed GDLs as a function of stress and MARV transmissivities for Altamont (a), Boardman (b), Cedar Rapids (c), and Omaha (d).	8-14
Fig. 8.9.	Site average transmissivity of GDL as a function of percent fines of the cover soil. Error bars represent one standard deviation from the mean. ..	8-15
Fig. 8.10.	Permittivity of GDL using 10 mm head (a) and 50 mm head (b). Horizontal bars in each column represent the average for the data in the column. Two headed arrows represent manufacturers' MARV.	8-17
Fig. 8.11.	Site average permittivity as a function of percent fines of the cover soil. Error bars represent one standard deviation from the mean.	8-18

Fig. 8.12. Ply adhesion of GDL. Horizontal bars in each column represent the average the average for the data in the column. Two headed arrows represent manufacturers' MARV.	8-19
Fig. 8.13. Site average ply adhesion as a function of service life (a) and number of freeze- thaw cycles (b). Error bars represent one standard deviation from = mean.	8-22
Fig. 8.14. Peak interface shear strength envelope of GM-GDL interface for geosynthetics sampled from the Wisconsin site.....	8-24
Fig. 9.1. Configuration for the electrical resistivity survey used at the Altamont site.	9-2
Fig. 9.2. Placement of current electrode under the GM at the Altamont site.	9-3
Fig. 9.3. Raw (a) and smoothed (b) distribution of voltage drop from electrical resistivity survey of conventional cover at Altamont site (scale in mV).	9-4
Fig. 9.4. Contour (a) and surface plots (b) of electrical resistivity data from conventional cover at Polson site. Suspect areas marked with red circles and location of intentional defect shown with solid yellow circle.	9-5
Fig. 9.5. Contour and surface plots of electrical resistivity survey of conventional cover at Omaha site (more detailed maps are presented on right). Suspect areas are marked with red oval; green box shows location of gash in GM in Fig. 9.6 (voltage amplitudes in mV).	9-6
Fig. 9.6. Gash in GM at Omaha site that was detected from electrical resistivity survey (lip balm container shown for scale).	9-7
Fig. 9.7. Antennae (200 MHz) used for GPR surveys at Altamont and Omaha sites.	9-9
Fig. 9.8. GPR reflection survey at Altamont site along survey line in Fig. 9.1. Profile shows both point reflector above ground (e.g., tools, cables, etc. on surface) and below ground (sensor cables, etc.).	9-10
Fig. 9.9. EM wave traces collected along survey line shown in Fig. 9.1.	9-11
Fig. 9.10. Tomographic images of EM wave velocity at Altamont site.	9-12
Fig. 9.11. GPR reflection survey across all three cover sections at Omaha site.	9-13
Fig. 9.12. Photograph of thick store-and-release cover at Omaha site showing thick upper storage layer, sand layer for capillary break (white layer), and lower interim cover layer. Note uniformity of layers and moist condition of storage layer and topsoil.	9-14
Fig. 9.13. Tomographic images of downhole EM wave velocity from the thick store-and-release cover at the Omaha site.	9-16

Fig. 10.1	Daily precipitation and percolation record (a) and water content vs. time at various depths (b) in first quarter of 1995 for the final cover test section in Wenatchee, WA described in Khire et al. (1997).	10-6
Fig. 10.2	Schematic of flux meter used to monitor a final cover (adapted from Malusis and Benson 2006).	10-7
Fig. 10.3	Storage and percolation (a) and water contents at various depths (b) as a function of time for thin store-and-release cover evaluated by ACAP in Sacramento, CA.	10-10
Fig. 10.4.	Typical profile of a sensor nest used for interpretive data (adapted from Benson et al. 2009). Labels to right of profile describe layers in cover profile. No sensors were placed in rip rap layer due to the large particle sizes and the negligible storage anticipated in this layer.	10-12
Fig. 10.5.	Moderate frequency TDR sensor ready to be pushed into cover profile. Type-T thermocouple (blue wire) is taped head of TDR sensor.	10-13
Fig. 10.6	Water balance quantities for ACAP test sections near Grand Junction, CO (from Benson et al. 2009).	10-15
Fig. 10.7.	Water contents in frost protection layer and radon barrier measured at same depth in up slope and down slope nests of Test Section A (adapted from Benson et al. 2009).	10-17
Fig. 10.8.	Comparison of water contents in frost protection layer in upslope (Probe 5) and down slope (Probe 12) interpretive monitoring nests in duplicate test sections (Test Sections A and B).	10-18

List of Tables

Table 2.1.	Climatic characteristics and slopes of ACAP sites.	2-5
Table 6.1.	Site characteristics and soil index properties for storage and barrier layers evaluated in this study.	6-2
Table 6.2.	Average as-built compaction and water content for storage and barrier layers evaluated in this study.	6-4
Table 6.3.	As-built hydraulic properties for storage and barrier layers evaluated in this study.	6-5
Table 6.4.	Field hydraulic conductivity for storage and barrier layers.	6-7
Table 6.5.	Saturated hydraulic conductivity measured in laboratory on specimens from in-service storage and barrier layers.	6-11
Table 6.6.	In-service saturated hydraulic conductivity for storage and barrier.	6-16
Table 6.7.	In-service dry unit weight and relative compaction for storage layers. ...	6-26
Table 6.8.	SWCC parameters for storage and barrier layers from 75-mm-diameter specimens.	6-32
Table 6.9.	SWCC parameters for storage and barrier layers from 150-mm-diameter specimens.	6-33
Table 6.10.	SWCC parameters for storage and barrier layers from 254-mm-diameter specimens.	6-34
Table 7.1.	Physical and chemical properties of exhumed GCLs.	7-5
Table 7.2.	Water Content, TCM, and MDR of exhumed GCLs.	7-6
Table 7.3.	USCS Classification and Arithmetic Mean Water Content, TCM, and MDR of Subgrade Soils.	7-6
Table 8.1.	Tensile properties of exhumed GMs (average reported, range of property in parenthesis).	8-3
Table 8.2.	Melt flow index (MFI) and oxidation induction time (OIT) of exhumed GMs (average reported, range of property in parenthesis).	8-8
Table 8.3.	Transmissivities and permittivities of exhumed GDLs (average reported, range of property in parenthesis).	8-12

Table 8.4.	Ply adhesions of exhumed GDLs (average reported range of property in parenthesis).....	8-20
Table 8.5	Shear strength parameters for the interface between the exhumed GDLs and GMs (average reported, range of property in parenthesis).	8-23
Table 8.6	Summary of reduction factors from previous studies and current study of exhumed geosynthetics.....	8-25
Table 10.1.	Water balance quantities for two ACAP test sections near Grand Junction, CO (from Benson et al. 2009).	10-16

EXECUTIVE SUMMARY

In this peer-reviewed study, final covers at test facilities and operating waste containment facilities were exhumed to evaluate how the properties of the cover materials changed 4.0-8.9 yr after installation (6.3 yr on average). Field tests were conducted, samples were collected, laboratory testing was performed, and data analyses were conducted. The findings demonstrate that engineering properties of cover soils change while in service and that long-term engineering properties should be used as input to models employed for performance assessments. Recommendations for appropriate input are made based on the data that were collected.

Changes in hydraulic properties occurred in all cover soils evaluated due to the formation of soil structure, regardless of climate, cover design, or service life. The saturated hydraulic conductivity and the α parameter for the soil water characteristic curve (SWCC) increased, which reflects formation of larger pores due to pedogenic processes such as wet-dry and freeze-thaw cycling. Larger changes were observed for soils with lower as-built saturated hydraulic conductivity and soils with a greater proportion of clay particles in the fines fraction. Hydraulic properties of the cover soils were similar when exhumed, regardless of the as-built condition. Test scale had a significant effect on the hydraulic properties, with conditions near field-scale obtained using 0.3-m test specimens.

Substantial changes were also observed in some geosynthetic clay liners (GCLs). Analysis showed that GCLs have very low saturated hydraulic conductivity ($< 5 \times 10^{-11}$ m/s) when placed on a moist subgrade (water content $> 10\%$) and covered with a geomembrane and cover soil soon after installation. GCLs installed under other conditions can be much more permeable. GCLs that underwent and maintained complete hydration with osmotic swell retained low hydraulic conductivity even when Na was replaced by Ca and Mg provided they did not dehydrate. GCLs that undergo osmotic swell and are covered with a geomembrane surcharged with cover soils are expected to retain low hydraulic conductivity provided the geomembrane remains intact.

Changes in geomembranes and geosynthetic drainage layers were modest or small. Analysis of antioxidants in geomembranes showed that antioxidant depletion was reasonably consistent with expectations based on first-order kinetics and laboratory-measured depletion rates. Based on antioxidant depletion, the minimum service life of geomembranes is on the order of 50-125 yrs. Actual service lives may be longer but are difficult to predict based on the limited information available today.

Because changes in the engineering properties of cover materials are commonplace, and significant in some cases, monitoring of covers should be conducted to ensure they are functioning as intended. Monitoring using pan lysimeters combined with secondary measurements collected for interpretive purposes (water content, temperature, vegetation surveys, etc.) is recommended. Future research investments should explore how remote sensing technologies can be used for cover monitoring.

This study represents a snap shot in the evolution of final covers approximately 5 to 10 yr after construction. Additional research investments are needed to more accurately and completely define very long-term properties of earthen and geosynthetic cover materials corresponding to 100s or 1000s of years. These research investments should include analog studies of natural environments where earthen and natural polymeric materials exist as well as accelerated laboratory experiments that can be used to develop predictive degradation models.

ACKNOWLEDGEMENT

This research study was funded by a consortium consisting of the U.S. Nuclear Regulatory Commission's Office of Nuclear Regulatory Research (through a grant to the University of Wisconsin-Madison Water Resources Institute under an interagency agreement, IA-RES-08-132, with the U. S. Geological Survey State Water Resources Research Institute Program), the National Science Foundation (Grant No. CMMI-0625850), the U.S. Environmental Protection Agency, the U.S. Department of Energy, the Environmental Research and Education Foundation, Colloid Environmental Technologies Corporation, Veolia Environmental Services, and Waste Connections, Inc. This support is gratefully acknowledged.

The research report was peer reviewed by an expert panel consisting of Charles D. Shackelford, John D. McCartney, and George R. Koerner. The authors of the research report considered and incorporated their comments and suggestions when finalizing the report.

ABBREVIATIONS

Acronyms

ACAP	Alternative Cover Assessment Program
BC	bound cations
CEC	cation exchange capacity
CMH	chilled mirror hygrometer
CMP	common midpoint
D	diameter
DW	deionized water
ET	evapotranspiration
GCL	geosynthetic clay liner
GDL	geosynthetic drainage layer
GM	geomembrane
GPR	ground penetrating radar
H	depth of water in outer ring of SDRI
HDPE	high density polyethylene
H _b	height of water in bubbling tube in BH relative to base of borehole
I	infiltration rate
ICP-OES	inductively coupled plasma – optical emissions spectrometry
I _s	ionic strength
K	hydraulic conductivity
L _f	depth of the wetting front
LLDPE	linear low density polyethylene
MARV	minimum average role value
MDR	charge ratio of monovalent to divalent soluble cations
MFI	melt flow index

MSW	municipal solid waste
OIT	oxidation induction time
PET	potential evapotranspiration
Q	volumetric flow rate
RMD	ratio of monovalent to divalent cations in a solution
SC	soluble cations
SDRI	sealed double-ring infiltrometer
SI	swell index
SW	standard water (0.01 M CaCl ₂)
SWCC	soil water characteristic curve
TDR	time domain reflectometry
BH	borehole permeameter
TCM	total soluble cations charge per mass
USCS	Unified Soil Classification System
USEPA	US Environmental Protection Agency

Western Symbols

Ca	calcium
Cl	chlorine
K	potassium
K _F	field-measured saturated hydraulic conductivity
K _s	saturated hydraulic conductivity
K _{sa}	as-built saturated hydraulic conductivity
K _{SDRI}	field-measured hydraulic conductivity with SDRI
K _{si}	in-service saturated hydraulic conductivity
K _{BH}	field-measured hydraulic conductivity with BH permeameter

n	shape parameter in van Genuchten's equation
n_{LS}	shape parameter in van Genuchten's equation from large-scale tests
n_{SS}	shape parameter in van Genuchten's equation from small-scale tests
n_a	shape parameter in van Genuchten's equation from as-built test section
Na	sodium
Mg	magnesium
p	p statistic from t-test
t	t statistic from t-test
X_m	mole fraction of monovalent cations

Greek Symbols

α	shape parameter in van Genuchten's equation
α_a	shape parameter in van Genuchten's equation from as-built test section
α_{LS}	shape parameter in van Genuchten's equation from large-scale tests
α_{SS}	shape parameter in van Genuchten's equation from small-scale tests
γ_{dmax}	maximum dry unit weight on compaction curve
θ	volumetric water content
θ_r	residual volumetric water content
θ_s	saturated volumetric water content
Θ	effective saturation
σ	standard deviation

1. INTRODUCTION

The final cover controls the amount of liquid entering a waste containment system and therefore directly affects the amount of leachate generated within the waste mass and the potential flux of contaminants to ground water. As a result, the final cover generally is regarded as one of the most important components in a waste containment system with respect to long-term performance. This is particularly true for wastes with very long life spans (e.g., mining wastes, radioactive wastes) that can pose a very long-term threat to ground water. Consequently, considerable interest has developed in understanding the long-term performance of final covers.

Although the importance of final covers has been recognized, their performance has remained largely undocumented. Until recently, few studies regarding the performance of final covers have been conducted and no systematic studies have assessed how the engineering properties of cover materials change during the service life of a cover. Consequently, modeling exercises conducted to predict the long-term performance of containment facilities are clouded with uncertainty due to scant information on appropriate input parameters for cover soils and other barrier materials.

During the last two decades, several studies were initiated in the US and abroad to assess the long-term performance of modern final covers under realistic conditions (Melchior 1997, Dwyer 2001, Albright et al. 2004). The most comprehensive of these studies is the Alternative Cover Assessment Program (ACAP), which evaluated the performance of 27 different final cover profiles at 12 locations in 8 states in the US (Albright et al. 2004). The covers were evaluated for a period ranging from 4-8 yr in climates ranging from arid (Apple Valley, CA) to humid (Albany, GA) to seasonal semi-arid with extreme fluctuations in temperature (Underwood, ND). Conventional covers relying on hydraulic barriers (compacted clay barriers, geosynthetic clay liners, polymeric geomembranes, and combinations thereof) and alternative covers relying on store-and-release principles were evaluated in ACAP via extensive monitoring of the water balance, state variables, and meteorological conditions.

Monitoring of the ACAP test sections ceased between October 2004 and August 2007 (the ACAP test section in Monticello, UT is an exception; it is still being monitored). Subsequently, the test sections were exhumed to evaluate how the engineering properties of the cover materials (soils and geosynthetics) changed during their service life. Field tests were conducted and samples were collected and tested in the laboratory. The specific objectives were to

- characterize changes in the engineering properties of the cover materials directly relevant to assessing hydrologic effectiveness,
- identify conditions that induce changes in the engineering properties of cover materials and ultimately affect percolation into waste,
- identify soil types and design and construction approaches that result in covers that are less prone to temporal change and therefore have more predictable performance, and

- recommend approaches to verify the hydrologic performance of final covers based on lessons learned from ACAP and the findings of the exhumation program.

This peer-reviewed report consists of 11 sections, including this introduction. Section 2 provides background on ACAP, describes the as-built profiles and properties of the test sections, and summarizes information from previous studies on factors that can lead to temporal change in the engineering properties of cover materials. Section 3 describes the methods used to exhume the ACAP test sections. Field test methods are described in Section 4 and laboratory test methods are described in Section 5. Findings regarding earthen cover materials are described in Section 6, findings regarding geosynthetic clay liners are described in Section 7, and findings regarding geomembranes and geosynthetic drainage layers are described in Section 8. Outcomes from geophysical assessments are described in Section 9. Lessons learned and practical applications for design, construction, and monitoring are described in Section 10. Conclusions and recommendations are provided in Section 11. Data from the field and laboratory experiments are contained in the appendices.

2. BACKGROUND: ACAP TEST SECTIONS

Twenty-seven tests sections were constructed in ACAP at 12 sites in 8 states. Locations of the field sites are shown in Fig. 2.1 and a summary of cover types and climate characteristics is given in Table 2.1. This diverse group of field sites represents a broad range of climatological conditions as well as types of soil and vegetation. The average annual precipitation ranges from 119 mm (Apple Valley, CA) to 1263 mm (Albany, GA). Snowfall is appreciable at 6 sites (Helena and Polson, MT; Omaha, NE; Cedar Rapids, IA; Monticello, UT; and Underwood, ND).

The cover profiles evaluated in ACAP are shown in Figs. 2.2 and 2.3. A broad variety of covers were evaluated that could be employed for a wide range of wastes, including municipal solid waste (MSW), hazardous waste (HW), low-level radioactive waste (LLRW), and mixed waste (MW). Covers were evaluated that relied on conventional resistive barrier layers as well as alternative approaches that rely on water balance principles, including storage and release of water under unsaturated conditions. One of the covers (Monticello, UT) was used to contain radioactive wastes associated with cleanup of a historic uranium mill tailings site.

Twelve are conventional covers and 15 are store-and-release covers. Side-by-side comparisons were conducted at 9 sites. Five of the conventional covers had compacted soil (clay) barriers and 7 had composite barriers (geomembrane over earthen/mineral barrier). Two of the conventional covers with composite barriers used a geosynthetic clay liner (GCL) as the earthen/mineral barrier. Nine of the store-and-release covers were monolithic covers (i.e., a thick layer of finer textured soil overlain by topsoil) and 6 were capillary barriers. All of the capillary barriers employed a simple two-layer fine-over-coarse design where the primary purpose of the capillary break was to enhance the storage capacity of the overlying finer-textured layer. Capillary barrier designs employing textural contrasts to facilitate lateral diversion were not evaluated. In this report, a "barrier layer" refers to the clay and/or geosynthetic materials (GCL or geomembrane) used to provide hydraulic resistance (block flow). A "storage layer" refers to a fine-textured soil layer used to store infiltrating water in a store-and-release cover. The storage layer resides below the topsoil (approx. 300 mm thick) and above a capillary break or foundation layer (if present).

All of the sites were vegetated with a mixture of annual and perennial grass mixtures. Three of the sites (Apple Valley, CA; Monticello, UT; Polson, MT) also included shrubs and two sites (Albany, GA; Cedar Rapids, IA) had hybrid poplar trees with an understory of grasses. The test sections were sloped at 5 or 25%, depending on the predominant slope (e.g., top deck vs. side slope) of the waste containment facility at each site (Table 2.1).

Construction of all but two of the ACAP test sections was completed by Fall 2000 (Apple Valley, CA and Underwood, ND were added later in the program). Each test section was constructed with soils available on site or nearby using methods and procedures typical of practice for construction of final covers. Full-scale construction equipment was used to place the soils and to compact the soil barrier layers. For the test sections with a composite barrier, a single 9-mm-diameter hole was cut in the geomembrane near the center of the test section. This hole was intended to represent a typical construction defect and was sized based on recommendations in Giroud and Bonaparte (1989).

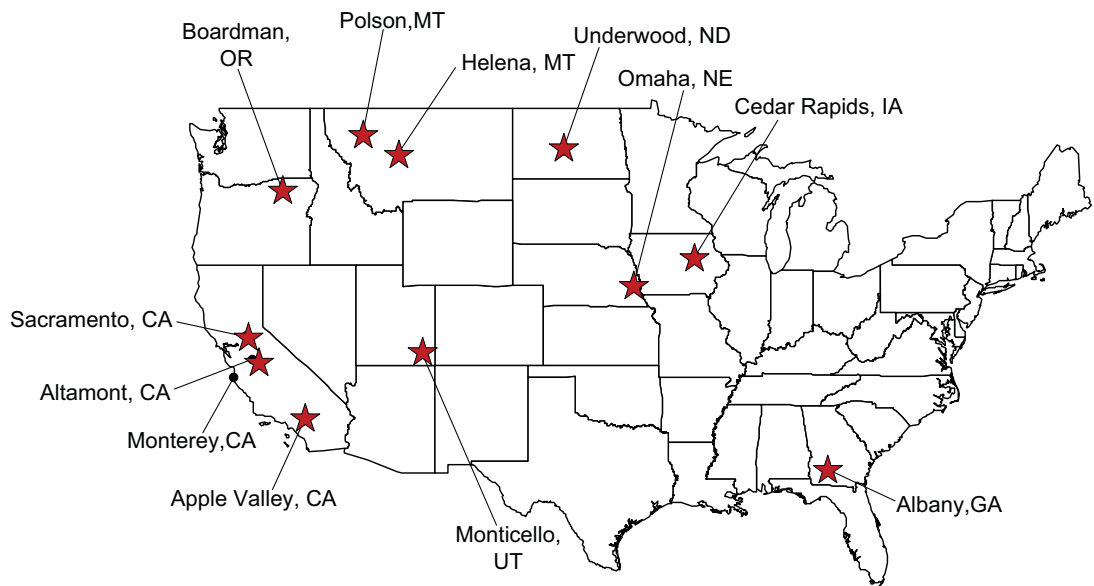


Fig. 2.1. Locations of ACAP field sites. Sites exhumed in this study marked with a star.

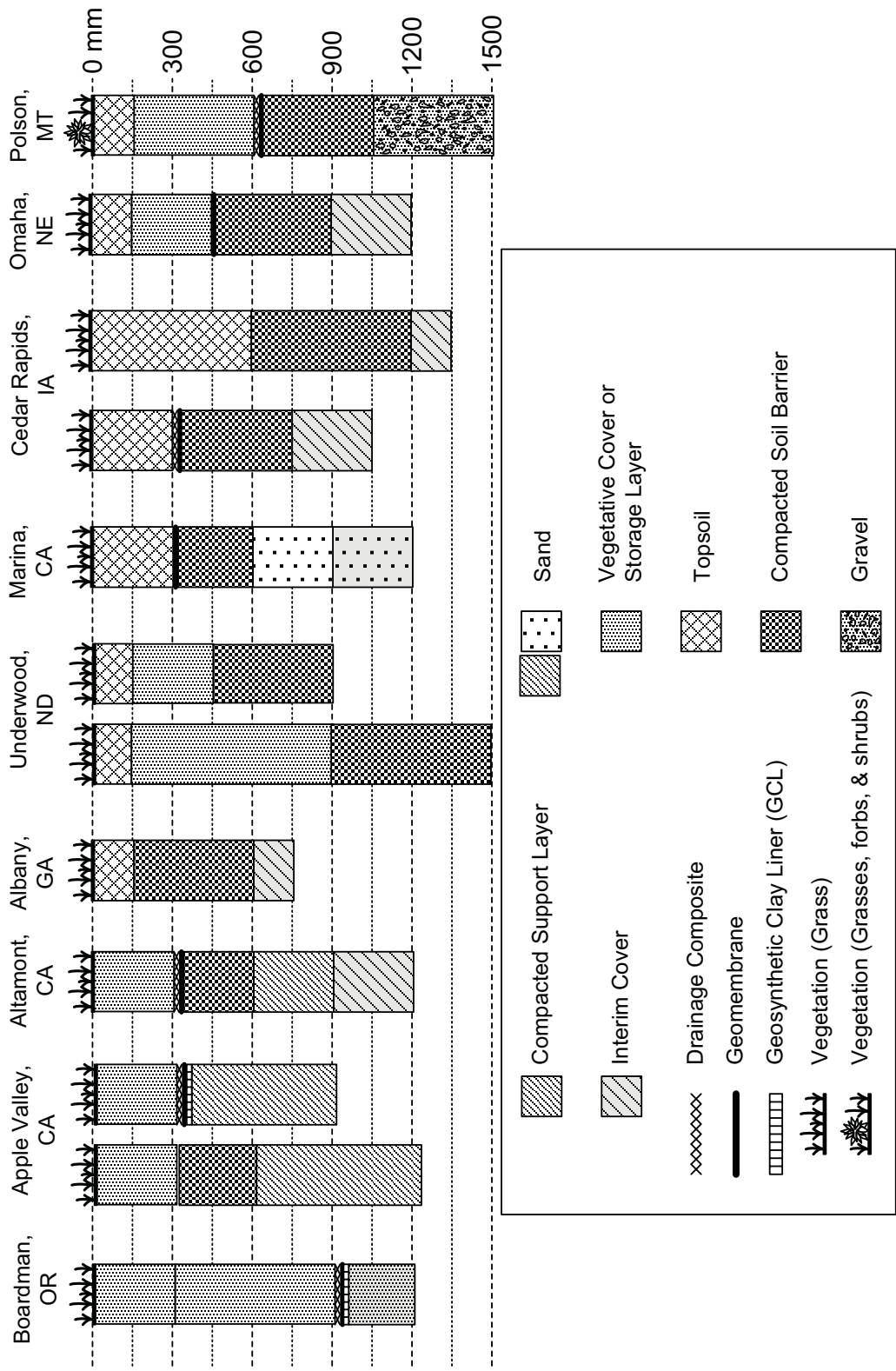


Fig. 2.2. Profiles of conventional covers evaluated by ACAP.

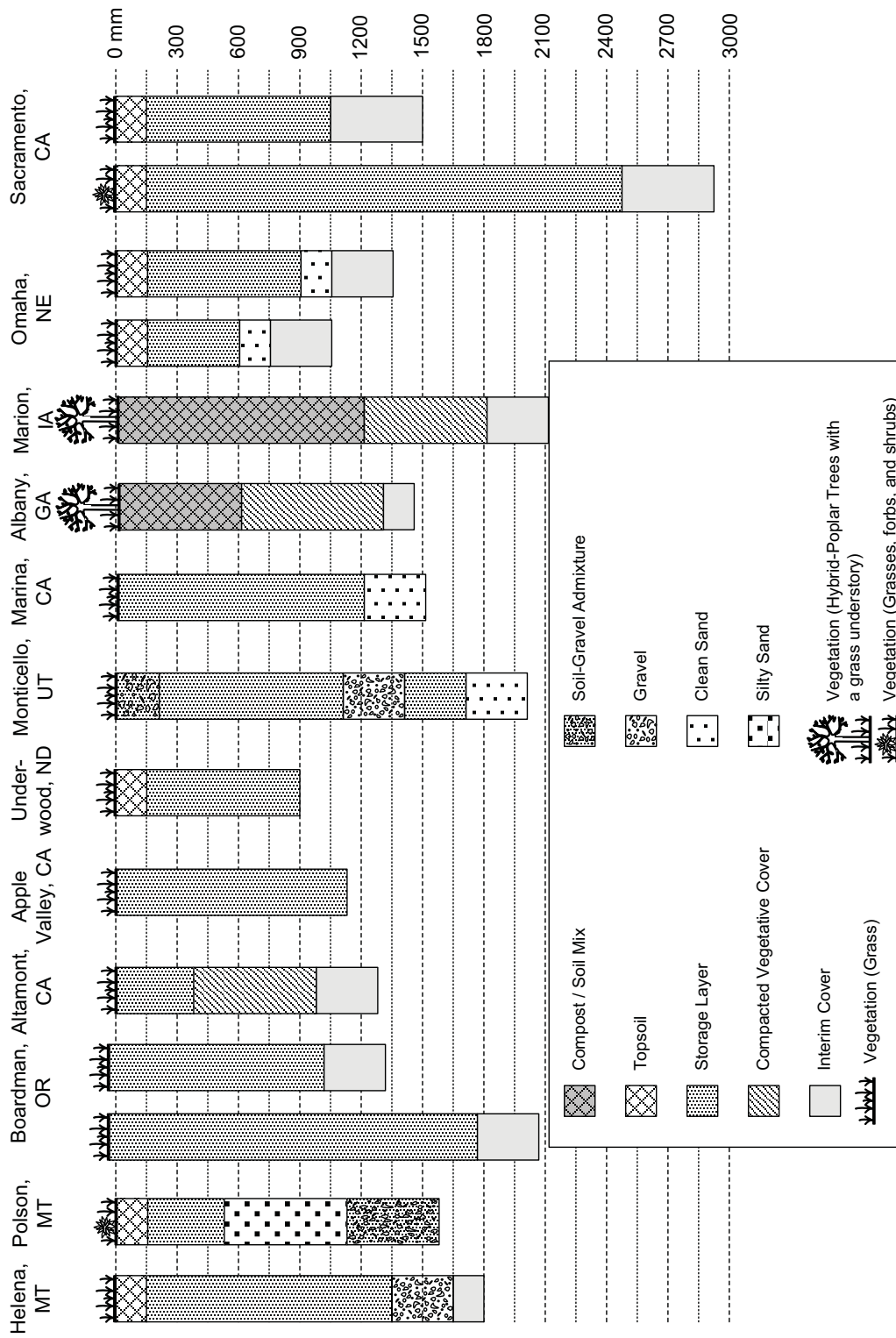


Fig. 2.3. Profiles of store-and-release covers evaluated by ACA

Table 2.1. Climatic characteristics and slopes of ACAP sites.

Site	Service Life (yr)	Slope (%)	Average Annual Precipitation (mm/yr)	Avg. Precipitation /Potential Evapotranspiration	Climate ^a
Altamont, CA	6.6	5	358	0.31	Semi-arid
Apple Valley, CA	4.9	5	119	0.06	Arid
Boardman, OR	6.8	25	225	0.23	Semi-arid
Helena, MT	8.9	5	289	0.44	Semi-arid
Marina, CA	3.8	25	466	0.46	Semi-arid
Monticello, UT	7.1	5	385	0.34	Semi-arid
Polson, MT	8.8	5	380	0.58	Sub-humid
Sacramento, CA	6.0	5	434	0.33	Semi-arid
Underwood, ND	4.1	25	442	0.47	Semi-arid
Albany, GA	4.0	5	1263	1.10	Humid
Cedar Rapids, IA	5.7	25	915	1.03	Humid
Omaha, NE	7.8	25	760	0.75	Humid

^aBased on UNESCO climate definitions described in Hill (1996).

Installing a single hole resulted in an areal defect frequency 10 times larger than is typical in practice (approx. 5 holes/ha, Giroud and Bonaparte 1989). However, installing less than one hole was not possible. A description of construction of each test section can be found in Bolen et al. (2001) and Roesler et al. (2002).

2.1 ACAP Lysimeters

A key feature of the ACAP test sections was a large (10 m x 20 m) pan-type lysimeter (Fig. 2.4) used for direct measurement of surface runoff (R), soil water storage (S), lateral drainage (L, conventional covers only), and percolation (P_c) from a full-depth cover profile. The base and sidewalls of each lysimeter were comprised of linear low-density polyethylene (LLDPE) geomembrane (GM). The GM in the base of the lysimeter was overlain with a geocomposite drainage layer (GDL) to protect the GM and to transmit water from the base of the cover profile to a collection and measurement system. Tests were conducted on the lysimeters during construction to ensure that each lysimeter was free of leaks (Bolen et al. 2001). Diversion berms on the surface are used to prevent run-on and collect run-off as well as to delineate the edges of the lysimeter. Methods used to install the lysimeters are described in Benson et al. (1999).

Each cover profile was constructed within the lysimeter and in a perimeter buffer area at least 3 m wide to reduce boundary effects and to provide an area for annual sampling of soil and vegetation. Prior to constructing the cover profile, a layer of soil simulating the existing interim cover on the waste was placed on top of the GDL at the base of the lysimeter to replicate the field condition above the waste as closely as practical. The interim cover layer was covered with a root barrier layer (a non-woven geotextile studded with nodules containing trifluralin, a root inhibitor) to prevent root intrusion into the geocomposite drainage layer and the percolation collection system. Inclusion of the root barrier probably results in less water being transpired than might occur in an actual cover, where roots can grow through the interim cover and possibly into the waste. However, the root barrier prevents plants from having access to water retained in the collection and measurement system that would otherwise become deep drainage in an actual containment facility.

2.2 Data Collection

Percolation, lateral flow, and surface runoff were routed by pipes to basins equipped with redundant instruments (pressure transducer, tipping bucket, and float switch) each capable of measuring flows with a precision < 1 mm/yr (Benson et al. 2001). Soil water content was measured in three nests located at the quarter points along the centerline of each test section (Fig. 2.4). Each nest contained 4 to 6 low-frequency (40 MHz) time domain reflectometry (TDR) probes (Campbell and Anderson 1998) in a vertical stack. The central nest also contained co-located thermal dissipation sensors (Phene et al. 1992) for monitoring soil water potential. Soil water storage was determined by integration of the point measurements of water content. The TDR probes were calibrated with the soils in which they were placed (Kim and Benson 2002). The thermal dissipation sensors were calibrated in Warden silt loam.

Meteorological parameters (precipitation, air temperature, relative humidity, solar radiation, wind speed, and wind direction) were measured with a weather station

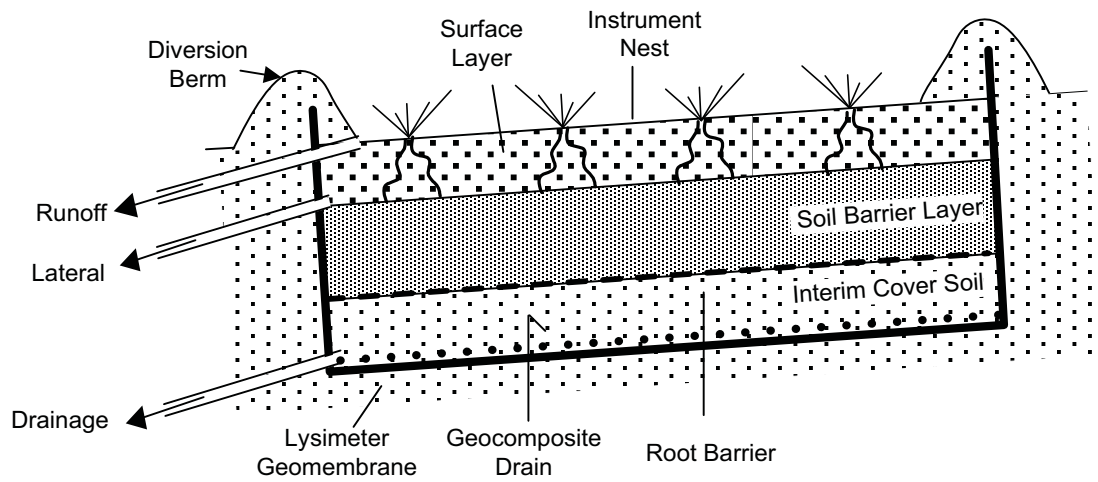


Fig. 2.4. Schematic of ACAP lysimeter (not to scale).

mounted in the buffer area. All data were collected and recorded by a datalogger every 15 min and were normally stored on one-hour intervals. At times of intense activity (e.g., an intense rain event with high surface runoff), data were stored at time intervals as short as every 15 s.

Evapotranspiration (ET) was estimated as the difference between precipitation (P) and the sum of the other components of the water balance. Potential evapotranspiration (PET) was computed using the Penman-Monteith method with on-site meteorological data (Roesler et al. 2002).

2.3 Calibration and Data Quality Control

Annual site visits were made for calibration, quality control checks, and characterization. The flow measurement systems (dosing basins, tipping bucket gauges, pressure transducers) were calibrated annually and the meteorological instruments received annual maintenance and calibration checks. Intact samples were collected in thin-wall sampling tubes (76-mm-diameter) for laboratory tests to evaluate the accuracy of the TDR probes. Comparisons between oven-dry water contents and those obtained with the TDR probes generally were in close agreement ($\pm 2\%$) (Albright et al. 2004).

2.4 Cover Soils

An extensive sampling program was conducted during construction to characterize the in-place cover soils. Four disturbed samples (20-L buckets) and four intact samples were collected from each lift of soil immediately after placement. Two of the intact samples were collected in thin-wall sampling tubes (76-mm diameter) and two were collected as hand-carved blocks (200-mm diameter). The disturbed samples were analyzed for particle size distribution, Atterberg limits, organic matter content, and compaction behavior. The intact samples were tested to determine the saturated hydraulic conductivity and the soil water characteristic curve (SWCC). Results of all of the tests are contained in Gurdal et al. (2003). Properties of the as-built cover soils are described in Sec. 6.

2.5 Geosynthetics

The GCLs, GMs, and GDLs were typical materials used for construction of waste containment systems. All were installed using methods typical of practice. The GCLs were North American needle-punched products (Bentomat or Bentofix) containing granular sodium bentonite ($\approx 3\text{-}5 \text{ kg/m}^2$). LLDPE geomembranes were used to construct all elements of each lysimeter. However, at two of the sites (Altamont and Apple Valley), textured high-density polyethylene (HDPE) GMs were used to construct the composite barrier within the cover profile. All GDLs had 5-mm geonet cores that were sandwiched between two non-woven geotextiles thermally-bonded to the geonet. The Underwood site had 200 g/m^2 geotextiles on both sides of the geonet, whereas all other GDLs had 270 g/m^2 geotextiles.

3. EXHUMATIONS

Twenty-four final cover test sections from ACAP were exhumed. The ACAP sites where exhumations were conducted are marked with a star in Fig. 2.1. In addition, exhumations to collect geosynthetic samples were conducted at two conventional full-scale covers at operating MSW landfills in Wisconsin and Michigan that employed a composite barrier layer (GM over a GCL) as the hydraulic barrier. Profiles for these full-scale sites are shown in Fig. 3.1. Service lives of the ACAP test sections are summarized in Table 2.1 and those of the MSW landfill covers are in Fig. 3.1. A gallery of photographs from the field activities is in Appendix A.

Each exhumation included a series of field tests to evaluate the saturated hydraulic conductivity of the barrier layer (conventional covers) or the storage layer (store-and-release covers), collection of a set of large intact soil samples from the barrier and/or storage layers for laboratory testing, collection of geosynthetic samples from the lysimeter or the barrier layer in profiles of conventional covers with composite barriers, inspection of soil structure within test pits excavated in the test sections, and geophysical surveys (conventional covers with composite barriers only). The objective was to define the in-service properties of the cover materials so that comparisons could be made with the as-built condition in the context of site conditions and material types.

3.1 Soil Sampling and Field Testing

The field hydraulic conductivity tests were conducted using sealed double-ring infiltrometers (SDRI) and borehole (BH) permeameters. These tests were conducted to determine the saturated hydraulic conductivity at two scales and at different depths in the storage or barrier layer. SDRI and BH tests were chosen due to their complementary characteristics. SDRIs provide a single, large-scale measurement (cross-sectional area = 2.25 m²) of saturated hydraulic conductivity at the ground surface. In comparison, BH tests are performed at a smaller scale (cross-sectional area = 0.07 m²) and can be replicated at multiple locations and depths. Photographs showing the BH and SDRI tests are in Figs. 3.2 and 3.3

Prior to field testing, at least 300 mm of surface soil was removed so that the tests would be conducted on the storage layer or the barrier layer as opposed to the surface layer. Hydraulic conductivities measured with SDRIs and BHs are assumed to represent conditions at saturation, although saturation could not be ensured in the field. Results from the field hydraulic conductivity tests are referred to as saturated hydraulic conductivities in this report.

Intact block samples were collected from each test section for measurement of hydraulic properties in the laboratory. Block samples were collected at multiple locations and depths following the procedure in ASTM D 7015 (Fig. 3.4). All block samples were trimmed into PVC rings with a diameter of 365 mm. Both ends of the sample were sealed with plastic sheeting and the sample was secured between wooden endplates. All samples were transported by truck to the University of Wisconsin-Madison where they were stored in a 100% humidity room prior to testing. Hydraulic properties of block samples collected from barrier and storage layers are described in this report, as these layers control the performance of conventional or store-and-release covers.

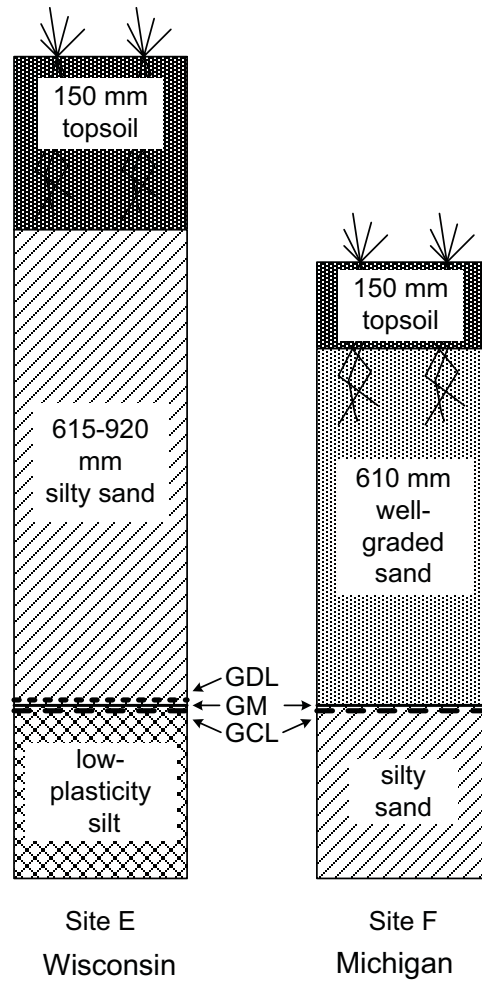


Fig. 3.1. Profiles of the final covers at full-scale MSW landfills in Wisconsin (Site E) and Michigan (Site F). GDL = geosynthetic drainage layer, GM = geomembrane, and GCL = geosynthetic clay liner. Service life of Wisconsin site is 4.7-5.8 yr (depending on test pit). Service life of Michigan site is 3.1 yr.



Fig. 3.2. BH test conducted during exhumation of ACAP test section in Helena, MT.



Fig. 3.3. SDRI test conducted at ACAP test facility in Polson, MT. Upper photograph shows inner and outer rings after installation. Lower photograph shows water-filled SDRI with Mariotte bottle in the rear.



Fig. 3.4. Block sample being collected at ACAP test facility in Underwood, ND. Upper photograph shows sample partially trimmed into ring. Lower photograph shows sample in ring and ready for separation from subgrade.

3.2 Sampling of Geosynthetics

Soils overlaying the composite barrier layer were removed from a test pit approximately 4 m x 4 m. The cover soils were removed using an excavator until the excavation was within approximately 150 mm of the uppermost geosynthetic layer. The remaining soil was then removed by hand. After the cover soil was removed, the geosynthetics were visually inspected and appeared undamaged by the excavation procedure. Rectangular sections (2 m x 2 m) of GDL (if present) and GM were removed from the floor of each test pit by cutting the perimeter with a sharp utility knife (Fig. 3.5). These samples were rolled, labeled, and transported to the laboratory for testing.

Samples of the GCLs were collected after the geomembrane was removed using the procedures described in ASTM D 6072-08. A minimum of 6 square samples (0.3 m x 0.3 m) were collected at each site with a GCL. The perimeter of each GCL sample (0.3 m x 0.3 m) was scored and cut with a sharp utility knife while the GCL remained on the subgrade (Fig. 3.6a). GCL surrounding the sampling area was pulled back, and a rigid PVC plate (0.3 m x 0.3 m) was slid under the sample (Fig. 3.6b). The GCL sample was then wrapped with plastic sheeting to prevent loss of moisture, placed in plastic tubs, and covered with at least 0.15 m of loose soil for protection during transport and storage. A bulk sample of the subgrade immediately beneath the GCL sample (<20 mm depth) was also collected for determination of water content, particle size distribution, and chemical analysis of the pore water. No recommendation is made in ASTM D 6072-08 as to how GCL samples should be transported and stored prior to permeation. One concern is the impact of stress relief prior to testing. To assess this issue, two alternate stress states were tested using split samples from the Boardman, OR and Eau Claire, WI sites. One state consisted of burying GCLs beneath at least 0.5 m of soil in a large plastic tub (referred to as “with overburden pressure” henceforth). The other method consisted of storing the GCLs in a shallow plastic tub beneath a thin (<0.15 m depth) soil layer (referred to as “without overburden pressure”). Duplicate samples collected adjacently were used for this evaluation. Statistical analysis of hydraulic conductivity tests conducted on the duplicate samples showed that no statistically significant difference between hydraulic conductivities obtained from the two stress states (Scalia 2009).

3.3 Geomorphological Surveys

Geomorphological surveys were conducted in test pits to map the soil structure that developed while the test sections were in service. These surveys are described in Albright et al. (2006) and Benson et al. (2008)

3.4 Geophysical Surveys

Geophysical surveys were conducted using electrical resistivity and ground penetrating radar on test sections containing composite barriers with a compacted fine-grained soil layer for the earthen/mineral component. The electrical resistivity surveys were conducted to detect defects in the geomembrane. Ground penetrating radar surveys were conducted to evaluate moisture within the cover profile.

The electrical resistivity method depicted in Fig. 3.7 detects an electrical current that flows through defects in the geomembrane (Van et al. 1991, Frangos 1997). A current electrode is placed below the geomembrane via a small excavation and the electrical

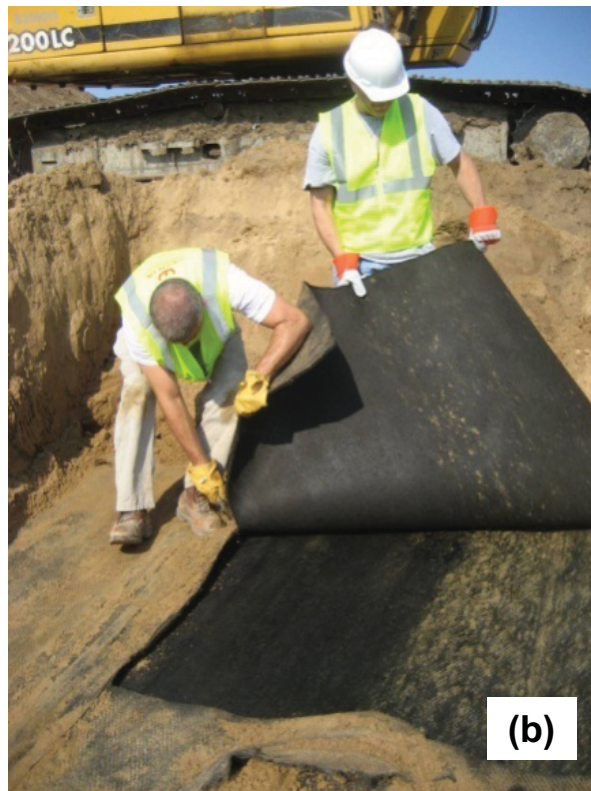


Fig. 3.5. Removing cover soils over a composite barrier layer (a) and removing a sample of geosynthetic drainage layer (b). Both photographs are from final cover at Wisconsin MSW landfill.

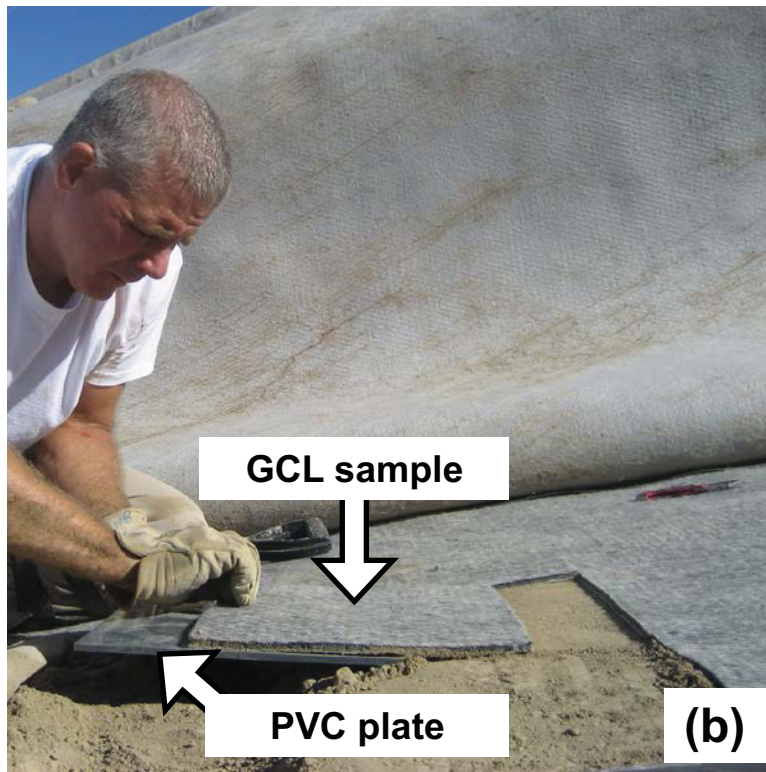
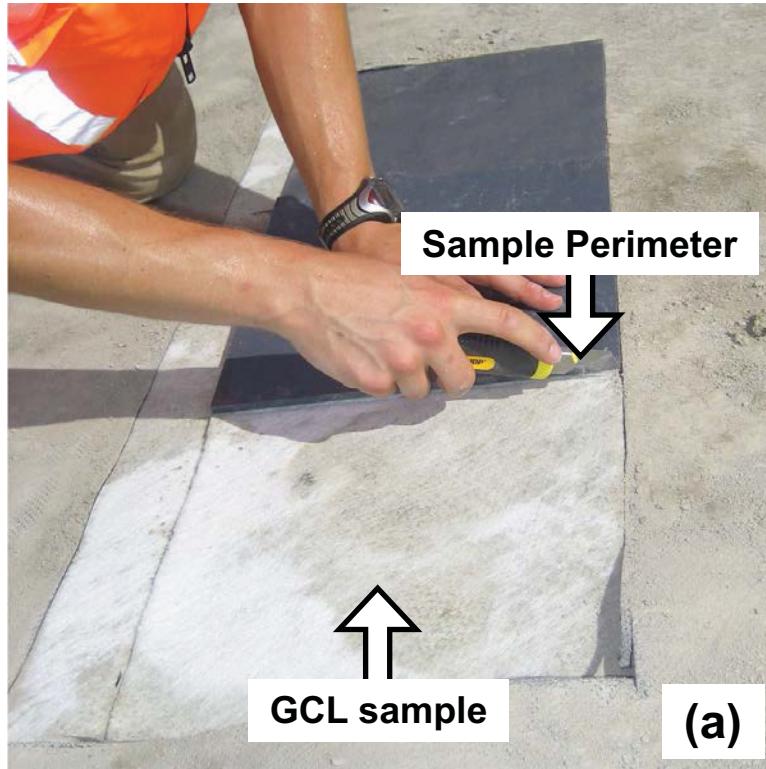


Fig. 3.6. Exhumation of GCL samples: cutting around perimeter with razor knife (a) and delicately sliding sample onto rigid plastic plate (b).

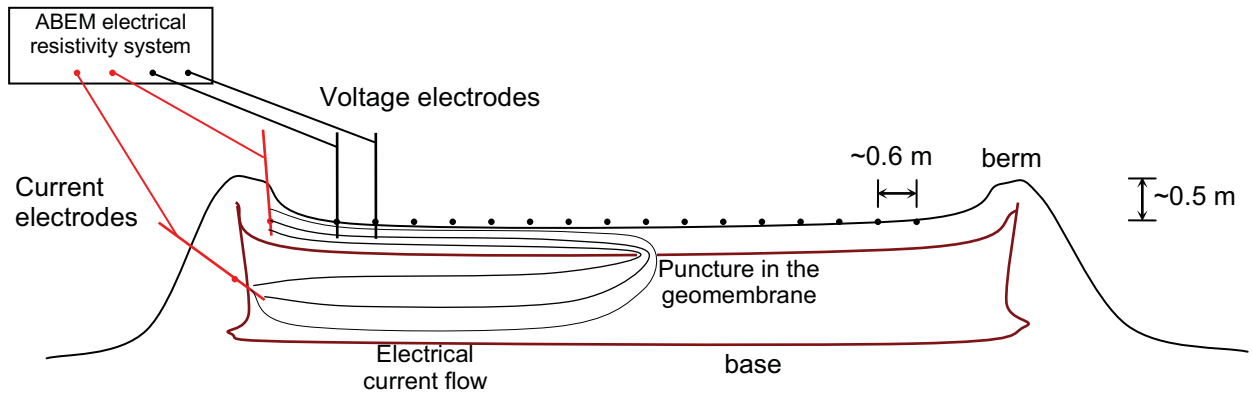


Fig. 3.7. Typical setup for evaluating punctures in geomembranes using electrical resistivity measurements (adapted from Frangos 1997 and Darilek and Miller 1998).

circuit is closed with a second current electrode placed on the surface of the test section. The potential drop on the surface of the cover is measured with an array of potential electrodes (Fig. 3.7). Large equipotential drops indicate concentration of electrical flow lines and provide the data needed to locate defects in the geomembrane (Fig. 3.8).

Electrical resistivity surveys yield non-destructive signals of the locations of holes, punctures, or other defects in the geomembrane. Typical electrical resistivity techniques monitor changes in potential distribution (e.g., pole-pole configuration to evaluate leaks over time, Van et al. 1991) or electrical current through the liner (Frangos 1997). Both methodologies require a closed electrical circuit with a resistance much smaller than the resistivity of the geomembrane (a large electrical contrast is required to identify defects). This requirement may limit use of the methodology to final covers in more humid areas. Assessing the efficacy of the method for final covers in semi-arid areas was a goal of the testing program.

The ground penetrating radar surveys were run in reflection and transmission modes to evaluate the moisture content distribution and homogeneity of the site (Schmalholz et al. 2004, Hanafy and al Hagrey 2006). Reflection data were collected using 100 and 200 MHz antennae in reflection and common midpoint (CMP) surveys (Fig. 3.9). The velocity and reflection amplitudes obtained from these surveys are functions of the volumetric water content and the salinity of the pore water. Transmission downhole surveys were also conducted to provide complementary data (Fig. 3.10).

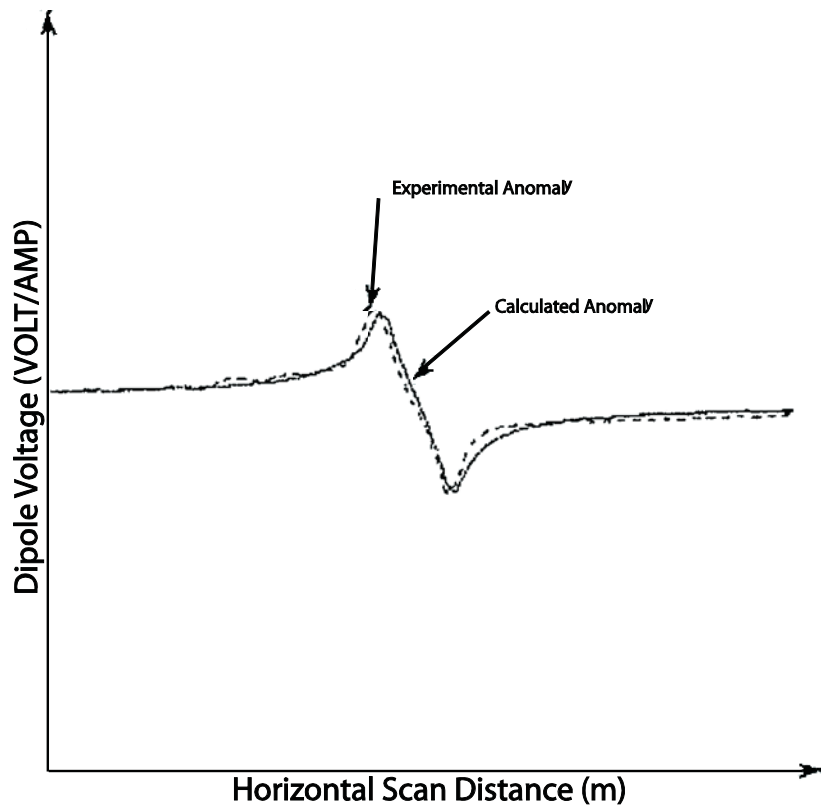
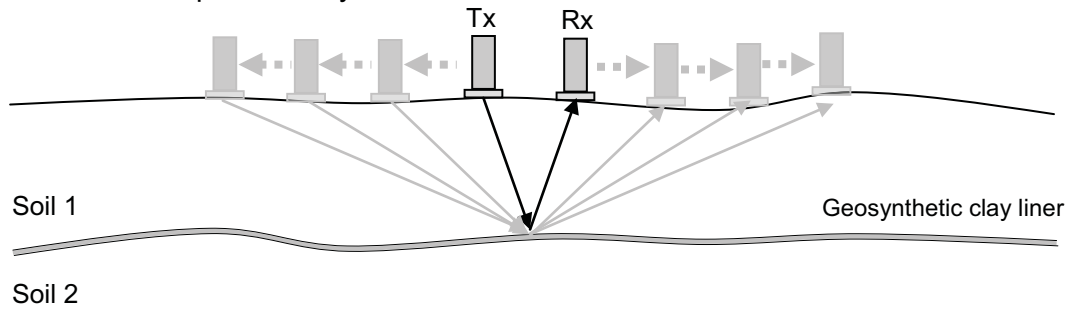
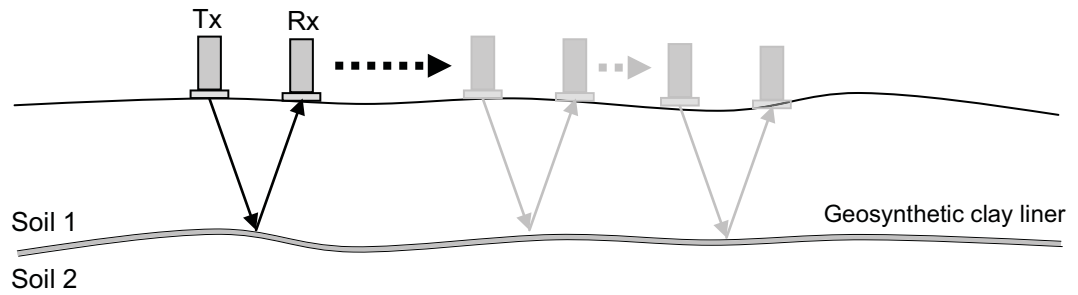


Fig. 3.8. Typical voltage drop over a hole in a geomembrane: experimental measurements and theoretical response (adapted from Parra 1988).

a) Common mid-point survey

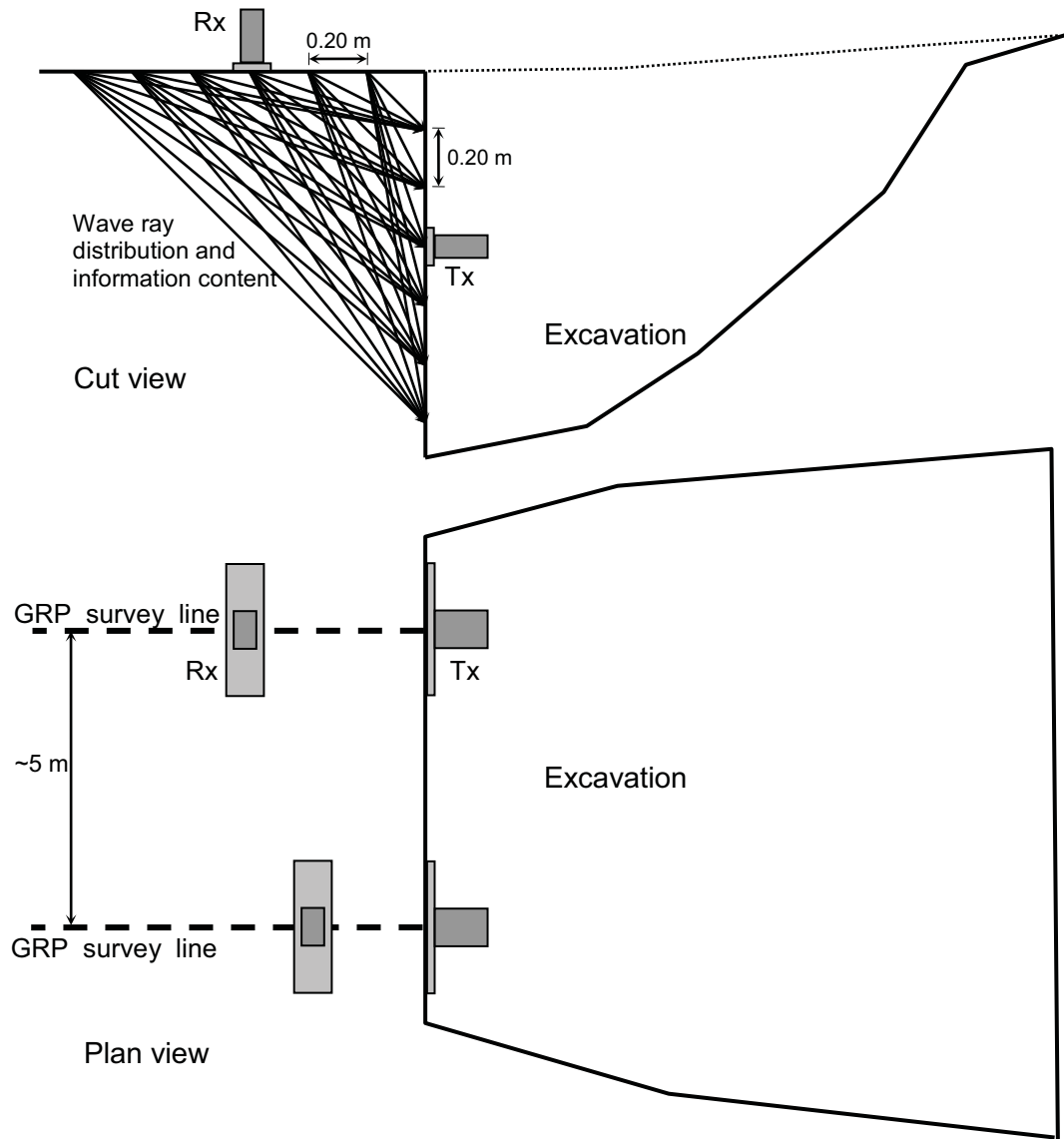


b) Reflection survey



Tx = transmitter
Rx = receiver

Fig. 3.9 Common mid-point (a) and reflection survey (b) configurations for ground penetrating radar.



Tx = transmitter
 Rx = receiver

Fig. 3.10. Downhole setup for ground penetrating radar.

4. FIELD TEST METHODS

4.1. Sealed Double-Ring Infiltrometer (SDRI) Tests

SDRI tests were performed on 12 of the ACAP test sections according to the methods in ASTM D 5093. Both the inner and outer rings were square, with the sides of the inner ring 1.5 m wide and the outer ring 2.25 m wide. A trenching machine was used to excavate trenches for the outer ring, whereas shovels and hand tools were used to excavate trenches for the inner ring to minimize disturbance of soil in the test area. Granular bentonite was used to seal the outer ring and hydrated bentonite paste was used to seal the inner ring.

The flow rate was expected to be high due to the presence of soil structure. The test duration also was sufficiently long to assume that the wetting front had propagated through the entire cover. Water draining into the basin used to collect percolation from the lysimeter confirmed that the wetting front had passed through the cover profile. Therefore, tensiometers generally were not used to determine the depth of the wetting front.

Infiltration rate was monitored using either a flexible plastic bag or a Mariotte bottle in cases where the infiltration rate was high. The saturated hydraulic conductivity was calculated as follows (Daniel 1989):

$$K_{\text{SDRI}} = I \frac{L_f}{H + L_f} \quad (4.1)$$

where I is the infiltration rate, L_f is the thickness of the wetted soil beneath the SDRI, and H is the height of the water in the outer ring.

The cross-sectional area of the SDRI was used to determine the effective diameter of a circle with an equivalent area of the inner ring so that hydraulic conductivities from the SDRIs could be compared with the hydraulic conductivities from all other tests, which had circular cross-sections. The SDRIs were assigned an effective diameter of 1.69 m (cross sectional area = 2.25 m²). Data from the SDRI tests are presented in Appendix B.

4.2 Borehole Tests

BH tests were conducted according to ASTM D 6391 using a 300-mm-diameter casing and 100-mm-diameter standpipe constructed of PVC tubing. The casing is larger than normal (most BH tests in practice have a 100-mm-diameter casing and 25-mm-diameter standpipe) to provide a larger scale measurement of hydraulic conductivity that could incorporate macroscopic features.

All boreholes were excavated using hand tools and were prepared with a flush surface at the bottom of the casing. The depth of the borehole was typically 300 or 600 mm below the surface of the storage or barrier layer to obtain hydraulic conductivity measurements at different depths. Alternating layers of bentonite paste and granular bentonite were used to seal the casing.

Constant head tests were conducted using a Mariotte bottle when possible. However, in several cases, falling head tests were necessary because the flow rates were too high

for a Mariotte bottle. Hydraulic conductivities for all constant head tests were calculated using the solution presented in Hvorslev (1949):

$$K_{BH} = \frac{Q}{2.75DH_b} \quad (4.2)$$

where Q is the steady-state volumetric flow rate, D is the casing diameter, and H_b is the height of the bubble tube above the bottom of the borehole. All falling head tests were analyzed using the method presented by Chaisson (2005). Data from the BH tests are presented in Appendix C.

4.3 Hydraulic Conductivity from Peak Lysimeter Flow Rates

Hydraulic conductivity at the lysimeter scale was estimated using the peak daily flow rate recorded by the lysimeter for test sections that transmitted at least 10 mm of percolation in a single year. Less than 10 mm of percolation was considered too small to make a reliable estimate of hydraulic conductivity. The computations were made using two approaches. A unit downward gradient and steady-state flow conditions were assumed in both approaches. Relatively uniform water contents and matric potentials were present on the days these computations were made. Thus, assuming a unit gradient and steady flow was reasonable.

In the first approach, the saturated hydraulic conductivity was assumed to equal the peak daily percolation rate (i.e., unit gradient saturated flow). However, because the peak daily flow generally occurred when the cover profile was unsaturated, a second computation was made to adjust for unsaturated conditions. In this case, the saturated hydraulic conductivity was estimated using the van Genuchten-Mualem equation (van Genuchten 1980):

$$K_{sat} = \frac{K(\theta)}{\Theta^{1/2} \left[1 - (1 - \Theta^{1/m})^m \right]^2} \quad (4.3)$$

where K(θ) is the unsaturated hydraulic conductivity (set equal to the peak daily flow), m = 1-1/n where n is the van Genuchten fitting parameter from the SWCC, and Θ is the effective saturation:

$$\Theta = \frac{\theta - \theta_r}{\theta_s - \theta_r} \quad (4.4)$$

In Eq. 4.4, θ is the average volumetric water content in the storage or barrier layer at the time of the peak daily flow (measured with water content reflectometers, Albright et al. 2004), θ_s is the saturated water content, and θ_r is the residual water content (see Sec. 6 for n, θ_s, and θ_r for each test section).

Because the soils were unsaturated, the largest pores probably were not conducting flow. Consequently, the field hydraulic conductivities computed using the peak lysimeter flows probably are lower than the saturated hydraulic conductivity. However, these field hydraulic conductivities should represent the highest hydraulic conductivities operative at the field sites that were evaluated.

5. LABORATORY TEST METHODS

5.1. Hydraulic Properties of Earthen Materials

Prior to hydraulic conductivity testing, the block samples were trimmed to a diameter of 305 mm and height of 150 mm. Trimmed specimens were then tested in flexible-wall permeameters using the procedure in ASTM D 5084 (Method C). Testing conditions for each test are summarized in Appendix D. The hydraulic gradients ranged from 4 to 11 depending on the hydraulic conductivity of the specimen. All specimens were tested at an effective stress of 10 kPa using a backpressure of 275 kPa.

Following permeation, a fraction of the 305-mm specimens were trimmed to a diameter of 152 mm and height of 75 mm and re-tested following the same procedure. These specimens were subsequently trimmed again to a diameter of 75 mm and height of 38 mm and re-tested. Tests were conducted on specimens of different size to evaluate whether the hydraulic conductivity varied with scale. Data from the saturated hydraulic conductivity tests conducted in the laboratory are presented in Appendix D.

After the hydraulic conductivity tests were performed, the SWCCs were measured in accordance with ASTM D 6836. The pressure plate extractor method (Method B) was used to determine the wet end of the SWCC (suctions < 1 MPa) and a chilled mirror hygrometer (CMH) (Method D) was used to determine the dry end of the SWCC (suctions > 1 MPa). The SWCC data are presented in Appendix E. Test specimens used in the 75-mm-diameter hydraulic conductivity tests were trimmed to 73 mm diameter and 25 mm height for pressure plate testing. In several cases, the 305-mm-diameter hydraulic conductivity specimens were trimmed to 250 mm diameter, and the 150-mm-diameter specimens were trimmed to 50 mm height for large-scale pressure plate testing. These large-scale SWCC tests allowed for the inclusion of more pedogenic features and are assumed to be more representative of the field SWCCs.

Samples for CMH testing were prepared using the method presented by Gee et al. (1992). Intact samples were trimmed from pressure plate samples prior to testing, placed in polyethylene cups with a 38 mm diameter and height of 5 mm, and tested using a Decagon WP4 Dewpoint Potentia-Meter. After each test the sample was air dried for approximately 30 min, re-sealed, allowed to equilibrate for 24 h, and then tested again.

5.2 Properties of Geosynthetic Clay Liners

5.2.1 Saturated Hydraulic Conductivity

Hydraulic conductivity tests were conducted on GCL specimens in flexible-wall permeameters following the procedures in ASTM D 5084-03 and ASTM D 6766-06. The falling head method was employed. Backpressure was not applied to approximate the field condition. The average effective stress was selected to represent the in situ condition, and ranged between 15 kPa and 24 kPa depending on the cover thickness. An average hydraulic gradient of 125 was applied to all specimens. This hydraulic gradient is higher than in the field, but is typical for GCL testing. In addition, Shackelford et al. (2000) show that hydraulic gradient has negligible impact on the hydraulic conductivity of GCLs when the hydraulic gradient is less than 500.

Specimens having a diameter of 152 mm were cut from the GCL field samples using a sharp razor knife. The GCL sample was retained on the rigid plastic sampling plate during cutting to avoid disturbing any structure within the bentonite. After cutting, geotextile fibers around the perimeter were trimmed back with scissors. Thickness of the GCL specimen was then measured with calipers at six equidistant points around the GCL perimeter and the mass of the specimen was recorded. A thin frosting of bentonite paste, composed of new Na bentonite hydrated in the permeant water, was applied to the perimeter of the specimen to prevent sidewall leakage.

Two permeant waters were employed: 0.01 M CaCl₂ solution, which is commonly referred to as “standard water” (SW), and Type II deionized water (DW). All GCLs were permeated with SW. A portion of the GCLs were tested with DW, particularly those GCLs with high hydraulic conductivity to SW. Solutions similar to SW have been used extensively for permeating GCLs exhumed from final covers (Egloffstein 2001, 2002; Lin and Benson 2000; Benson et al. 2007), but SW has been used only once for GCLs removed from composite barriers (Meer and Benson 2007). DW was selected as a permeant water that would not introduce cation exchange reactions.

Hydraulic conductivity tests were conducted until the termination criteria stipulated in ASTM D 5084-03 were met. For specimens that exhibited high hydraulic conductivity ($> 10^{-9}$ m/s), rhodamine WT dye (5 mg/L) was added to the influent liquid at the conclusion of testing to determine if sidewall leakage was occurring. No indication of sidewall leakage was found in any test. The effluent lines and effluent were also monitored throughout testing for bentonite particle migration. No particles were observed visually in the effluent lines and effluent.

5.2.2 Swell Index

Swell index (SI) of bentonite from the GCLs was measured using 2 g of oven dry bentonite removed from each GCL sample. Methods described in ASTM D 5890-04 were followed. All tests were conducted with deionized water (DW) as the hydrating solution. Duplicate tests were run for each sample, but the SI were identical.

5.2.3 Soluble Cations, Bound Cations, and Cation Exchange Capacity

Soluble cations (SC), bound cations (BC), and cation exchange capacity (CEC) were determined following the procedures in the draft ASTM standard “Standard Test Method for Measuring Exchangeable Cations and Cation Exchange Capacity of Inorganic Fine Grained Soils,” which is being balloted by ASTM Subcommittee D18.04. Chemical analysis of extracts from the SC and BC tests was conducted using inductively coupled plasma optical emission spectroscopy (ICP-OES) following USEPA Method 6010 B. BC mole fractions were calculated as the ratio of total charge per unit mass of bentonite associated with a particular cation to the CEC.

Strength and relative abundance of SC (cations that can be released by rinsing with water) were quantified by the total soluble cations charge per mass (TCM) and the monovalent-to-divalent ratio (MDR). TCM is defined as the total charge of monovalent and divalent SC per mass of soil solid. MDR is defined as the ratio of the total charge of monovalent cations relative to the total charge of divalent cations. These mass and charge-based metrics are used in lieu of the more conventional ionic strength (I) and

ratio of monovalent to divalent cations (RMD), which are based on solution concentrations (Kolstad et al. 2004) and are generally employed to describe permeant liquids. Using mass-based metrics for soluble cations precludes the need for dilution corrections that account for differences in liquid-to-solid ratio in the field and the laboratory extracts.

5.2.4 Subgrade Soils

Pore water in the subgrade was characterized using a batch test method similar to the procedure described in ASTM D 6141-04. Meer and Benson (2007) indicate that this method “provides a relatively simple and expedient method to generate a test liquid representative of flow-through conditions.” DW was used as the eluent with a liquid-to-solid ratio of 1.3. The soil-water mixture was placed in a sealed 250-mL bottle and rotated for 24 h. The solution was then separated by centrifugation and vacuum filtered through 0.45 μm filter paper. Concentrations of the major cations (Ca, Mg, Na, and K) in the eluent were then measured using ICP-OES following USEPA Method 6010 B.

5.3 Properties of Geomembranes and Geosynthetic Drainage Layers

5.3.1 Tensile Strength of Geomembranes

Tensile strength of the GM samples was measured using the wide-strip method (ASTM D 4885) and the narrow-strip dumbbell method (ASTM D 638). The sample size of the wide-strip method was 232 mm by 232 mm. All samples were tested in the machine direction using a cross-head speed of 10 mm/min (D 4885) or 51 mm/min (D 638). The grip separation was 102 mm for specimens tested using D 4885 and 65 mm for specimens tested using D 638. All test specimens were cut from samples using a hydraulic press and were conditioned at 21 °C and 50 to 70% relative humidity prior to testing. Loading was conducted with a screw-driven MTS Sintech 10/GL load frame equipped with Curtis Geo-Grips (load capacity = 44.5 kN). Three specimens were tested from each GM sample using both test methods.

5.3.2 Ply Adhesion of Geosynthetic Drainage Layers

Ply adhesion of the GDL samples was measured following the procedure in ASTM D 7005. Five test specimens with dimensions of 100 mm x 200 mm were punched by the hydraulic press from each sample. All tests were conducted using the MTS Sintech 10/GL load frame equipped with Curtis Geo-Grips using a cross-head speed of 300 mm/min. The specimens were tested in the machine direction at 21°C and 50±5% relative humidity. Both sides of the specimens were tested.

5.3.3 Interface Shear Strength

Interface shear strength between the GMs and GDLs was measured following the method in ASTM D 5321 using a displacement rate of 1 mm/min. Stark et al. (1996) show that displacement rate has no effect on the interface shear strength between geosynthetics provided the displacement rate is between 0.029 and 36.7 mm/min. All tests were terminated at 60 mm of displacement. Normal stresses between 12 and 60 kPa were applied to bracket conditions existing in the field. All test specimens (300 mm x

400 mm) were cut from the exhumed samples using a razor knife. A minimum of three specimens was tested from each test pit.

5.3.4 Hydraulic Properties

Transmissivity of the GDL was measured in the machine direction using a hydraulic gradient of 1.0 following the procedure in ASTM D 4716. Test specimens (305 mm x 356 mm) were cut from the GDL samples using a hydraulic press. Tests were conducted using normal stresses of 24, 48, and 480 kPa. The lower confining stresses (24 and 48 kPa) were used to simulate field conditions for covers with a surface layer 900 to 2200 mm thick (Fig. 2.2). The higher confining stress (480 kPa) was used to obtain data for comparison with the manufacturers' minimum average role value (MARV)¹. Transmissivity of the GDL was computed as the quotient of the flow rate per unit area and the unit hydraulic gradient. Because turbulent flow may have occurred in the GDLs during testing, the transmissivities in this report should not be extrapolated to higher hydraulic gradients.

Permittivity of the GDL was measured following the constant head procedure in ASTM D 4491. Tests were conducted with a head of 50 mm to provide a direct comparison with measurements conducted during construction or MARV permittivities, and with a 10-mm head to represent a more realistic in-service condition. Circular specimens (50-mm diameter) were punched from the bulk field samples using a hydraulic press. Fresh de-aired DW was used as the permeant liquid.

5.3.5 Melt Flow Index and Oxidation Induction Time

Melt flow index (MFI) and oxidation induction time (OIT) were measured on one sample of GM from each site. The MFI is an index of the condition of the GM and increases as the GM polymer is degraded by chain scission. OIT is a measure of the amount of antioxidant within the GM. Antioxidants are added to the GM polymer to inhibit oxidative degradation of the polymer. MFI was determined following ASTM D 1238 Method A 190/2.16. OIT was determined using ASTM D 3895. All MFI and OIT tests were conducted by TRI Environmental Inc. of Austin, Texas.

¹The MARV represents a lower bound material property for a geosynthetic material. The engineering property of interest is measured on a collection of samples collected from a geosynthetic roll. The MARV is the mean of these measurements less two standard deviations.

6. EARTHEN BARRIER AND STORAGE LAYERS

Over the service life of a final cover, the hydraulic properties of earthen layers evolve due to the formation of soil structure in response to natural processes such as insect and animal burrowing, plant root growth, freeze-thaw cycling, wet-dry cycling, and distortion (Chamberlain and Gow 1979, Beven and Germann 1982, Benson and Othman 1993, Benson et al. 1995, Albrecht and Benson 2001). These processes create cracks, fractures, and other larger-scale features that are generally referred to as macropores. Formation of macropores alters the network of pores controlling retention and movement of water in the field, which is reflected in changes in the hydraulic properties (e.g., K_s and SWCC).

Although formation of soil structure in natural and engineered systems is well documented, data quantifying changes in the hydraulic properties of cover soils in response to changes in structure are scant (Suter et al. 1993, Khire et al. 2000, Albright et al. 2006, Benson et al. 2007, Kelln et al. 2009). The objective of this portion of the study was to determine the in-service hydraulic properties of cover soils used in the ACAP test sections, to quantify how the hydraulic properties changed over the service life of the test section, to identify factors that may be responsible for these changes, and to determine soil properties and site conditions that result in less propensity for change in soil properties. The focus was on the soil layer intended to control percolation: the barrier layer in a conventional cover or the storage layer in a store-and-release cover.

6.1. Soil Characteristics

Particle size characteristics of soils from the ACAP sections are described in Table 6.1. Most of the soils were fine grained (i.e., $\geq 50\%$ of the material was finer than $75 \mu\text{m}$). The exceptions are the storage layer in covers at Apple Valley, CA; Helena, MT; and Sacramento, CA; and the clayey soil barrier in the conventional cover at Albany, GA. The soils classify as GC, SM, SC, SC-CL, CL, CL-ML or CL-CH in the Unified Soil Classification System (USCS), as described in ASTM D 2487. Atterberg limits for most of the soils fall between the U-line and A-line on the plasticity chart (Fig. 6.1) and in the region designated as CL, with the soils from Boardman (CL-ML), Polson (CL-ML), and Helena (CH) being exceptions. The storage layer in the store-and-release cover at Apple Valley, CA was designated as non plastic (NP) and therefore is not shown in Fig. 6.1.

As-compacted dry unit weight and gravimetric water content of each storage and barrier layer are presented in Table 6.2 along with the compaction characteristics of the cover soils. Relative compaction of the storage and barrier layers ranged from 83% to 102% of the maximum dry unit weight (γ_{dmax}) for standard Proctor effort, with an average of 92%. The as-compacted water content ranged from 3% dry of optimum to 5% wet of optimum, with an average of 0.6% wet of optimum water content.

Hydraulic properties of the as-built storage and barrier layers are summarized in Table 6.3. These properties were measured on specimens trimmed from large-scale intact block samples collected during construction. As-built saturated hydraulic conductivities (K_{sa}) were determined in flexible wall permeameters using the falling headwater–rising tailwater method described in ASTM D 5084 (Method C). SWCCs were determined using the pressure plate extractor method and the chilled mirror hygrometer method in ASTM D 6836 (Methods B and D). Geometric means of K_{sa} and the van Genuchten α parameter are

Table 6.1. Site characteristics and soil index properties for storage and barrier layers evaluated in this study.

Site Location	Climate	Service Life (yr)	Unified Soil Classification	Particle Size Distribution				Atterberg Limits	
				Gravel (%)	Sand (%)	Fines (%)	Clay < 2 μm (%)	Plasticity Index	Liquid Limit
Store-and-Release Covers									
Altamont, CA	Semi-Arid	6.6	CL-CH	1.4	10.5	88.1	34.11	19	45
Apple Valley, CA	Arid	4.9	SM	35.0	52.0	13.0	8.0	NP	NP
Boardman, OR	Semi-Arid	6.8	CL-ML	0.2	15.9	83.9	12.4	4	24
Cedar Rapids, IA	Humid	5.7	SC-CL	2.2	45.9	51.8	25.5	16	35
Helena, MT	Semi-Arid	8.9	SC	1.9	53.6	44.5	29.8	47	67
Monticello, UT	Semi-Arid	7.1	CL	2.9	22.3	74.8	21.4	17	32
Omaha, NE	Humid	7.8	CL	0.0	0.6	99.4	27.8	26	44
Underwood, ND	Semi-Arid	4.1	CL	5.5	27.9	66.6	25.2	23	39
Polson, MT	Sub-Humid	8.8	CL-ML	0.8	6.1	93.2	17.9	7	28
Sacramento, CA Thin	Semi-Arid	6.0	GC	31.1	27.9	41.0	14.7	18	32
Sacramento, CA Thick	Semi-Arid	6.0	CL	6.4	21.8	71.8	17.9	22	39
Conventional Covers with Clay Barriers									
Albany, GA	Humid	4.0	SC	6.0	63.1	30.8	23.0	13	28
Apple Valley, CA	Arid	4.9	CL	0.0	19.0	81.0	26.3	10	29
Cedar Rapids, IA	Humid	5.7	SC-CL	1.5	46.3	52.2	22.3	19	33
Underwood, ND	Semi-Arid	4.1	CL	3.5	35.8	60.8	25.2	21	38
Conventional Covers with Composite Barriers									
Altamont, CA	Semi-Arid	6.6	CL-CH	1.4	8.0	90.6	36.9	20	45
Cedar Rapids, IA	Humid	5.7	SC-CL	1.4	45.9	52.8	25.0	17	32
Omaha, NE	Humid	7.8	CL	0.0	1.0	99.0	27.8	17	32
Polson, MT	Sub-Humid	8.8	CL-ML	0.9	7.5	91.7	17.3	7	28

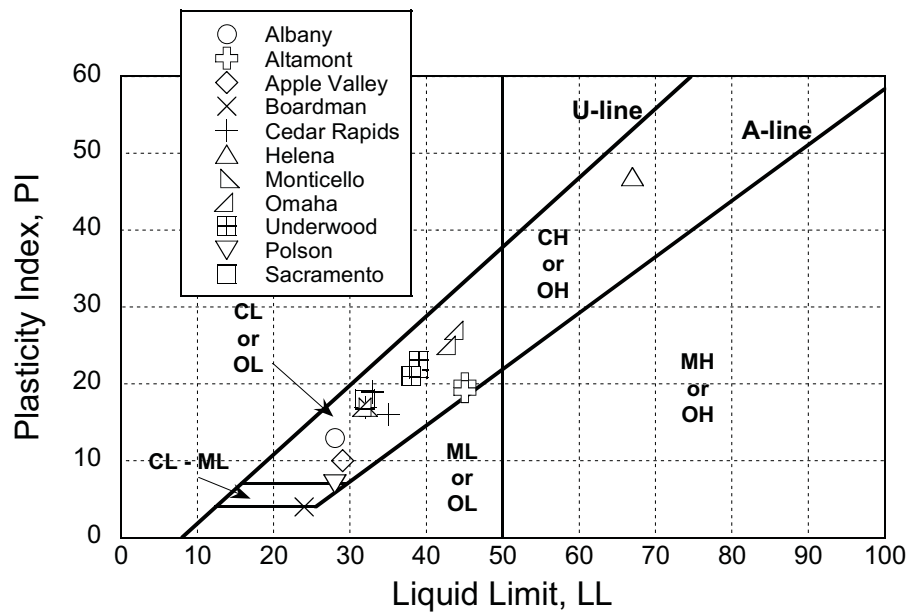


Fig. 6.1. Plasticity chart showing Atterberg limits of storage and barrier layers evaluated in this study.

Table 6.2. Average as-built compaction and water content for storage and barrier layers evaluated in this study.

Site Location	Std. Proctor Max. Dry Unit Wt., γ_{dmax} (kN/m ³)	Std. Proctor Optimum Water Content, w_{opt} (%)	As-Built Dry Unit Wt., γ_{dc} (kN/m ³)	As-Built Water Content, w_c (%)	As-Built Relative Compaction (%)	As-Built $w_c - w_{opt}$ (%)
Store-and-Release Covers						
Altamont, CA	18.1	15.9	16.2	18.1	89.6	2.2
Apple Valley, CA	NA	NA	NA	NA	NA	NA
Boardman, OR	17.1	17.1	14.2	20.5	83.2	4.2
Cedar Rapids, IA	17.7	15.2	15.6	20.1	87.9	5.0
Helena, MT	15.4	22.4	14.0	26.6	91.1	4.2
Monticello, UT	17.7	15.2	15.1	12.3	85.6	-2.9
Omaha, NE	16.5	19.3	14.6	18.2	88.8	-1.5
Underwood, ND	16.6	19.4	16.1	18.3	97.2	-1.1
Polson, MT	16.4	18.9	15.1	16.9	92.1	-2.0
Sacramento, CA Thin	17.6	16.5	16.5	16.1	93.6	-0.4
Sacramento, CA Thick	16.0	21.7	15.3	21.3	95.2	-0.5
Conventional Covers with Clay Barriers						
Albany, GA	18.1	15.7	16.8	15.8	93.0	0.1
Apple Valley, CA	19.3	12.5	17.6	15.2	91.0	2.7
Cedar Rapids, IA	19.2	12.2	17.8	15.0	92.8	2.8
Underwood, ND	17.4	16.8	17.6	15.1	101.5	-1.7
Conventional Covers with Composite Barriers						
Altamont, CA	18.2	15.2	17.0	12.8	93.4	-2.4
Cedar Rapids, IA	19.3	12.1	17.7	15.3	91.6	3.2
Omaha, NE	16.6	18.8	15.1	20.0	90.6	1.2
Polson, MT	16.9	18.6	16.1	16.5	95.6	-2.1

Table 6.3. As-built hydraulic properties for storage and barrier layers evaluated in this study.

Site Location	Saturated Hydraulic Conductivity			SWCC Parameters							
	K_{sa} (m/s)		No. Tests	α_a (kPa ⁻¹)	n_a		θ_{sa}		θ_{ra}	No. SWCC Tests	
	Geometric Mean	σ_{lnKsa}			Geometric Mean	$\sigma_{ln\alpha}$	Mean	σ			Mean
Store-and-Release Covers											
Altamont, CA	6.6×10^{-9}	1.90	4	0.0030	0.56	1.42	0.05	0.34	0.02	0.00	7
Apple Valley, CA	6.4×10^{-7}	0.36	2	NA	NA	NA	NA	NA	NA	NA	NA
Boardman, OR	1.3×10^{-7}	1.05	36	0.0138	0.65	1.50	0.09	0.39	0.02	0.00	29
Cedar Rapids, IA	9.7×10^{-9}	2.63	8	0.0016	0.55	1.63	0.26	0.33	0.02	0.00	8
Helena, MT	1.5×10^{-9}	0.80	16	0.0018	0.28	1.19	0.02	0.34	0.03	0.00	13
Monticello, UT	1.4×10^{-7}	1.97	8	0.0028	0.91	1.38	0.11	0.30	0.02	0.00	8
Omaha, NE - Thin	4.8×10^{-8}	2.35	8	0.0050	0.16	1.35	0.13	0.38	0.05	0.00	3
Omaha, NE - Thick	5.6×10^{-8}	0.71	4	0.0024	0.84	1.56	0.28	0.37	0.03	0.00	7
Underwood, ND	1.8×10^{-9}	0.46	2	0.0170	NA	1.22	NA	0.42	NA	0.00	1
Polson, MT	4.0×10^{-9}	0.84	8	0.0027	0.32	1.27	0.03	0.30	0.04	0.00	7
Sacramento, CA - Thin	1.9×10^{-8}	4.46	6	0.0064	0.12	1.20	0.05	0.32	0.01	0.00	2
Sacramento, CA - Thick	3.2×10^{-9}	2.07	18	0.0035	1.15	1.32	0.10	0.29	0.01	0.00	12
Conventional Covers with Clay Barriers											
Albany, GA	4.0×10^{-10}	0.81	5	0.0024	1.23	1.58	0.42	0.31	0.01	0.00	5
Apple Valley, CA	1.7×10^{-10}	0.84	8	0.0045	1.13	1.27	0.05	0.35	0.07	0.00	8
Cedar Rapids, IA	1.7×10^{-10}	0.55	8	0.0022	0.48	1.49	0.12	0.30	0.01	0.00	3
Underwood, ND - Thick	1.2×10^{-9}	0.53	4	0.0021	NA	1.37	NA	0.35	NA	0.00	1
Underwood, ND - Thin	4.6×10^{-10}	1.77	4	0.0028	NA	1.32	NA	0.36	NA	0.00	1
Conventional Covers with Composite Barriers											
Altamont, CA	1.6×10^{-9}	0.31	4	0.0018	0.29	1.54	0.03	0.39	0.01	0.00	2
Cedar Rapids, IA	1.5×10^{-10}	0.73	8	0.0011	0.20	1.66	0.11	0.35	0.03	0.00	3
Omaha, NE	1.5×10^{-8}	1.35	6	0.0021	0.53	1.52	0.16	0.37	0.01	0.00	4
Polson, MT	4.2×10^{-9}	0.69	8	0.0027	0.29	1.25	0.05	0.31	0.02	0.00	8

Note: σ = standard deviation, α and n = van Genuchten parameters, θ_s = saturated volumetric water content, θ_r = residual volumetric water content.

presented because these properties are log-normally distributed. Arithmetic means are presented for n , θ_s , and θ_r because these properties are normally distributed (Gurdal et al. 2003). The standard deviation (σ) of each property is also presented in Table 6.3. Standard deviations of $\ln K_{sa}$ and $\ln \alpha$ are reported to correspond with the geometric means of these properties.

6.2 Field Hydraulic Conductivity

Field hydraulic conductivities obtained from the SDRI and BH tests and peak flows in the lysimeters are summarized in Table 6.4. The BH hydraulic conductivities (K_{BH}) reported in Table 6.4 correspond to the geometric mean of all BH data for a test section. The standard deviation was determined for $\ln K_{BH}$ due to the log-normal distribution of hydraulic conductivity data (Russo and Bouton 1992, Benson 1993, Gurdal et al. 2003). Hydraulic conductivities from the SDRIs and BHs for conventional and store-and-release covers are shown in Fig. 6.2a. The hydraulic conductivities from field testing were typically between 1×10^{-8} and 1×10^{-5} m/s, but were as high as 1.1×10^{-1} m/s and as low as 3.0×10^{-9} m/s. Hydraulic conductivities computed from the peak flows from the lysimeter using both methods (see Sec. 4.3) typically bracket the field hydraulic conductivities obtained with the BHs and SDRIs (Table 6.4).

Hydraulic conductivities from the SDRIs and BHs are compared in Fig. 6.2. Similar hydraulic conductivities (within an order of magnitude) were obtained with the SDRIs and BHs, although lower hydraulic conductivities typically were obtained from the SDRI tests on the clay barriers in conventional covers with composite barriers. The most significant difference between hydraulic conductivities obtained with the SDRI and BHs was at Apple Valley. The BHs yielded much higher hydraulic conductivities due to cracks within the testing area. These cracks expanded due to erosion during testing, and functioned as preferential flow paths. Similar features were not observed in the cross-section of the inner ring of the SDRI when it was dismantled.

A t-test was conducted at a significance level of 0.05 to compare the hydraulic conductivities from the SDRIs and BHs for each cover type (Appendix F). The t-tests indicated that hydraulic conductivities from both field methods are statistically similar for store-and-release covers and conventional covers with clay barriers (store-and-release: $t = -1.098$ and $p = 0.139$; clay barrier: $t = -0.690$, $p = 0.270$). A statistically significant difference was observed for the conventional covers with composite barriers ($t = -6.114$, $p = 1.84 \times 10^{-5}$), but this data set consisted of only three points. When the entire data set is considered (i.e., all cover types in a pool), hydraulic conductivities for the BHs and SDRIs were found to be statistically similar ($t = 1.551$, $p = 0.149$).

The overall field hydraulic conductivity (K_F) for each test section was calculated as the geometric mean of all field tests for a test section (SDRI and BHs). Although hydraulic conductivities calculated from peak lysimeter flows provide an estimate of the field hydraulic conductivity at lysimeter scale, they were not included in the overall field hydraulic conductivity due to the imprecision in the hydraulic conductivity computed using this method. Box plots for K_F are shown in Fig. 6.3a. Storage layers from store-and-release covers have the highest K_F (geometric mean = 1.7×10^{-6} m/s), clay barriers from conventional covers have slightly lower K_F (geometric mean = 6.5×10^{-7} m/s), and clay barriers from conventional covers with composite barriers have the lowest K_F (geometric mean = 2.0×10^{-7} m/s).

Table 6.4. Field hydraulic conductivity for storage and barrier layers.

Site	Lysimeter Peak Flow		Sealed Double-Ring Infiltrometer K _{SDRI} (m/s)	Two-Stage Borehole		Field Hydraulic Conductivity K _F (m/s)	
	Unit Gradient Calc. (m/s)	van Genuchten-Mualem Calc. (m/s)		K _{BH} (m/s)	σ lnK _{BH}		K _{BH} /K _{SDRI}
Store-and-Release Covers							
Altamont	7.5x10-8	1.1x10-6	7.0x10-7	6.8x10-7	0.79	1	6.8x10-7
Apple Valley	3.2x10-8	-	-	7.1x10-6	0.18	-	7.1x10-6
Boardman	-	-	-	1.3x10-5	2.44	-	2.0x10-6
Helena	-	-	1.4x10-7	2.6x10-8	1.23	0.2	1.8x10-8
Monticello	-	-	8.5x10-7	4.4x10-5	5.58	51	1.1x10-6
Omaha 1	9.8x10-8	1.8x10-4	-	1.7x10-6	0.59	-	7.5x10-6
Omaha 2	8.1x10-8	8.1x10-4	-	7.5x10-6	0.64	-	8.5x10-6
Polson	-	-	8.9x10-8	1.8x10-7	0.23	2	7.7x10-8
Underwood	-	-	-	1.2x10-6	0.58	-	1.2x10-6
Sacramento Thin	1.4x10-7	1.3x10-4	2.1x10-6	5.8x10-7	0.71	0.3	7.5x10-7
Sacramento Thick	-	-	7.8x10-7	1.4x10-6	0.58	2	1.3x10-6
Conventional Covers with Clay Barriers							
Albany	3.6x10-7	-	2.0x10-6	1.7x10-6		1	1.8x10-6
Apple Valley	2.6x10-8	1.8x10-6	5.6x10-7	2.1x10-5	3.05	38	1.2x10-5
Cedar Rapids	1.2x10-7	2.4x10-7	1.3x10-8	3.5x10-8	1.66	3	2.8x10-8
Underwood Thick	-	-	-	4.9x10-7	1.54	-	4.9x10-7
Underwood Thin	-	-	-	3.5x10-7	1.13	-	3.5x10-7
Conventional Covers with Composite Barriers							
Altamont	-	-	4.1x10-8	8.0x10-8	0.32	2	7.0x10-8
Cedar Rapids	-	-	2.1x10-8	1.2x10-7	0.56	6	8.4x10-8
Omaha	-	-	-	1.7x10-6	0.59	-	1.7x10-6
Polson	-	-	1.4x10-8	3.5x10-7	0.25	25	1.3x10-7

Notes: - indicates no data available or less than 10 mm/yr percolation, σ = standard deviation.

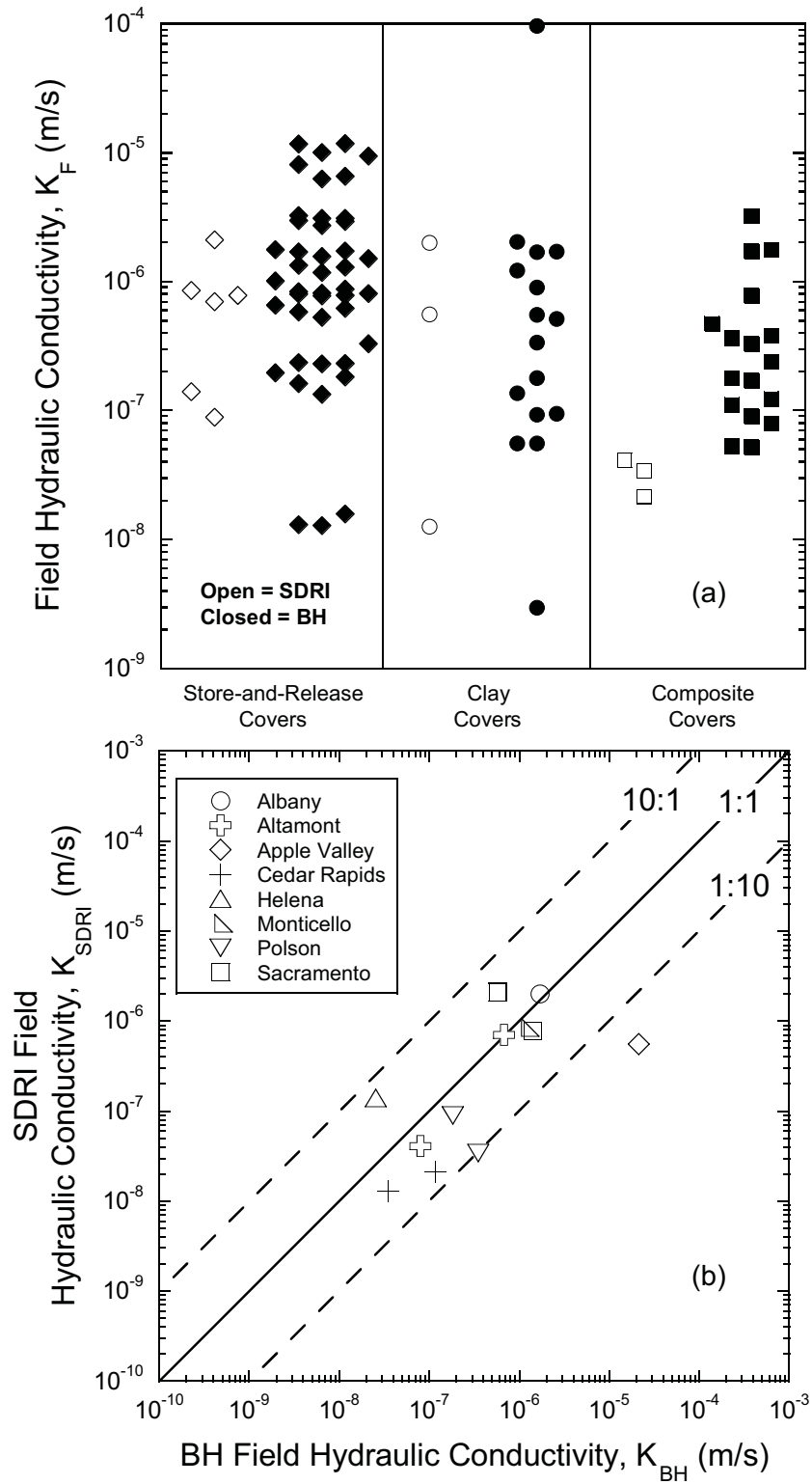


Fig. 6.2. Field hydraulic conductivity determined by SDRIs and BHs from each cover type (a) and hydraulic conductivity from SDRIs versus hydraulic conductivity from BHs for individual test sections (b).

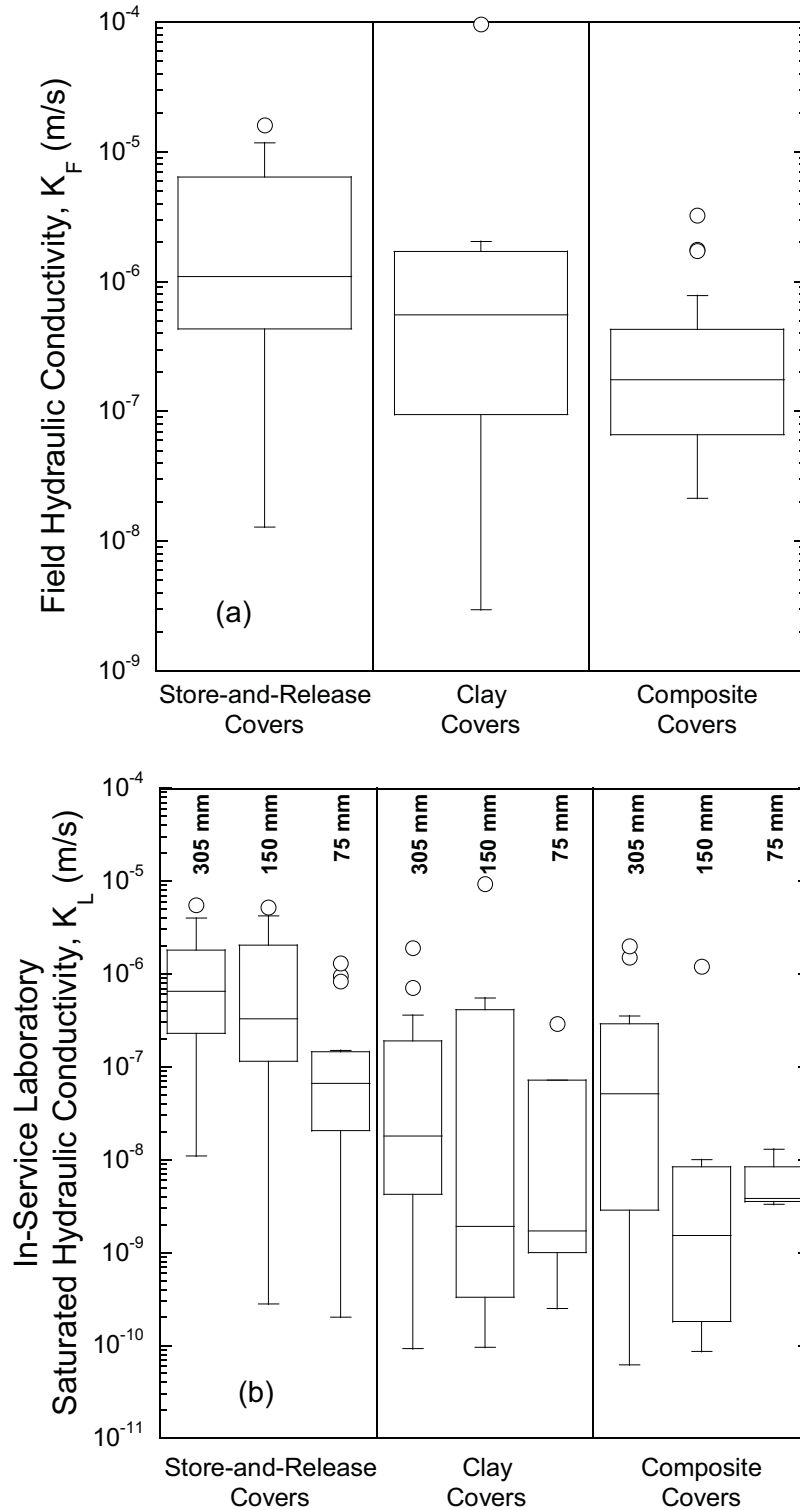


Fig. 6.3. Saturated hydraulic conductivity from SDRI and BH tests (a) and laboratory tests on 305-, 150- and 75-mm-diameter specimens for each cover type (b). The solid line within the box represents the median, the box encloses 50% of the data, and outliers are indicated with a circle.

The sequence of these hydraulic conductivities is consistent with the method in which the soils were placed and exposed while in service. Earthen barrier layers in conventional covers are placed with high effort to achieve low hydraulic conductivity, whereas storage layers are placed with modest effort to promote root development and to provide storage capacity. The lower K_F of the clay in composite barriers indicates that the geomembrane helps maintain lower hydraulic conductivity during the service life of conventional covers. Field tests conducted in Germany by Melchior (1997, 2002) also showed that clay barriers beneath geomembranes were better protected than clay barriers alone in test sections simulating conventional covers. However, the clay barriers beneath geomembranes did have higher hydraulic conductivity than required by regulation. For example, K_F was required to be less than 1×10^{-9} m/s at Cedar Rapids ($K_F = 8.4 \times 10^{-8}$ m/s) and Omaha ($K_F = 1.7 \times 10^{-6}$ m/s) and less than 1×10^{-8} m/s at Altamont ($K_F = 7.0 \times 10^{-8}$). The reason for the increase in hydraulic conductivity of clay barriers beneath geomembranes is not known with certainty. The geomembrane was effective in preventing root intrusion. However, freeze-thaw cycling and thermally-driven wet-dry cycling may have contributed to development of structure, which was evident when the clay was inspected.

6.3 Laboratory Hydraulic Conductivity

Hydraulic conductivities measured in the laboratory on the 305-mm, 150-mm, and 75-mm-diameter specimens are presented in Table 6.5 and shown in Fig. 6.3b. The laboratory hydraulic conductivities (K_L) reported in Table 6.5 are the geometric mean of all K_L for the specified specimen size for a given test section. The standard deviation is reported in terms of $\ln K_L$.

Box plots of the laboratory hydraulic conductivities are shown by cover type in Fig. 6.3b. Storage layers in store-and-release covers have higher K_L on average than clay barriers in conventional covers, whereas clay barriers from conventional covers have similar K_L regardless of whether they are from a cover with a clay barrier only or a composite barrier. The lower hydraulic conductivity for the conventional covers is consistent with the field hydraulic conductivities described in the previous section.

Scaling is evident for all three cover types, with K_L of the 305-mm-diameter specimens consistently greater than K_L from the 150-mm and 75-mm-diameter specimens. On average, K_L from the 305-mm-diameter specimens was 13 times greater than K_L from the 75-mm-diameter specimens for store-and-release covers, 3 times greater for conventional covers with only a clay barrier, and 4 times greater for conventional covers with a composite barrier.

Statistical analysis was conducted using t-tests to evaluate whether the hydraulic conductivities measured at different scales were statistically different. Hydraulic conductivities of the small-scale specimens (150-mm and 75-mm-diameter) were found to be statistically similar for all test sections at a significance level of 0.05 (Appendix F). Hydraulic conductivities of the 305-mm-diameter specimens were found to be statistically different from the hydraulic conductivities of the smaller specimens at several test sections. Therefore, hydraulic conductivities of the 150-mm and 75-mm specimens were combined for analysis (herein referred to as small-scale laboratory hydraulic conductivity, K_{L-SS}) and hydraulic conductivities of the 305-mm-diameter specimens (herein referred to as large

Table 6.5. Saturated hydraulic conductivity measured in laboratory on specimens from in-service storage and barrier layers.

Site	305 mm		150 mm		75 mm				
	K_S (m/s)	$\sigma_{In,Ks}$	No.	K_S (m/s)	$\sigma_{In,Ks}$	No.	K_S (m/s)	$\sigma_{In,Ks}$	No.
Store-and-Release Covers									
Altamont, CA	1.2×10^{-6}	1.38	3	3.5×10^{-9}	-	1	1.1×10^{-9}	-	1
Apple Valley, CA	2.9×10^{-6}	-	1	-	-	0	-	-	0
Boardman, OR	4.8×10^{-7}	0.51	9	1.7×10^{-7}	1.05	4	6.8×10^{-8}	0.78	4
Cedar Rapids, IA	-	-	-	3.3×10^{-6}	0.64	2	-	-	0
Helena, MT	1.9×10^{-7}	1.24	4	2.8×10^{-7}	0.28	2	4.5×10^{-8}	1.02	2
Monticello, UT	1.2×10^{-6}	1.37	9	1.6×10^{-6}	0.58	4	2.5×10^{-7}	1.76	4
Omaha, NE Thin	3.0×10^{-6}	0.30	3	2.7×10^{-6}	-	1	1.5×10^{-7}	-	1
Omaha, NE Thick	2.0×10^{-6}	0.67	4	1.1×10^{-6}	2.01	3	3.2×10^{-7}	2.06	3
Polson, MT	1.3×10^{-7}	0.26	2	3.7×10^{-7}	-	1	1.9×10^{-8}	-	1
Underwood, ND	3.5×10^{-7}	0.80	3	2.8×10^{-7}	-	1	8.8×10^{-8}	-	1
Sacramento, CA Thin	1.3×10^{-7}	1.84	4	3.7×10^{-10}	0.40	2	3.5×10^{-10}	0.78	2
Sacramento, CA Thick	1.6×10^{-7}	1.30	4	8.6×10^{-8}	0.47	2	8.0×10^{-9}	-	1
Conventional Covers with Clay Barriers									
Albany, GA	3.6×10^{-7}	-	2	9.3×10^{-6}	-	2	1.0×10^{-9}	-	2
Apple Valley, CA	5.6×10^{-8}	3.16	3	5.3×10^{-9}	1.46	2	6.5×10^{-10}	1.36	2
Cedar Rapids, IA	8.0×10^{-10}	2.00	5	2.0×10^{-10}	0.73	4	-	-	0
Underwood, ND Thick	1.0×10^{-7}	1.85	3	4.1×10^{-7}	-	1	2.9×10^{-7}	-	1
Underwood, ND Thin	1.9×10^{-7}	-	1	5.5×10^{-7}	-	1	7.2×10^{-8}	-	1
Conventional Covers with Composite Barriers									
Altamont, CA	5.1×10^{-7}	1.59	4	1.1×10^{-7}	3.39	2	7.0×10^{-9}	0.87	2
Cedar Rapids, IA	2.8×10^{-10}	2.08	4	2.8×10^{-10}	1.40	5	-	-	0
Omaha, NE	2.3×10^{-7}	-	1	-	-	0	-	-	0
Polson, MT	4.6×10^{-8}	0.15	2	6.7×10^{-9}	-	1	3.3×10^{-9}	-	1

Note: - indicates no data are available.

scale laboratory hydraulic conductivity, K_{L-LS}) were analyzed independently. A graph of K_{L-LS} versus K_{L-SS} is presented in Fig. 6.4. The K_{L-LS} are within a factor of 10 of K_{L-SS} for most test sections. However, K_{L-LS} is as much as 640 times greater than K_{L-SS} .

A comparison of the field and large-scale laboratory hydraulic conductivities (K_F vs. K_{L-LS}) is in Fig. 6.5a. Much of the data scatter within 1 order of magnitude of the equality line, although more points fall above the equality line than below. The geometric mean K_F is 3.8 times the geometric mean K_{L-LS} , and K_F can be as much as 306 K_{L-LS} . The difference is larger for the small-scale hydraulic conductivities; K_F typically is one or more orders of magnitude higher than the small-scale laboratory hydraulic conductivity (K_{L-SS}), and as much as 6000 times higher. These comparisons illustrate that large-scale laboratory tests yield hydraulic conductivities that are more representative of the field hydraulic conductivity compared to more conventional small-scale laboratory hydraulic conductivity tests (75-150 mm diameter), although even K_{L-LS} may underestimate K_F . Benson et al. (1994) and Trast and Benson (1995) report similar findings; they show that 300-mm-diameter samples adequately represented field conditions, whereas field hydraulic conductivity generally was underestimated when evaluated using smaller specimens.

The hydraulic conductivity varies with scale of the volume of solid tested because the soil structure that is captured varies with the scale of the test. As illustrated in Fig. 6.6, the hydraulic conductivity can vary more than four orders of magnitude between small-scale tests on conventional test specimens (75 mm) and the scale of the entire lysimeter (effective diameter = 16 m). Even the SDRI, which is the largest field test typically conducted in practice, does not necessarily test a large enough volume to capture the hydraulic conductivity at the scale of the entire lysimeter. Bias during sample trimming contributes to the scale effect. The most intact part of a sample is typically retained when trimming samples to a smaller size; otherwise the specimen tends to collapse during trimming. As a result, structure contributing to higher hydraulic conductivity of a larger specimen is removed, and the hydraulic conductivity is reduced.

These findings indicate that tests conducted on small-scale test specimens that are commonly used in practice (i.e., 75-mm diameter) will provide an under estimate of the hydraulic conductivity of storage and barrier layers that have been in service. If laboratory tests are to be conducted to assess the in-service condition of the storage layer or barrier layer in a final cover, the test specimen should be as large as practical. Specimens having a minimum diameter of at least 300 mm are recommended.

6.4 Comparison of In-Service and As-Built Hydraulic Conductivity

An in-service hydraulic conductivity (K_{si}) was computed for each test section as the geometric mean of all SDRI, BH, and K_{L-LS} for the test section. A summary of the K_{si} is in Table 6.6 and a comparison of K_{si} and the as-built hydraulic conductivity (K_{sa} , see Sec. 6.1) is shown in Fig. 6.7. For all but one site, K_{si} falls within the range of 7.5×10^{-8} and 6.0×10^{-6} m/s regardless of cover type (the exceptions are the conventional covers at Cedar Rapids). This range is indicated in Fig. 6.7a as the band labeled "in-service hydraulic conductivity." The geometric mean in-service hydraulic conductivity is 4.4×10^{-7} m/s.

The in-service hydraulic conductivities shown in Fig. 6.7 are essentially independent of the as-built hydraulic conductivities (Fig. 6.7). This indicates that larger changes in hydraulic

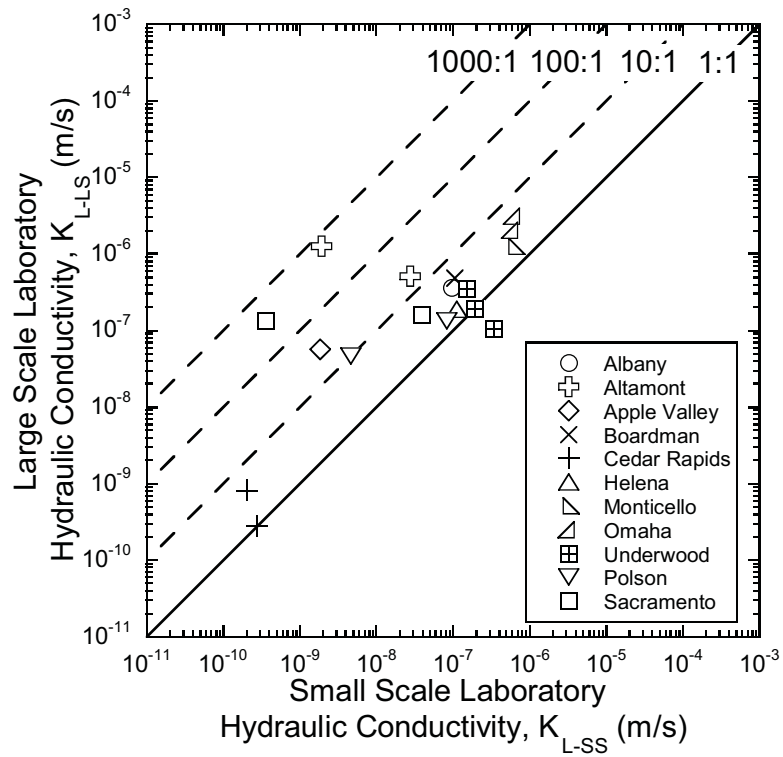


Fig. 6.4. Saturated hydraulic conductivity of large-scale (305 mm) laboratory specimens versus small-scale (150 and 75-mm-diameter) laboratory specimens.

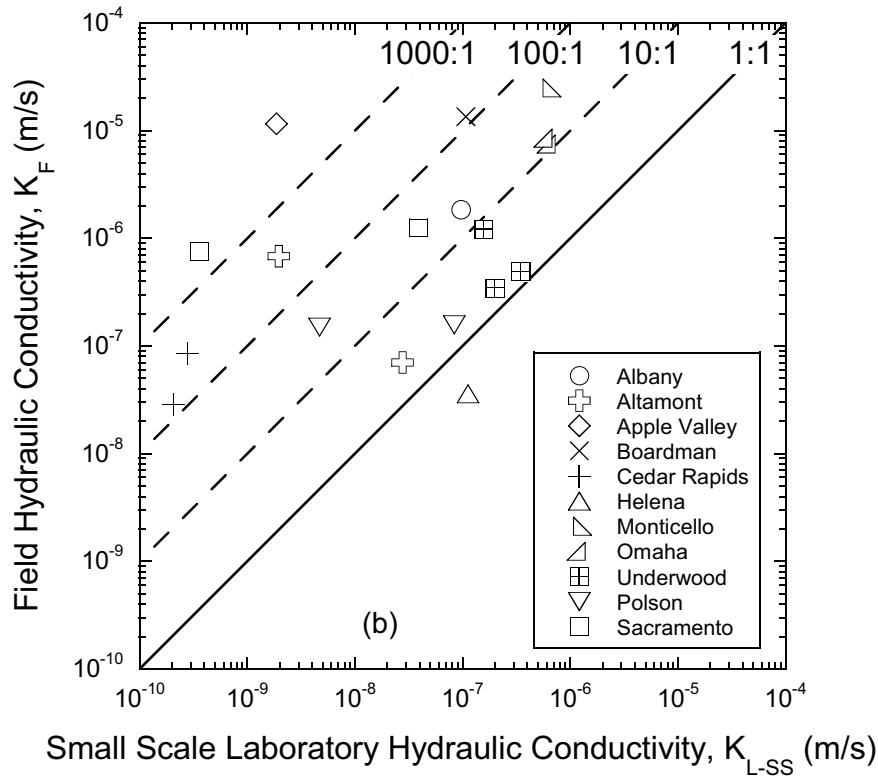
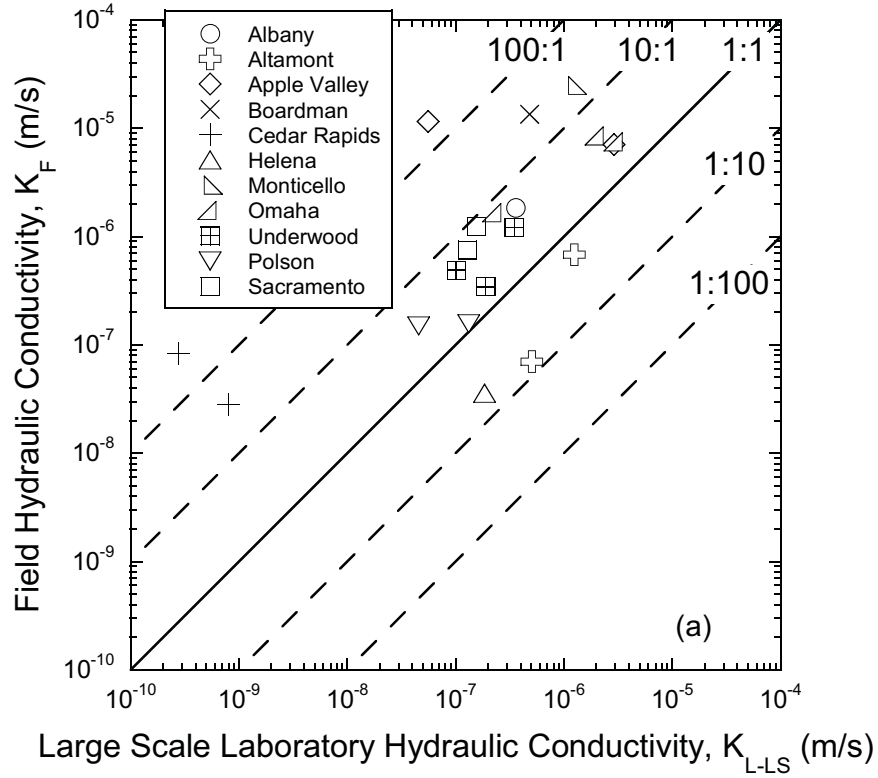


Fig. 6.5. Field hydraulic conductivity from SDRI and BH versus large-scale (305 mm) laboratory saturated hydraulic conductivity (a) and small scale (150 and 75-mm) laboratory saturated hydraulic conductivity (b).

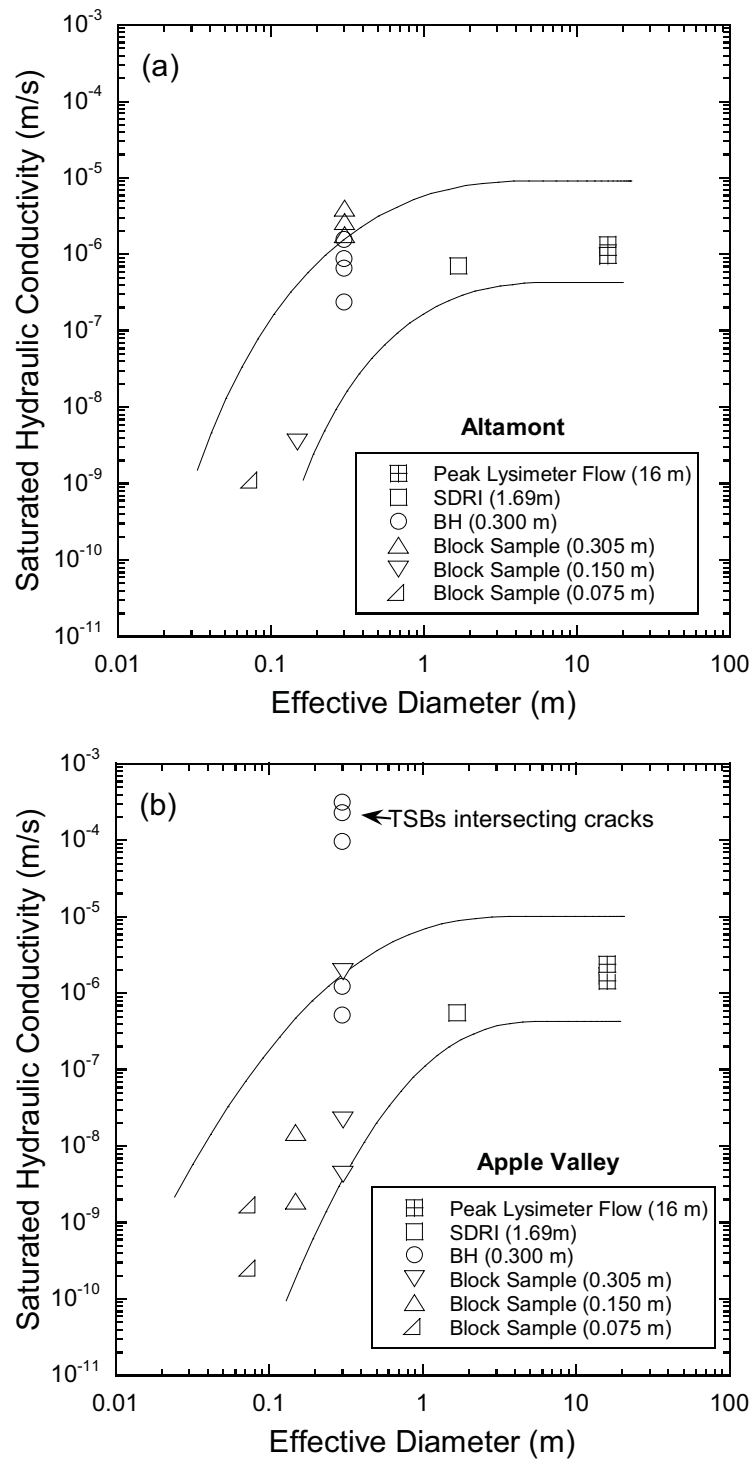


Fig. 6.6. Saturated hydraulic conductivity versus effective diameter for the Altamont store-and-release cover (a) and Apple Valley clay barrier (b). Trend lines drawn by hand.

Table 6.6. In-service saturated hydraulic conductivity for storage and barrier layers.

Site Location	In-Service Saturated Hydraulic Conductivity, K_{si} (m/s)	Saturated Hydraulic Conductivity Ratio, K_{si}/K_{sa}
Store-and-Release Covers		
Altamont, CA	8.6×10^{-7}	129
Apple Valley, CA	5.3×10^{-6}	8
Boardman, OR	8.6×10^{-7}	7
Cedar Rapids, IA	3.3×10^{-6}	342
Helena, MT	7.5×10^{-8}	51
Monticello, UT	1.2×10^{-6}	9
Omaha, NE Thin	2.2×10^{-6}	45
Omaha, NE Thick	3.9×10^{-6}	70
Underwood, ND	7.1×10^{-7}	395
Polson, MT	1.6×10^{-7}	39
Sacramento, CA Thin	3.4×10^{-7}	18
Sacramento, CA Thick	5.0×10^{-7}	156
Conventional Covers with Clay Barriers		
Albany, GA	1.1×10^{-6}	2650
Apple Valley, CA	2.0×10^{-6}	11522
Cedar Rapids, IA	4.8×10^{-9}	28
Underwood, ND Thick	2.5×10^{-7}	214
Underwood, ND Thin	3.1×10^{-7}	668
Conventional Covers with Composite Barriers		
Altamont, CA	1.7×10^{-7}	104
Cedar Rapids, IA	6.6×10^{-9}	43
Omaha, NE	1.1×10^{-6}	75
Polson, MT	1.5×10^{-7}	36

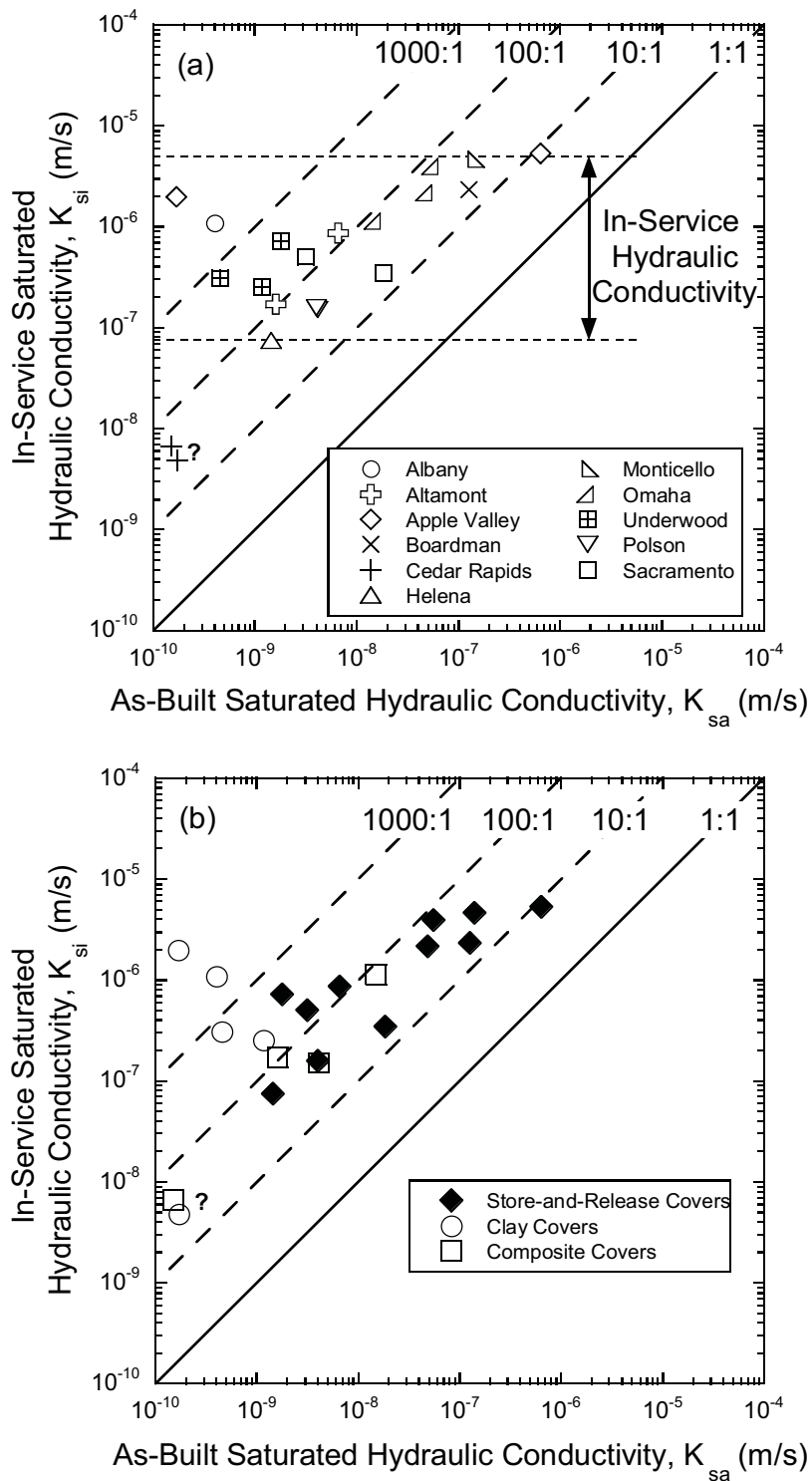


Fig. 6.7. In-service saturated hydraulic conductivity (K_{si}) versus as-built hydraulic conductivity (K_{sa}) by site (a) and cover type (b). “?” signifies apparent outliers.

conductivity occurred for sites that had lower K_{sa} , as illustrated in Fig. 6.8. Regardless of the initial condition, the in-service hydraulic conductivity is at least 10 times higher than the as-built hydraulic conductivity. For sites with lower K_{sa} , the in-service hydraulic conductivity can be more than 10,000 times higher than K_{sa} .

The largest increases in hydraulic conductivity occurred in the clay barriers in conventional covers that were not covered by a geomembrane. These barrier layers were intentionally compacted into a dense monolithic condition so that they would have low hydraulic conductivity, but also were exposed to processes such as wet-dry and freeze-thaw cycling that introduce structure into the soil. These structural features act as preferential flow paths that control hydraulic conductivity (Kleppe and Olson 1985, Albrecht and Benson 2001), transforming a monolithic barrier layer with very low hydraulic conductivity into a structured and permeable soil layer. Because the initial hydraulic conductivity is low, the change in hydraulic conductivity due to the introduction of structure is larger.

6.5 Factors Affecting Changes in Hydraulic Conductivity

6.5.1 Service Life

The relationship between K_{si}/K_{sa} (i.e., the increase in hydraulic conductivity while in service) and service life is shown in Fig. 6.9. The trend implies that the increase in hydraulic conductivity diminishes as the service life increases because the largest K_{si}/K_{sa} corresponds to the test sections with the shortest service life. However, there is no trend between K_{si}/K_{sa} and service life for test sections in service for at least 4.9 yr, and there is no systematic trend in K_{si}/K_{sa} between those test sections with short service life (< 4.1 yr) and those having a longer service life (> 4.9 yr). A more logical explanation is that the apparent trend with service life actually is a reflection of the trend between K_{si}/K_{sa} and K_{sa} . That is, the test sections with a short service life also had low K_{si}/K_{sa} and therefore underwent the largest increase in hydraulic conductivity (i.e., the trend with service life is spurious). This conclusion is consistent with previous laboratory and field studies, which have shown that “healing” of structure in final covers is unlikely (Corser and Cranston 1991, Khire et al. 1997, Melchior 1997, Albrecht and Benson 2001).

6.5.2 Climate

The effect of climate on K_{si}/K_{sa} is shown in Fig. 6.10. Climate has no noticeable effect on K_{si}/K_{sa} . The geometric mean K_{si}/K_{sa} is 89 in humid and sub-humid climates and 93 in arid and semi-arid climates. A t-test at a significance level of 0.05 on the logarithmically transformed data confirmed that K_{si}/K_{sa} was statistically similar for the two categories of climate ($t = -0.051$ and $p = 0.480$). Similarly, a t-test comparing K_{si}/K_{sa} only for conventional covers showed no statistically significant difference between K_{si}/K_{sa} for both categories of climates ($t = -1.419$ and $p = 0.103$). This finding contrasts anecdotal reports, which suggest that clay barriers in drier climates are more readily or severely damaged by environmental exposure. The findings of this study indicate that significant alterations in hydraulic conductivity can occur in all climates.

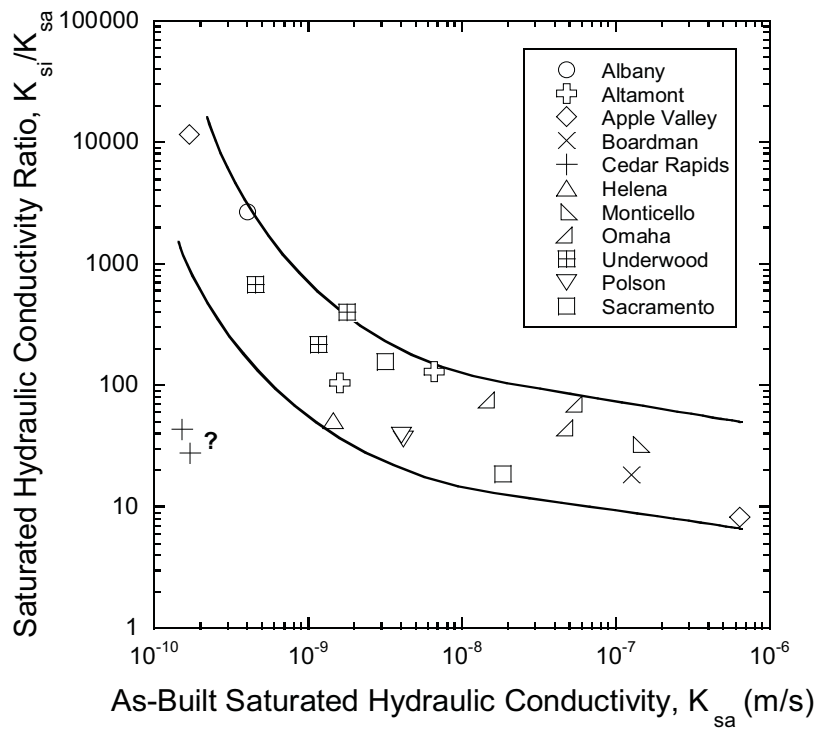


Fig. 6.8. Saturated hydraulic conductivity ratio (K_{si}/K_{sa}) versus as-built saturated hydraulic conductivity (K_{sa}). Trend lines drawn by hand. “?” signifies outliers.

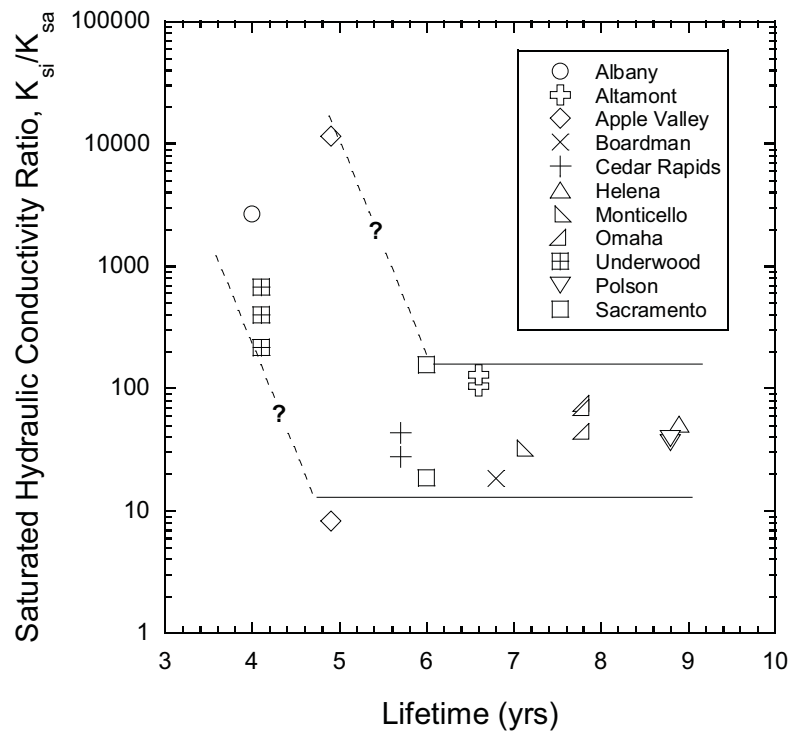


Fig. 6.9. Saturated hydraulic conductivity ratio versus service life of test section. Trend lines drawn by hand.

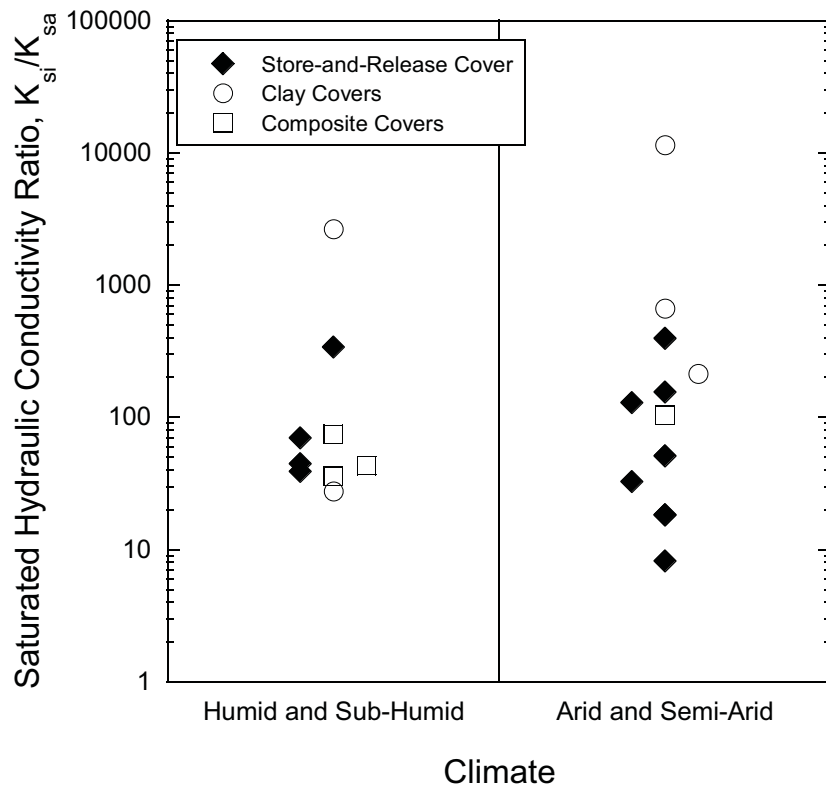


Fig. 6.10. Saturated hydraulic conductivity ratio versus climate presented by cover type.

6.5.3 Soil Composition

Several studies have suggested that soils with lower plasticity or a greater fraction of coarse particles have lower propensity for volume change, and therefore are less susceptible to formation of structure and alterations in hydraulic conductivity in response to environmental stresses (Chamberlin and Gow 1979, Kleppe and Olson 1985, Albrecht and Benson 2001, Eigenbrod 2003, Benson et al. 2007). To evaluate whether the data collected in this study are consistent with these trends, relationships between K_{si}/K_{sa} and plasticity index (PI), 2 μm clay content, activity, and relative proportions of finer and coarser particles were explored. Graphs showing how K_{si}/K_{sa} varies with these compositional variables are presented in Figs. 6.11 and 6.12. When both coarse and fine-grained soils are considered, clay content is the only compositional variable having a statistically significant (significance level = 0.05) effect on K_{si}/K_{sa} (Fig. 6.11b). However, when only fine-grained soils are considered, the ratio of silt content to fines content also has a statistically significant effect on K_{si}/K_{sa} at a significance level of 0.05 (Fig. 6.12). Essentially no trend was obtained with PI (no statistical significance at the 0.05 level), and the largest K_{si}/K_{sa} was obtained for a low plasticity soil (Apple Valley, Fig. 6.11a).

The influence of clay content is consistent with findings reported by Kleppe and Olson (1985) and Albrecht and Benson (2002). Soils with higher clay content experience greater shrinkage cracking when desiccated and have lower as-compacted hydraulic conductivity. Therefore, soils with higher clay content that undergo desiccation should exhibit larger K_{si}/K_{sa} (Fig. 11b). However, because soils with higher clay content also have lower K_{sa} , covers constructed with soils having higher clay content may not have higher in-service hydraulic conductivity even if K_{si}/K_{sa} for the soil is large (e.g., Fig. 6.7b).

For fine-grained soils, smaller increases in hydraulic conductivity were obtained when the fines contained a greater proportion of silt particles (Fig. 6.12b). These soils also had higher K_{sa} , and thus were not as susceptible to large increases in hydraulic conductivity. Because soils with high silt content are less cohesive, cracks and other defects do not remain open as readily as in more clayey soils. Silt particles are also mobilized easily and can fill cracks and other features as soil structure develops, thereby reducing the impact of structure on hydraulic conductivity (Eigenbrod 2003).

6.5.4 Compaction Conditions

Formation of soil structure is known to have greater impact on hydraulic properties of soil layers placed in a dense monolithic condition because the flow paths change significantly (Benson et al. 2007). Conditions that lead to a monolithic structure include compaction to higher dry unit weight or at higher water content, which results in remolding of clods and eliminate interclod voids (Benson and Daniel 1990). Thus, greater changes in hydraulic properties are anticipated with higher dry unit weight or relative compaction or with higher compaction water content.

Graphs of K_{si}/K_{sa} vs. compacted dry density (γ_{dc}) and relative compaction are shown in Fig. 6.13. A summary of the in-service dry unit weight and relative compaction is in Table 6.7. The hydraulic conductivity increases up to 2 orders of magnitude for γ_{dc} between 14 and 15 kN/m^3 , up to 3 orders of magnitude for γ_{dc} between 15 and 17 kN/m^3 , and as much as 4 orders of magnitude for γ_{dc} between 17 and 18 kN/m^3 (Fig. 6.13a). Larger increases in

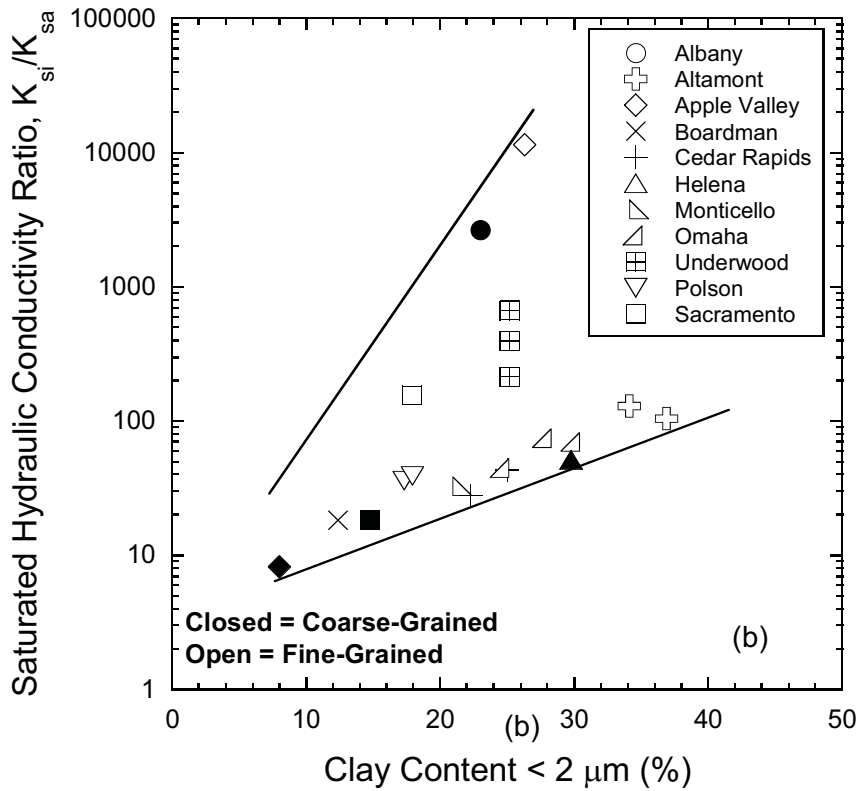
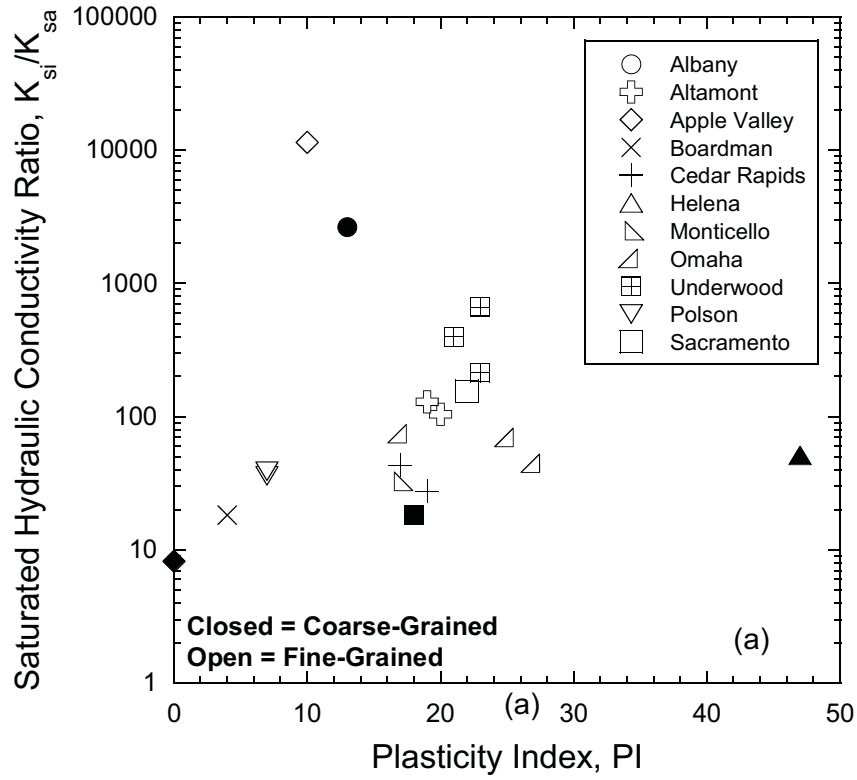


Fig. 6.11. Saturated hydraulic conductivity ratio versus plasticity index (a), clay content (< 2 μm) (b), and activity (c). PI = 0 indicates soil is non plastic.

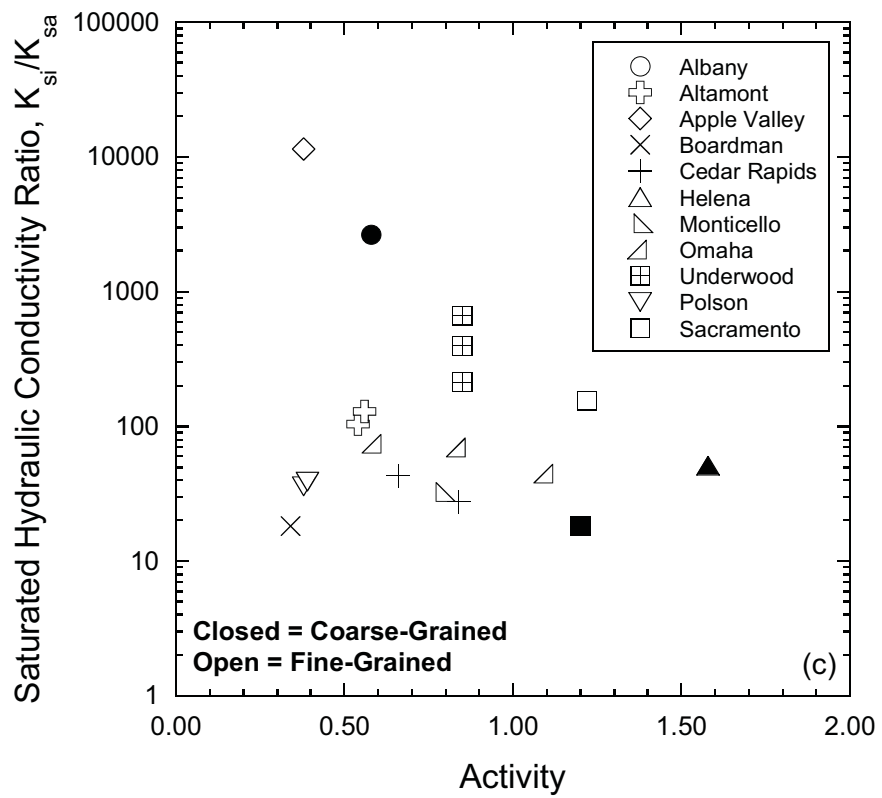


Fig. 6.11. Saturated hydraulic conductivity ratio versus plasticity index (a), clay content ($< 2 \mu\text{m}$) (b), and activity (c). PI = 0 indicates soil is non plastic (continued).

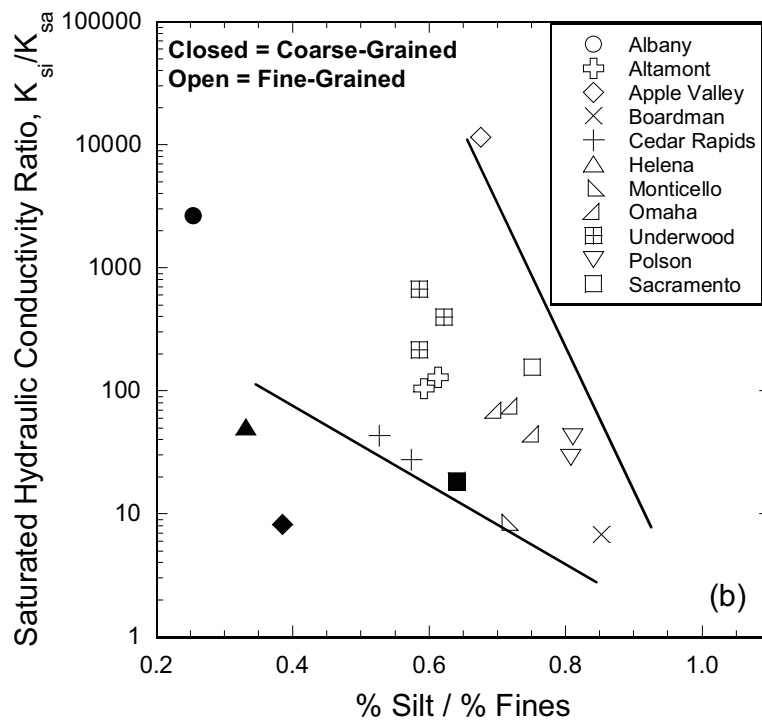
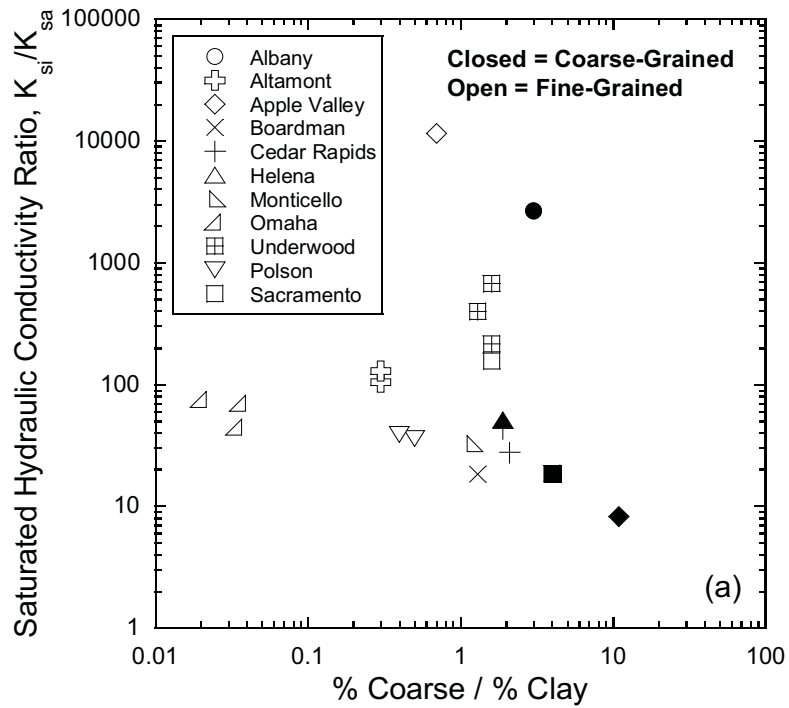


Fig. 6.12. Saturated hydraulic conductivity versus coarse fraction ($\% > 75 \mu\text{m}$) over clay content ($\% < 2 \mu\text{m}$) (a) and ratio of silt content ($\%$ between 2 and $75 \mu\text{m}$) to fines content ($\% < 75 \mu\text{m}$) (b).

Table 6.7. In-service dry unit weight and relative compaction for storage layers.

Site	Number of Samples	In-Service Dry Unit Weight, γ_{di} (kN/m ³)		In-Service Relative Compaction (%)	
		Mean	Standard Deviation	Mean	Standard Deviation
Altamont, CA	3	16.7	0.79	91.9	4.3
Boardman, OR	5	16.5	0.83	98.1	4.5
Cedar Rapids, IA	2	15.3	1.18	86.1	6.7
Helena, MT	3	12.7	0.51	82.3	3.3
Monticello, UT	5	15.9	0.55	90.7	4.0
Omaha, NE	6	14.0	0.64	83.8	3.2
Underwood, ND	3	15.0	0.28	90.8	1.7
Poison, MT	1	14.1	NA	86.1	NA
Sacramento, CA Thin	4	15.9	1.29	91.4	8.7
Sacramento, CA Thick	2	14.3	1.04	89.1	6.5

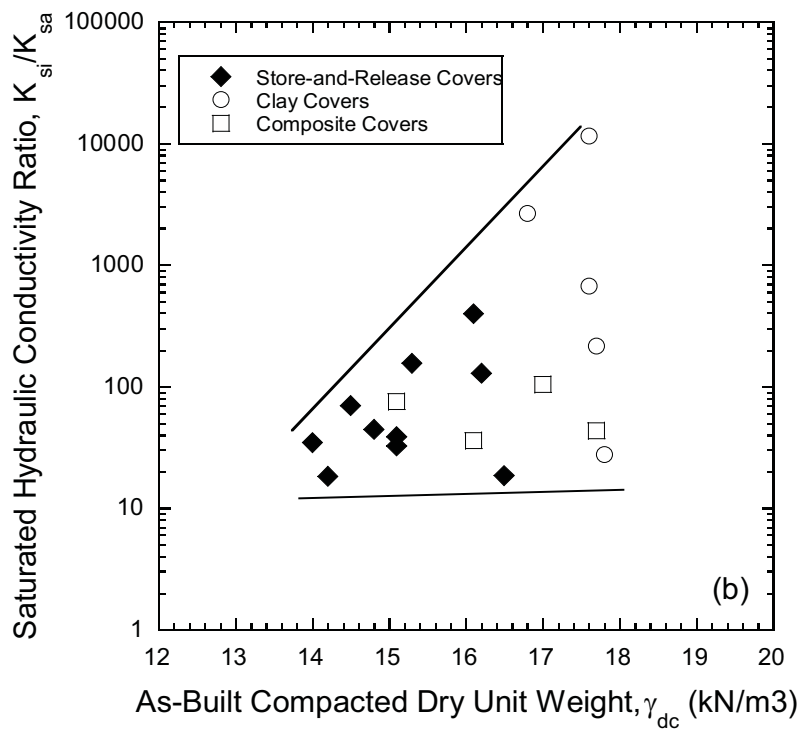
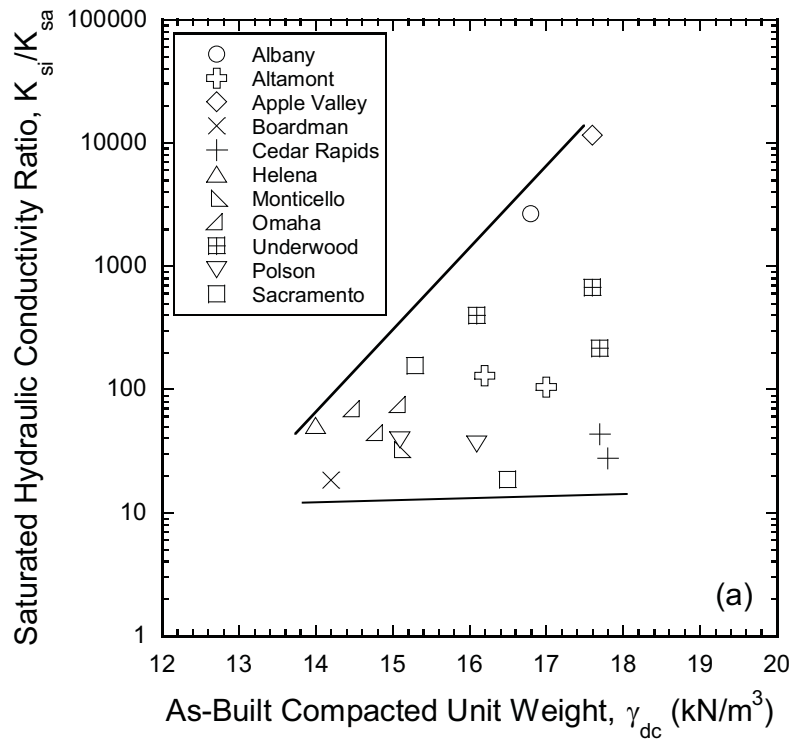


Fig. 6.13. Saturated hydraulic conductivity ratio versus as-built compacted dry unit weight by site (a) and cover type (b).

hydraulic conductivity occurred for the clay barriers in conventional covers, which are compacted to higher dry unit weight (Fig. 6.13b) or relative compaction (Fig. 6.13c) specifically to reduce structure and achieve low hydraulic conductivity (Benson and Daniel 1990). Thus, the trends in Fig. 6.13 are consistent with the trend between K_{si} and K_{sa} shown in Fig. 6.8; i.e., larger increases in hydraulic conductivity occur in storage and barrier layers with lower as-built hydraulic conductivity due to a larger change in soil structure. These trends are statistically significant at the 0.05 level.

The effect of as-compacted water content is shown in Fig. 6.14 in terms of water content relative to optimum water content ($w_c - w_{opt}$). Larger increases in hydraulic conductivity (higher K_{si}/K_{sa}) occur when the compaction water content is higher. This occurs because fine-textured soils compacted wet of optimum water content have lower as-built hydraulic conductivity and less structure than fine-textured soils compacted dry of optimum water content (Benson and Daniel 1990). The largest increases in hydraulic conductivity correspond to compacted clay barriers used as the sole hydraulic barrier in a conventional cover. These clay barriers generally are compacted to have very low as-built hydraulic conductivity and experience greater exposure to environmental conditions than composite barriers in conventional covers. Thus, they should exhibit the largest K_{si}/K_{sa} .

6.5.5 Effect of Freeze-Thaw and Wet-Dry Cycles

Several studies have shown that freeze-thaw and wet-dry cycling form soil structure that results in increases in hydraulic conductivity (Kleppe and Olson 1985, Benson and Othman 1993, Benson et al. 1995, Albrecht and Benson 2001, Eigenbrod 2003). Thus, the effect of freeze-thaw and wet-dry cycling on hydraulic conductivity was evaluated. A freeze-thaw cycle was defined as a period of at least 24 hr during which the soil temperature at the midpoint of the layer of interest was below 0°C followed by a 24 hr period with temperatures greater than 0°C (Benson et al. 1995). A wet-dry cycle was defined as an increase in volumetric water content of at least 2% (as measured in situ using TDR) followed by a 2% or greater decrease in volumetric water content. Smaller changes in water content were not considered because the resolution of the method used to measure water content in situ was approximately 2% (Benson and Bosscher 1999), even though Albrecht and Benson (2001) indicate that smaller changes in water content can cause cracking of fine-textured soils.

Graphs showing K_{si}/K_{sa} as a function of the number of freeze-thaw and wet-dry cycles are shown in Fig. 6.15. At least one freeze-thaw cycle occurred in nine of the test sections that were studied, and all test sections experienced at least four wet-dry cycles. For both freeze-thaw and wet-dry cycling, there is no apparent or statistically significant (significance level = 0.05) trend with number of cycles (Fig. 6.15). This suggests that all storage and barrier layers underwent a sufficient number of wet-dry and freeze-thaw cycles to develop the structure required to induce the maximum change in hydraulic conductivity. This inference is consistent with the findings of Albrecht and Benson (2001) and Miller et al. (1998), who found that cracks caused by desiccation form during the first drying event and that the maximum hydraulic conductivity is achieved after only one cycle. Similarly, Chamberlain et al. (1990), Zimmie and LaPlante (1990), and Podgorney and Bennett (2006), show that changes in hydraulic conductivity do not occur as the number of cycles increases substantially. Chamberlain et al. (1990) conducted tests for up to 15 freeze-thaw cycles, Zimmie and LaPlante (1990) conducted tests up to 30 freeze-thaw cycles, and Podgorney and Bennett (2006) conducted tests for as many as 150 freeze-thaw cycles. None of these

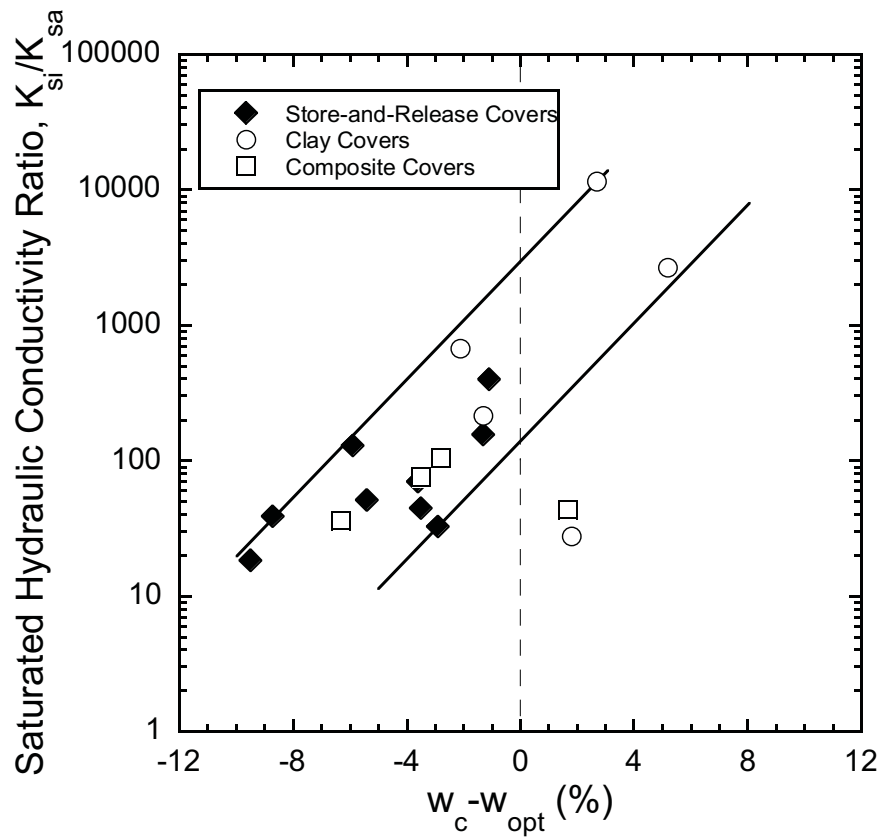


Fig. 6.14. Saturated hydraulic conductivity ratio versus water content relative to optimum water content.

studies reported secondary changes in saturated hydraulic conductivity at a greater number of cycles. Thus, the absence of a trend with number of wet-dry and freeze-thaw cycles is not unexpected.

6.6 Soil Water Characteristic Curves

SWCCs were measured on a subset of the specimens subjected to hydraulic conductivity testing. Geometric and arithmetic means of the SWCC parameters for each site are presented in Table 6.8 for tests conducted on 73 mm specimens, Table 6.9 for tests conducted on 150 mm specimens, and Table 6.10 for tests conducted on 254 mm specimens. The geometric mean and the standard deviation of the logarithmic transform are reported for the lognormally distributed α , whereas arithmetic means and standard deviations are reported for the normally distributed n , θ_s , and θ_r . Similar mechanisms cause alterations in hydraulic conductivity and the SWCC (Benson et al. 2007). Thus, this section only provides a synopsis of how the SWCC parameters changed while in service.

The in-service α and n obtained from tests on 73-mm specimens are shown as a function of the as-built α and n in Fig. 6.16. The in-service α ranges from 0.0012 to 0.05 kPa⁻¹, or 0.3 to 27 times the as-built α . The geometric mean of the ratio of in-service to as-built α (α_i/α_a) is 2.2. This increase in α corresponds to a decrease in the air-entry suction, which is indicative of the development of larger pores associated with formation of soil structure (Benson et al. 2007). The lowest in-service α were obtained for the specimens from Cedar Rapids, which also had the lowest in-service hydraulic conductivity. The in-service n range from 1.15 to 1.35 [the clay barriers at Cedar Rapids ($n = 1.49$ - 1.49) and the storage layer at Boardman ($n = 1.57$) are exceptions], or 0.7 to 1.1 times larger than the as-built n . On average, n decreased by a factor of 1.1 while in service. This modest decrease in n indicates that the pore size distribution has broadened only slightly, and suggests that the changes in soil structure consisted primarily of formation of large pores without altering the distribution of smaller pores (i.e., the smaller pores still governed).

The in-service saturated volumetric water content (θ_{si}) is shown in Fig. 6.17 as a function of the as-built saturated volumetric water content (θ_{sa}), which was determined using weight-volume computations. For nearly all sites, θ_s increased while in service (the test sections in Cedar Rapids and one test section in Altamont are the exceptions), which corresponds to an increase in porosity or a decrease in dry unit weight (both are uniquely related) due to formation of soil structure (i.e. the soil has become looser).

The effect of scale on the SWCC parameters is shown in Fig. 6.18 in terms of the ratio of α or n determined at a larger scale (LS, 254-mm and 150-mm-diameter) to that determined using a conventional small-scale (SS, 73-mm-diameter) test specimen (Wang and Benson 2004). On average, the α parameter is 4.4 times larger for 150-mm specimens and 19.6 times larger for the 254-mm specimens compared to α for the conventional size test specimens. In contrast, n of the larger-scale specimens is essentially equal to n of the conventional small-scale test specimens (on average, $n_{LS}/n_{SS} = 0.97$ at 150 mm and 0.99 at 254 mm when the outlier for Boardman at 150 mm is excluded, Fig. 6.18b). The increase in α with the size of the test specimen is indicative of the additional structure and larger pores included in the larger test volumes.

Table 6.8. SWCC parameters for storage and barrier layers from 75-mm-diameter specimens.

Site Location	Number of SWCCs	α (kPa ⁻¹)		n		θ_s		θ_r	
		Geometric Mean	$\sigma_{ln\alpha}$	Arithmetic Mean	σ	Arithmetic Mean	σ	Arith. Mean	σ
Store-and-Release Covers									
Altamont, CA	2	0.0043	0.07	1.25	0.03	0.37	0.02	0.00	0.00
Apple Valley, CA	-	-	-	-	-	-	-	-	-
Boardman, OR	4	0.0060	1.09	1.57	0.15	0.39	0.02	0.00	0.01
Cedar Rapids, IA	-	-	-	-	-	-	-	-	-
Helena, MT	1	0.0483	-	1.15	-	0.52	-	0.00	-
Monticello, UT	7	0.0203	0.64	1.28	0.06	0.41	0.01	0.00	0.00
Omaha, NE Thin	1	0.0128	-	1.25	-	0.46	-	0.00	-
Omaha, NE Thick	3	0.0226	0.44	1.22	0.04	0.48	0.02	0.00	0.00
Underwood, ND	1	0.0065	-	1.26	-	0.42	-	0.00	-
Polson, MT	1	0.0098	-	1.34	-	0.43	-	0.00	-
Sacramento, CA Thin	4	0.0067	0.48	1.27	0.03	0.43	0.05	0.00	0.00
Sacramento, CA Thick	2	0.0132	1.11	1.23	0.06	0.47	0.07	0.00	0.00
Conventional Covers with Clay Barriers									
Albany, GA	-	-	-	-	-	-	-	-	-
Apple Valley, CA	2	0.0052	0.33	1.19	0.00	0.37	0.03	0.00	0.00
Cedar Rapids, IA	5	0.0012	0.53	1.49	0.14	0.29	0.01	0.01	0.01
Underwood, ND Thick	1	0.0030	-	1.34	-	0.43	-	0.00	0.00
Underwood, ND Thin	-	-	-	-	-	-	-	-	-
Conventional Covers with Composite Barriers									
Altamont, CA	2	0.0093	0.80	1.23	0.05	0.37	0.01	0.00	0.00
Cedar Rapids, IA	6	0.0014	0.40	1.45	0.08	0.30	0.01	0.00	0.00
Omaha, NE	-	-	-	-	-	-	-	-	-
Polson, MT	-	-	-	-	-	-	-	-	-

Note: - indicates no data are available and σ = standard deviation

Table 6.9. SWCC parameters for storage and barrier layers from 150-mm-diameter specimens.

Site Location	Number of SWCCs	α (kPa ⁻¹)		n		θ_s		θ_r	
		Geom. Mean	$\sigma_{\ln\alpha}$	Arith. Mean	σ	Arith. Mean	σ	Arith. Mean	σ
Store-and-Release Covers									
Boardman, OR	1	0.0174	-	1.25	-	0.52	-	0.00	-
Monticello, UT	3	0.1095	0.36	1.25	0.02	0.45	0.02	0.00	0.00
Omaha, NE Thick	1	0.0274	-	1.25	-	0.46	-	0.00	-
Underwood, ND	1	0.0886	-	1.18	-	0.46	-	0.00	-
Conventional Covers with Clay Barriers									
Apple Valley, CA	1	0.0063	-	1.25	-	0.42	-	0.00	-
Underwood, ND Thick	1	0.0070	-	1.24	-	0.38	-	0.00	-

Note: - indicates no data are available and σ = standard deviation.

Table 6.10. SWCC parameters for storage and barrier layers from 254-mm-diameter specimens.

Site Location	α_i (kPa ⁻¹)	n	θ_s	θ_r
Store-and-Release Covers				
Altamont, CA	0.1949	1.15	0.44	0.00
Helena, MT	0.3312	1.13	0.51	0.00
Monticello, UT	0.1160	1.24	0.54	0.01
Omaha, NE Thick	0.2567	1.17	0.45	0.00
Underwood, ND	0.3230	1.17	0.46	0.00
Conventional Covers with Clay Barriers				
Apple Valley, CA	0.2004	1.11	0.37	0.00
Conventional Covers with Composite Barriers				
Altamont, CA	0.0159	1.24	0.41	0.00

Note: 1
SWCC
per site.

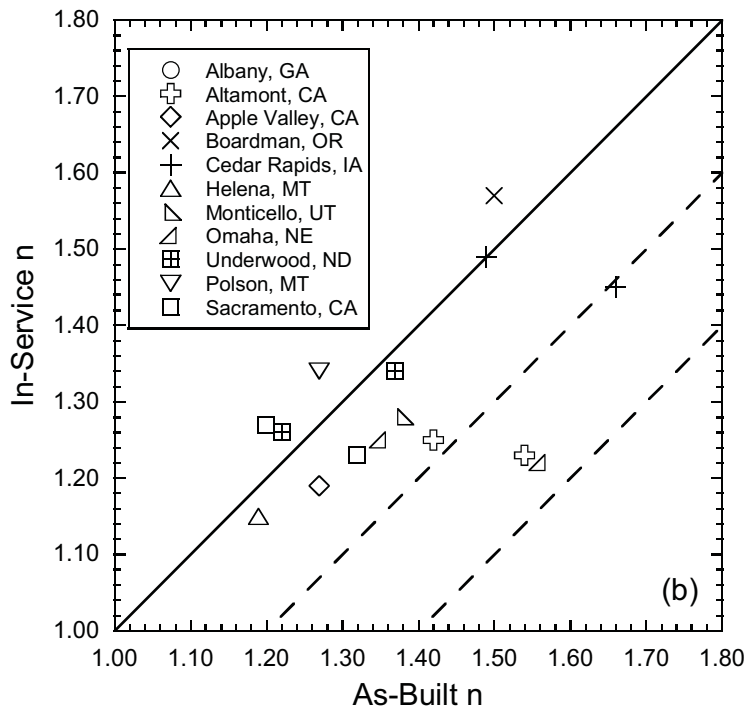
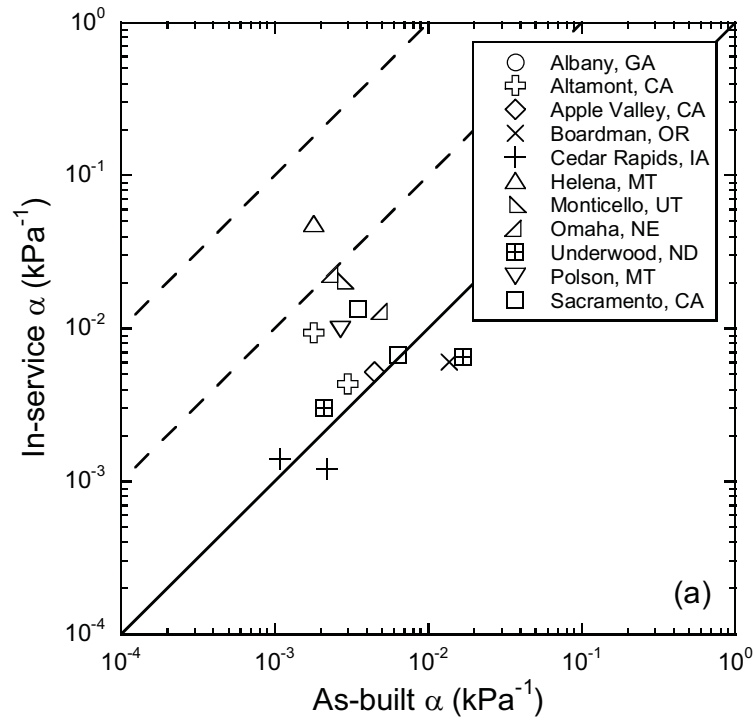


Fig. 6.16. In-service α parameter versus as-built α parameter (a) and in-service n parameter versus as-built n parameter (b).

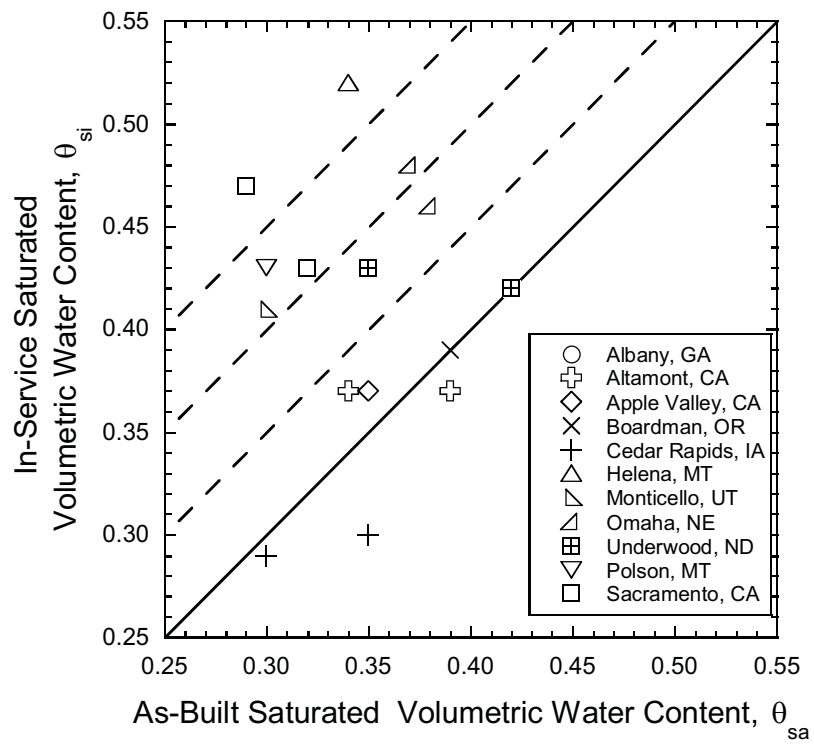


Fig. 6.17. In-service saturated volumetric water content versus as-built saturated volumetric water content.

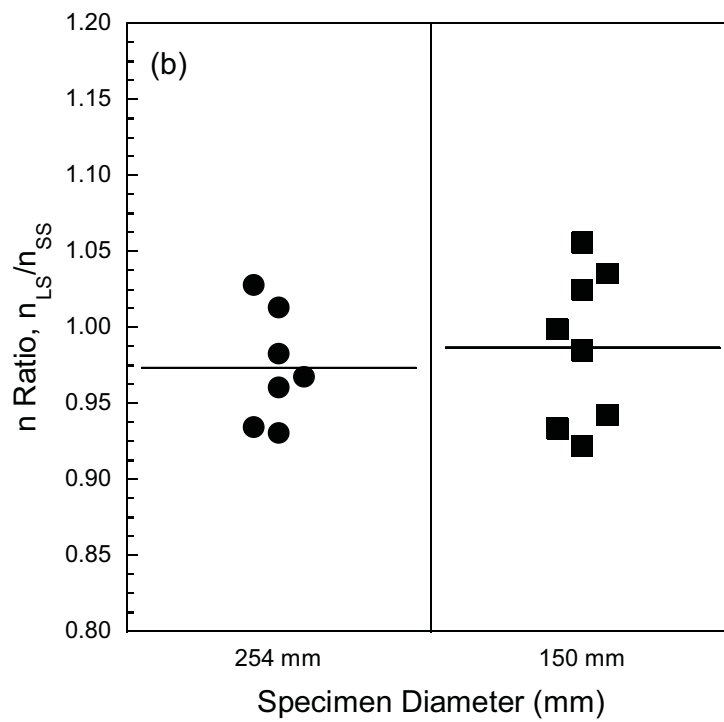
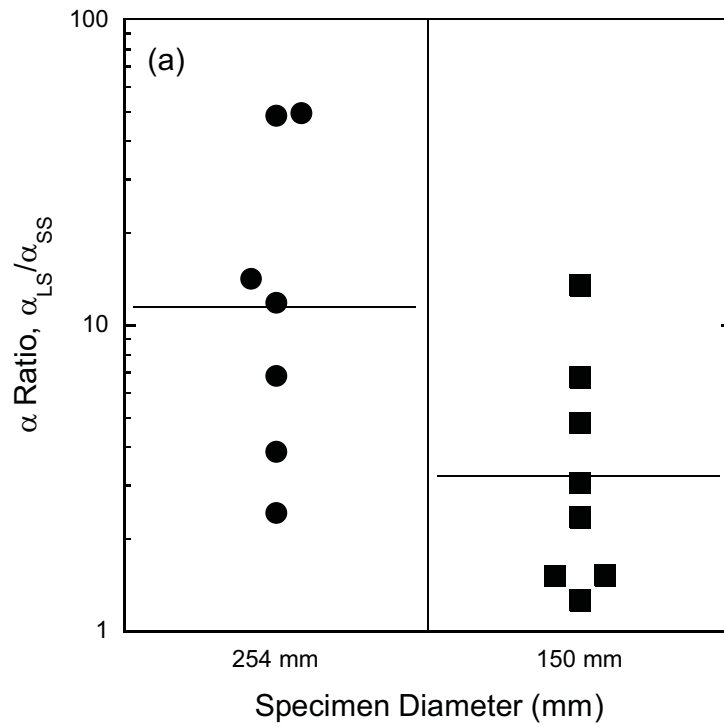


Fig. 6.18. The ratio of α (a) and n (b) from large-scale testing (254 or 150 mm) to small scale testing (75 mm). Horizontal lines are medians.

6.7 Summary of Findings for Earthen Storage and Barrier Layers

The following conclusions and recommendations are made based on the findings presented in this section:

1. Similar saturated hydraulic conductivities were obtained with the BH and SDRI tests (within 10x). Saturated hydraulic conductivities based on peak flows in the lysimeters that were computed with and without accounting for degree of saturation generally bracketed the saturated hydraulic conductivities measured with the BHs and SDRIs. Thus, both the SDRI and BHs generally provided a good estimate of the saturated hydraulic conductivity operative in the field.
2. Storage layers in the store-and-release covers had the highest saturated hydraulic conductivity followed by the clay barriers in conventional covers without a geomembrane. The lowest saturated hydraulic conductivities were obtained from clay barriers in composite barriers. These differences reflect the higher compactive energy used to construct resistive barrier layers and the protection afforded by the geomembrane in composite barriers. However, the hydraulic conductivities did not differ appreciably between cover types ($< 10x$), and the clay barriers in all of the conventional covers had higher saturated hydraulic conductivity than existed in the as-built condition.
3. The saturated hydraulic conductivity of in-service storage and barrier layers that were evaluated is sensitive to scale. Saturated hydraulic conductivities determined from testing conventional small-scale specimens (< 76 -mm diameter) in the laboratory are appreciably lower (more than 1000x in some cases) than the actual field hydraulic conductivity. Large-scale laboratory tests (> 300 -mm diameter) yield saturated hydraulic conductivities similar to, but slightly lower than (within 10x) the true field hydraulic conductivity. When the in-service condition of covers is evaluated using laboratory tests, intact samples should be large enough to yield a test specimen having a diameter of at least 300 mm.
4. For the covers that were evaluated, in-service saturated hydraulic conductivities of storage and barrier layers in the field falls between 7.5×10^{-8} and 6.0×10^{-6} m/s regardless of the initial saturated hydraulic conductivity. The geometric mean saturated hydraulic conductivity in the field is 4.4×10^{-7} m/s. If available, a site-specific saturated hydraulic conductivity that reflects in-service conditions should be used for performance predictions. If not, the geometric mean saturated hydraulic conductivity observed in this study (4.4×10^{-7} m/s) can be used to predict performance for typical in-service conditions.
5. Alterations in saturated hydraulic conductivity occurred in all climates and for barrier and storage layers in all cover types that were evaluated. Changes in the saturated hydraulic conductivity were similar regardless of climate (wet or dry) and no barrier type was found to be immune to an alteration in hydraulic conductivity. Wet-dry cycling appears to have a major role in the alterations in hydraulic conductivity. Storage and barrier layers in all cover types evaluated, including those with composite barriers, experience wet-dry cycling and corresponding alterations in hydraulic conductivity.

6. Smaller changes in saturated hydraulic conductivity occur in storage and barrier layers constructed with soils having lower clay content and fines containing a greater proportion of silt. Similar inferences cannot be made using PI and activity; neither is a good indicator of the propensity for change in hydraulic conductivity. Fine-grained soils used to construct storage and barrier layers should have lower clay content and fines containing a greater fraction of silt, when practical.
7. Larger increases in saturated hydraulic conductivity were associated with soils compacted to higher dry unit weight and higher water content. Storage and barrier layers should be compacted to lower dry unit weight and at drier water contents to the extent practical to reduce the change in hydraulic conductivity that occurs while in service.
8. Changes in the SWCC parameters typically are smaller than the changes in saturated hydraulic conductivity (2.2x for θ and 1.1x for n , on average). Nevertheless, these changes in hydraulic properties may have an equally important effect on hydrology. The α parameter is also influenced significantly by test scale. The α parameter from the largest-scale tests conducted in this study (254-mm diameter) was 19.6x larger than α from conventional small-scale tests, on average. Parameters from the large-scale tests conducted in this study are believed to be representative of the field condition.

7. GEOSYNTHETIC CLAY LINERS

Geosynthetic clay liners (GCLs) are factory-manufactured barrier layers containing sodium (Na) bentonite that are used in lieu of compacted soil barriers. In a final cover, a new GCL typically has a saturated hydraulic conductivity of approximately 10^{-11} m/s (Shan and Daniel 1991; Shackelford et al. 2000; Jo et al. 2001, 2005; Kolstad et al. 2004). Recent studies on GCLs exhumed from final covers have shown, however, that the low hydraulic conductivity of GCLs is not necessarily maintained throughout the service life of a final cover. For example, hydraulic conductivities in the range of 10^{-7} to 10^{-6} m/s have been reported for GCLs exhumed from final covers after 2.0 to 11.0 yr of service (Melchior 2002, Benson et al. 2007, Meer and Benson 2007).

The high hydraulic conductivities observed in exhumed GCLs have been attributed to loss of swelling capacity of the bentonite coupled with formation of cracks and other macroscopic features during dehydration. During re-wetting, swelling of the bentonite is insufficient to seal off these features, which results in high hydraulic conductivity. The loss of swelling capacity is caused by replacement of Na bound to the clay surface by calcium (Ca) and magnesium (Mg), which prevents osmotic swelling in the interlayer of montmorillonite (the primary clay mineral in bentonite). Water entering the GCL from overlying cover soils has been suggested as the primary source of the Ca and Mg (Melchior 2002, Benson et al. 2007, Meer and Benson 2007, Benson and Meer 2009).

Lin and Benson (2000) suggest that GCLs deployed in composite barrier layers (i.e., GCL overlain by a geomembrane) are unlikely to experience cation exchange and wet-dry cycling, and thus will retain low hydraulic conductivity. This hypothesis has remained largely unverified because field data regarding the condition of GCLs in composite barriers are scant (Melchior 2002, Meer and Benson 2007). Thus, understanding the in-service condition of GCLs in composite barriers, and comparing this condition to previous studies on GCLs used as the sole barrier layer, was the primary objective of this part of the study. However, in contrast to covers where a GCL is the sole barrier layer, covers with composite barriers have performed well in a broad variety of climates. Benson et al. (2007) report percolation rates between 2.6 and 4.1 mm/yr over a 6-yr period for a cover containing a GCL laminated with geofilm and Albright et al. (2004) report percolation rates ranging from 0 to <0.1 mm/yr for two final covers constructed with composite barriers containing a GCL overlain by a HDPE GM that had service lives between 4 and 5 yr. Despite this good record, understanding alterations in GCLs that occur while in service is important to understanding long-term performance.

GCLs in composite barriers were exhumed from four sites: the ACAP test sections in Apple Valley, CA and Boardman, OR (Fig. 2.2) and the final covers at the operating MSW landfills in Wisconsin and Michigan (Fig. 3.1). Data from these exhumed GCLs are compared to data reported in Meer and Benson (2007) for GCLs exhumed from covers with and without an overlying GM. Profiles of the covers exhumed by Meer and Benson (2007) are shown in Fig. 7.1. A compilation of the GCL data from this study can be found in Appendices G-O.

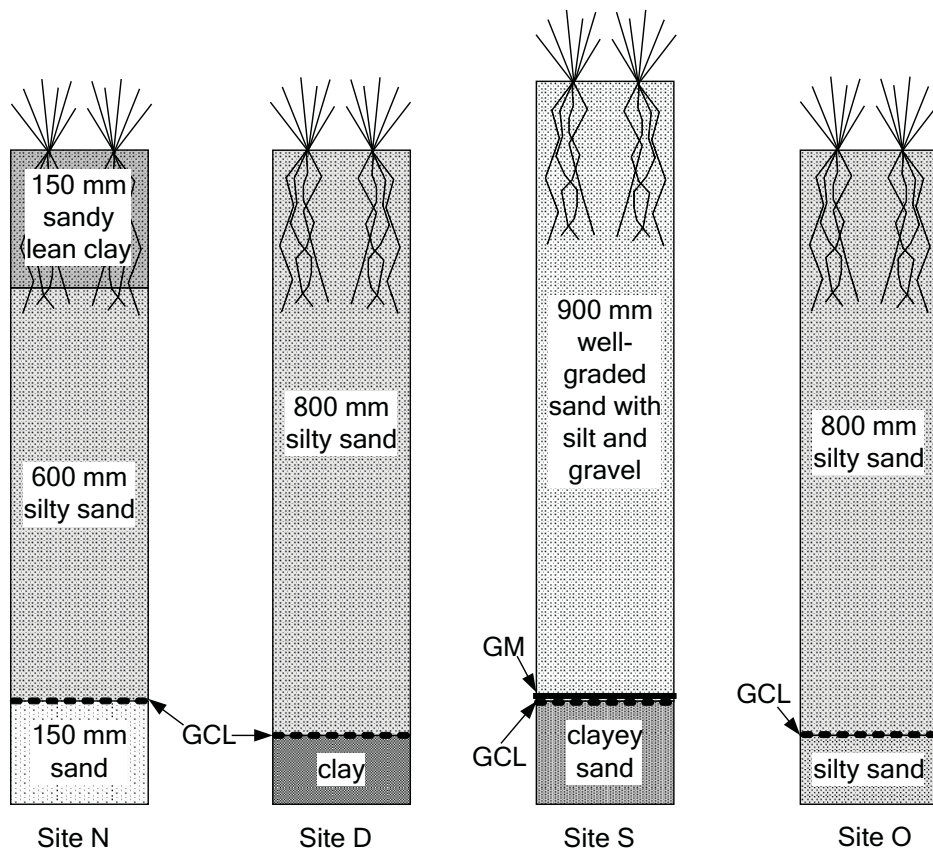


Fig. 7.1. Profiles of final covers evaluated by Meer and Benson (2007). The service life varied from 4.1 to 11.1 yr.

7.1 Background on GCLs

GCLs containing Na-bentonite typically have hydraulic conductivities ranging from 6×10^{-12} to 2×10^{-11} m/s when permeated with dilute aqueous solutions using conventional test methods and under stresses characteristic of final covers (Petrov and Rowe 1997, Shackelford et al. 2000, Jo et al. 2001, Kolstad et al. 2004, Meer and Benson 2007). Na-bentonite in GCLs has low hydraulic conductivity because much of the water in the bentonite is bound to the clay mineral surface and unavailable for flow (Mesri and Olson 1971, Mitchell 1993, Shang et al. 1994). The association of water molecules with the clay surface during hydration is manifested as swelling, which seals off macroscopic flow paths that can control hydraulic conductivity. Thus, the hydraulic conductivity of a GCL and bentonite swell are often related (Shackelford et al. 2000, Jo et al. 2001, Kolstad et al. 2004, Benson and Meer 2009).

Swelling of bentonite occurs in two distinct phases: the crystalline phase and the osmotic phase (Norrish and Quirk 1954). Crystalline swelling occurs first as water molecules move into the interlayer space hydrating the mineral surface and associated cations. Crystalline swelling causes the interlayer to separate by a distance corresponding to several water molecules (McBride 1994). Completion of crystalline swelling corresponds to a gravimetric water content in bentonite of approximately 35% (Mooney et al. 1952, Norrish and Quirk 1954, Martin 1960). Osmotic swelling follows crystalline swelling as water molecules flow into the interlayer region in response to the concentration gradient between the interlayer region and the free pore water. Bentonites that have undergone osmotic swell have water content exceeding 35%, and in many cases have water contents in excess of 100%.

Osmotic swelling can produce far greater swell than crystalline swelling alone (McBride 1994), and is responsible for the high swelling capacity and low hydraulic conductivity of Na bentonite in DW. The magnitude of osmotic swell is a function of the ionic strength of the pore water, with greater swell occurring when the pore water is more dilute (Norrish and Quirk 1954, McBride 1994, Kolstad et al. 2004, Jo et al. 2004). Osmotic swelling only occurs, however, when cations occupying the interlayer space are predominantly monovalent. When divalent cations are predominant, only crystalline swelling occurs (Norrish and Quirk 1954, McBride 1994).

Chemical interactions that affect swelling concurrently affect hydraulic conductivity. Interactions that prevent osmotic swell (e.g., replacement of Na by divalent cations prior to osmotic swell) result in higher hydraulic conductivity, whereas interactions that promote osmotic swell (e.g., permeation by dilute pore water with monovalent cations) result in lower hydraulic conductivity (Jo et al. 2001, Kolstad et al. 2004).

Bentonites that undergo osmotic swelling can retain relatively low hydraulic conductivity under stresses typical of covers (10-30 kPa) even if the Na is subsequently replaced by divalent cations, provided that osmotic swelling persists. For example, Egloffstein (2001, 2002) permeated Na-bentonite GCLs with a 0.3-M CaCl_2 solution after 20 d of permeation with DW (which promoted osmotic swelling). After 3 yr of permeation with the CaCl_2 solution, at which time complete replacement of Na by Ca was assumed, the hydraulic conductivity of the GCL was only 3×10^{-10} m/s. Similarly, Jo et al. (2005) show that permeation of Na-bentonite GCLs with dilute CaCl_2 solutions (< 40 mM) that are known to induce osmotic swelling resulted in hydraulic conductivity less than 6×10^{-10} m/s even though more than 94 pore volumes of flow passed through the bentonite and all of

the Na was replaced by Ca. Lee and Shackelford (2005) show that replacement of Na by Ca in GCLs initially prehydrated with DW (promoting osmotic swell) and then permeated with dilute CaCl_2 solutions results in hydraulic conductivities no greater than 3.5×10^{-10} m/s. Similar results have been reported by Gleason et al. (1997) and Shackelford et al. (2000) for Na-bentonites permeated with dilute solutions of divalent cations mimicking soil eluents.

GCLs that have undergone osmotic swelling can retain low hydraulic conductivity even with a preponderance of bound divalent cations because water molecules associated with osmotic swelling are strongly associated with the clay surface. Osmotic pressures associated with concentration differences in the interlayer and the bulk pore water during exchange have insufficient energy to remove these tightly bound water molecules. However, if these water molecules are extracted by a source with greater energy, much higher hydraulic conductivities may be realized because montmorillonites containing primarily divalent cations do not undergo osmotic swelling when rehydrated (Meer and Benson 2007). This is the reason why a GCL that has undergone replacement of Na by divalent cations coupled with desiccation can be many orders of magnitude more permeable (ex., 10^{-7} m/s) than a new GCL (Melchior 1997, Lin and Benson 2000, Egloffstein 2001, Benson et al. 2007, Benson and Meer, 2009). Similarly, rapid exchange relative to the rate of hydration induced by permeation with a concentrated solution of divalent cations (effectively producing Ca bentonite prior to full osmotic hydration) yields hydraulic conductivities on the order of 10^{-7} m/s (Jo et al. 2005).

Replacement of Na by Ca and Mg while GCLs are in service is well documented. Downward percolation of pore water containing Ca and Mg from overlying cover soils is generally cited as the source of divalent cations for exchange (Egloffstein 2001, Melchior 2002, Meer and Benson 2007, Benson et al. 2007). However, Meer and Benson (2007) showed extensive replacement of Na by Ca and Mg in a GCL exhumed from a composite barrier layer, and attributed the exchange to diffusion of divalent cations into the GCL from the subgrade. Bradshaw (2008) has also shown that divalent cations migrate into GCLs covered by a GM during and after hydration on a subgrade. However, the extent of exchange that commonly occurs in the field in GCLs covered with a GM has not been well documented.

7.2 Properties of Exhumed GCLs

All GCL samples were tested for saturated hydraulic conductivity, water content, SI, and composition of bound and soluble cations. The GCLs were permeated with a 0.01 M CaCl_2 solution, which is commonly referred to as standard water (SW). Some GCLs were also permeated with deionized water (DW), including GCLs where high hydraulic conductivity was obtained with SW. Water content and soluble cations in the subgrade were also evaluated for interpretive purposes. Properties of the GCLs are summarized in Tables 7.1 and 7.2. Properties of the subgrades are summarized in Table 7.3.

7.2.1 GCL Water Content and Cation Exchange

Swell index (SI) and the mole fraction monovalent cations (X_m) of the exhumed GCLs are shown in Fig. 7.2 along with the data from Meer and Benson (2007) for a GCL in a composite barrier (Site S) and GCLs that were the sole barrier layer in final cover (Sites D, N, and O). At the Wisconsin and Michigan sites, GCLs were exhumed from regions

Table 7.1. Physical and chemical properties of exhumed GCLs.

Site ID	Swell Index (mL/2 g)	Grav. Water Content (%)	Hydraulic Conductivity (m/s)		Exchange Complex (mole fraction)			
			SW	DW	Na	K	Ca	Mg
New ^a	^a 36	-	^a 1.2 x 10 ⁻¹¹	1.1 X 10 ⁻¹¹	^a 0.74	^a 0.02	^a 0.22	^a 0.03
	^a 34	-	^a 1.7 x 10 ⁻¹¹	1.0 X 10 ⁻¹¹	^a 0.65	^a 0.02	^a 0.27	^a 0.03
Apple Valley	20.5	53	1.1 x 10 ⁻¹¹	-	0.32	0.01	0.48	0.18
	18.0	55	1.0 x 10 ⁻¹¹	-	0.33	0.01	0.49	0.17
	22.0	53	9.3 x 10 ⁻¹²	-	0.39	0.01	0.43	0.17
	19.8	56	1.3 x 10 ⁻¹¹	1.0 X 10 ⁻¹¹	0.35	0.01	0.47	0.16
	13.0	53	1.5 x 10 ⁻¹¹	-	0.25	0.01	0.57	0.17
	20.5	61	1.2 x 10 ⁻¹¹	-	0.30	0.01	0.50	0.19
	20.0	57	1.4 x 10 ⁻¹¹	-	0.29	0.01	0.51	0.19
Boardman	16.5	59	1.6 x 10 ⁻¹¹	-	0.34	0.01	0.49	0.16
	12.0	22	1.8 x 10 ⁻⁸	-	0.37	0.03	0.41	0.20
	14.0	21	2.0 x 10 ⁻⁸	-	0.45	0.03	0.52	0.00
	20.0	21	4.1 x 10 ⁻⁹	-	0.52	0.03	0.29	0.16
	16.5	21	1.5 x 10 ⁻⁸	-	0.59	0.03	0.24	0.14
	16.0	17	2.3 x 10 ⁻⁹	-	0.46	0.03	0.33	0.18
	14.0	20	8.5 x 10 ⁻⁹	-	0.46	0.03	0.33	0.18
	17.0	18	2.1 x 10 ⁻⁹	2.0 X 10 ⁻¹¹	0.43	0.03	0.35	0.19
	13.0	19	4.5 x 10 ⁻⁸	-	0.41	0.02	0.37	0.20
Wisconsin (W-01)	15.0	20	1.5 x 10 ⁻⁹	-	0.54	0.03	0.28	0.15
	18.0	21	1.9 x 10 ⁻⁸	-	0.52	0.03	0.29	0.16
	8.0	70	4.7 x 10 ⁻¹¹	-	0.06	0.01	0.71	0.21
	8.0	64	4.2 x 10 ⁻¹¹	-	0.06	0.01	0.70	0.22
	10.0	58	4.0 x 10 ⁻¹¹	-	0.05	0.01	0.69	0.25
Wisconsin (W-02)	10.0	60	2.3 X10 ⁻¹¹	-	0.05	0.02	0.72	0.22
	8.0	58	^b 1.3 x 10 ⁻⁸	-	0.05	0.01	0.70	0.25
	10.0	56	^b 1.6 x 10 ⁻⁷	-	0.06	0.02	0.66	0.26
	10.0	56	^b 1.3 x 10 ⁻⁷	2.5 X 10 ⁻¹⁰	0.03	0.01	0.70	0.26
	11.0	63	^b 2.1 x 10 ⁻⁸	-	0.04	0.00	0.71	0.25
	9.0	60	^b 1.5 x 10 ⁻⁸	-	0.04	0.01	0.69	0.25
	11.0	68	3.3 x 10 ⁻¹¹	-	0.05	0.01	0.67	0.27
Michigan (M-03)	10.0	67	3.2 x 10 ⁻¹¹	-	0.05	0.01	0.69	0.25
	8.0	61	3.7 x 10 ⁻¹¹	-	0.05	0.02	0.72	0.21
	8.0	61	^b 6.5 x 10 ⁻⁹	8.9 X 10 ⁻¹¹	0.03	0.03	0.95	0.00
Michigan (M-05)	10.0	61	^b 2.6 x 10 ⁻⁹	9.3 X 10 ⁻¹¹	0.01	0.03	0.96	0.00
	10.0	65	^b 3.3 x 10 ⁻⁹	1.2 X 10 ⁻¹⁰	0.01	0.02	0.97	0.00
	13.0	43	3.8 x 10 ⁻⁹	1.3 X 10 ⁻¹¹	0.14	0.03	0.83	0.00
Michigan (M-05)	12.0	46	2.1 x 10 ⁻⁷	1.4 X10 ⁻¹¹	0.14	0.04	0.83	0.00
	13.0	45	1.1 x 10 ⁻⁸	1.3 X 10 ⁻¹¹	0.13	0.03	0.84	0.00

^a Tests conducted by Meer and Benson (2007)

^b Preferential flow observed

Table 7.2. Gravimetric Water Content, TCM, and MDR of exhumed GCLs.

Site	Water Content (%)		TCM (cmol ⁺ /kg)		MDR	
	Mean	Std. Dev.	Mean	Std. Dev.	Mean	Std. Dev.
Apple Valley	52	3	5.5	0.9	0.96	0.02
Boardman	20	2	9.2	0.6	0.99	0.01
Wisconsin (W-01)	62	5	2.6	1.0	0.85	0.10
Wisconsin (W-02)	59	5	2.8	1.5	0.77	0.19
Michigan (M-03)	63	2	2.5	0.5	0.70	0.02
Michigan (M-05)	45	2	8.4	0.4	0.95	0.00

Table 7.3. USCS Classification and Arithmetic Mean Water Content, TCM, and MDR of Subgrade Soils.

Site	Soil Classification	Water Content (%)		TCM (cmol ⁺ /kg)		MDR	
		Mean	Std. Dev.	Mean	Std. Dev.	Mean	Std. Dev.
Apple Valley	SW	9.8	0.0	0.73	0.09	0.74	0.08
Boardman	ML	2.3	0.2	0.97	0.12	0.76	0.03
Wisconsin (W-01)	ML-CL	14.2	1.6	0.63	0.08	0.62	0.08
Wisconsin (W-02)		14.9	1.2	0.58	0.15	0.64	0.07
Michigan (M-03)	SM	15.9	0.0	0.46	0.09	0.52	0.02
Michigan (M-05)		8.5	0.0	1.20	0.15	0.76	0.04

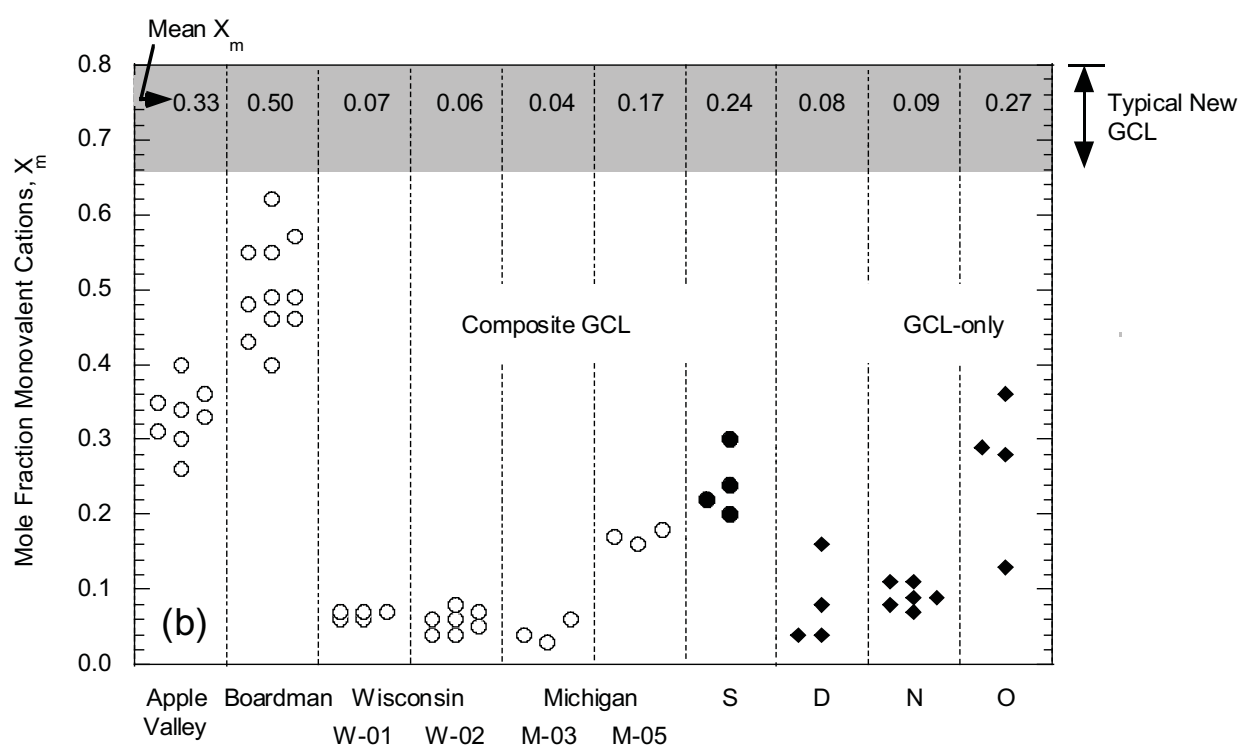
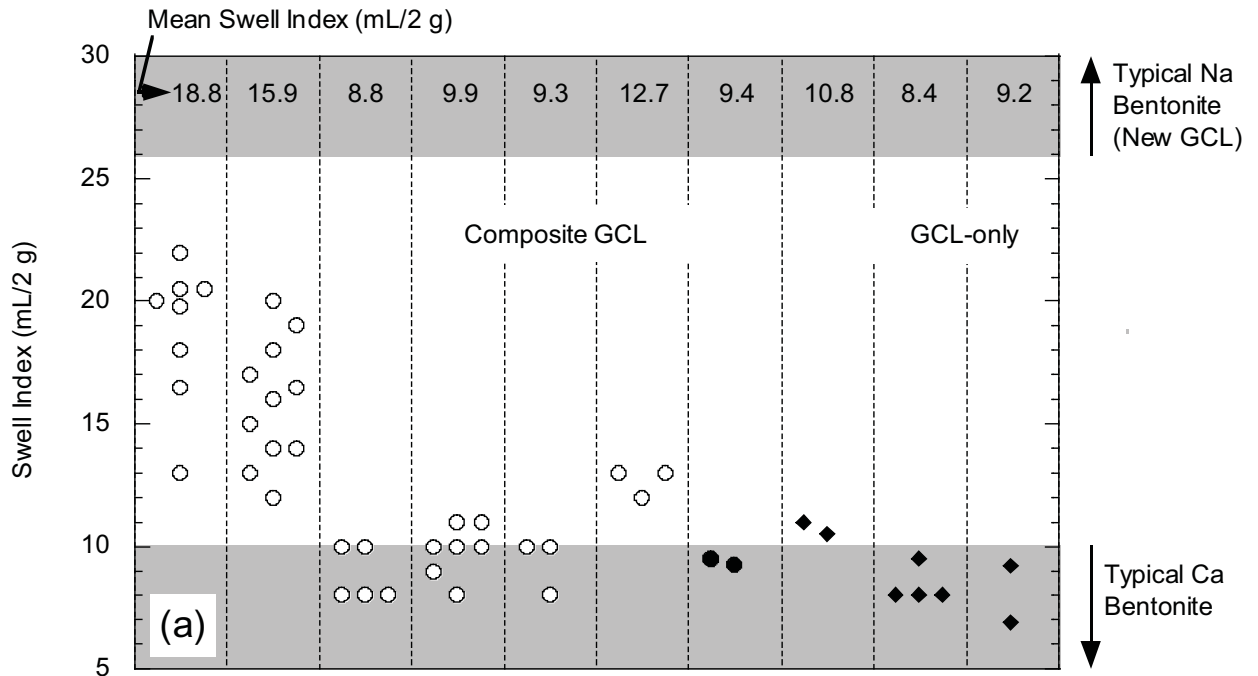


Fig. 7.2. Swell index in DW (a) and mole fraction monovalent bound cations (b) for GCL-only and composite GCL covers. Data are from this study (open symbols) and Meer and Benson (2007) (closed symbols).

constructed in different years. These areas are treated separately and are designated as W-01 and W-02 (Wisconsin 2001, 2002) and M-03 and M-05 (Michigan 2003, 2005).

Swell indices typical of Ca-bentonite (5-10 mL/2 g) and Na-bentonite (26-36 mL/2 g) are denoted in Fig. 7.2a, and the X_m typical of a new GCL (> 0.65) is marked in Fig. 7.2b. Cation exchange and loss of swell are common and extensive in GCLs deployed in composite barriers. At four of the six sites, the GCLs exhumed from composite barriers had SI near those typical of Ca-bentonite (7-11 mL/2 g) and concurrently low X_m (i.e., bound cations predominantly divalent). These SI and X_m are consistent with those for the GCLs exhumed by Meer and Benson (2007). Two of six sites (Apple Valley and Boardman) in this study had SI and the X_m falling between the SI and the X_m for Na and Ca bentonite.

GCLs installed in composite barrier layers are assumed to be protected from downward percolation of overlying soil eluents. However, cation exchange and loss of swell from multivalent cations is not prevented by the overlying GM, and is limited in only some cases. Multivalent cations may still enter the GCL by advective transport from underlying soil pore water during hydration, diffusion from underlying soil pore water, or a combination of both mechanisms (Meer and Benson 2007, Bradshaw 2008). Given the similarity of the SI and X_m of the GCLs exhumed in this study and those in Meer and Benson (2007), transport of cations from the subgrade appears to be equally important as downward percolation of soil eluent. Eventually, GCLs in most composite barriers probably will undergo complete cation exchange and have swell indices typical of Ca bentonite once sufficient quantity of divalent cations migrate into the GCL.

Gravimetric water content of exhumed GCLs is shown in Fig. 7.3a along with data from Meer and Benson (2007). GCLs exhumed from composite barriers exhibit less overall variation in water content (20% - 63%) than GCLs not covered by a GM (43% - 180%) as reported in Meer and Benson (2007). At a given site, the water content varies by at most 12% for GCLs in composite barriers, compared to 49% for GCLs used as the sole barrier layer. Moreover, the average water content varies between 45 and 62% for six of the seven sites where the GCL was part of a composite barrier, but between 43 and 180% for GCLs used without a GM. More consistent in-situ water content in GCLs from composite barriers is likely a result of the overlying GM eliminating cyclic percolation into the GCL.

Water content of the exhumed GCLs from composite barriers varies systematically with the water content of the subgrade, as shown in Fig 7.3b. For example, the driest exhumed GCLs (Boardman) were installed on the driest subgrade (water content = 2.4%), whereas the wettest exhumed GCL (Site D, Meer and Benson 2007) was installed on the wettest subgrade (water content = 19%). Subgrades underlying composite barriers in this study tend to have lower water contents than subgrades underlying GCLs installed as the sole barrier (i.e., from Meer and Benson (2007)), which is due to the GM preventing downward percolation.

7.2.2 Hydraulic Conductivity

Hydraulic conductivities of the GCLs exhumed in this study are shown in Fig. 7.4 along with hydraulic conductivities of GCLs exhumed by Meer and Benson (2007). Circles show hydraulic conductivities obtained using SW (open – this study; closed – Meer and

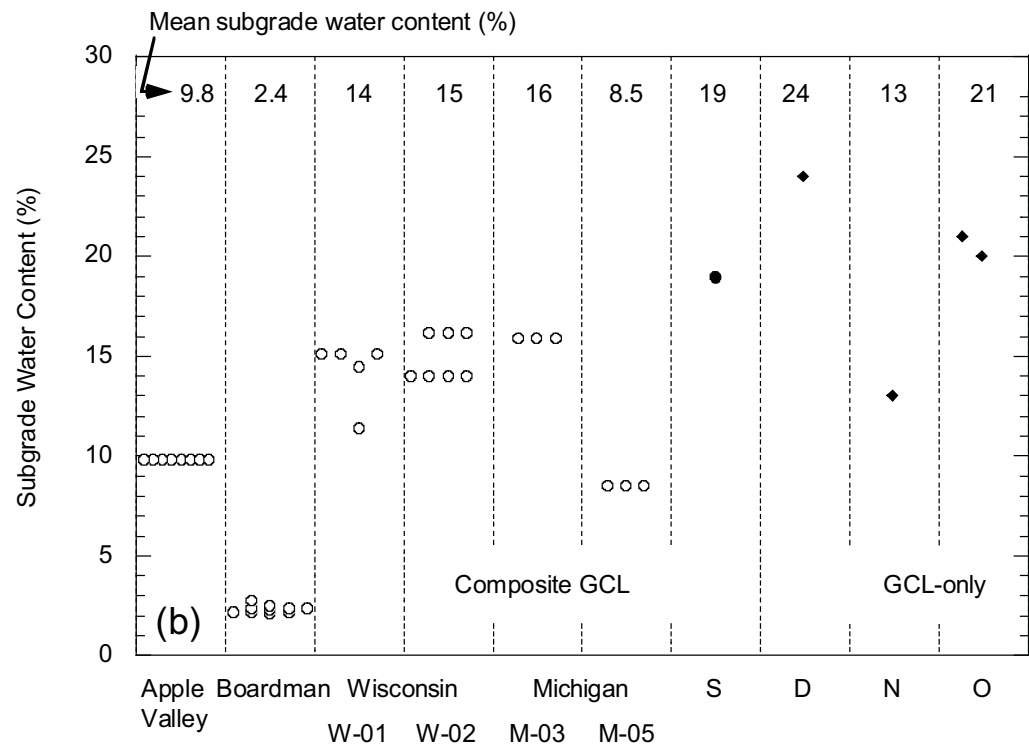
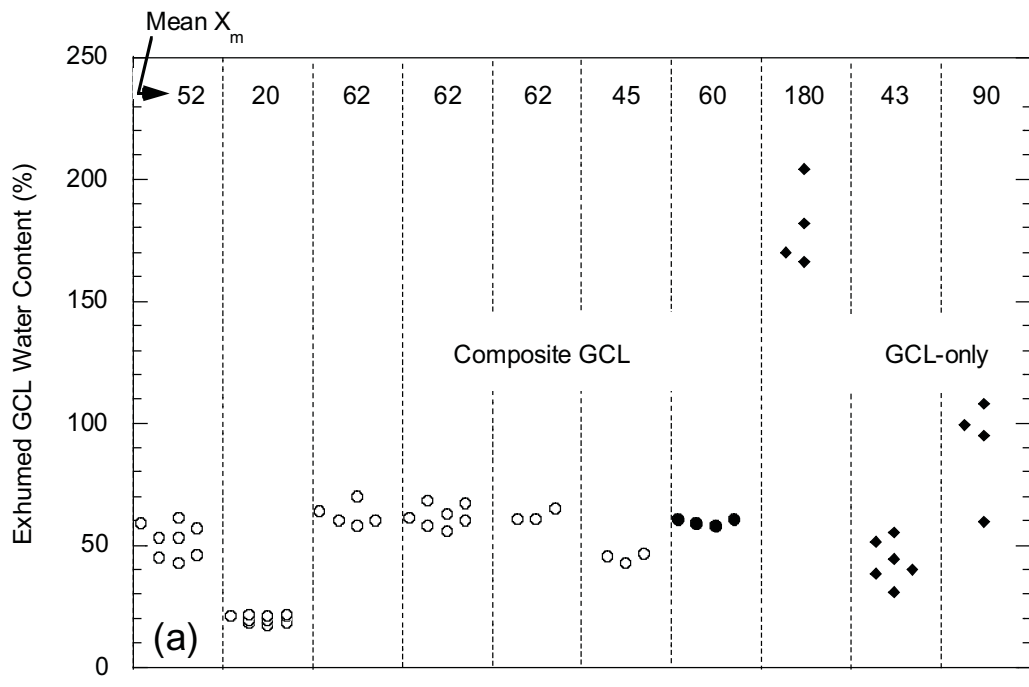


Fig. 7.3. Gravimetric water content of exhumed GCLs (a) and subgrades (b) for covers where GCLs were in composite barriers or the sole barrier layer. Data are from this study (open symbols) and Meer and Benson (2007) (closed symbols).

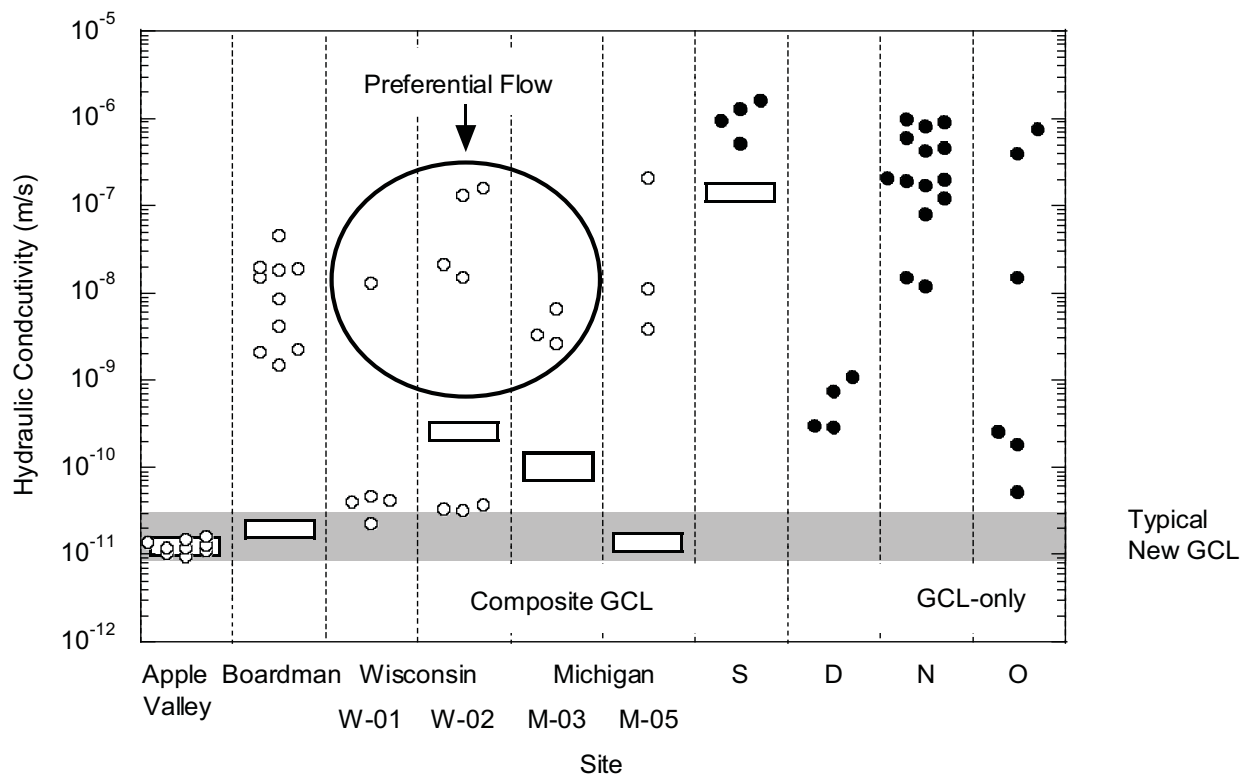


Fig. 7.4. Hydraulic conductivity of exhumed GCLs from covers where GCLs were in composite barriers or the sole barrier layer. Data are from this study (open symbols) and Meer and Benson (2007) (closed symbols). Circles represent hydraulic conductivity to SW; shaded boxes represent hydraulic conductivity to DW. GCLs permeated with DW at Wisconsin site (W-02) are duplicates of GCLs that had high hydraulic conductivity to SW.

and Benson (2007) (e.g., Site S in Fig. 7.4) and Benson et al. (2007) did not find similar sensitivity to water type. For the GCLs that they exhumed, GCLs having high hydraulic conductivity to SW also had high hydraulic conductivity to DW.

Because actual pore waters contain a mixture of cations (Meer and Benson 2007, Benson and Meer 2009), the actual hydraulic conductivity of the GCLs exhumed in this study probably exists between the hydraulic conductivities to SW and DW. However, a definitive inference regarding the actual in-service hydraulic conductivity is not possible. Nevertheless, the sensitivity to water type and the high hydraulic conductivity to SW, both of which are atypical of a new GCL, indicates that covering a GCL with a GM does not preclude alteration of the GCL while it is in service.

After terminating the hydraulic conductivity tests, GCLs with high hydraulic conductivity were permeated with dye to detect if preferential flow was occurring. Preferential flow was observed in the GCLs from one area of the Michigan site (M-03) and both areas of the Wisconsin site that had high hydraulic conductivities (see call out in Fig. 7.4). Preferential flow in GCLs from Site E occurred along nearly all of the bundles of needle-punched fibers and was concomitant with dark mineral precipitates. Preferential flow along fiber bundles also occurred at the Michigan site (M-03), but in only 5% of the bundles. GCLs exhibiting preferential flow behaved differently than the other GCLs exhumed in this study and are separated out in the remaining discussion.

Hydraulic conductivities of the GCLs are shown in Fig. 7.5 as a function of SI (Fig. 7.5a) and X_m (Fig. 7.5b). GCLs that exhibited preferential flow are shown as closed symbols. Data are reported for tests conducted with SW and DW. New GCLs permeated with SW and GCLs from Site S permeated with SW and DW by Meer and Benson (2007) are also shown in Fig. 7.5. Data from GCLs that did not exhibit preferential flow fall into two bands corresponding to higher hydraulic conductivity and lower hydraulic conductivity. The band with higher hydraulic conductivity shows strong sensitivity to SI and X_m , whereas the band with lower hydraulic conductivity has much less sensitivity to SI and X_m . Higher hydraulic conductivities correspond almost exclusively to GCLs permeated with SW [one data point for DW from Meer and Benson (2007) is in this region], whereas lower hydraulic conductivities correspond to data from GCLs permeated with SW and DW.

7.2.3 Effect of Subgrade Condition

The relationship between hydraulic conductivity to SW and exhumed water content is shown in Fig. 7.6a. When the GCLs with preferential flow are excluded, low hydraulic conductivity is obtained consistently when the water content of the GCL exceeds 50%. For lower water contents, the hydraulic conductivity consistently is higher. Meer and Benson (2007) report a similar step relationship, except the transition occurred at a water content of 85%. The data from Site S from Meer and Benson (2007) and the GCLs with preferential flow in this study do not follow this trend.

The relationship between water content of the exhumed GCL and the subgrade water content is shown in Fig. 7.6b. Water content of GCLs increases as the water content of the subgrade increases, as has also been shown in laboratory studies (Daniel et al. 1993, USEPA 1996, Thiel and Criley 2005). Subgrade water content also influenced the soluble and bound cations in the bentonite, as shown in Fig. 7.7. GCLs that had lower

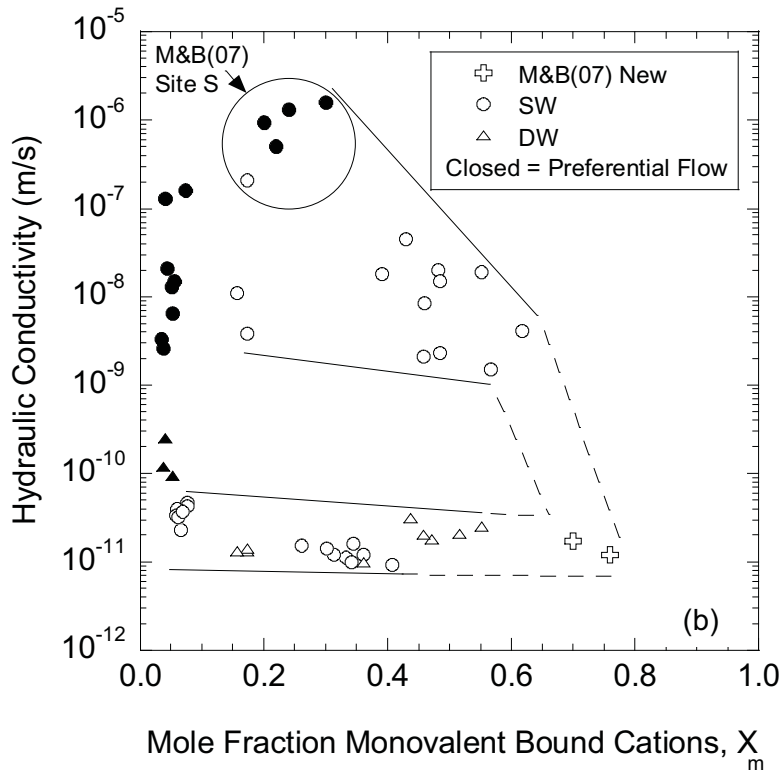
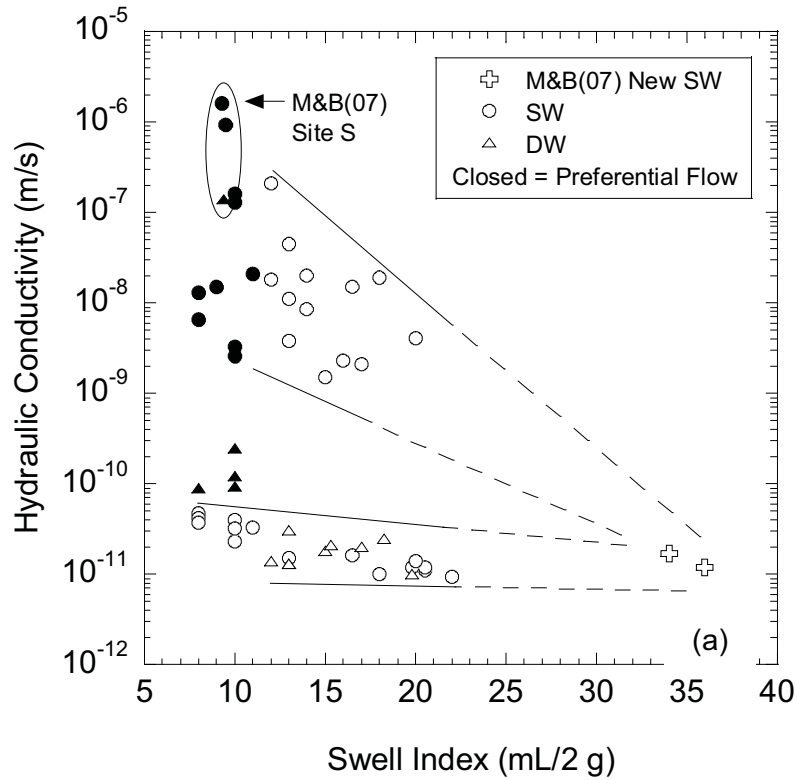


Fig. 7.5 Hydraulic conductivity versus (a) swell index in DW and (b) mole fraction bound sodium for exhumed GCLs from composite barriers. Data for new GCL are from Meer and Benson (2007).

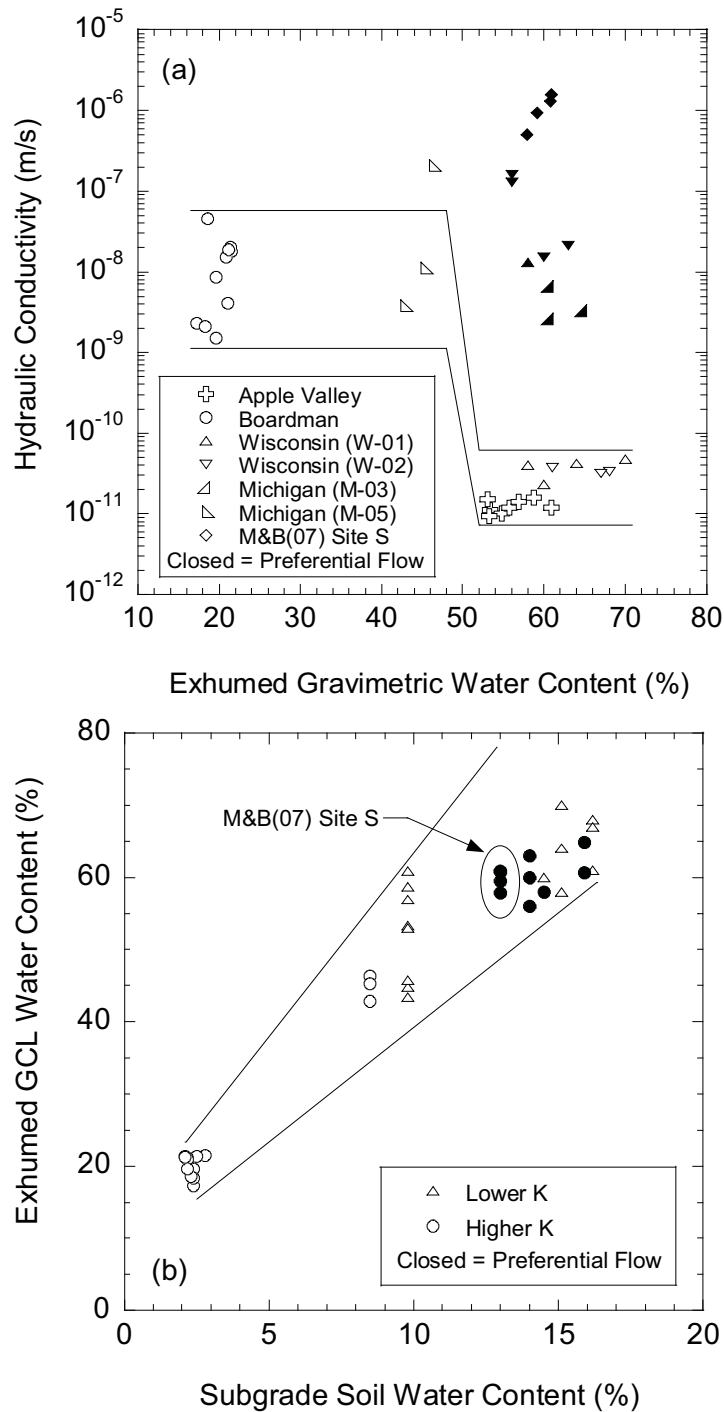


Fig. 7.6. Hydraulic conductivity of exhumed GCLs vs. water content (a) and water content of exhumed GCLs versus corresponding water content of subgrade (b). GCLs with lower K had hydraulic conductivities $< 5 \times 10^{-11}$ m/s, whereas GCLs with higher K had hydraulic conductivities $> 1 \times 10^{-9}$ m/s.

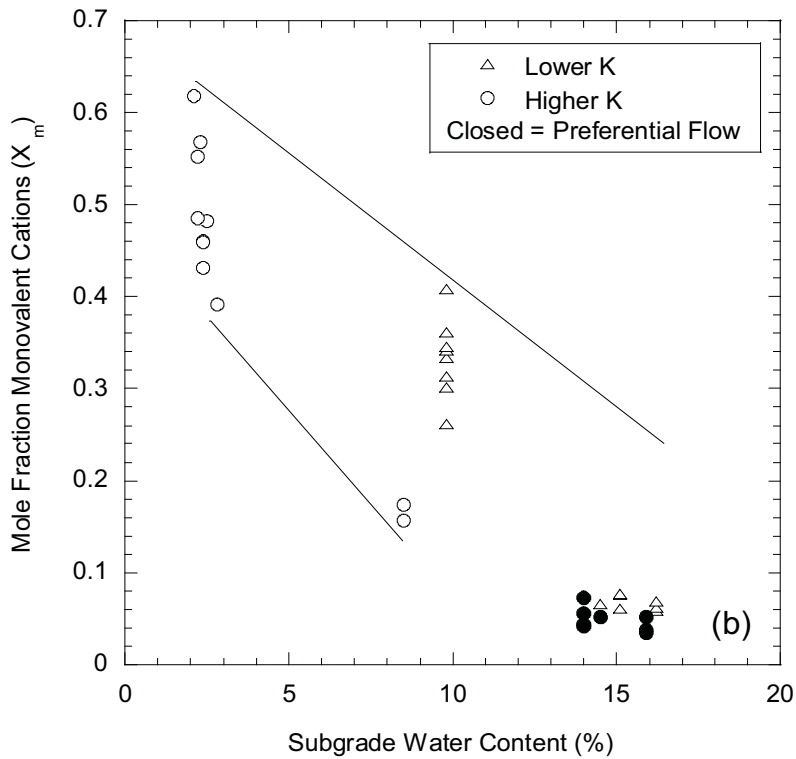
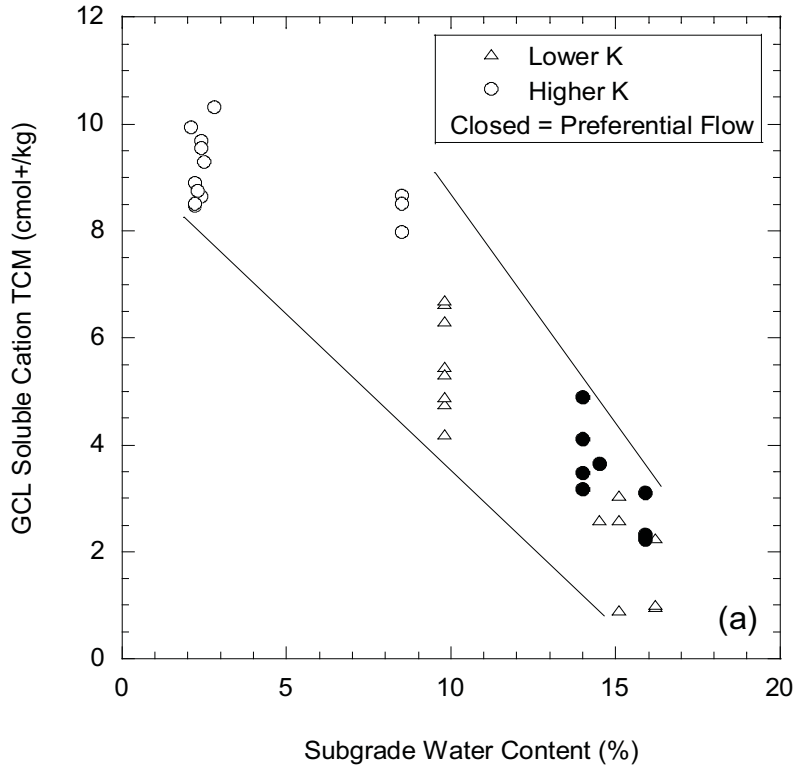


Fig. 7.7. TCM (a) and X_m (b) of GCL versus water content of subgrade. GCLs with lower K had hydraulic conductivities $< 5 \times 10^{-11}$ m/s, whereas GCLs with higher K had hydraulic conductivities $> 1 \times 10^{-9}$ m/s.

TCM (Fig. 7.7a) and lower X_m (Fig. 7.7b) were from subgrades having higher water content. Most importantly, when the GCLs with preferential flow are excluded, low hydraulic conductivity ($<5 \times 10^{-11}$ m/s) to SW was achieved consistently when the subgrade water content was at least 10%.

The subgrade also influences the total charge of soluble cations in the bentonite, but has less impact on the relative abundance of monovalent and divalent cations (Fig. 7.8). As shown in Fig. 7.8a, TCM of the GCL increases as TCM of the subgrade increases, but the relative abundance of monovalent and divalent cations in the GCL (as indicated by MDR) is nearly independent of the relative abundance in the subgrade (Fig. 7.8b). The GCLs with preferential flow are an exception; MDR for these GCLs is comparable to the MDR of the subgrade, which may indicate that these GCLs are closer to equilibrium than those without preferential flow (perhaps due to preferential flow). Most importantly, when GCLs with preferential flow are excluded, low hydraulic conductivity to SW is consistently obtained when the GCL has $\text{TCM} < 7 \text{ cmol}^+/\text{kg}$ and the subgrade pore water has $\text{TCM} < 0.8 \text{ cmol}^+/\text{kg}$. More dilute pore water in the GCL (lower TCM) promotes osmotic swelling of the bentonite, and therefore lower hydraulic conductivity to SW even if the Na on the bentonite has been replaced by divalent cations.

Type of subgrade was also evaluated as a factor that might contribute to the sensitivity of some GCLs to the type of permeant water. Hydraulic conductivity to SW and DW is shown in Fig. 7.9 as a function of the USCS classification of the subgrade. Greatest sensitivity to the permeant water was obtained for the subgrades classified as SM, SC, ML, and ML-CL. However, there is no apparent reason why soils having these classifications would be responsible for sensitivity to the type of permeant water.

7.2.4 Service Life and Cover Soil Thickness

Service life and thickness of the cover soil over the GM were evaluated as factors that may have contributed to sensitivity to the type of permeant water and the high hydraulic conductivity to SW. Hydraulic conductivity to SW and DW are shown as a function of service life and thickness of the cover soil in Fig. 7.10. There is no systematic relationship between the hydraulic conductivities to SW or DW and service life or thickness of the cover soil. High hydraulic conductivities to SW occurred for both the shortest (3.1 yr) and longest (6.7 yr) service lives, and low hydraulic conductivities to DW were observed across the full range of service lives.

7.3 Key Factors to Successful GCL Performance

The aforementioned discussion has shown that GCLs in composite barriers are altered by their environment even though they are covered by a GM. When GCLs that exhibit preferential flow paths are excluded, GCLs in composite barriers that are Hydrated sufficiently on a moist subgrade with modest TCM retain low hydraulic conductivity and are insensitive to water type. In contrast, GCLs that do not hydrate sufficiently and/or hydrate on a subgrade with lower water content and higher TCM can have high hydraulic conductivity to SW and can be very sensitive to water type.

This behavior is in marked contrast to new GCLs, which have essentially identical hydraulic conductivities to SW and DW when permeated for durations similar to the tests conducted in this study (< 30 d) (Jo et al. 2001, 2005, Kolstad et al. 2004). Moreover, the GCLs exhumed in this study have hydraulic conductivity to SW as much as four orders

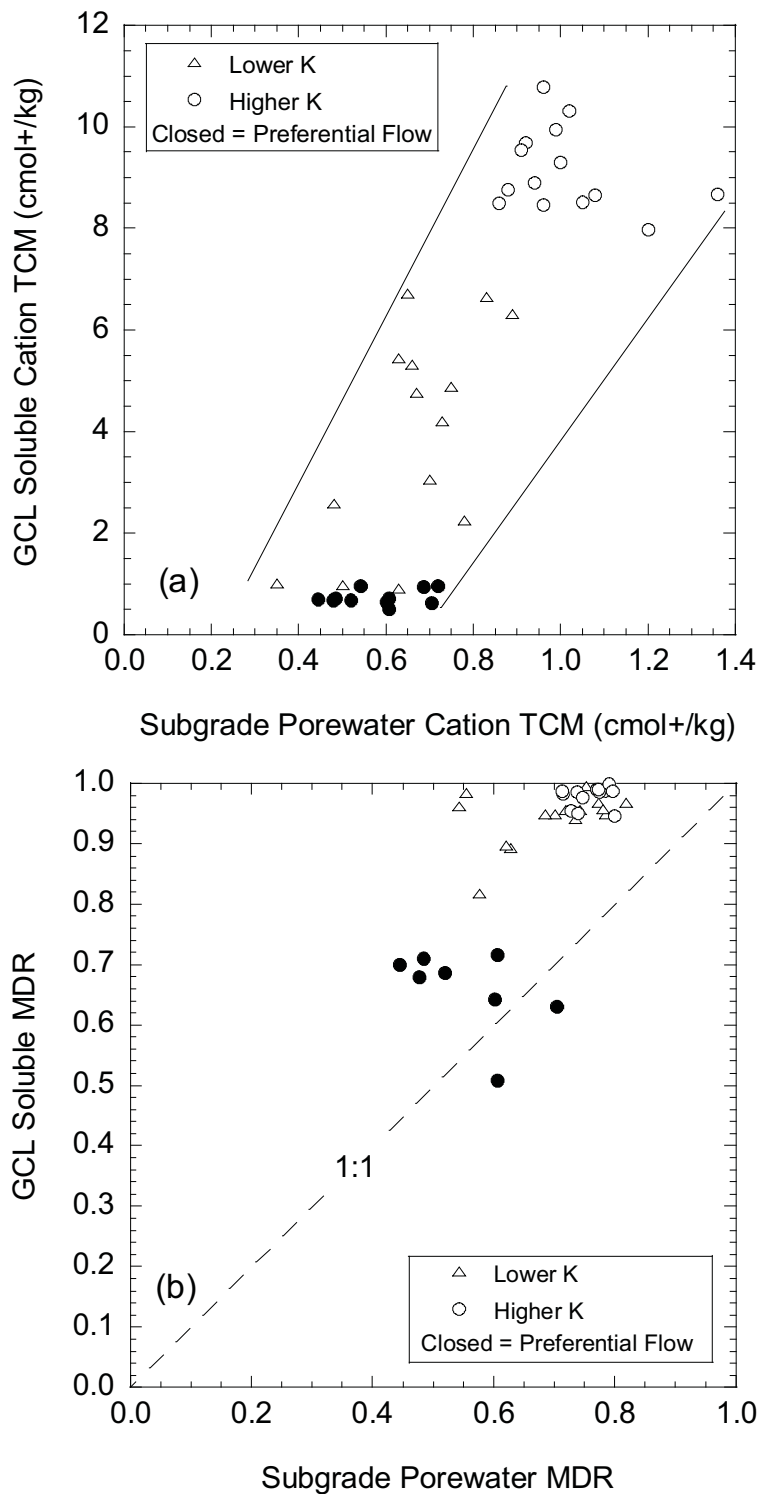


Fig. 7.8. TCM of GCL vs. TCM of subgrade (a) and MDR of GCL vs. MDR of subgrade (b). GCLs with lower K had hydraulic conductivities $< 5 \times 10^{-11}$ m/s, whereas GCLs with higher K had hydraulic conductivities $> 1 \times 10^{-9}$ m/s.

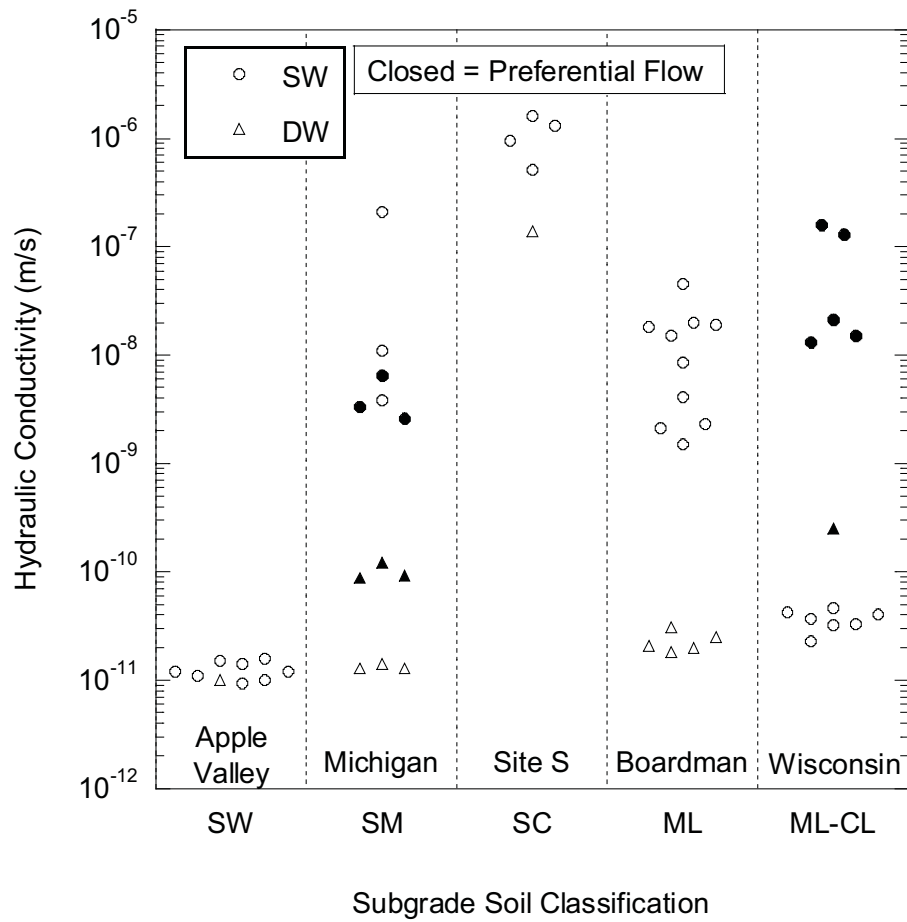


Fig. 7.9. Hydraulic conductivities of GCLs exhumed in this study as a function of USCS classification of subgrade. Compilation of data from Meer and Benson (2007) Site S and from this study.

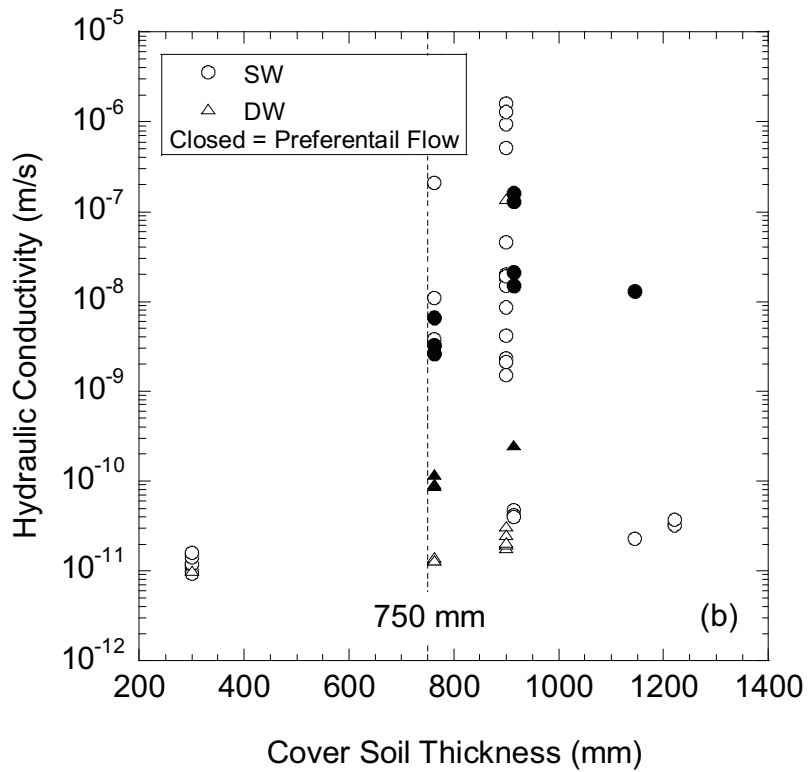
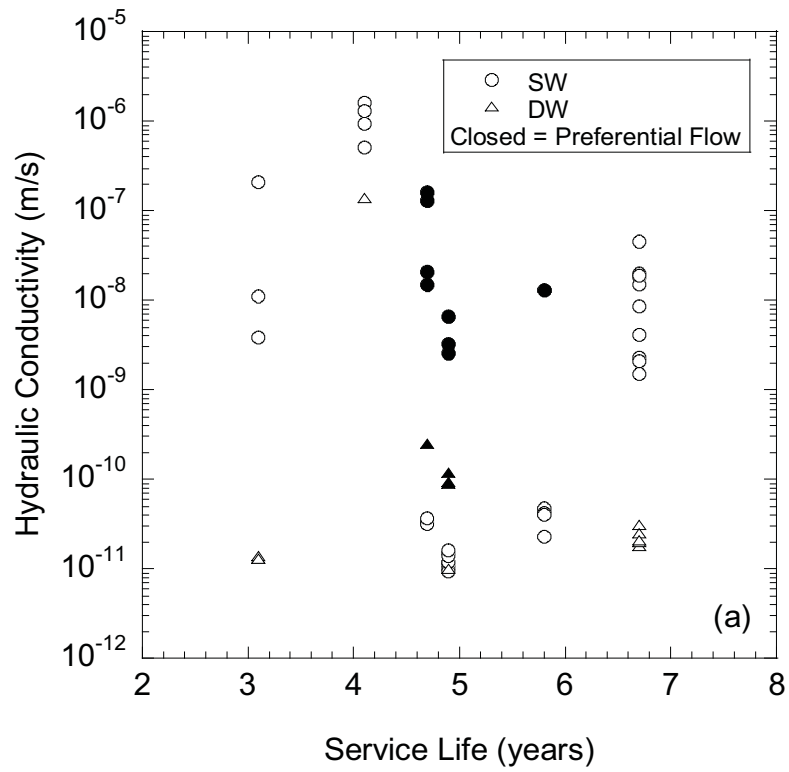


Fig. 7.10. Hydraulic conductivity of exhumed GCLs permeated with SW and DW vs. service life (a) and thickness of overlying soil (b). Data are from this study and Site S in Meer and Benson (2007).

of magnitude higher than the hydraulic conductivity reported after very long-term permeation with solutions similar to SW ($\sim 2 \times 10^{-10}$ m/s) that result in complete replacement of Na by Ca and/or Mg (Egloffstein 2001, Jo et al. 2005, Benson et al. 2007). These findings indicate that alterations that occur within composite barriers can introduce unique sensitivity to GCLs, and suggest that the sensitivity is affected by the hydration state. In a composite barrier, hydration of the GCL occurs gradually over a period of approximately 30 d as water migrates upward from the subgrade in the liquid and vapor phases. The amount of hydration depends on the water content of the subgrade (Daniel et al. 1993, USEPA 1996, Bradshaw 2008). If the subgrade is sufficiently moist to induce osmotic swelling of the bentonite (i.e., water content at least 35%) before divalent cations from the subgrade replace the Na, the swollen structure of the bentonite will be retained and permeation with SW or DW will yield low hydraulic conductivity (even if divalent cations in the permeant water replace Na in the bentonite). For example, at the Apple Valley and Wisconsin sites, the GCL had a water content > 53% and hydraulic conductivities to DW and SW in the range of 9×10^{-12} to 5×10^{-11} m/s, even though divalent cations replaced 48% of the Na (on average) at the Apple Valley site and 90% at the Wisconsin site (GCLs with preferential flow at Site E excluded). Moreover, the GCLs at the Apple Valley and Wisconsin sites exhibited the paste-like consistency of bentonite that had undergone osmotic swell (Fig. 7.11a) at exhumation. Pore water in the subgrade at the Apple Valley and Wisconsin sites (Table 7.3) was also more dilute ($\text{TCM} < 0.8 \text{ cmol}^+/\text{kg}$), which promotes osmotic swell.

In contrast, if the subgrade has insufficient moisture to promote or complete osmotic swell, and divalent cations replace a substantial portion of the Na in the bentonite, then the hydraulic conductivity of the GCL to SW can be orders of magnitude higher because osmotic swell is precluded as Ca in SW replaces the remaining Na in the bentonite. For example, the GCLs from the Boardman and Michigan (M-03) sites had water content < 46%, substantial replacement of Na by divalent cations, high hydraulic conductivity to SW, and a granular structure characteristic of a GCL that had not undergone osmotic swell (Fig. 7.11b). Pore water in these subgrades also was more concentrated ($\text{TCM} > 0.8 \text{ cmol}^+/\text{kg}$, Table 7.3), which inhibits osmotic swell.

The GCL from Site S in Meer and Benson (2007) and the GCLs from the Wisconsin and Michigan sites with preferential flow are exceptions. The data for these GCLs, which group together in Figs. 7.6a and 7.8b, are inconsistent with the data for the other GCLs. The GCL from Site S also did not have the paste-like consistency associated with bentonite that had undergone osmotic swell and contained cracks typically associated with wet-dry cycling (Fig. 7.12a). This GCL may have undergone hydration, cation exchange, and then dehydration, even though the GCL was overlain by a GM. However, information regarding the installation and service life of the GCL at Site S is insufficient to confirm whether this sequence of processes could have occurred. Because the GCL from Site S had relatively low X_m and SI (Fig. 7.2), the cracks probably did not swell shut during permeation and acted as preferential flow paths. Consequently, the GCL had similar hydraulic conductivity to SW and DW (Fig. 7.4). The GCLs with preferential flow paths from the Wisconsin and Michigan sites are highly unusual and are different from those at Site S. These GCLs had distinct preferential flow occur along bundles of needle-punching fibers (Fig. 7.12b). Mechanisms causing these flow paths were beyond the scope of this study, but cation exchange as water from the subgrade wicks upward through bundles of needle-punching fibers is a likely cause (Scalia 2009). Conditions leading to this phenomenon have not yet been identified.

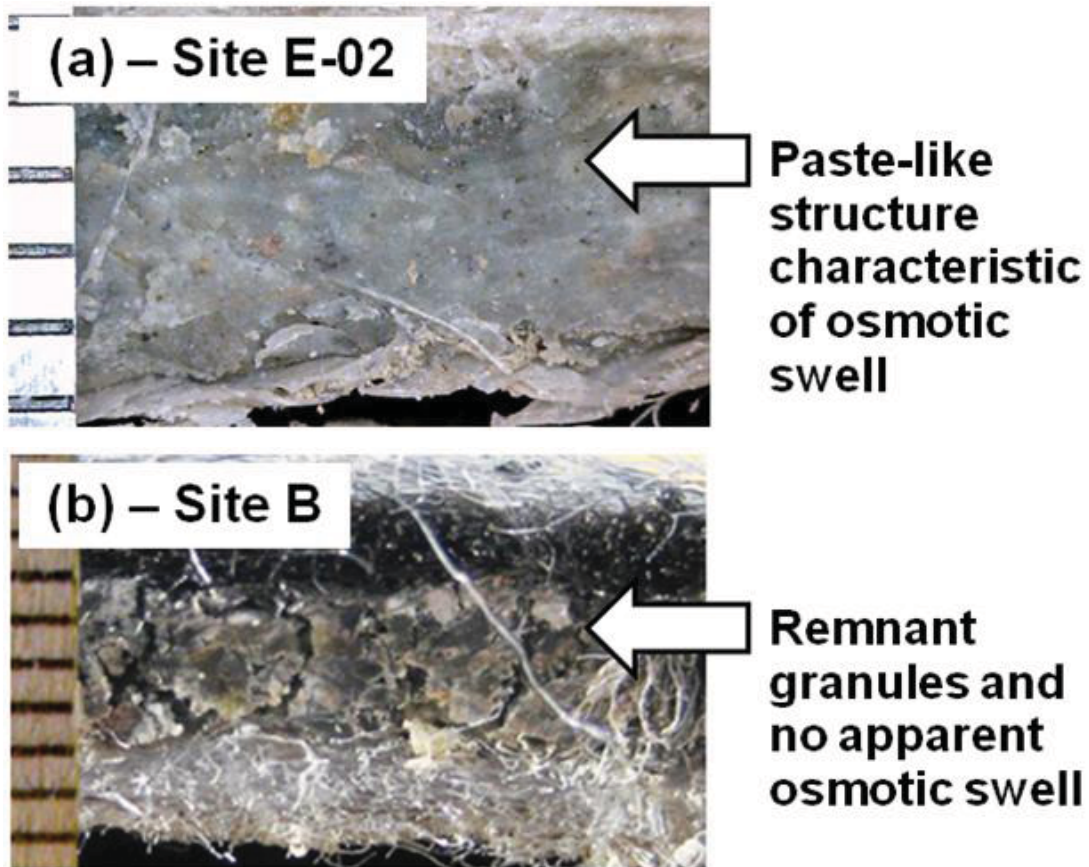


Fig. 7.11. Cross-sections of exhumed GCLs from Site E-02 (a) and Site B (b). Vertical scale in mm.

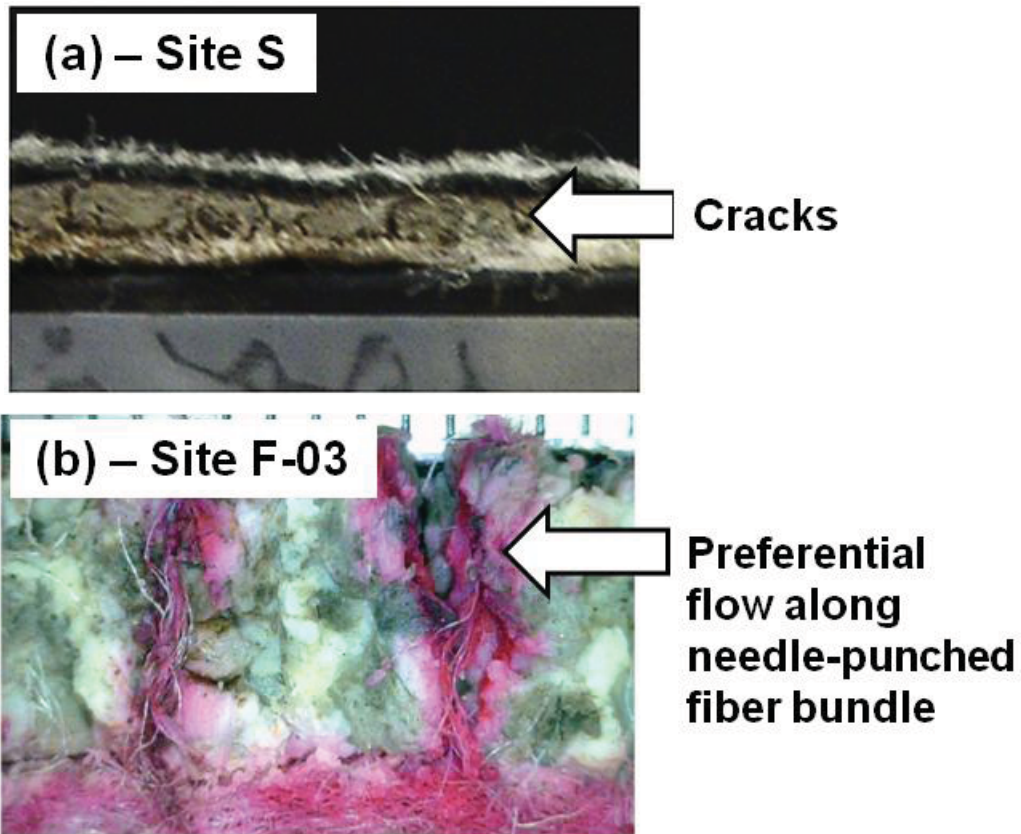


Fig. 7.12. Cross-sections of exhumed GCLs from Site S (a) and Site F-03 (b). Photo of GCL from Site S is from Meer (2004). Photo of GCL from Site F-03 is from after permeation with rhodamine WT dye. Vertical scale in mm.

7.4 Summary of Findings for GCLs

Based on the findings reported in this section, the following conclusions and recommendations are made regarding GCLs deployed in final covers:

1. Divalent cations will eventually replace the native Na in GCLs deployed in most composite barriers. Exchange appears to occur more rapidly and completely when the GCL is installed on a subgrade with higher water content.
2. GCLs hydrated to water content in excess of 50% tend to have low saturated hydraulic conductivity regardless of the amount of Na replaced by divalent cations or the type of permeant water. Therefore, conditions that promote rapid hydration to a water content > 50% are recommended to ensure that a GCL has low hydraulic conductivity regardless of the type of pore water migrating through the GCL.
3. The water content of GCLs exhumed from composite barriers is directly related to the water content of the subgrade underlying the GCL. Subgrades with water contents above 10% were associated with GCLs that had higher water contents (>50%) at exhumation. These GCLs also had low saturated hydraulic conductivity regardless of type of permeant water, unless the exhibited preferential flow paths. Subgrade compacted wet of optimum water content generally promote rapid hydration of bentonite in GCLs.
4. GCLs with more dilute pore water (lower GCL TCM) are associated with subgrades with more dilute pore water (lower subgrade TCM). GCLs that had low saturated hydraulic conductivity regardless of water type were exhumed from subgrades having TCM < 0.8 cmol⁺/kg.
5. Preferential flow was observed in some GCLs along bundles of needle-punched fibers. These GCLs had higher hydraulic conductivity to SW and DW and essentially complete replacement of Na by divalent cations. Conditions contributing to the formation of these flow paths have not been identified conclusively.
6. Subgrade with a minimum water content of 10% is recommended to ensure rapid hydration and osmotic swell in GCLs used in composite barriers. Provided that desiccation is prevented, GCLs placed under these conditions are likely to maintain low hydraulic conductivity (<5 x10⁻¹¹ m/s) to dilute permeant waters even after complete exchange of divalent for monovalent cations has occurred.
7. Even though cation exchange occurs in a GCL in a composite barrier, the GM still plays an important role by preventing desiccation and ensuring the integrity of a GCL. As shown in past studies, GCLs used as the sole barrier layer typically become very permeable within several years after installation, and cease functioning as a hydraulic barrier. GCLs that are not overlain by a geomembrane or geofilm should not be used in cover systems. However, when properly deployed, GCLs overlain by a geomembrane or geofilm function very effectively. Moreover, they are expected to function effectively so long as the geomembrane remains intact (i.e., the service life of the GCL is controlled by the service life of the geomembrane).

8. GEOMEMBRANES AND GEOSYNTHETIC DRAINAGE LAYERS

The conventional approach to estimate the change in engineering properties of geosynthetics during their service life is to apply a reduction (scaling) factor to the as-manufactured engineering properties to account for degradation mechanisms such as installation damage, creep, and clogging (Koerner 2005). Most of the reduction factors currently in use are estimates based on laboratory durability experiments or engineering judgment; little field data exist to confirm that scaling factors currently in use are consistent with conditions existing in the field. Despite this shortcoming, the field-performance record for final covers constructed with geosynthetic materials generally has been excellent (Bonaparte et al. 2002, Albright et al. 2004). Nevertheless, as more emphasis is placed on long-term performance assessments of waste containment facilities, greater reliance on reduction factors based on field performance data will be necessary (National Research Council 2007).

Engineering properties of geosynthetic drainage layers (GDLs) and geomembranes (GMs) exhumed from the ACAP test sections and the Wisconsin MSW landfill were evaluated in this part of the study. Locations from which the geosynthetics were obtained are shown in Fig. 8.1. GDLs from the Apple Valley, Cedar Rapids, Helena, Omaha, Polson, and Underwood sites were exhumed from the bottom of lysimeters. GDLs from the Altamont and Boardman sites were collected from the bottom of lysimeters and from the drainage layer above the GM in the cover. GDLs from the full-scale cover in Wisconsin were from the drainage layer above the GM in the cover. GM samples from the Cedar Rapids, Helena, and Underwood sites were collected from the bottom of lysimeters. GM samples from the Boardman and Omaha sites were from the bottom of lysimeters and from the barrier layer in the cover. Mechanical, hydraulic, and polymeric properties of the exhumed geosynthetics were measured in the laboratory and compared to MARVS reported by the geosynthetic manufacturers. Reduction factors were computed from the measured properties and the MARVs. The MARV was used as a surrogate in lieu of as-built properties, which were not available for all of the geosynthetics used to construct the lysimeters.

Photographs of the laboratory tests are in Appendix P. The mechanical test data are compiled in Appendix Q and the hydraulic test data are compiled in Appendix R. Data describing interface strengths between the GDLs and GMs are in Appendix S.

8.1 Properties of Geomembranes

8.1.1 Tensile Strength

Tensile properties of the exhumed GMs are summarized in Table 8.1. Break strengths from the narrow strip tests on the GMs are shown in Fig. 8.2. Strain at break and at yield from the narrow-strip tests is shown in Fig. 8.3. The horizontal solid line in each column represents the average narrow-strip break strength for each site. The horizontal line with arrows in each column represents the MARV break strength reported by the manufacturer. A distinct difference between the break strengths of the HDPE and LLDPE GMs was not observed. In fact, the range of break strengths for the LLDPE GMs encompasses the range of break strengths for the HDPE GMs.

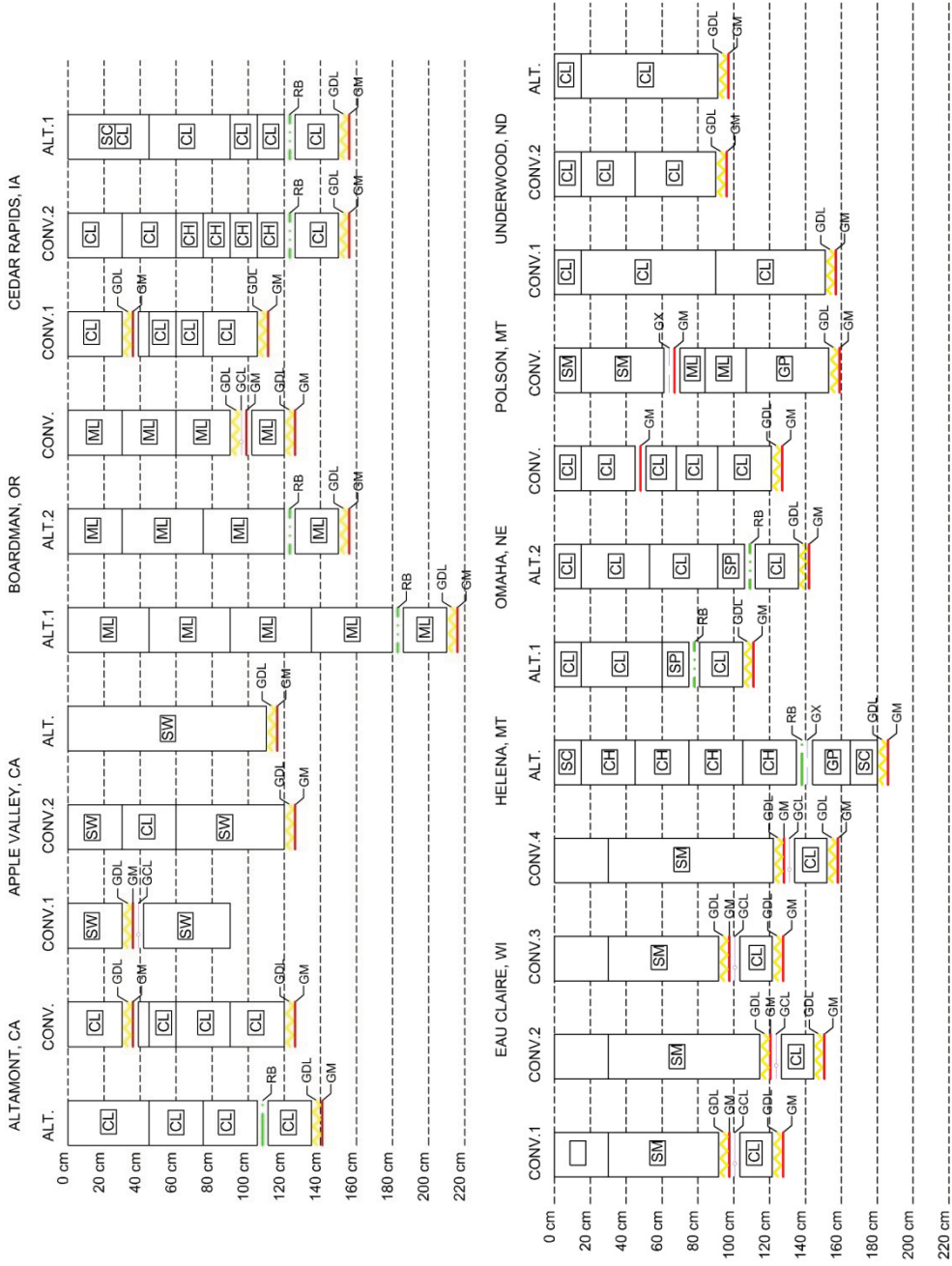


Fig. 8.1. Profiles of covers at sites where geosynthetics were exhumed. GCL = geosynthetic clay liner, GDL = geosynthetic drainage layer, GM = geomembrane, GX = geotextile, RB = root barrier.

Table 8.1. Tensile properties of exhumed GMs (average reported, range of property in parenthesis).

Location	No. of Specimens	Wide Strip Tensile Strength (N/m)			Narrow Strip Tensile Strength (N/m)		
		Yield Strength (N/m) average (min. - max.)	Yield Elongation (%) average (min. - max.)	Break Strength (N/m) average (min. - max.)	Yield Strength (N/m) average (min. - max.)	Yield Elongation (%) average (min. - max.)	Break Strength (N/m) average (min. - max.)
Altamont, CA	6	25200 (24,900 - 26,500)	17.4 (16.7 - 18.0)	30500 (26,000 - 31,800)	9.3 (7.7 - 10.4)	46100 (38,100 - 50,900)	600.0 (507.4 - 651.30)
Apple Valley, CA	9	28200 (26,900 - 29,900)	15.4 (14.7 - 15.8)	29670 (24,200 - 33,800)	7.1 (6.4 - 7.8)	30800 (20,300 - 39,600)	380.3 (158.2 - 511.4)
Boardman, OR	9	17200 (15,700 - 17,900)	18.5 (17.1 - 19.8)	11400 (9600 - 12,800)	6.4 (5.1 - 7.6)	27300 (20,700 - 35,900)	468.9 (407.8 - 562.1)
Cedar Rapids, IA	9	18500 (17,900 - 19,000)	26.8 (23.1 - 33.5)	17200 (13,500 - 19,800)	9.8 (7.7 - 10.4)	35800 (32,300 - 40,200)	465.9 (406.7 - 495.5)
Wisconsin	12	13900 (12,900 - 14,900)	22.3 (17.9 - 34.9)	12300 (9200 - 15,500)	8.0 (3.6 - 11.7)	27900 (16,200 - 34,900)	412.8 (187.9 - 587.2)
Helena, MT	3	17300 (16,700 - 17,700)	17.8 (18.3 - 26.9)	18400 (17,900 - 18,800)	8.6 (7.7 - 9.1)	23800 (20,800 - 27,700)	393.6 (357.0 - 443.3)
Omaha, NE	12	20500 (17,800 - 23,000)	19.7 (11.2 - 30.0)	20300 (14,000 - 24,400)	8.2 (5.1 - 10.3)	37900 (7000 - 53,400)	487.6 (12.0 - 593.8)
Polson, MT	3	23200 (21,600 - 25,900)	16.5 (15.4 - 18.0)	25700 (24,400 - 27,500)	7.7 (6.4 - 9.0)	25300 (14,500 - 31,100)	281.9 (73.1 - 431.5)
Underwood, ND	9	21100 (20,200 - 22,100)	36.0 (23.6 - 49.5)	22800 (20,400 - 26,400)	11.7 (10.3 - 13.1)	52500 (46,200 - 58,200)	536.2 (500.9 - 584.8)

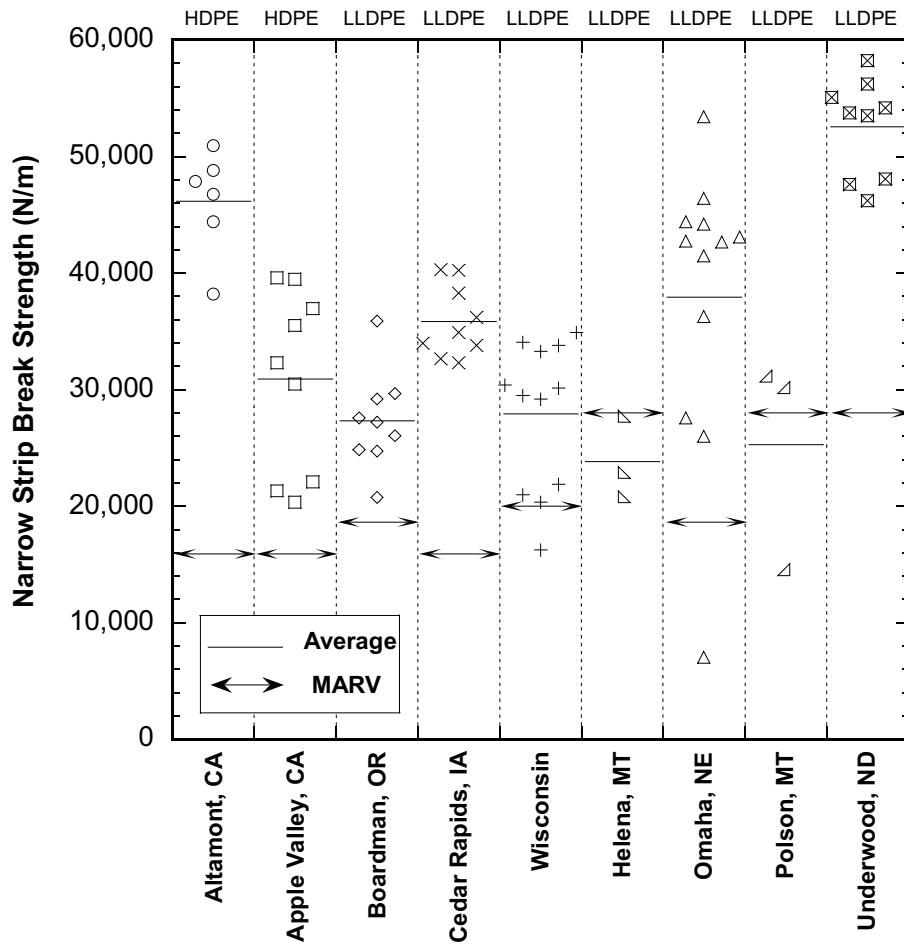


Fig. 8.2. Narrow strip break strengths for the geomembrane samples. Horizontal bars in each column represent the average for the data in the column. Polymer types are noted at the top of each column. Two headed arrows represent manufacturer's MARV.

At all sites except Helena and Polson, the average narrow-strip break strength is higher (1.4 to 2.9 times) than the MARV tensile strength. In contrast, the average narrow strip break strength was 0.8 and 0.9 times the MARV break strength for the GMs from Helena and Polson. Individual tests also had break strengths below the MARV at the Wisconsin and Omaha sites (one test each), even though the average narrow-strip break strength at these sites was greater than the MARV break strength. These specimens, along with the specimens from Helena and Polson, were examined to determine if these GMs had visible defects that may have contributed to their lower tensile strength. However, no defects were evident. The average break strain exceeded the MARV break strain at all sites except Helena, Polson, and Wisconsin (Fig. 8.3). Helena and Polson also exhibited narrow-strip break strengths lower than the MARV.

Yield and break strengths determined from the narrow-strip and wide-strip tensile tests are compared in Fig. 8.4. Yield strengths determined by both test methods are similar, regardless of the polymer. However, higher yield strengths were obtained for the HDPE GMs than the LLDPE GMs. On average, the yield strength from the narrow-strip test is the same as the yield strength from the wide-strip test, and 100% of the narrow-strip yield strengths fall within a factor of 2 of the wide-strip strengths. The exception is for low strengths, where higher yield strengths were obtained from the wide-strip method than the narrow-strip method. Defects incurred while the GM was in service may have contributed to these lower yield strengths from the narrow-strip method. These specimens also broke at lower strains, which is indicative of a defect.

8.1.2 OIT and MFI

Polymer properties of the GMs are summarized in Table 8.2. The comparison with the MARVs suggest that most of the GMs maintained properties exceeding the minimum standard reported by the manufacturer during their service life (GMs from the Helena, Polson, and Wisconsin sites are exceptions). This finding is supported by the MFI and OIT data in Fig. 8.5 (as done previously, a solid horizontal line represents the average for the site and a horizontal line with arrows represents the MARV). MFI is an indicator of polymer degradation, and becomes larger as chain-scission reactions produce smaller polymer molecules (Grassie and Scott 1985). OIT represents the amount of antioxidant inhibitor available within the GM to prevent chain scission in response to oxidation.

For those sites where MARVs were available, MFIs of the exhumed GMs are similar to the MARV. MFIs exceeding the MARV were recorded at the Wisconsin and Underwood sites. The retention of OIT, as shown in Fig. 8.5a, indicates that a significant amount of antioxidant was retained and inhibited polymer degradation. This retention of antioxidant is consistent with the absence of a noticeable increase in MFI.

OIT of the exhumed GMs is shown as a function of service life in Fig. 8.6. The OIT data in Fig. 8.6 are normalized relative to the MARV OIT (130 min) reported by the manufacturer of the HDPE and LLDPE GMs used at the Wisconsin, Helena, Polson, and Underwood sites. Antioxidant depletion rates for the exhumed LLDPE and HDPE GMs were determined assuming that antioxidant loss occurs in accordance with first-order kinetics (Hsuan and Koerner 1998, Sangam 2002):

$$\text{OIT}_t = \text{OIT}_0 e^{-St} \quad (8.1)$$

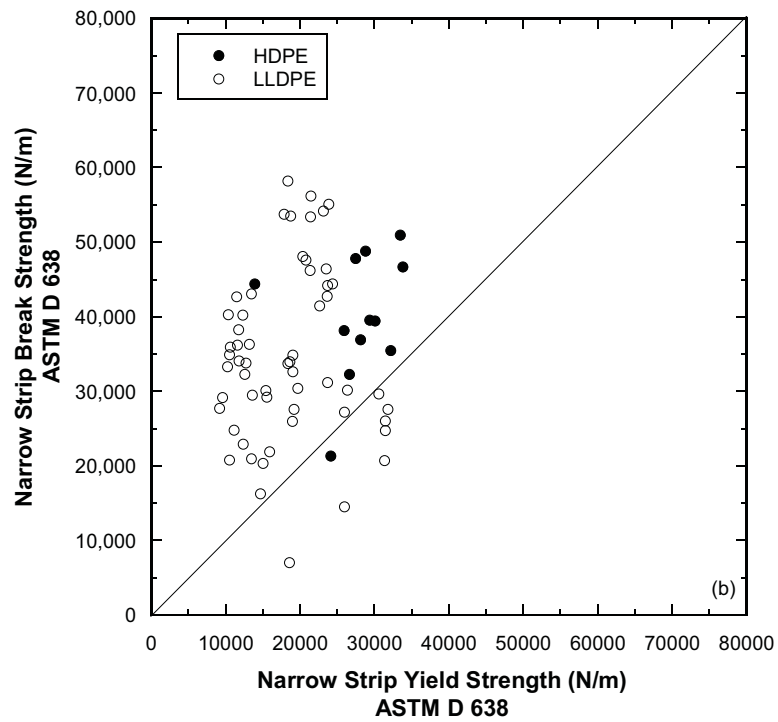
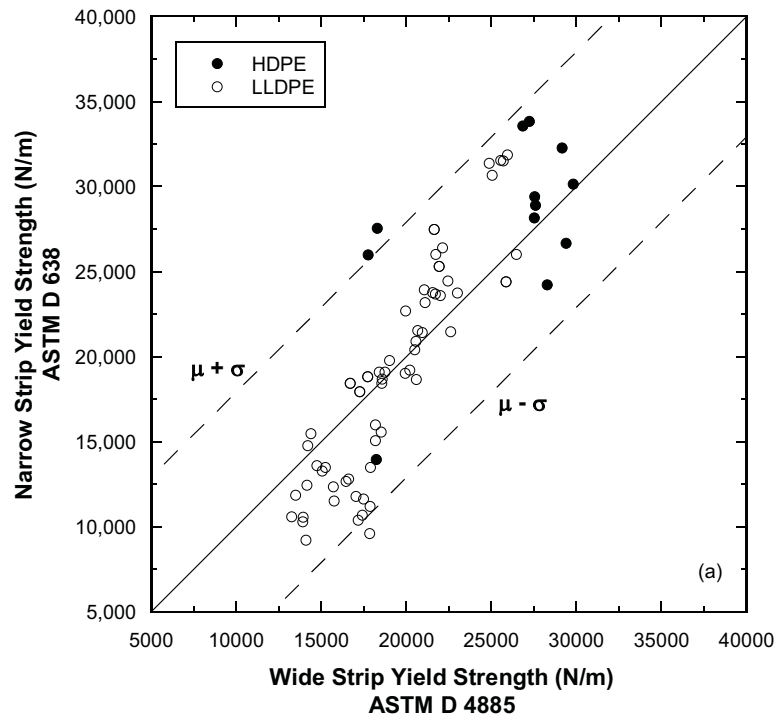


Fig. 8.4 Comparison between narrow-strip and wide-strip yield strengths (a) and narrow strip break and narrow strip yield strengths (b).

Table 8.2. Melt flow index (MFI) and oxidation induction time (OIT) of exhumed GMs (average reported, range of property in parenthesis).

Location	No. of Specimens	Melt Flow Index (MFI) (g/10min)	Oxidation Induction Time (OIT) (min)
		average min. - max.	average
Altamont, CA	1	0.20 -	74 -
Apple Valley, CA	1	0.24 -	79 -
Boardman, OR	1	0.40 -	102 -
Cedar Rapids, IA	1	0.32 -	120 -
Wisconsin	4	0.38 (0.35 - 0.39)	112 (106 - 118)
Helena, MT	1	0.24 -	78 -
Omaha, NE	1	0.45 -	101 -
Polson, MT	1	0.20 -	80 -
Underwood, ND	1	0.37 -	129 -

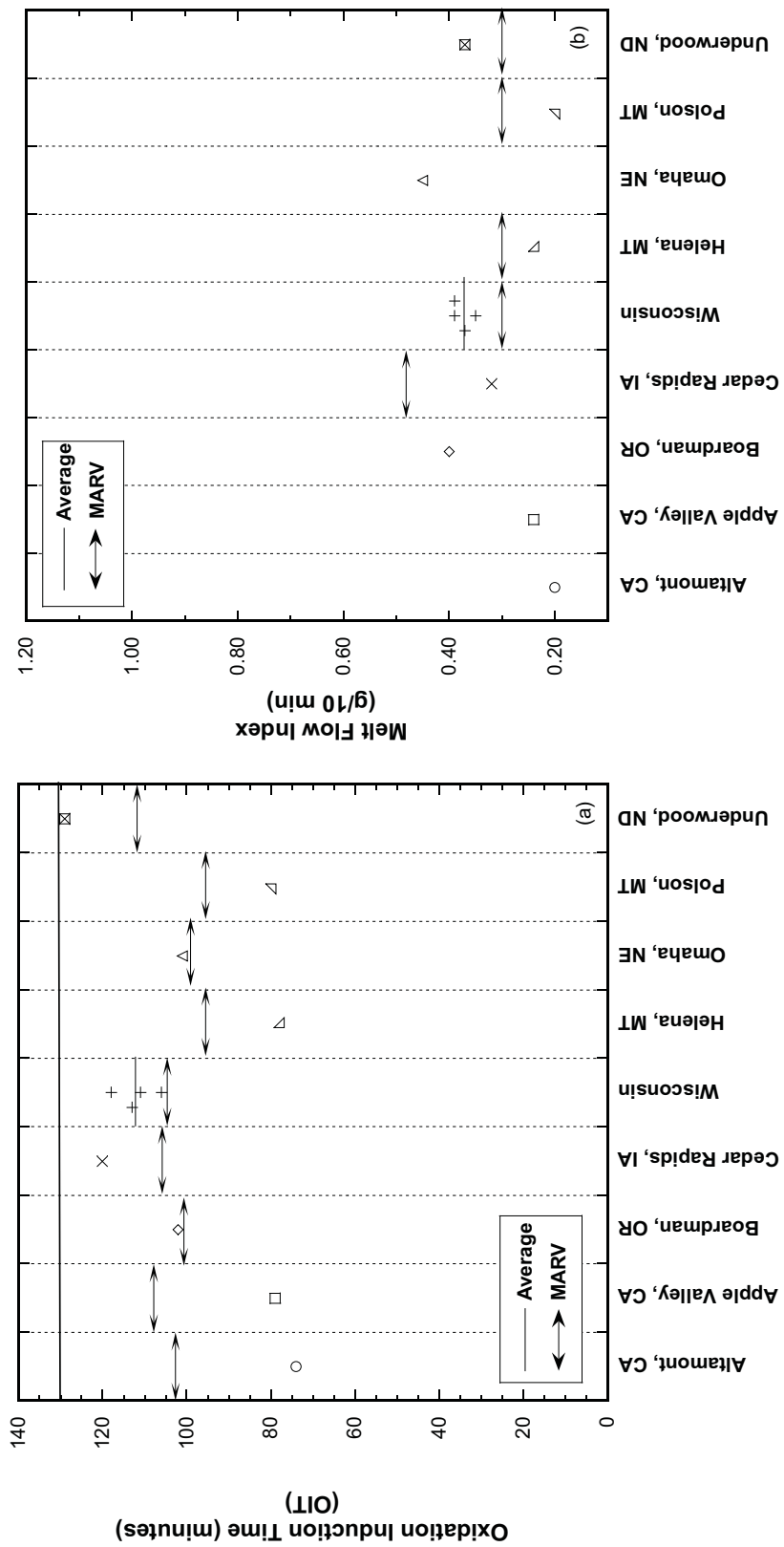


Fig. 8.5. Oxidation induction time (OIT) (a) and melt flow index (MFI) (b) for the geomembrane. OIT and MFI were measured by TRI Environmental, Inc. of Austin, Texas. Horizontal bars in each column represent the average for the data in the column. Solid line at 130 min in OIT graph represents the manufacturers' MARV. Two headed arrows represent the OIT estimates of the exhumed samples calculated by the Arrhenius equation.

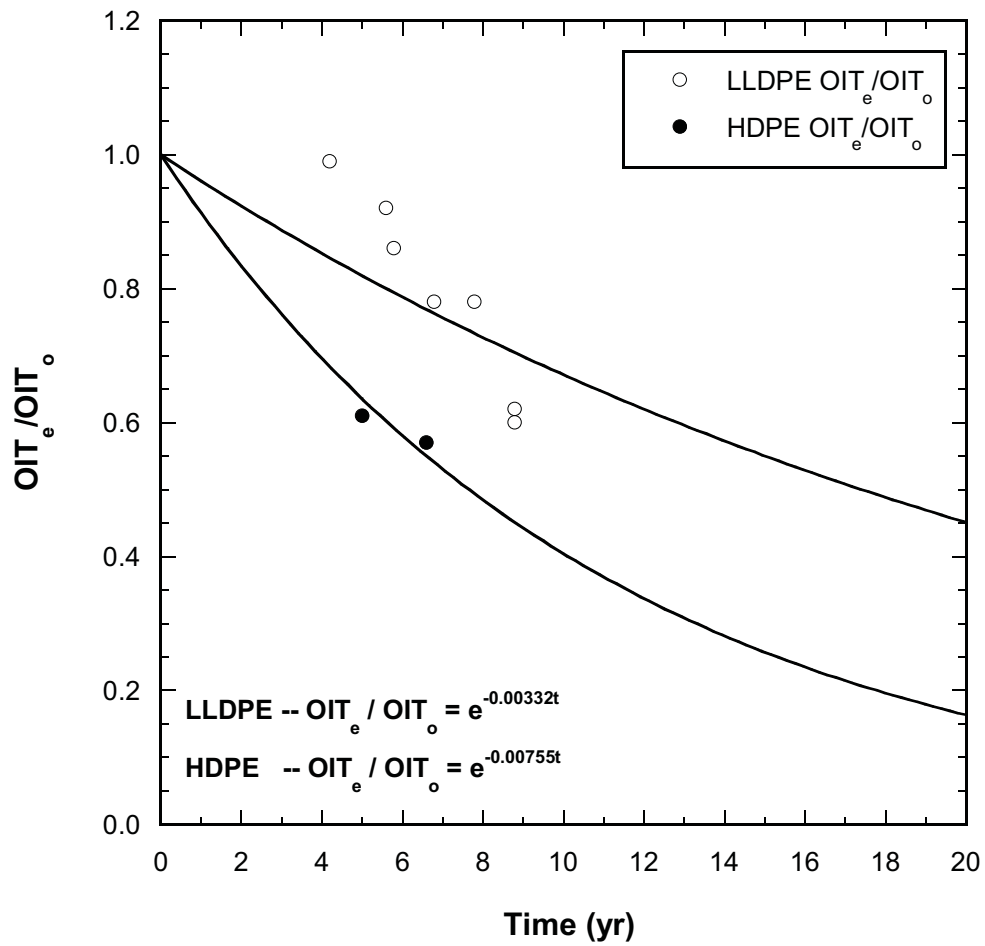


Fig. 8.6. OIT of exhumed geomembranes normalized by MARV and OIT as a function of time. OIT_e = exhumed OIT. OIT_o = MARV OIT.

where S = the first-order depletion rate, OIT_0 is the initial OIT (assumed = 130 min), and OIT_t is the OIT at time = t . Non-linear least-squares regression yielded a depletion rate of 0.0076 1/month for the HDPE GMs and 0.0033 1/month for the LLDPE GMs. Because the data set is limited and the initial OIT was not known, these depletion rates are considered to be estimates. Moreover, use of ASTM D 3895 to determine the depletion rates may have resulted in an over-estimate of the amount of antioxidant depletion. Despite these shortcomings, the depletion rates shown in Fig. 8.6 are consistent with depletion rates reported by others for HDPE GMs immersed in water at 15 °C, which range between 0.0029 and 0.0053 1/month (Hsuan and Koerner 1998, Sangam and Rowe 2002, Gulec et al. 2004). Thus, they are considered to be reasonable, if not precise.

8.2 Properties of Geocomposite Drainage Layer

8.2.1. Transmissivity

Transmissivities and permittivities of the exhumed GDLs are summarized in Table 8.3. Exhumed samples of the GDL from Apple Valley and Polson were not large enough to conduct transmissivity tests. Thus, transmissivity data for these sites are not available. At a given site, the transmissivity varies by at most a factor of 9 (24 kPa), 6 (48 kPa), or 5 (480 kPa). The average transmissivity varies less than a factor of 6 between the test sites at a confining stress of 48 kPa, and the differences between sites are larger at higher stresses. For example, as the stress is increased from 24 kPa to 48 kPa, the ratio of highest to lowest average transmissivity increases from 3.2 to 3.4. Similarly, from 48 kPa to 480 kPa, the ratio increases from 3.4 to 5.9.

Transmissivity of the GDL at a hydraulic gradient of 1 is shown in Fig. 8.7 for confining stresses of 24 and 480 kPa. Averages are shown in Fig. 8.7 with a solid horizontal line, and the MARV is shown as a line with arrows. MARVs at the test gradient (1.0) and at 480 kPa confining stress were only available for the Wisconsin, Helena, and Underwood sites. MARVs for Altamont, Boardman, Cedar Rapids, and Omaha were reported for a gradient of 0.1 and for a confining stress of 100 kPa. However, all GDLs were tested at the same stresses and a unit gradient. Thus, for the Altamont, Boardman, Cedar Rapids, and Omaha sites, the transmissivities are graphed as a function of confining stress and shown along with the MARV at 100 kPa (Fig. 8.8). As shown in Figs. 8.7 and 8.8, transmissivities of the exhumed GDLs are below the MARV for all sites except Cedar Rapids. For the MARVs reported at a gradient of 1.0 and 480 kPa, the average transmissivity of the exhumed GDL was 1.6 to 2.6 times lower than the MARV. For the other sites, the average transmissivities were approximately equal to the MARV (Cedar Rapids) or approximately 5 times lower than the MARV (Altamont, Boardman, and Omaha).

Modest amounts of soil were present in many of the geotextiles, and the geonets contained a coating of fines in some cases, but there was not direct relationship between the presence of soil particles and transmissivity. Soil type overlying the GDL was explored as a factor contributing to the variation in average transmissivity between the sites. Transmissivity of the GDL could not be related systematically to soil classification of the cover soil. The Altamont, Boardman, Cedar Rapids, Omaha, and Underwood sites had fine-grained soil (CL) over the GDLs, and these sites also had the minimum (Altamont) and maximum (Cedar Rapids) transmissivity under 48 and 480 kPa. The effect of fines content of the cover soil on the transmissivity is shown in Fig. 8.9. Each point represents the site average

Table 8.3. Transmissivities and permittivities of exhumed GDLs (average reported, range of property in parenthesis).

Location	Transmissivity (m ² /s)				Permittivity (s ⁻¹)		
	No. of Specimens	24 kPa	48 kPa	480 kPa	No. of Specimens	10 mm head	50 mm head
Altamont, CA	12	1.4x10 ⁻⁴ (3.5x10 ⁻⁵ - 3.3x10 ⁻⁴)	8.2x10 ⁻⁵ (3.1x10 ⁻⁵ - 1.7x10 ⁻⁴)	2.7x10 ⁻⁵ (1.3x10 ⁻⁵ - 9.7x10 ⁻⁵)	12	0.69 (0.48 - 0.83)	0.48 (0.20 - 0.58)
Apple Valley, CA	-	-	-	-	4	1.00 (0.87 - 1.11)	0.79 (0.74 - 0.84)
Boardman, OR	9	1.6x10 ⁻⁴ (5.7x10 ⁻⁵ - 3.4x10 ⁻⁴)	1.0x10 ⁻⁴ (4.3x10 ⁻⁵ - 1.6x10 ⁻⁴)	4.7x10 ⁻⁵ (2.3x10 ⁻⁵ - 7.9x10 ⁻⁵)	8	0.64 (0.42 - 0.90)	0.54 (0.39 - 0.70)
Cedar Rapids, IA	6	3.3x10 ⁻⁴ (2.8x10 ⁻⁴ - 4.8x10 ⁻⁴)	2.8x10 ⁻⁴ (1.8x10 ⁻⁴ - 3.9x10 ⁻⁴)	1.6x10 ⁻⁴ (8.4x10 ⁻⁵ - 2.3x10 ⁻⁴)	4	1.07 (0.57 - 1.47)	0.83 (0.62 - 1.01)
Wisconsin	42	4.5x10 ⁻⁴ (1.9x10 ⁻⁴ - 1.6x10 ⁻³)	-	1.4x10 ⁻⁴ (6.2x10 ⁻⁵ - 2.8x10 ⁻³)	56	0.58 (0.21 - 1.19)	0.41 (0.11 - 0.76)
Helena, MT	3	2.4x10 ⁻⁴ (2.3x10 ⁻⁴ - 2.5x10 ⁻⁴)	2.3x10 ⁻⁴ (2.2x10 ⁻⁴ - 2.3x10 ⁻⁴)	1.3x10 ⁻⁴ (1.3x10 ⁻⁴ - 1.4x10 ⁻⁴)	4	1.21 (0.72 - 2.23)	0.49 (0.26 - 0.70)
Omaha, NE	9	1.6x10 ⁻⁴ (1.0x10 ⁻⁴ - 2.3x10 ⁻⁴)	1.4x10 ⁻⁴ (8.2x10 ⁻⁵ - 2.2x10 ⁻⁴)	7.4x10 ⁻⁵ (3.9x10 ⁻⁵ - 1.2x10 ⁻⁴)	12	0.54 (0.20 - 0.96)	0.34 (0.07 - 0.60)
Underwood, ND	9	2.3x10 ⁻⁴ (1.3x10 ⁻⁴ - 4.2x10 ⁻⁴)	2.1x10 ⁻⁴ (1.2x10 ⁻⁴ - 3.6x10 ⁻⁴)	8.9x10 ⁻⁵ (4.6x10 ⁻⁵ - 1.6x10 ⁻⁴)	12	0.89 (0.40 - 1.13)	0.53 (0.15 - 0.77)

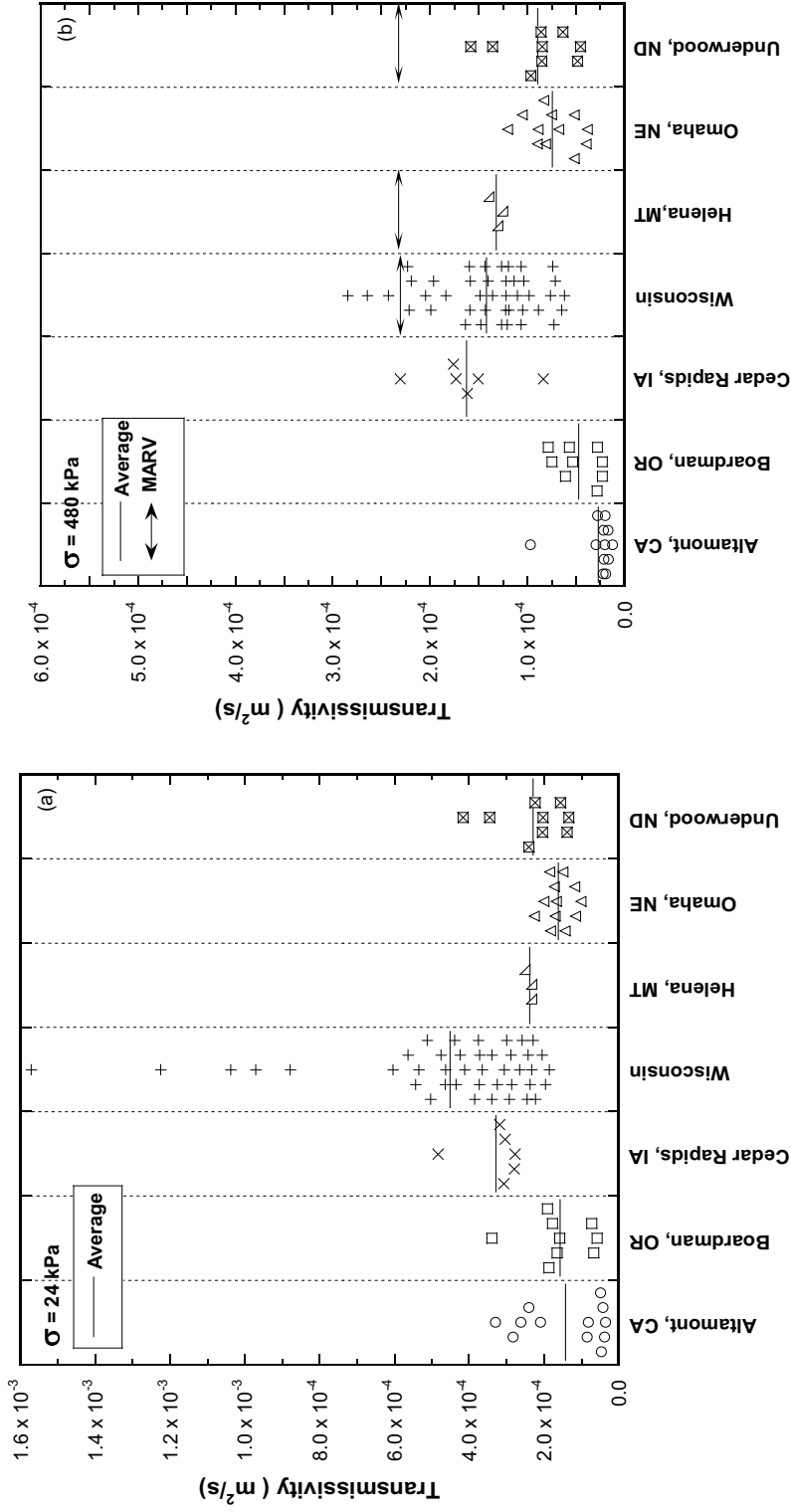


Fig. 8.7. Transmissivity of GDL under normal stress of 24 kPa (a) and 480 kPa (b). Horizontal bars in each column represent the average for data in the column.

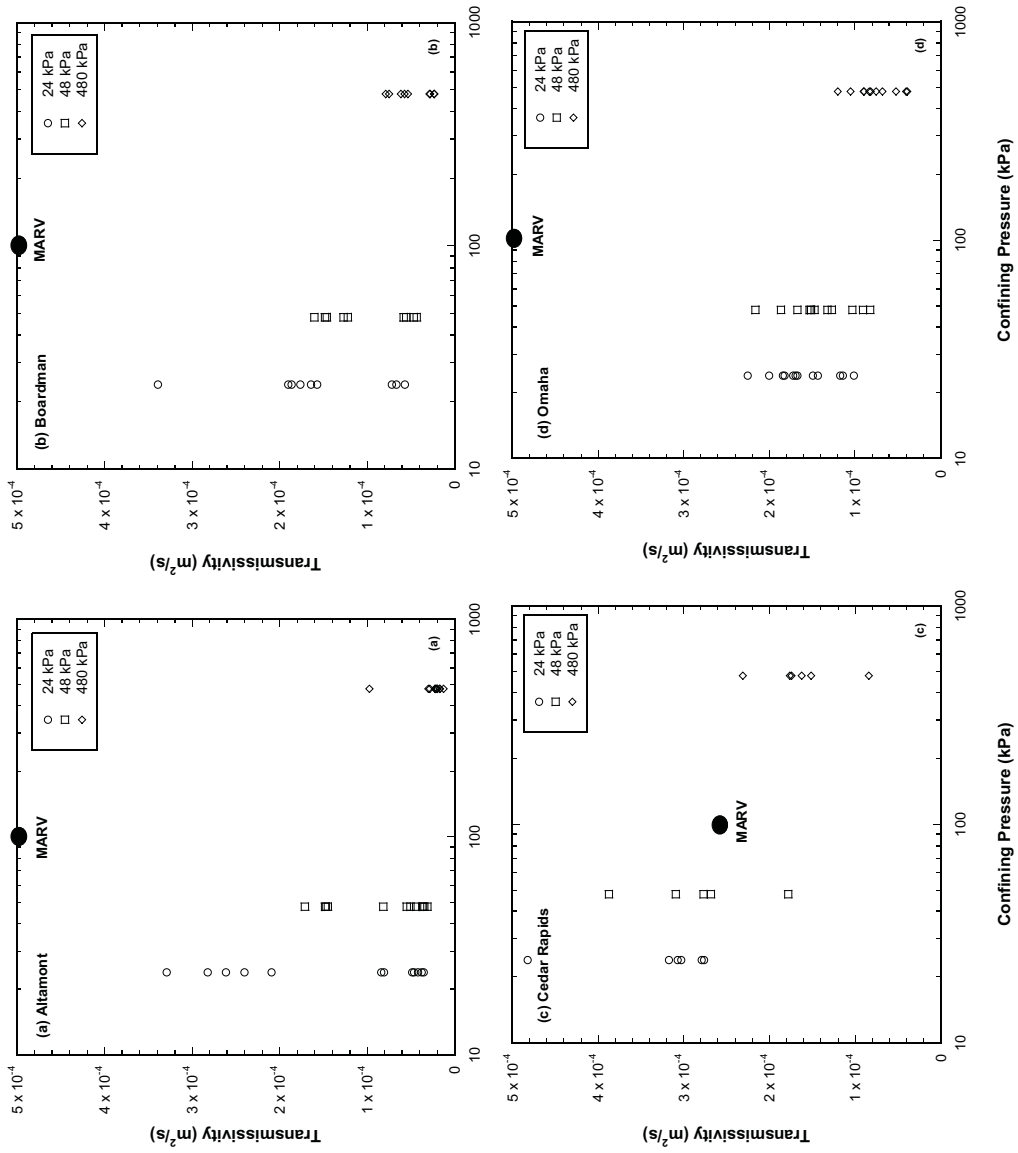


Fig. 8.8 Transmissivity of exhumed GDLs as a function of stress and MARV transmissivities for Altamont (a), Boardman (b), Cedar Rapids (c), and Omaha (d).

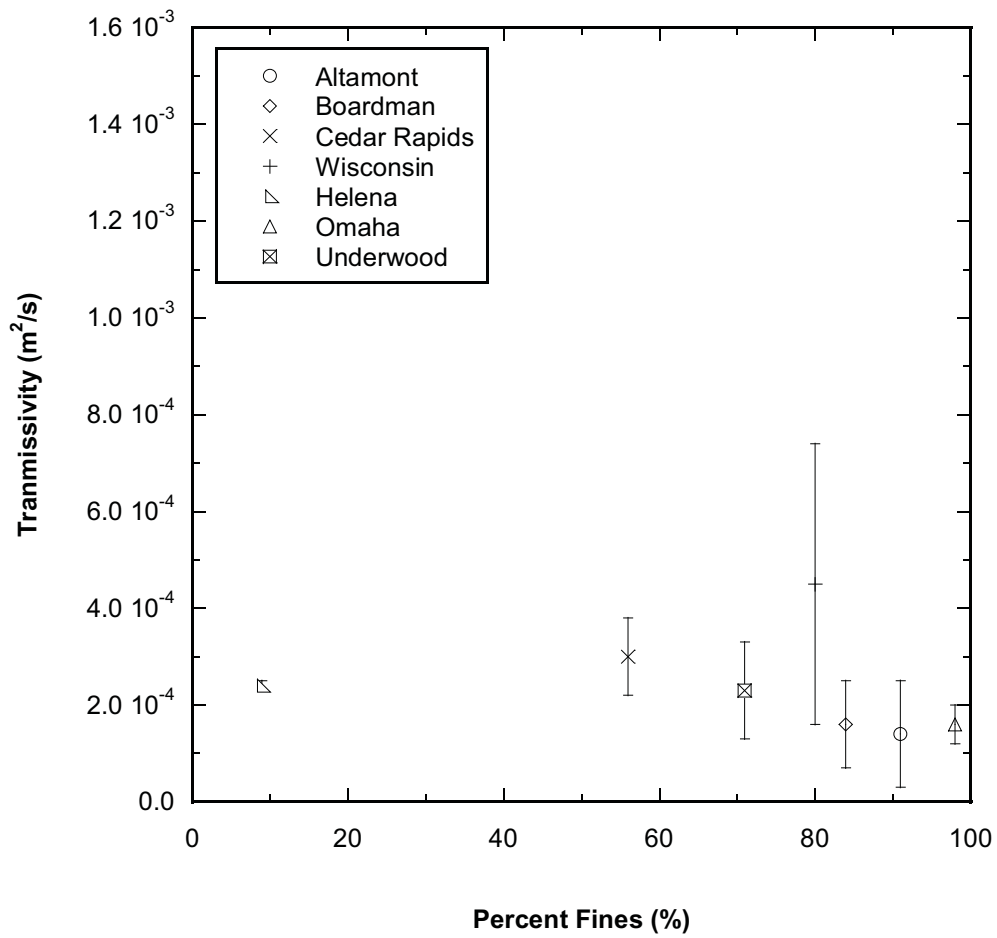


Fig. 8.9. Site average transmissivity of GDL as a function of percent fines of the cover soil. Error bars represent one standard deviation from the mean

transmissivity and the error bars correspond to one standard deviation from the mean. There is a slight decrease in transmissivity with increasing percent fines when the fines content is greater than 50%.

The apparent opening size (AOS) of the GT component of the exhumed GDLs ranged between 0.18 and 0.21 mm, which meets the conventional filtration design criteria reported in Koerner (2005) for both coarse and fine-grained soils (AOS < 0.6 mm for soils with < 50% fines; < 0.3 mm for > 50% fines). The absence of clogging of the GDLs suggests that this relatively simple method for filtration design of GTs is sufficient for final covers.

8.2.2. Permittivity

Permittivity of the GDL at each site is shown in Fig. 8.10 with a solid horizontal line, The MARV is shown as a line with arrows. The permittivity at each site ranged nearly one order of magnitude both at 10 mm head and 50 mm head. Samples from Apple Valley, Cedar Rapids, and Helena had slightly higher permittivities (1.00 , 1.07 , and 1.21 s^{-1}) under 10 mm head than those from other sites. The same trend was observed for the permittivities under 50 mm head at Apple Valley and Cedar Rapids (0.79 s^{-1} and 0.83 s^{-1}), but not for Helena. The average permittivity at each site ranges between 0.54 s^{-1} and 1.21 s^{-1} for 10 mm head and 0.34 s^{-1} and 0.83 s^{-1} for 50 mm head.

As with transmissivity, there was no apparent effect of soil classification on permittivity of the exhumed GDLs, but there was a slight trend with percent fines in the cover soil (Fig. 8.11). Each point in Fig. 8.11 represents the site average permittivity and the error bars represent one standard deviation from the mean. For fines content greater than 50%, the permittivity decreases slightly with percent fines.

MARVs were only available for the GDLs from the Wisconsin, Helena, and Underwood sites. For these sites, the average permittivity of the GDL was 3.8 and 4.6 times lower than the MARV permittivity.

8.2.3. Ply Adhesion

Ply adhesions of the exhumed GDLs are shown in Fig. 8.12 and tabulated in Table 8.4. Site averages are shown on the graphs with a solid horizontal line, and the MARV is shown as a line with arrows. MARVs were not available for the Altamont, Apple Valley, Boardman, and Omaha sites. The average ply adhesion for the Cedar Rapids, Helena, and Underwood sites range between 1.1 and 3.2 times higher than the MARV. For the Wisconsin site, the average ply adhesion is 1.2 times lower than the MARV.

Ply adhesion varies by as much as a factor of 33 at each site, and the average ply adhesion ranges between 290 and 840 N/m between sites. These averages may be grouped into three categories: high (740 – 840 N/m; Altamont, Boardman, and Underwood), medium (420-570 N/m; Wisconsin and Helena), and low (290-350 N/m, Apple Valley, Cedar Rapids, and Omaha). Uneven bonding between the geonet and geotextile was a key factor affecting the ply adhesion. Inspection prior to testing showed that the bond between the geotextile and geonet had separated in some regions, and specimens with greater bond separation had lower ply adhesion. In addition, for the specimens with low ply adhesion, a clean

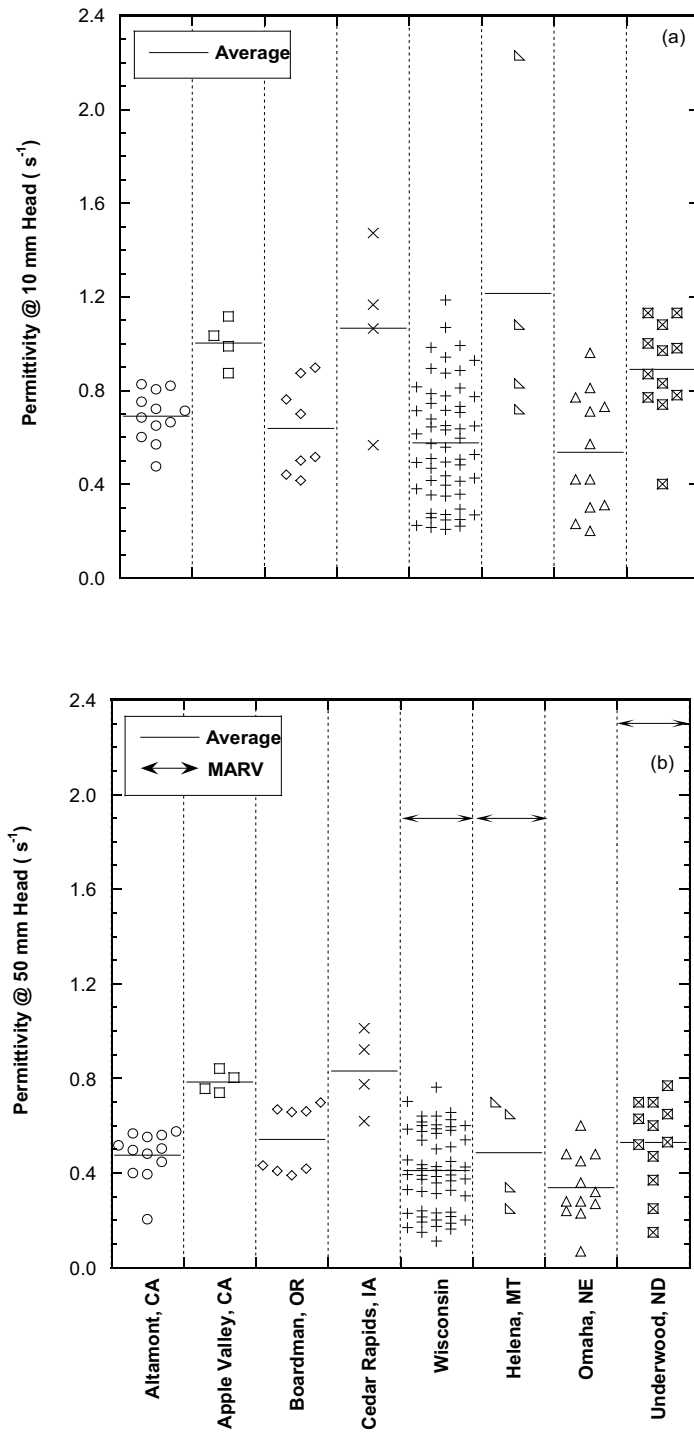


Fig. 8.10. Permittivity of GDL using 10 mm head (a) and 50 mm head (b). Horizontal bars in each column represent the average for the data in the column. Two headed arrows represent manufacturers' MARV.

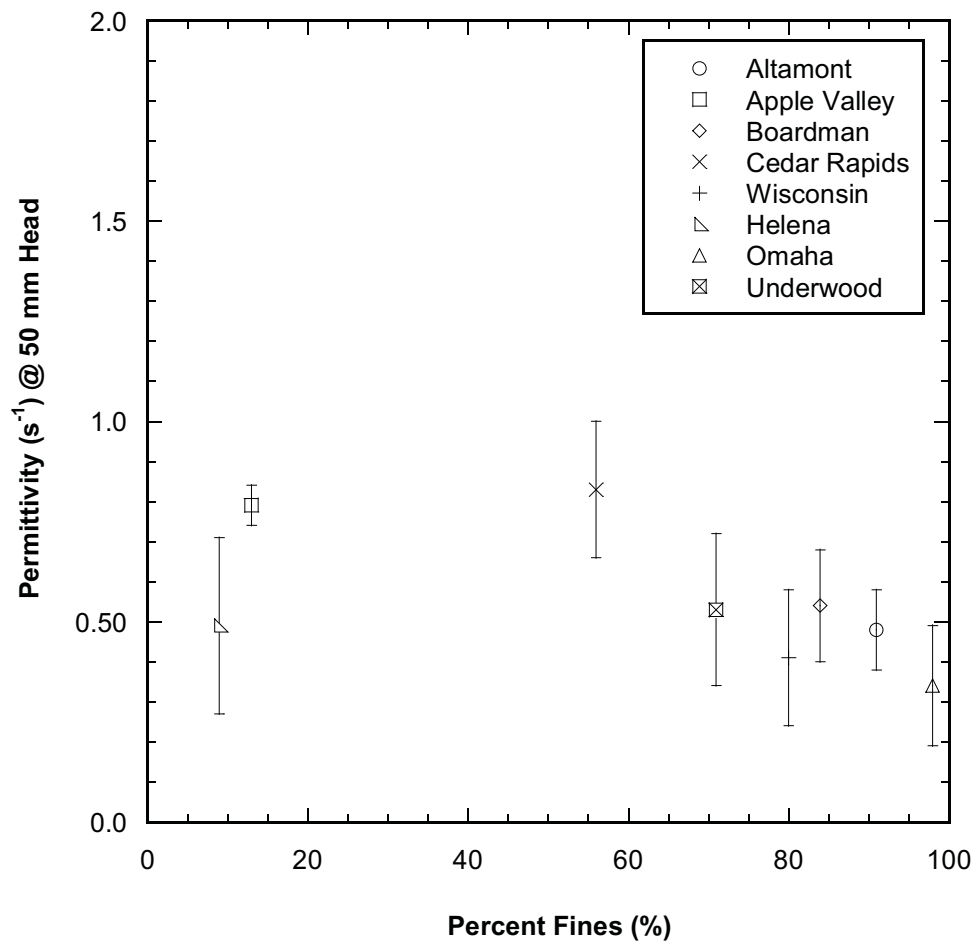


Fig. 8.11. Site average permittivity as a function of percent fines of the cover soil. Error bars represent one standard deviation from the mean.

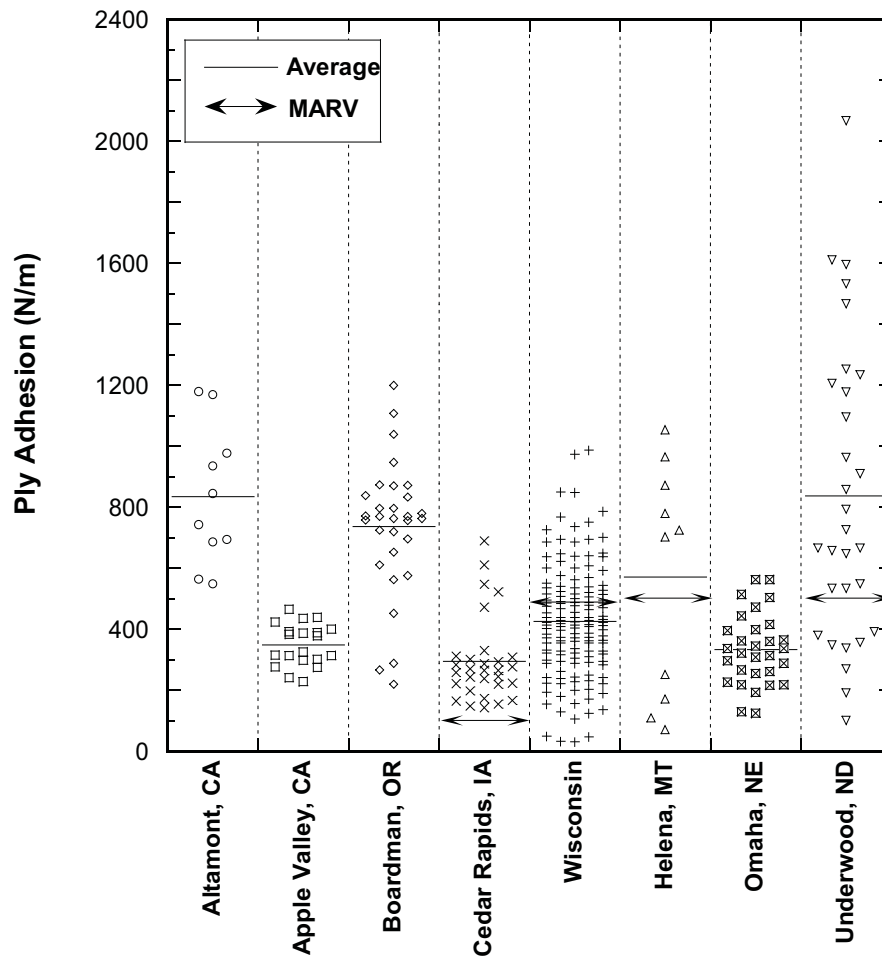


Fig. 8.12. Ply adhesion of GDL. Horizontal bars in each column represent the average the average for the data in the column. Two headed arrows represent manufacturers' MARV.

Table 8.4. Ply adhesions of exhumed GDLs (average reported range of property in parenthesis).

Location	Ply Adhesion (N/m)	
	No. of tested sides	average min. - max.
Altamont, CA	10	830 (550 - 1180)
Apple Valley, CA	20	350 (230 - 470)
Boardman, OR	30	740 (220 - 1200)
Cedar Rapids, IA	30	290 (140 - 690)
Wisconsin	140	420 (30 - 990)
Helena, MT	10	570 (70 - 1050)
Omaha, NE	30	330 (120 - 560)
Underwood, ND	30	840 (100 - 2070)

separation occurred between the geotextile and geonet (no tearing or delamination was evident), suggesting that the bond between the geosynthetics was never strong.

Service life and freeze-thaw cycles were considered as factors that may have influenced ply adhesion of the GDLs. For example, expansion of water during freezing may have expanded the GDL and affected the bond strength between geonet and geotextile. Similarly, polymer degradation might have damaged the bonding. As shown in Fig. 8.13, however, site-average ply adhesion does not vary systematically with service life or number of freeze-thaw cycles.

8.3 Interface Shear Strength

Shear strength parameters for the GDL-GM interfaces are summarized in Table 8.5. Envelopes corresponding to peak strengths for the GDL-GM interface for the Eau Claire site are shown in Fig. 8.14 as an example. Similar envelopes were obtained from the other sites (see Appendix S). The interface friction angles range from 30° to 41° between sites, and between 34° and 41° at sites where more than one envelope was measured.

No interface shear tests were available from the manufacturers. Thus, a direct comparison between interface shear strengths of the exhumed geosynthetics and a MARV could not be made. However, Stark et al. (1996) conducted interface shear tests on similar materials, and reported peak interface friction angles ranging between 30° and 32° and adhesions ranging between 5 and 17 kPa. Comparison of the strength parameters of the exhumed geosynthetics and those reported by Stark et al. (1996) suggests that no decrease in the peak interface shear strength appears to have occurred.

8.4. Reduction Factors for Design

A summary of engineering properties of exhumed geosynthetics from past studies and the current study is in Table 8.6. This table includes a column labeled property ratio, which is the ratio of the MARV to the engineering property measured in this study, or the ratio of the initial property to engineering property of the exhumed geosynthetic material in previous studies. A reduction factor for each property was estimated by rounding up the largest property ratio measured in this study and past studies to the nearest 0.5. Reduction factors recommended by Koerner (2005) are also summarized in Table 8.6. Based on the data in Table 8.6, the following inferences are made:

- The yield and break strengths of HDPE and LLDPE GMs were nearly always larger than the MARV. When the studies by Eith and Koerner (1997) and Rowe et al. (2003) are considered, the property ratio ranges between 0.3 and 1.2. Rounding the maximum property ratio up to the nearest 0.5 yields a reduction factor of 1.5 on yield and break strength.
- Permittivity of the GDLs exhumed in this study were at most a factor of 4.6 times lower than the MARV. Property factors ranging between 0.3 and 3.7 have reported by Hytiris and Berkhout (1996), Mannsbart and Christopher (1997), Reitz and Holtz (1997), and Black and Holtz (1997). Koerner (2005) recommends a composite reduction factor between 7 and 180 to account for soil clogging and blinding, creep reduction of voids, intrusion into voids, chemical clogging, and biological clogging mechanisms. Rounding

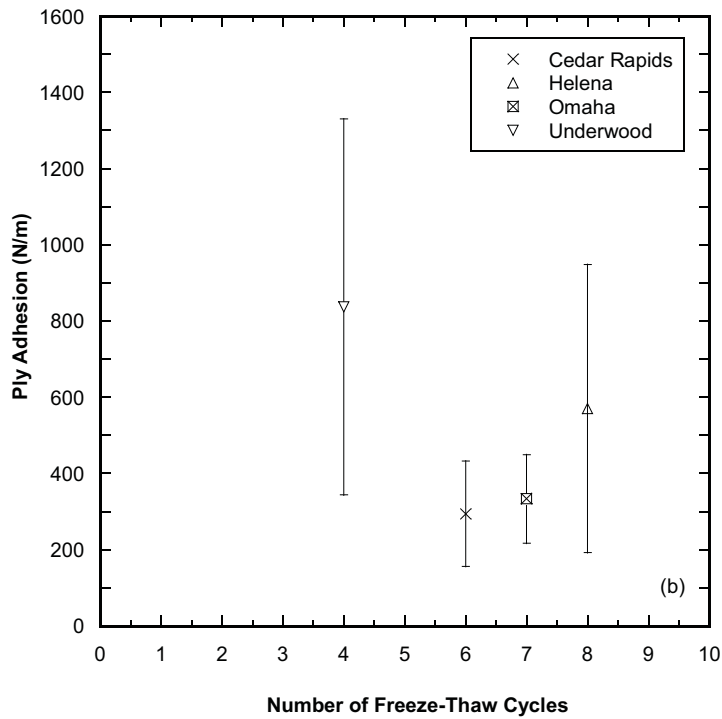
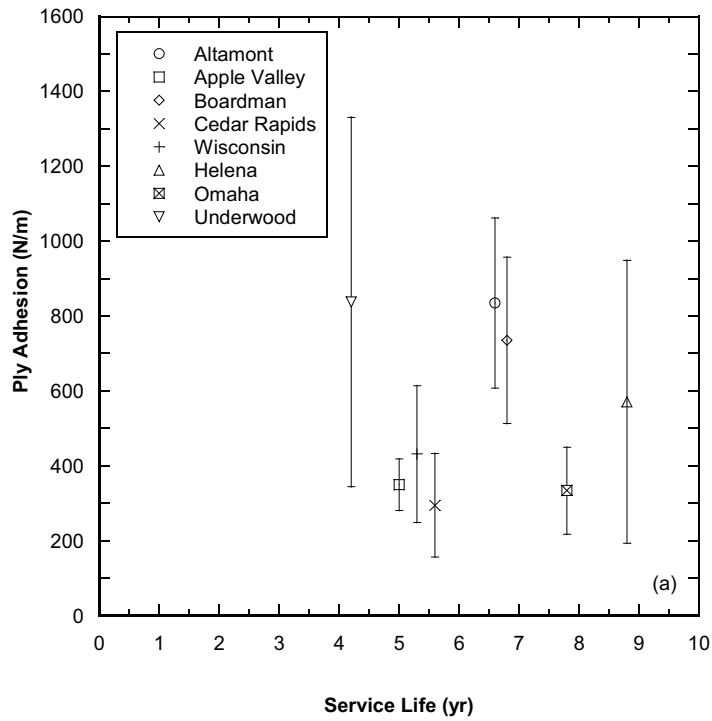


Fig. 8.13. Site average ply adhesion as a function of service life (a) and number of freeze-thaw cycles (b). Error bars represent one standard deviation from the mean.

Table 8.5. Shear strength parameters for the interface between the exhumed GDLs and GMs (average reported, range of property in parenthesis).

Location	Interface Shear Strength Parameters (GM - GDL)		
	No. of Envelopes	δ° average min. - max.	a (kPa) average min. - max.
Altamont, CA	1	30 -	12 -
Apple Valley, CA	1	34 -	19 -
Wisconsin	4	34 (33 - 35)	12 (5 - 17)
Helena, MT	1	40 -	25 -
Omaha, NE	3	41 (37 - 44)	12 (9 - 16)
Underwood, ND	3	41 (38 - 45)	13 (8 - 16)

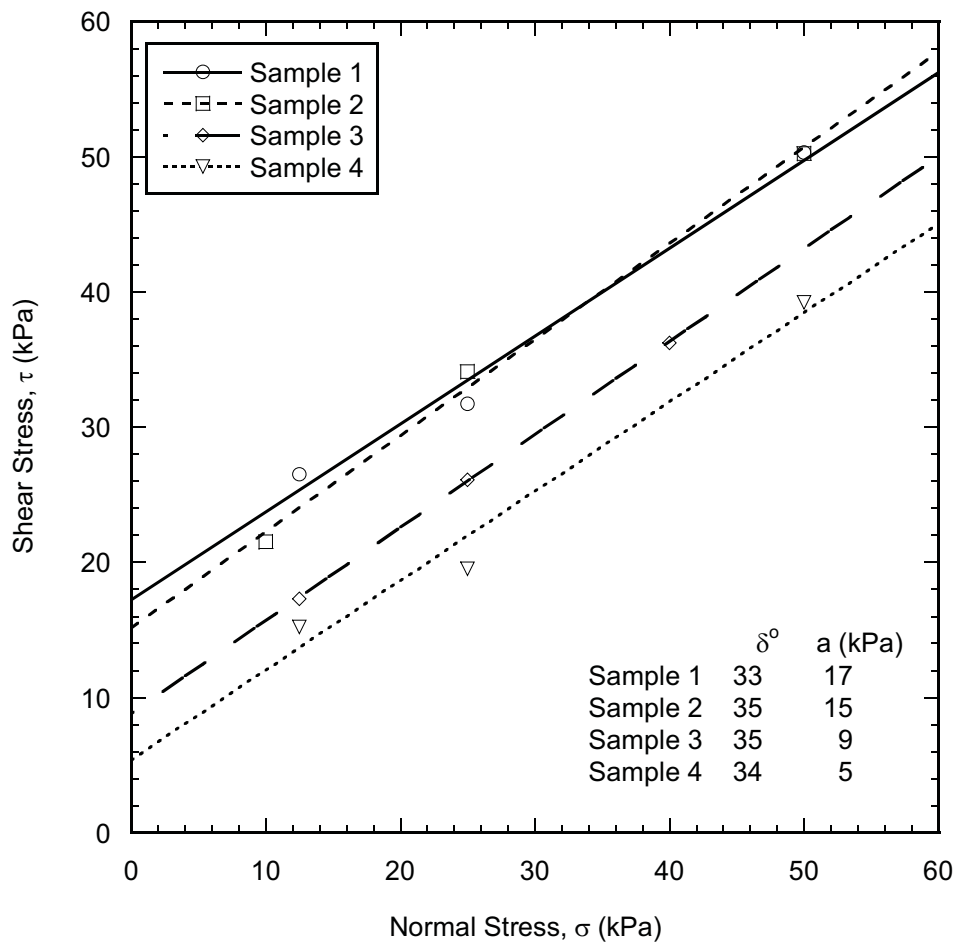


Fig. 8.14. Peak interface shear strength envelope of GM-GDL interface for geosynthetics sampled from the Wisconsin site

Table 8.6. Summary of reduction factors from previous studies and current study of exhumed geosynthetics.

Property	Source	Average or Range of Original Material	Average or Range of Exhumed Material	Property Ratio
Yield Strength (kN/m)	Eith and Koerner (1996)	21	29.7	0.7
	Rowe et al. (2003)	30	37	1.2
Yield Strain (%)	Eith and Koerner (1996)	10	18	-
	Rowe et al. (2003)	15	11	-
Break Strength (kN/m)	Current study for HDPE GMs	15.8	20.3 - 50.9	0.3 - 0.5
	Current study for LLDPE GMs	15.8	7 - 58.2	0.4 - 1.2
Break Strain (%)	Current study for HDPE GMs	100	158 - 651	0.2
	Current study for LLDPE GMs	250 - 500	12 - 594	1.8
Permittivity (s ⁻¹)	Hytiris and Berkhout (1996)	2.44	2.32	1.1
	Mannsbart and Christopher (1997)	0.47 - 2.50	0.23 - 0.79	2.0 - 3.7
	Reitz and Holtz (1997)	-	-	1.3 - 2.5
	Black and Holtz (1999)	0.10 - 2.70	0.30 - 2.00	0.3 - 1.8
	Koerner (2005)	-	-	7.2 - 180
	Current study	1.9 - 2.3	0.1 - 1.0	3.9 - 4.6
Transmissivity (m ² /s)	Hytiris and Berkhout (1996) at 200 kPa	0.29	0.28	1.1
	Koerner (2005) at 200 kPa	-	-	2.3 - 5.0
	Current study at 480 kPa	2.3x10 ⁻⁴	1.3x10 ⁻⁴ - 2.8x10 ⁻³	1.6 - 5.0
Ply Adhesion (N/m)	Current study	90 -500	30 - 2070	0.3 - 1.2

Note: For current study, property of original material was assigned the MARV.

up the largest property ratio in this study to the nearest 0.5 yields a reduction factor for permittivity of 5.0.

- Transmissivity of the GDLs exhumed in this study were a factor of 1.6 to 5.0 times lower than the MARV. Slightly smaller factors (1.1 and 1.2) are reported by Hytiris and Berkhout (1996), but they studied a drainage layer in contact with much coarser soils than those considered in this study. Rounding up the largest property ratio in this study to the nearest 0.5 yields a reduction factor of 5.0.
- The ply adhesion measured in this study ranged from 0.3 – 1.2 times the MARV. No other data on ply adhesion of exhumed geosynthetics were found in the literature. Rounding the reduction factor up to the nearest 0.5 yields a recommended reduction factor of 1.5.
- No manufacturer's data were available for the interface shear strength for the GDL-GM interfaces. However, the interface strength properties of the geosynthetics exhumed in this study were comparable to or larger than those reported by Stark et al. (1996) for similar new geosynthetic materials. Thus, a reduction factor of 1.0 is recommended for GM-GDL interfaces.

These reduction factors account for installation damage and degradation during near-term service (< 10 yr). They do not apply to long-term conditions.

8.5 Summary of Findings for Geomembranes and Drainage Layers

Based on the findings reported in this section, the following conclusions are made:

1. The GMs generally retained their tensile strength and there was no evidence of embrittlement. Narrow-strip break strengths of the exhumed GMs exceeded the MARV at 7 sites and were slightly below the MARV (1.1-1.2x) at two sites. The break strain was higher than MARV at six sites and slightly lower than the MARV (1.2-1.7x).
2. Similar yield strengths were obtained from narrow and wide-strip tensile tests. HDPE GMs had slightly higher narrow strip yield strengths than LLDPE GMs. On average, the narrow strip yield strength was 0.99 times the wide-strip yield strength.
3. No measurable degradation of the GM polymer occurred, as indicated by MFIs being similar to the MARV. The absence of measurable degradation was consistent with the presence of substantial antioxidant inhibitor in all of the GMs (OIT > 74 min for all GMs, and > 100 min for Boardman, Cedar Rapids, Wisconsin, Omaha and Underwood sites).
4. Antioxidant depletion rates computed from the OIT data showed that the field depletion rate was 0.0076 1/month for HDPE and 0.0033 1/month for LLDPE. These rates are similar to laboratory-measured rates reported by others for GMs immersed in water. These rates can be used with Eq. 8.1 to make inferences regarding the minimum service life of GMs.
5. Transmissivity of the exhumed GDLs was lower than the MARV by a factor of 1.6 to 5.0 for all but one site, for which the site average transmissivity was equal to the MARV.

The decrease in transmissivity appears to be due to migration of fines into the GDL, as lower transmissivities were obtained for GDLs placed under soils with higher fines content. Thus, if practical, cover soils with lower fines content should be used over GDLs.

6. The site average permittivity of the exhumed GDLs was lower than the MARV by a factor of 3.9 to 4.6 for the Wisconsin, Helena, and Underwood sites. The decrease in the permittivity probably was due to migration of fines into the geotextile and geonet, as slightly lower permittivity was obtained for cover soils with higher fines content.
7. All of the GDLs that were evaluated had GTs meeting the AOS criterion in Koerner (2005), none of these GTs were clogged by fines, and none of the GDLs showed evidence of significant accumulation of fines in the core. Moreover, as cited above, only modest reductions in transmissivity and permittivity of the GDLs were measured. Thus, the relatively simple filter criterion based on fines content reported in Koerner (2005) is adequate for filtration design of GTs used in final covers.
8. Site average ply adhesion of the GDL ranged from 3.2 times higher to 1.2 times lower than the MARV. Some of the GDLs had very weak to non-existent bonding of the GDL and geonet.
9. Interface shear strength between the GDL and the GM appeared unaffected by in-service conditions. Interface friction angles between 30° and 45° were obtained.
10. Data from this part of the study were used to define reduction factors that account for installation damage and short-term service (< 10 yr) on engineering properties. The following reduction factors are recommended:

GDL permittivity:	6.0
GDL transmissivity:	6.0
GDL ply adhesion:	2.0
Geomembrane tensile strength:	1.5
GDL-geomembrane interface friction:	1.0

These reduction factors should be applied to the MARV. Additional study is needed to understand how the properties of geosynthetics change over longer periods of time.

9. GEOPHYSICAL EVALUATION

Geophysical surveys were conducted at the Altamont, Omaha, and Polson ACAP sites using the electrical resistivity and ground penetrating radar methods discussed in Section 3.4. These sites were selected because they included test sections with composite barriers and represent semi-arid (Altamont), sub-humid (Polson), and humid (Omaha) climates. The evaluation had two goals: (i) to determine if electrical resistivity methods could be used to detect the defect deliberately placed in the GM at each site (as well as any other defects created during construction) and (ii) to evaluate the utility of using ground-penetrating radar (GPR) to evaluate homogeneity of cover profiles.

9.1 Electrical Resistivity Surveys

The test configuration for the electrical resistivity survey at the Altamont site is shown in Fig. 9.1. Similar configurations were used at the Omaha and Polson sites. At the Omaha site, however, the survey was conducted only over the lower two-thirds of the test section to avoid a test pit excavated in the cover profile. Current electrodes were installed beneath the GM at each site in a small pit excavated outside and adjacent to the lysimeter wall. The sidewall of the lysimeter was cut open using a razor knife and the electrode was driven into the underlying soil with a hammer. A photograph of a current electrode being installed at the Altamont site is shown in Fig. 9.2. A single current electrode was installed beneath the GM at the Altamont site. Two current electrodes were installed beneath the GM at the Omaha and Polson sites. Contour plots of voltage drop (mV) on the surface of the conventional covers at the Altamont, Omaha, and Polson sites are shown in Figs. 9.3-9.5.

The raw data from the Altamont site were noisy (Fig. 9.3a) and thus a moving average technique was used reduce the noise (Fig. 9.3b). However, even with smoothing, there was no evidence of the hole deliberately placed in the GM in the center of the test section. Moreover, both images are dominated by a disturbance associated with the current electrode (large voltage drops occur near current sources and sinks). Consequently, two current electrodes were deployed beneath the GM at the Polson and Omaha sites.

Contour and surface plots of voltage drop at the Polson site are shown in Fig. 9.4. Several anomalies were detected at the Polson site, but none were associated with the intentionally placed defect at the center of the test section. The large voltage anomaly near the north edge of the test section was caused by the presence of the electrode.

Voltage drop contours along the surface of the test section at Omaha are shown in Fig. 9.5. Two zones exist with a very strong voltage drop; one is along the west edge of the test section and the other along the east edge. The high voltage drop profile along east of the survey was most likely caused by the test pit excavated in the eastern end of the test section and along the periphery of the survey area. The cause of the high voltage drops along the west edge of the test section is unknown. One hypothesis is a faulty weld where the GM was joined to the sidewall of the lysimeter. However, this hypothesis could not be confirmed. No anomalies were found near the defect intentionally placed in the GM. However, more detailed analysis of the data (insets in Fig. 9.5) showed an unexpected voltage anomaly (see green box), which suggested the presence of an unintended defect. Excavation of the GM in this location revealed an unintended gash in the GM that was approximately 50 mm long (Fig. 9.6).

Absence of a signal associated with the hole deliberately placed in the GM at all three sites was unexpected. Difficulty at the Altamont and Polson sites can be attributed to the thick and very

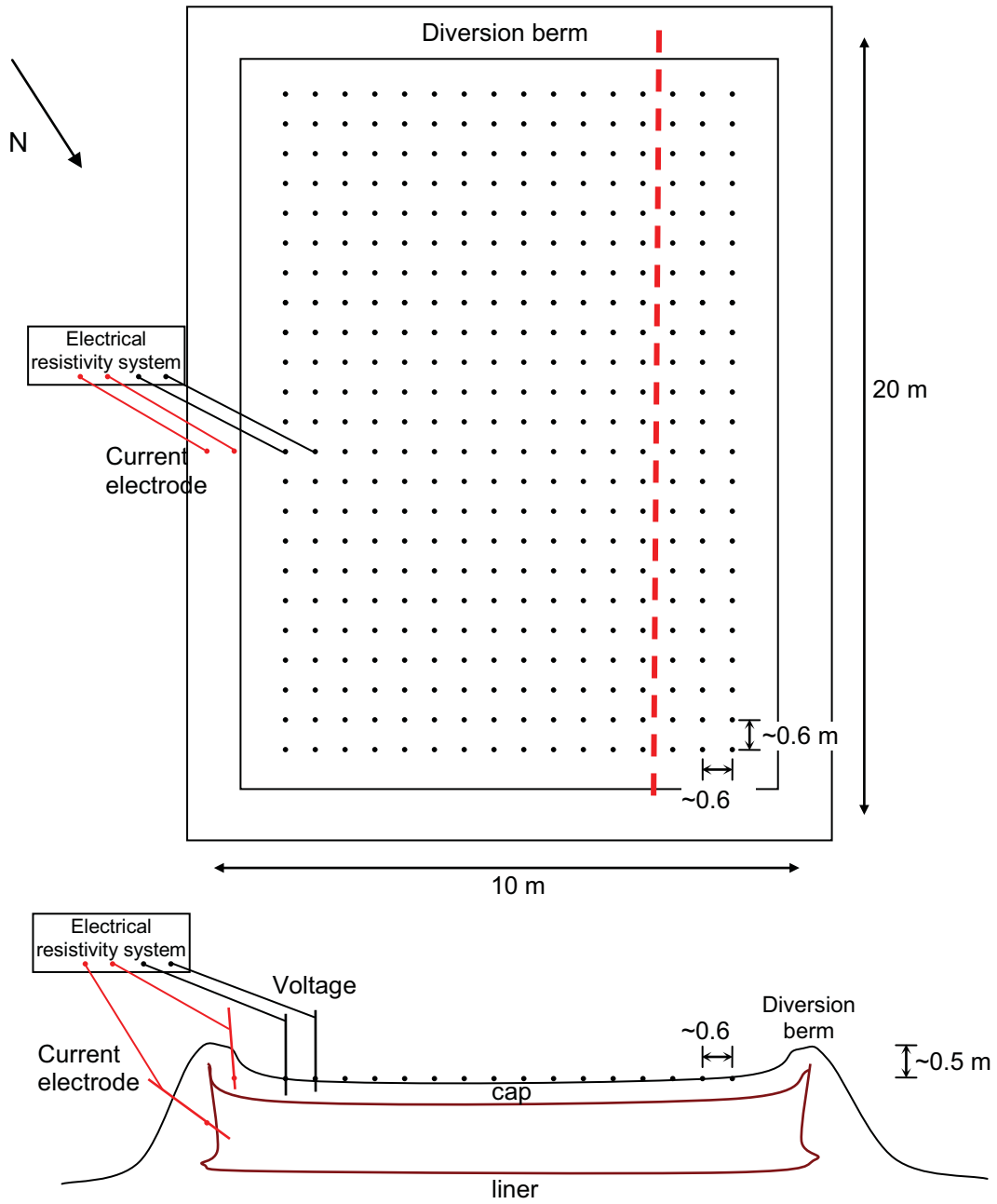


Fig. 9.1. Configuration for the electrical resistivity survey used at the Altamont site.

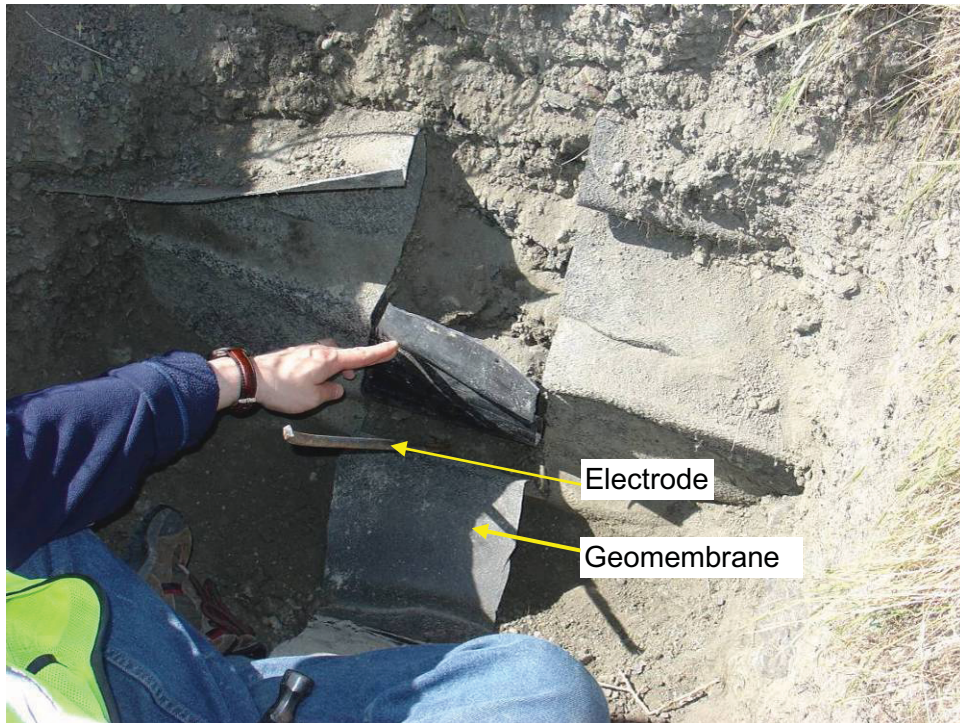


Fig. 9.2. Placement of current electrode under the GM at the Altamont site.

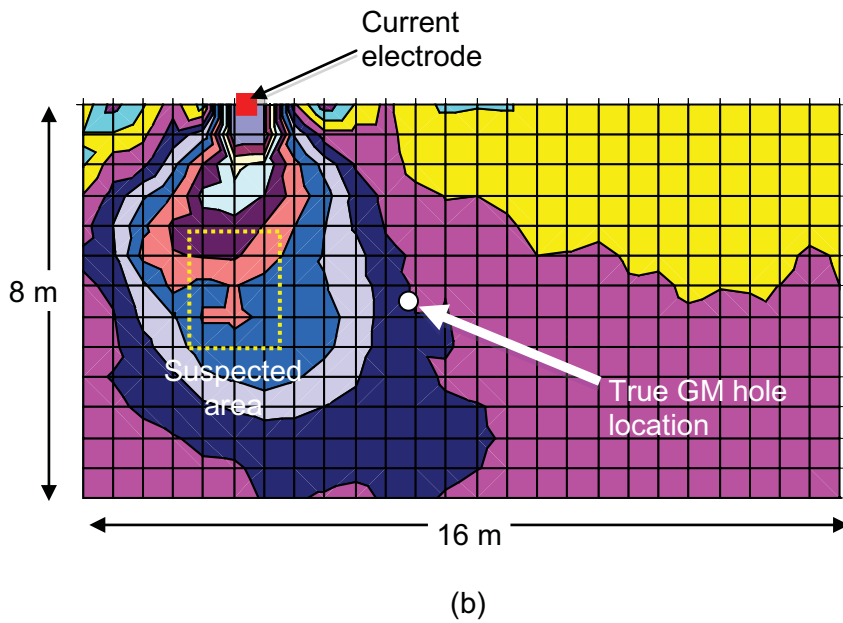
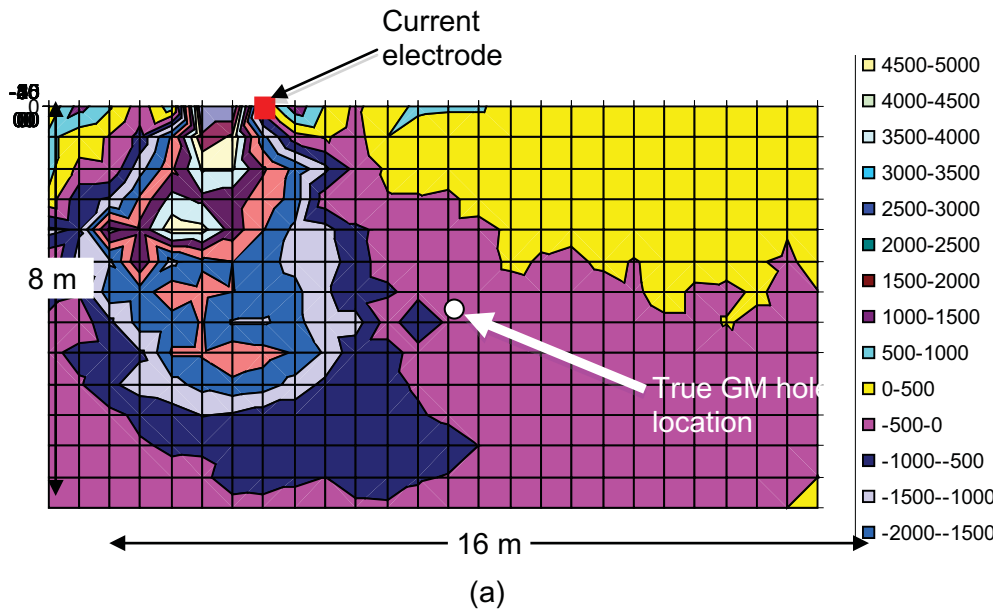


Fig. 9.3. Raw (a) and smoothed (b) distribution of voltage drop from electrical resistivity survey of conventional cover at Altamont site (scale in mV).

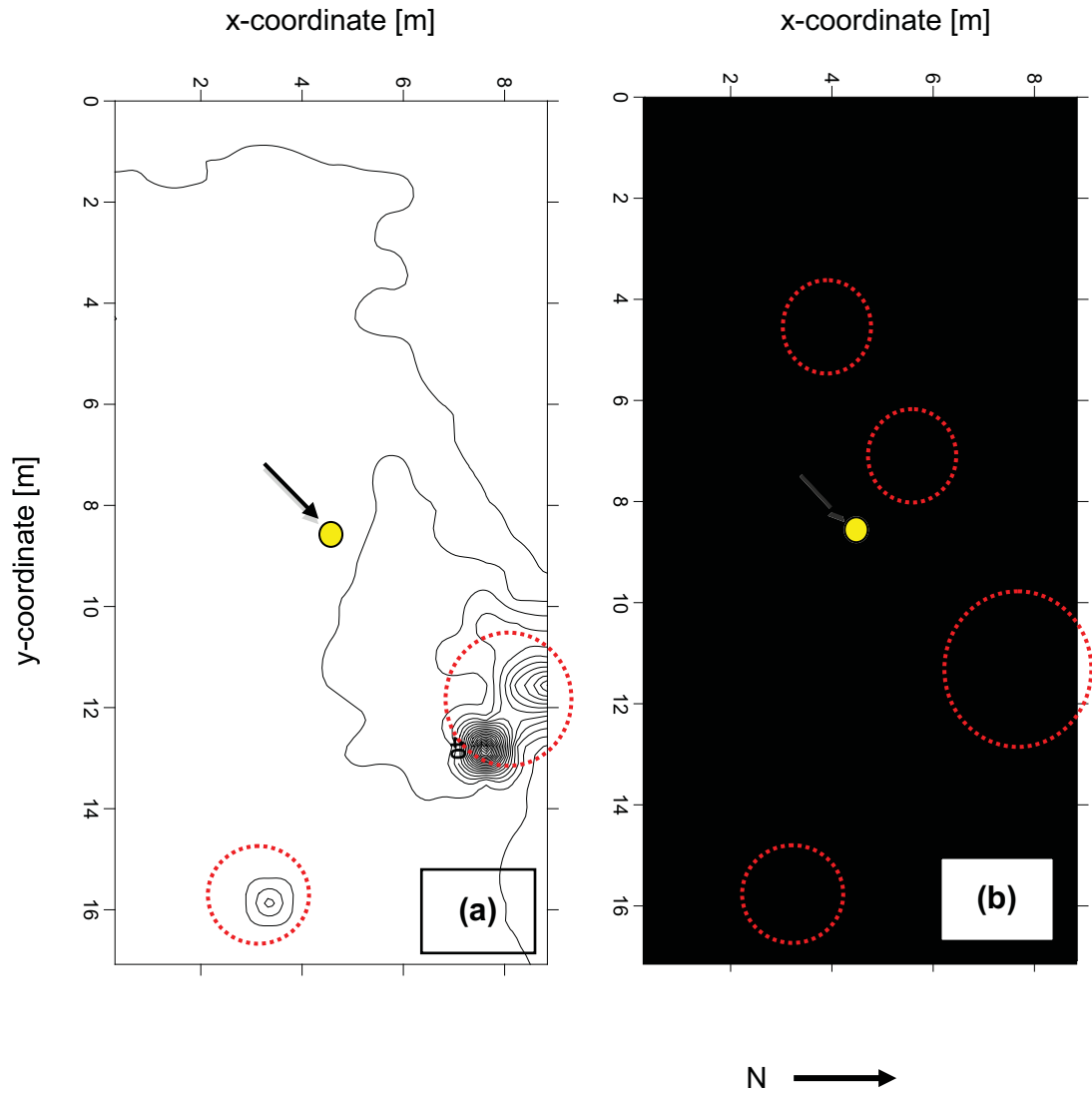


Fig. 9.4. Contour (a) and surface plots (b) of electrical resistivity data from conventional cover at Polson site. Suspect areas marked with red circles and location of intentional defect shown with solid yellow circle.

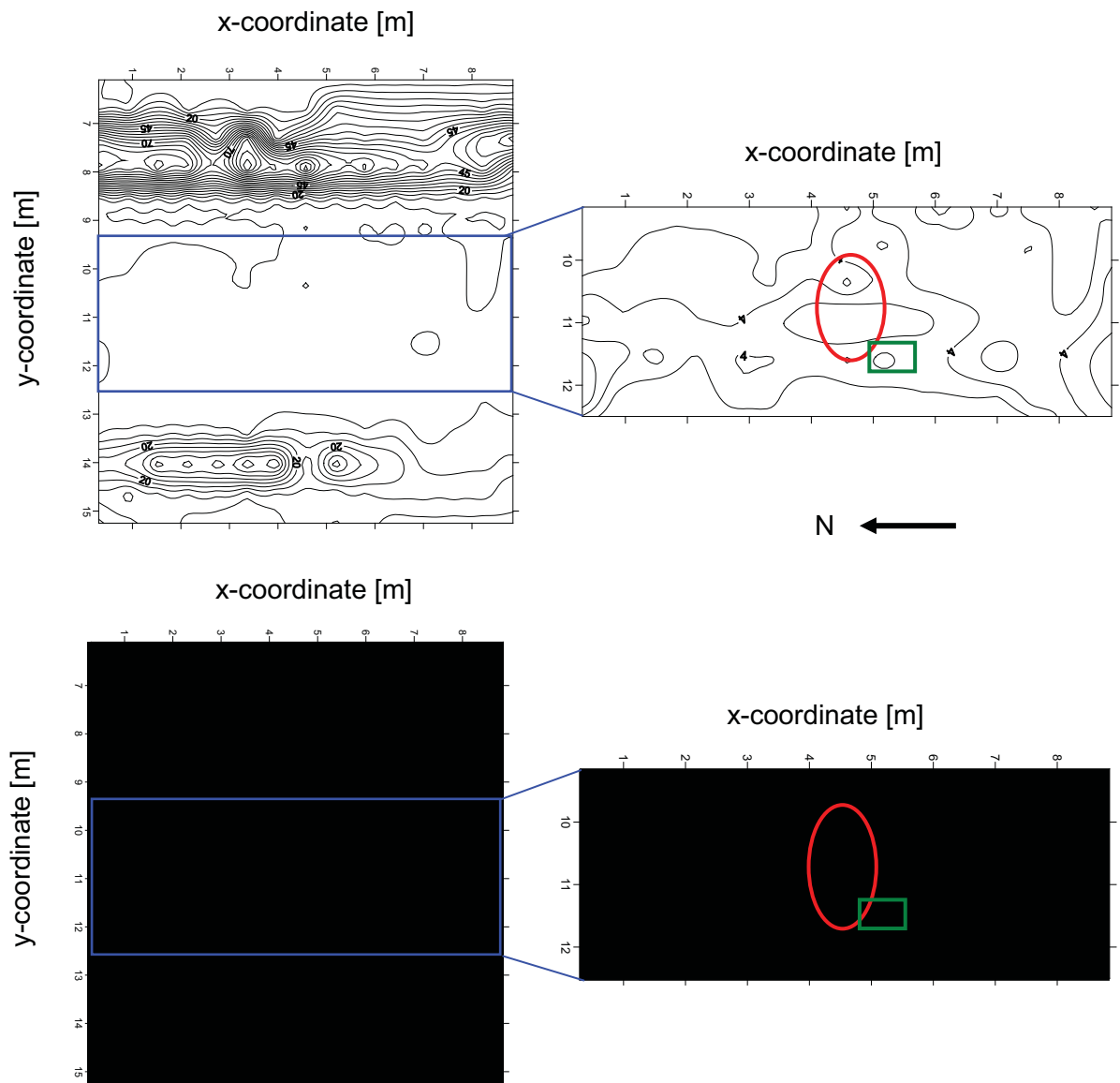


Fig. 9.5. Contour and surface plots of electrical resistivity survey of conventional cover at Omaha site (more detailed maps are presented on right). Suspect areas are marked with red oval; green box shows location of gash in GM in Fig. 9.6 (voltage amplitudes in mV).



Fig. 9.6. Gash in GM at Omaha site that was detected from electrical resistivity survey (lip balm container shown for scale).

dry surficial cover soils at both sites (e.g., see Fig. 9.2 for conditions at Altamont) and the presence of a polymeric GDL nearly devoid of water directly over the GM. Consequently, sufficient contrast may not have existed between the impedance of the GM (GM resistivity $\approx 10^8$ ohm-m, thickness = 0.001 m) and the overlying materials (soil electrical resistivity > 100 ohm-m, 0.5-m thickness) to permit detection of small defects. Under these conditions, the GM may not have behaved as an ideal dielectric and current may “leaked” through the GM, masking the hole. However, this hypothesis was not validated. In contrast, the soil at the Omaha site was moist and no GDL was present. Nevertheless, even at the Omaha site, the intentional defect in the GM could not be detected.

One commonality to all sites was the strong influence of the current electrode on the outcome of the survey. Using two current electrodes at the Omaha and Polson sites diminished this effect, but even at these sites the current electrodes impacted the survey. Using a more refined electrode configuration may have reduced these effects and improved resolution.

9.2 Ground Penetrating Radar Surveys

GPR surveys were conducted at the Altamont and Omaha sites. Two different GPR surveys were conducted at each site: a reflection survey along the ground surface and a downhole tomographic survey along the vertical face of a test pit (Fig. 3.10). Surveys at the Altamont site were conducted with a 200-MHz antennae to maximize resolution at small depths. At the Omaha site, GPR surveys were conducted with 100-MHz antennas to enhance penetration depth at the expense of resolution (Annan 2005). A photograph of the antennas is in Fig. 9.7.

The reflection survey at Altamont was conducted on the conventional cover with a composite barrier. Two horizontal reflectors were detected ≈ 0.6 m below ground surface (bgs) (compacted soil barrier) and ≈ 1.3 m bgs (interim cover) (Fig. 9.8). A number of less coherent reflectors are also present that are from cables, metal, and tools above and below the ground surface. Some other traces may indicate the presence of other layers, but these layers could not be confirmed.

Traces collected from the downhole survey at the Altamont site are shown in Fig. 9.9. These traces were corrected for amplitude before the first arrivals were determined and then time corrections were applied to properly represent the initial arrival time. Tomographic images were obtained from the corrected traces via inversion using the program GeoTom (Jackson and Tweeton 1996) (Fig. 9.10). Due the high contrast in wave velocity in air and soil, a non-linear inversion with curved rays was used.

As shown in Fig. 9.10, the surficial soil has an electromagnetic (EM) velocity greater than 0.22 m/ns, which corresponds to a real dielectric permittivity of approximately 2. This low permittivity indicates that the surficial soils were very dry, which hampered the electrical resistivity surveys.

A GPR reflection survey was conducted over all three covers at the Omaha site. The profile from the reflection survey is shown in Fig. 9.11. Two horizontal reflection horizons exist corresponding to the top and bottom of the storage layer and another corresponds to the top of the interim cover. A number of less coherent reflectors exist that cannot be explained without more information. For both of the store-and-release covers, amplitudes of the reflected signals were consistent, indicating a homogeneous distribution of water content and homogeneous soils profiles. Visual observations in the test pits during the exhumation also indicated that the soil was moist and uniform (Fig. 9.12).



Fig. 9.7. Antennae (200 MHz) used for GPR surveys at Altamont and Omaha sites.

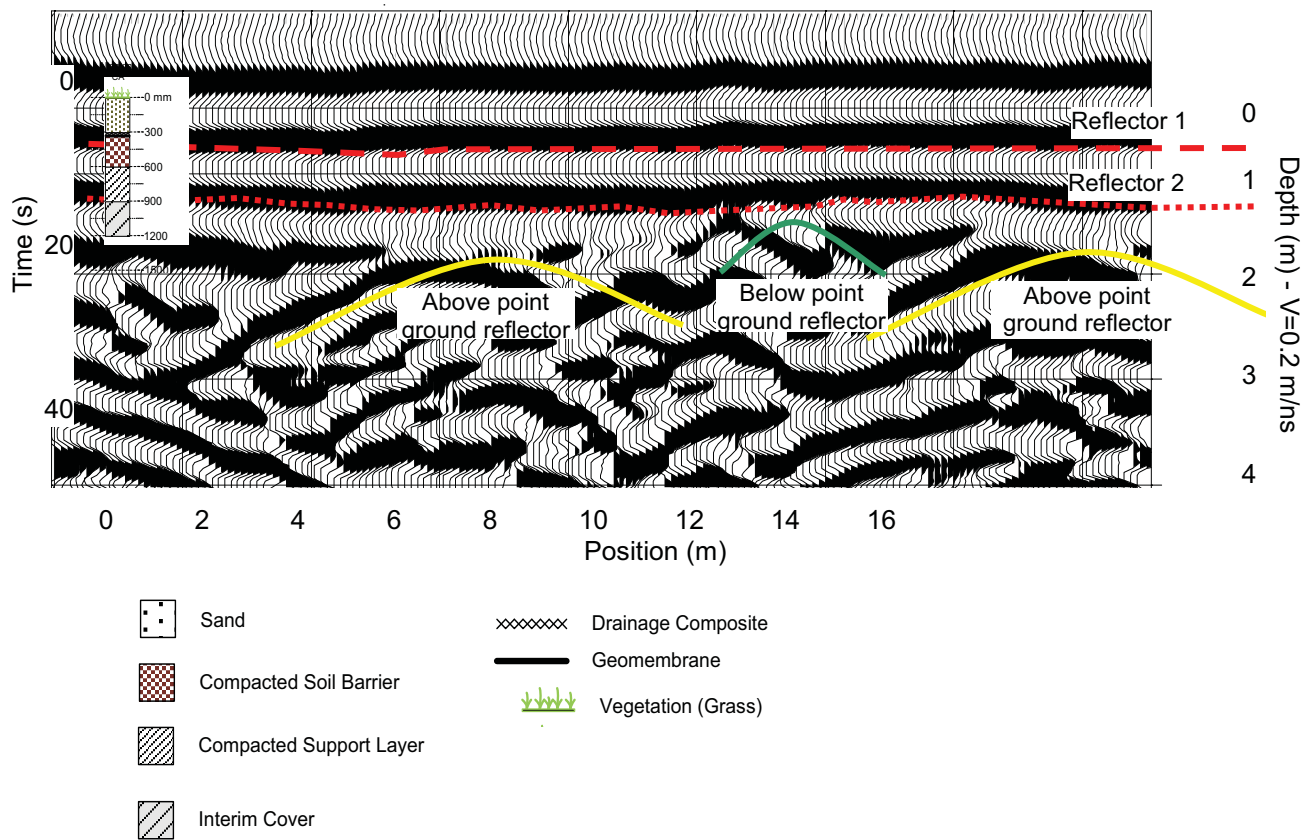


Fig. 9.8. GPR reflection survey at Altamont site along survey line in Fig. 9.1. Profile shows both point reflector above ground (e.g., tools, cables, etc. on surface) and below ground (sensor cables, etc.).

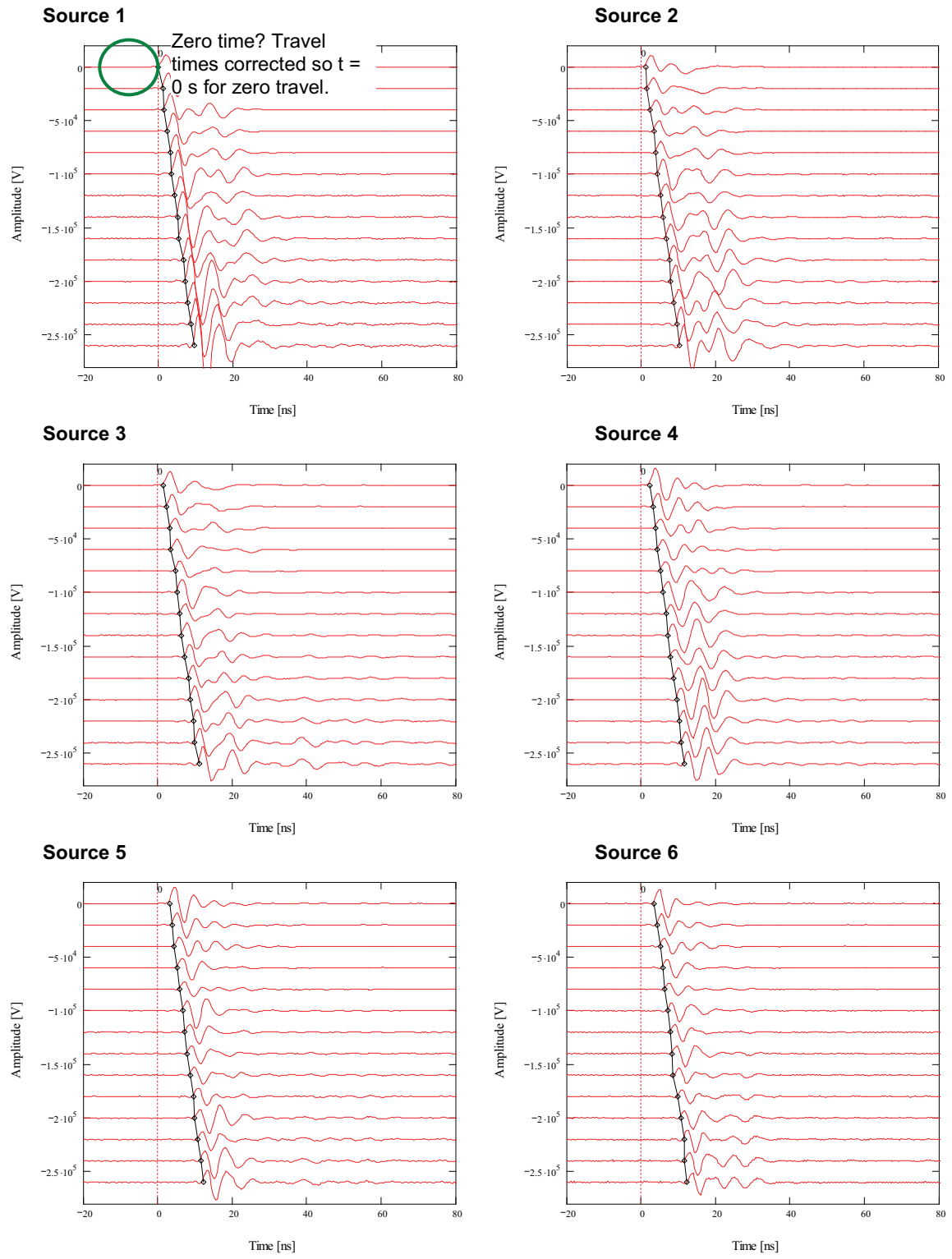


Fig. 9.9. Electromagnetic wave traces collected along survey line shown in Fig. 9.1.

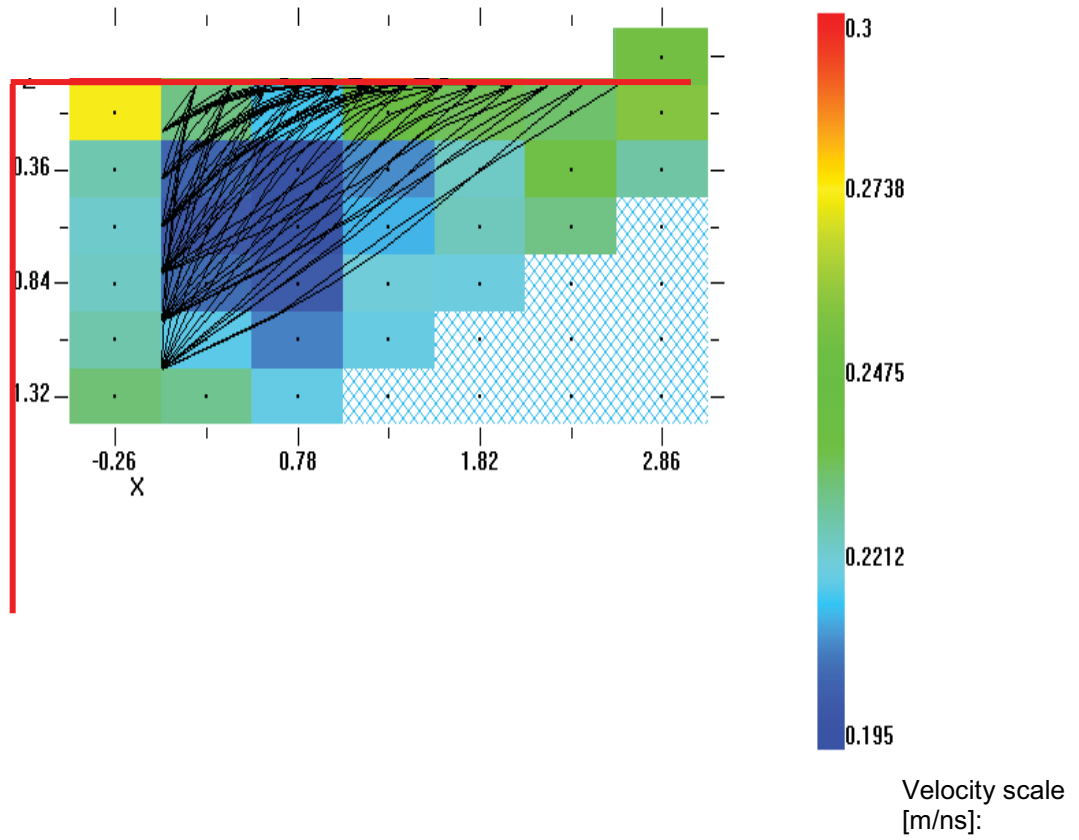


Fig. 9.10. Tomographic images of electromagnetic wave velocity at Altamont site.

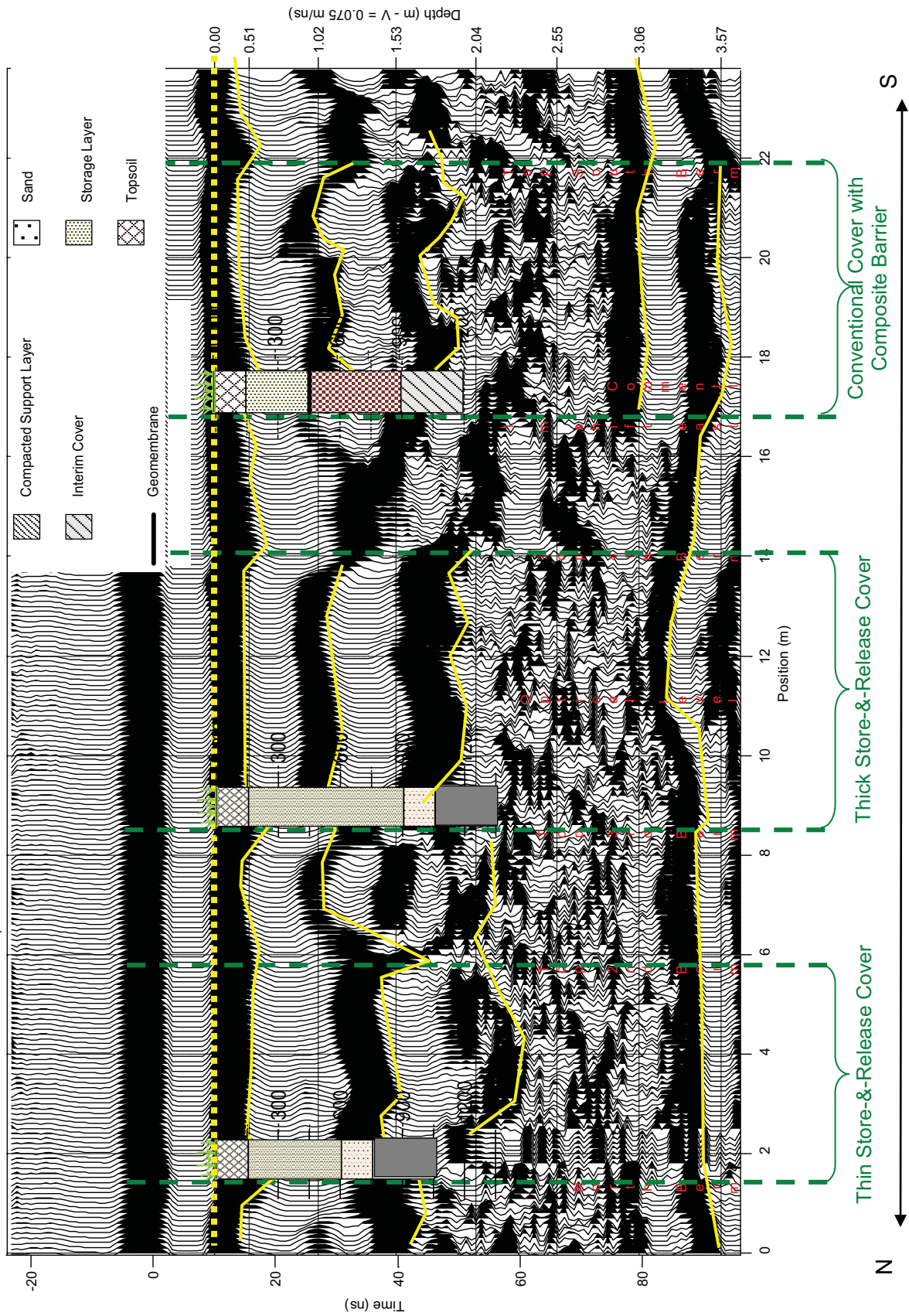


Fig. 9.11. GPR reflection survey across all three cover sections at Omaha site.



Fig. 9.12. Photograph of thick store-and-release cover at Omaha site showing thick upper storage layer, sand layer for capillary break (white layer), and lower interim cover layer. Note uniformity of layers and moist condition of storage layer and topsoil.

Results of the downhole tomographic survey at Omaha are presented in Fig. 9.13. The EM wave velocities are less than 0.15 m/ns, which corresponds to a real dielectric permittivity greater than 4. This velocity is lower than the velocity at Altamont because of the higher water content of the cover soils in Omaha.

9.3 Summary of Findings from Geophysical Surveys

Based on the findings presented in this section, the following conclusions are made:

1. Electrical resistivity surveys were not able to detect the small (≤ 10 mm) intentionally placed defects in the GMs at the field sites. However, the surveys were able to identify anomalies and larger defects in GMs, including a larger unintended gash in one GM. Resolution of electrical resistivity surveys may be improved by optimizing the electrode spacing.

Additional research on using electrical resistivity surveys as a periodic monitoring tool for evaluating composite barrier layers in covers is recommended.

2. GPR surveys can be used to assess the layering and homogeneity of cover soils. Reflection surveys at the Omaha site showed very different profiles corresponding to different cover types. Downhole surveys showed differences in water content between sites (e.g., Altamont vs. Omaha). Thus, by analogy, GPR potentially could be used to detect unanticipated variations in water content in a cover profile or significant geometric variations within barrier systems, such as disruptions in layers. Additional research on using GPR as a monitoring tool is recommended.

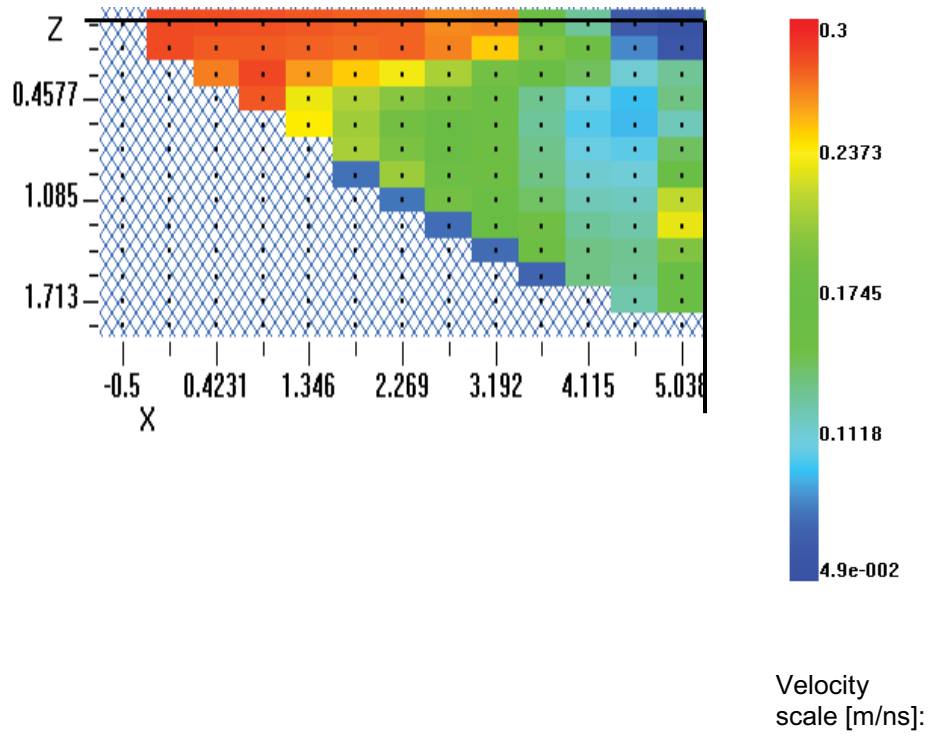


Fig. 9.13. Tomographic images of downhole EM wave velocity from the thick store-and-release cover at the Omaha site.

10. PRACTICAL IMPLICATIONS FOR DESIGN, PERFORMANCE ASSESSEMENT, AND MONITORING

The findings from this study have demonstrated that the properties of earthen and geosynthetic materials used in final covers change over time in response to interactions with the surrounding environment. Some materials undergo modest changes in engineering properties (e.g., geomembranes), whereas others undergo much larger changes (e.g., dense compacted clay barriers). Alterations in cover materials should be expected. Like all man-made structures, final covers are placed in a state of disequilibrium with the surrounding environment, which itself is changing continuously. Alterations to cover materials will continue to occur until an equilibrium condition exists, or the temporal change in the cover becomes consistent with the temporal changes of the surrounding landscape. This phenomenon is omnipresent and cannot be changed, and, therefore, must be considered by the designer and analyst.

Final covers should be designed for an as-built condition that is as close as practical to the anticipated equilibrium state. Performance assessments should consider changes in engineering properties that are likely to occur, and employ performance predictions based on the equilibrium state rather than the as-built condition. To confirm that the facility is functioning as intended, conventional environmental monitoring at the periphery (e.g., ground water monitoring wells, perimeter air monitoring) should be augmented by monitoring associated with engineering components (e.g., percolation rate from cover, geochemistry within the waste, contaminant flux from the base of the facility). Data collected from these monitoring points should be regularly compared to predictions made during performance assessments, with significant deviations noted as potential problems.

This section provides recommendations on design states that represent conditions closer to equilibrium, engineering parameters that can be used in modeling for realistic performance assessments, and methods for monitoring the hydrologic performance of final covers. These recommendations are based on the data collected during this study as well as the collective experience gained by the research team via ACAP. The covers evaluated in this study had service life ranging from 3.8 to 8.9 yr when they were exhumed.

Because ACAP was a large and comprehensive study including final covers in diverse climates that were constructed with a variety of soils, types of vegetation, and design strategies (e.g., conventional hydraulic resistance vs. store-and-release), these recommendations are believed to apply to most conditions that are encountered. However, not all possible scenarios could be evaluated by ACAP, and the service life of all covers was less than 10 yr. Thus, even though data from ACAP represent one of the longest-term and most comprehensive data sets in existence, the data may not represent very long term conditions (100s or 1000s of years) or all possible conditions. This limitation should be considered when interpreting and applying the recommendations presented henceforth.

10.1 Design Conditions

Sections 6-8 have illustrated relationships between the engineering properties of cover materials when the exhumations were conducted and as-built properties. These discussions illustrated the following tenets relevant to design:

1. For covers of typical thickness (< 3 m), the saturated hydraulic conductivity of earthen barrier and storage layers will increase over time in response to processes such as wet-dry and freeze-thaw cycling, with larger increases occurring in layers having lower as-built saturated hydraulic conductivity. Increases will occur until the saturated hydraulic conductivity is in the range of approximately 8×10^{-8} to 6×10^{-6} m/s. The changes occur regardless of climate, cover profile, or placement condition. Designers should acknowledge that these changes in properties will occur and select materials and placement conditions that result in earthen barrier and storage layers that have as-built saturated hydraulic conductivities within 8×10^{-8} to 6×10^{-6} m/s.
2. Smaller changes in hydraulic conductivity occurred in earthen barrier and storage layers that were constructed with soils having lower clay content and a fines fraction that had a greater proportion of silt-size particles. Although an effect of the coarse fraction could not be identified from the data collected in this study, soils with a greater fraction of coarse particles will be more resistant to volume change and therefore less prone to changes in soil structure and hydraulic properties (Kleppe and Olson 1985). When practical, earthen storage and barrier layers should be constructed using fine-textured soils containing a broad range of particles (coarse and fine) with a modest amount of clay-size particles. Soils classifying as SC, SM, ML, and SC-CL in the USCS are likely to be more resistant to changes in hydraulic properties over time compared to soils classifying as CL, CH, CL-CH, or CL-ML.
3. Earthen storage and barrier layers that are densely compacted tend to loosen over time and become more permeable. The porosity of most earthen storage and barrier layers evaluated in this study was between 0.35-0.45 when exhumed. Thus, to the extent practical, earthen storage and barrier layers should be compacted to a condition resulting in a porosity of approximately 0.40, which corresponds to a dry unit weight of approximately 15.5 kN/m^3 for a soil with a specific gravity of solids = 2.65. Alternatively, data from local analog sites could be used to define an equilibrium porosity and dry unit weight. Compaction wet of optimum water content should be avoided; compaction near optimum water content is recommended.
4. Geosynthetic clay liners (GCLs) used as barrier layers in final covers inevitably become altered as divalent cations common in the environment replace native Na in the bentonite. The impact of cation exchange depends greatly on the placement and boundary conditions. GCLs should be covered with a geomembrane and placed on a subgrade having an initial water content exceeding 10%. Under this condition, the bentonite will undergo osmotic swell and retain low saturated hydraulic conductivity ($< 5 \times 10^{-11}$ m/s) even if divalent cations replace the native Na provided that the overlying geomembrane remains intact (i.e., the service life of the GCL is controlled by the service life of the geomembrane). GCLs not covered by a geomembrane or placed on drier subgrades have the potential to become much more permeable, with saturated hydraulic conductivities on the order of 10^{-8} to 10^{-6} m/s.

5. The polymeric geosynthetic materials (geomembranes and geosynthetic drainage layers) evaluated in this study exhibited smaller changes in properties over time compared to the earthen materials or GCLs. This robust behavior is consistent with findings by others. Antioxidant depletion rates observed in this study and by others can be used with Eq. 8.1 to compute the minimum service life of geomembranes. For the depletion rates observed in this study, the minimum lifespan of geomembranes (assuming an initial oxidation time of 130 min and a final oxidation induction time of 1 min) ranges between 55 and 125 yr depending on the type of polymer employed. Rowe et al. (2010) report similar minimum life spans based on long-term prototype tests. This computation conservatively assumes that the service life of the geomembrane ends when the antioxidants are depleted. The actual lifetime should be longer, and methods to estimate the actual lifespan are in Koerner et al. (2005) and Rowe et al. (2009). Periodic inspection and replacement of geosynthetics may be necessary once these time frames have been reached.

10.2 Parameters for Performance Assessments

The data reported in this study represent conditions approximately 5-10 yrs after construction, and therefore do not necessarily represent long-term conditions that may exist in 100 or 1000 yr. However, given that many of the engineering properties of the exhumed materials coalesced around similar values regardless of the initial condition, the engineering properties measured during this exhumation study provide a reasonable first estimate of long-term properties. The following recommendations are made regarding engineering properties of cover materials that can be used in performance assessments in lieu of site-specific data:

1. The saturated hydraulic conductivity of fine-textured earthen storage and barrier layers can be assumed to range between 1×10^{-7} m/s and 5×10^{-6} m/s. This relatively narrow range of saturated hydraulic conductivities was obtained from a very broad range of as-built saturated hydraulic conductivities, which suggests that the saturated hydraulic conductivity reached an equilibrium condition during the study. Moreover, given that storage and barrier layers are constructed with fine-textured soils, saturated hydraulic conductivities higher than 5×10^{-6} m/s are unlikely unless a fundamental change in texture or mineralogy occurs during the service life of the cover. When site-specific information representing in service conditions is not available, typical conditions can be predicted using a saturated hydraulic conductivity of 5×10^{-7} m/s. Sensitivity analyses can be conducted using the aforementioned upper and lower bounds to assess the range of performance that may be encountered.
2. The porosity of earthen storage and barrier layers will likely range between 0.35 and 0.45. The porosity is equal to the saturated volumetric water content, which is used in hydrologic simulations of final covers. For such simulations, typical conditions can be simulated using a porosity of 0.40, but sensitivity analyses should be conducted using the aforementioned upper and lower bounds to assess the range of performance that may be encountered. As with the saturated hydraulic conductivity, the volumetric water content coalesced into a narrow range regardless of the as-built condition, which suggests that an equilibrium state was achieved.
3. The α -parameter in van Genuchten's equation, which is used to describe the SWCC for hydrologic simulations, varies between 0.01 and 0.33 kPa⁻¹ for field-scale barrier

and storage layers. The field-scale α is approximately 20 times larger than α measured in a conventional 75-mm-diameter laboratory test. When site-specific information representing in service conditions is not available, typical conditions can be predicted using $\alpha = 0.2 \text{ kPa}^{-1}$. As with the saturated hydraulic conductivity, the α -parameter coalesced into a narrow range regardless of the as-built condition, which suggests that an equilibrium state was achieved. Sensitivity analyses can be conducted using the aforementioned upper and lower bounds to assess the range of performance that may be encountered.

4. The n-parameter in van Genuchten's equation, which is used to describe the SWCC for hydrologic simulations, varies over a very small range (typically between 1.2 to 1.4). When site-specific information representing in service conditions is not available, typical conditions can be predicted using $n = 1.3$, and sensitivity analyses can be conducted using $n = 1.2$ and 1.4 to ascertain the range of performance that may be encountered.
5. GCLs covered with a geomembrane and placed on a subgrade with a gravimetric water content $> 10\%$ can be assumed to have a saturated hydraulic conductivity $\leq 5 \times 10^{-10} \text{ m/s}$ provided that cover soils are placed on top of the geomembrane soon after installation. This saturated hydraulic conductivity accounts for long-term impacts of cation exchange in the absence of dehydration, as described by Meer and Benson (2007). This condition will persist provided conditions inducing dehydration are precluded (e.g., large thermal cycles, root water uptake, evaporation) and mechanisms that cause mineralogical transformation of the montmorillonite are absent. An acceptable elapsed time for placing the cover soil over the geomembrane has not yet been identified, but no more than one week is reasonable. GCLs placed under other conditions may be much more permeable. A saturated hydraulic conductivity of 10^{-7} m/s is recommended for GCLs placed under other circumstances.
6. The permittivity and transmissivity of geosynthetic drainage layers can be assumed to be 6 times lower than the MARV after approximately 6 yr of service (average service life of the geosynthetics in this study). The rate of reduction for longer times remains unknown. A linear reduction in permittivity and transmissivity over time would be very conservative (reduction of 6 fold every 6 yr), given that natural filter layers will develop and provide greater protection of the drainage layer over time.
7. The tensile strength of geomembranes can be assumed to decrease by a factor of 1.5 over the first decade. Given that installation damage contributes to the initial reduction in tensile strength, a similar rate of reduction in tensile strength over the lifespan of the geomembrane should be very conservative.

10.3 Monitoring

Because the engineering properties of cover materials change over time, performance monitoring of covers is prudent to ensure that the cover is functioning as predicted in the performance assessment. Cover monitoring generally is conducted at two levels: (i) direct non-destructive performance monitoring and (ii) direct or indirect interpretive monitoring. Direct non-destructive monitoring consists of directly and continuously monitoring the primary performance variable using an in situ device. Interpretive monitoring consists of measuring secondary variables related to the primary

performance variable that can be used to understand or interpret data obtained from primary performance monitoring. Interpretive monitoring can be conducted directly using embedded sensors (e.g., water content or matric potential sensors) or indirectly using remote sensing methods such as ground penetrating radar or airborne radar systems. Indirect monitoring using remote sensing focuses on variables that have been shown to be strongly related to the primary performance variable.

Interpretive monitoring currently is conducted almost exclusively using direct methods. However, indirect remote sensing methods likely will become more important in the future, especially for long-term monitoring from remote locations. The knowledge base relating remotely sensed variables and cover performance is sparse at the current time. Research is needed that provides quantitative coupling between remotely sensed variables and cover performance.

10.3.1 Performance Monitoring

For many final covers, the primary performance variable generally is percolation from the base. Accordingly, performance monitoring of covers must consist of a method to continuously and non-destructively measure the percolation rate, i.e., the rate at which water is transmitted from the base of the cover. In effect, this requires that an in situ device be installed that can be used to collect and measure water transmitted from the base of the cover (Malusis and Benson 2006). This device must be large enough to represent field-scale conditions and simple enough to permit continuous long-term monitoring with little to no maintenance.

Indirect approaches, such as inferences made from water content or matric potential sensors, have been used to estimate the percolation rate from covers. These approaches rely on computations based on state variables (water content, matric potential) and constitutive functions (hydraulic conductivity vs. water content). These computations involve an assortment of assumptions that introduce large uncertainties into the estimated percolation rate (Gee and Hillel 1988, Benson et al. 2001, Malusis and Benson 2006).

Inability to detect or account for preferential flow is another serious shortcoming of indirect approaches. Data from sensors are point measurements characteristic of conditions within the soil matrix at the location of the sensor and not along cracks, fissures, or macropores. Consequently, water content data can provide a false impression regarding the effectiveness of a cover. Khire et al. (1997) provide an example of preferential flow in a 0.8-m-thick monolithic cover instrumented with water content sensors and a lysimeter. Pulses of percolation transmitted through preferential flow paths were regularly collected in the lysimeter shortly after precipitation events (Fig. 10.1a), but two months before the deepest sensors indicated that water was reaching the base of the cover (Fig. 10.1b). Consequently, indirect approaches to monitor percolation rate are not recommended for performance monitoring of covers.

Flux meters and pan lysimeters are the most commonly used devices for direct monitoring of percolation rate. Flux meters are tubes (< 0.3 m diameter) placed within the cover profile to monitor the rate at which water is flowing (Fig. 10.2). Water is collected in a wick at the base of tube and is transmitted to a metering device (a tipping bucket or a dielectric volume sensor). The volume of water collected in the metering device is measured periodically and subsequently discharged (Gee et al. 2002). Flux

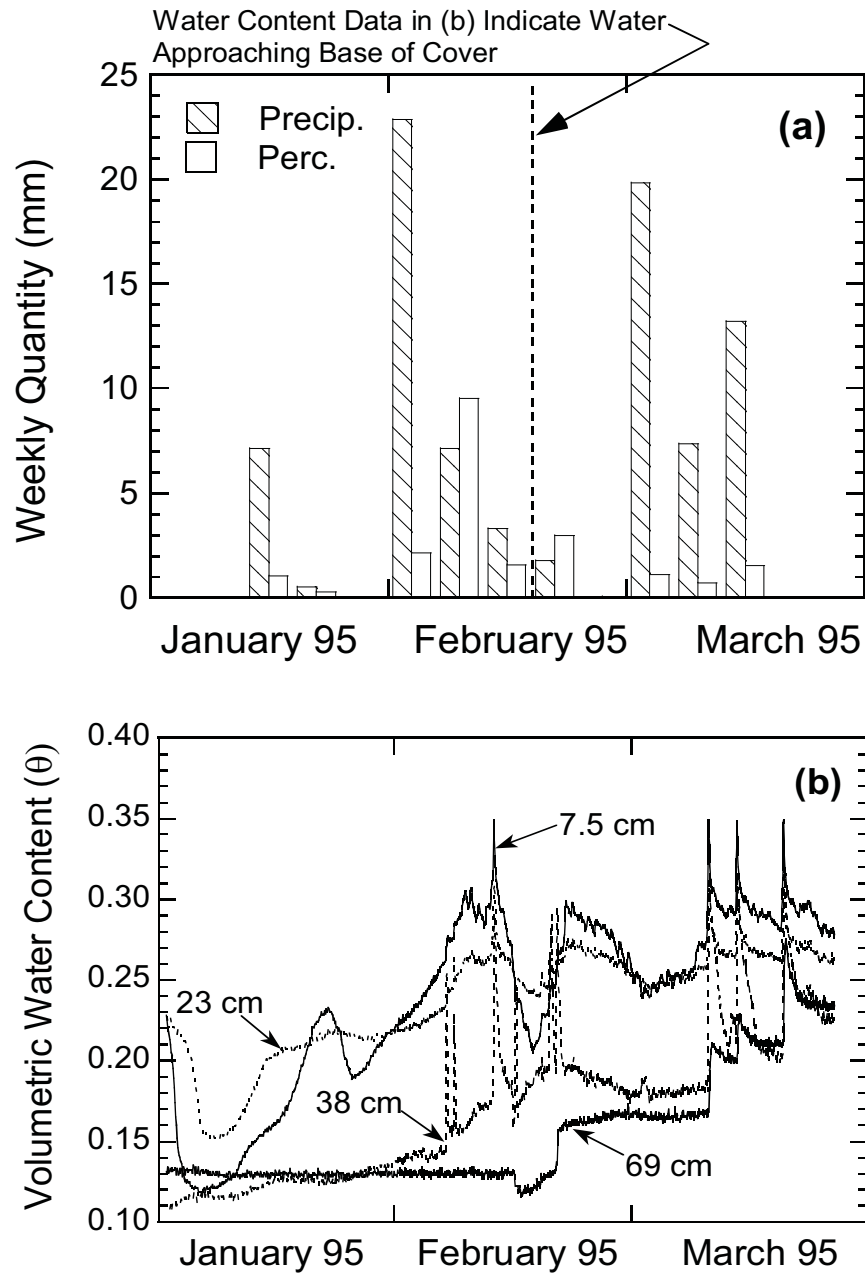


Fig. 10.1 Daily precipitation and percolation record (a) and water content vs. time at various depths (b) in first quarter of 1995 for the final cover test section in Wenatchee, WA described in Khire et al. (1997).

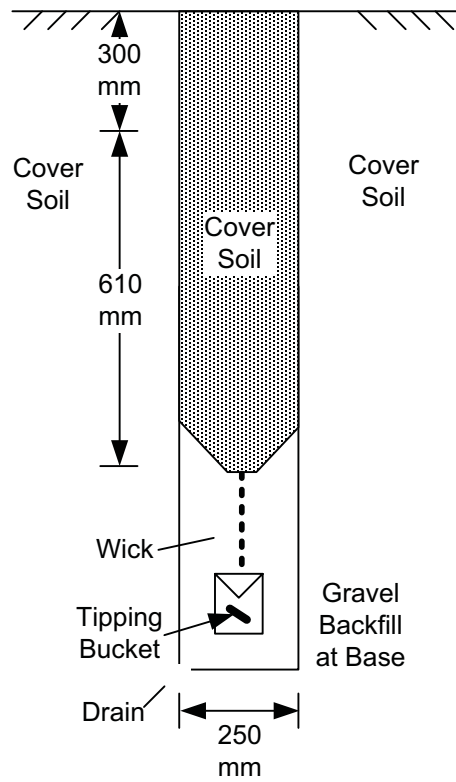


Fig. 10.2 Schematic of flux meter used to monitor a final cover (adapted from Malusis and Benson 2006).

meters are relatively inexpensive and are expedient to install. However, because flux meters are small, they may not capture the network of pores controlling flow in the field.

As illustrated in Fig 6.5, the saturated hydraulic conductivity at a scale of 0.3 m can be lower than the field-scale hydraulic conductivity. Consequently, the percolation rate measured by a flux meter may be lower than the actual field percolation rate. This issue cannot be overcome by adding more flux meters, as the bias introduced by scale is inherent at each measurement location.

Flux meters that employ dielectric metering devices in lieu of mechanical devices should have a longer service life and require less maintenance. However, all electronic metering systems have a finite service life (probably < 10 yr). Thus, flux meters will require periodic replacement.

Pan lysimeters, such as the ACAP lysimeter described in Sec. 2.1, consist of a large pan placed beneath the cover to collect percolation (Benson et al. 1994, 2001). Water collected in the pan is piped to a monitoring station where the flow is metered using manual or automated methods (automation is common because it permits remote monitoring). Lysimeters are advantageous because they provide a large-scale passive measurement of the percolation rate with minimal to no maintenance. Provided that the metering station is accessible from the surface, maintenance of metering devices (e.g., pressure transducers, tipping buckets, etc.) is expedient and cost effective. Disadvantages of lysimeters include higher installation cost compared to other monitoring methods and the impact of the artificial boundary imposed by the lysimeter pan.

The boundary imposed by the pan lysimeter is considered the most significant issue associated with lysimetry. A capillary break is formed by the drainage layer at the base of the lysimeter, which enhances storage within the cover profile and may reduce the percolation rate. The ACAP lysimeter included a geosynthetic root barrier and a layer of interim cover soil between at base of the cover to address this issue (Fig. 2.4). The root barrier prevents roots from entering the interim cover soil, and therefore precludes root water uptake from the interim soil layer. Consequently, once the interim cover soil is wetted for the first time, the soil will remain wet due to the capillary break effect from below and the lack of root water uptake. Thus, the capillary break effect becomes moot after the first wetting event.

Size of a lysimeter is particularly important. The lysimeter must be sufficiently large so that it provides a reliable spatially averaged percolation rate. This requires that the minimum dimension of the lysimeter be at least 3 times the spatial correlation length of the hydraulic properties of the cover soils (Benson et al. 2001). Engineered fill soils have a spatial correlation length ranging from 1-3 m (Benson 1991). Thus, the minimum dimension of a lysimeter should be no less than 9 m to account for cover soils exhibiting a high level of spatial correlation. The ACAP lysimeter (10 m x 20 m) was sized to ensure that this criterion was met. The lysimeters walls should also be oriented so that they do not induce focusing or divergence of flow.

10.3.2 Interpretive Monitoring

Interpretive performance monitoring consists of monitoring secondary variables that are related to the primary performance variable. Water content and temperature are the two

most commonly measured secondary variables employed for interpretive monitoring. Matric potential is also commonly measured as a secondary variable (Albright et al. 2004).

Interpretive monitoring data are used to interpret data collected from direct performance monitoring. This type of monitoring is particularly important when direct monitoring indicates that the performance of the final cover is unsatisfactory (e.g., the percolation rate is higher than a design standard) (Malusis and Benson 2006). Without data from secondary variables, the root cause of unsatisfactory performance can be difficult or impossible to determine, which hampers selection of an appropriate remedy.

Data from the ACAP site in Sacramento, CA illustrate the value of indirect non-destructive monitoring of secondary variables. Both store-and-release covers at Sacramento (Fig. 2.3) were intended to transmit no more than 3 mm/yr of percolation. However, during 2001-02 and 2003-04, approximately 100 mm of percolation was transmitted by the thinner cover (Fig. 10.3a). The reason for the high percolation rate was evident when the water content data were evaluated, either as soil water storage (Fig. 10.3a) or water contents at various depths (Fig. 10.3b).

During the Summers of 2001 and 2003, water stored during the previous winter was not completely removed (Fig. 10.3a). As a result, the cover had inadequate soil water storage capacity the following winters, which resulted in the two large percolation events. The secondary data in Fig. 10.3b provide clues to the unexpected behavior. Water contents within the upper 600 mm of the cover decreased during Spring and Summer 2001, but not to the extent that occurred in 2000 or in 2002, and very little depletion in water content occurred at depths greater than 600 mm in 2001. This suggests that the vegetation was not functioning as intended in 2001, and that the portion of the root zone deeper than 600 mm was nearly inactive. The water content data from Summer 2003 show a different phenomenon. The entire depth of the root zone was active in Summer 2003, but water removal ceased when the water content reached approximately 0.15, whereas water was removed until the water content reached 0.10-0.12 during Summer 2001 or 2003.

A vegetation survey conducted when the ACAP test sections were exhumed explained why the water contents did not diminish as greatly during the spring and summer later in the monitoring period (Smesrud et al. 2012). Vegetation initially established on the test sections at Sacramento consisted of a variety of perennial plants with a high wilting point potential (low water content at the wilting point). During the monitoring period, the perennial vegetation was succeeded by annual species that had a lower wilting point potential (higher water content at the wilting point), shallower roots, and a shorter period of active transpiration (Smesrud et al. 2012). A remedy was selected that included a management scheme to ensure that the intended species were maintained on the cover. This remedy could not have been selected reliably without the water content data collected for interpretive monitoring.

Vegetation surveys, such as the survey conducted at the Sacramento ACAP site, are an example of indirect interpretive monitoring. Other types of indirect interpretive monitoring might consist of reconnaissance surveys to evaluate other features such as erosion, subsidence, or biota intrusion (e.g., burrows) or satellite imagery to evaluate larger-scale patterns in water content distribution or vegetative status.

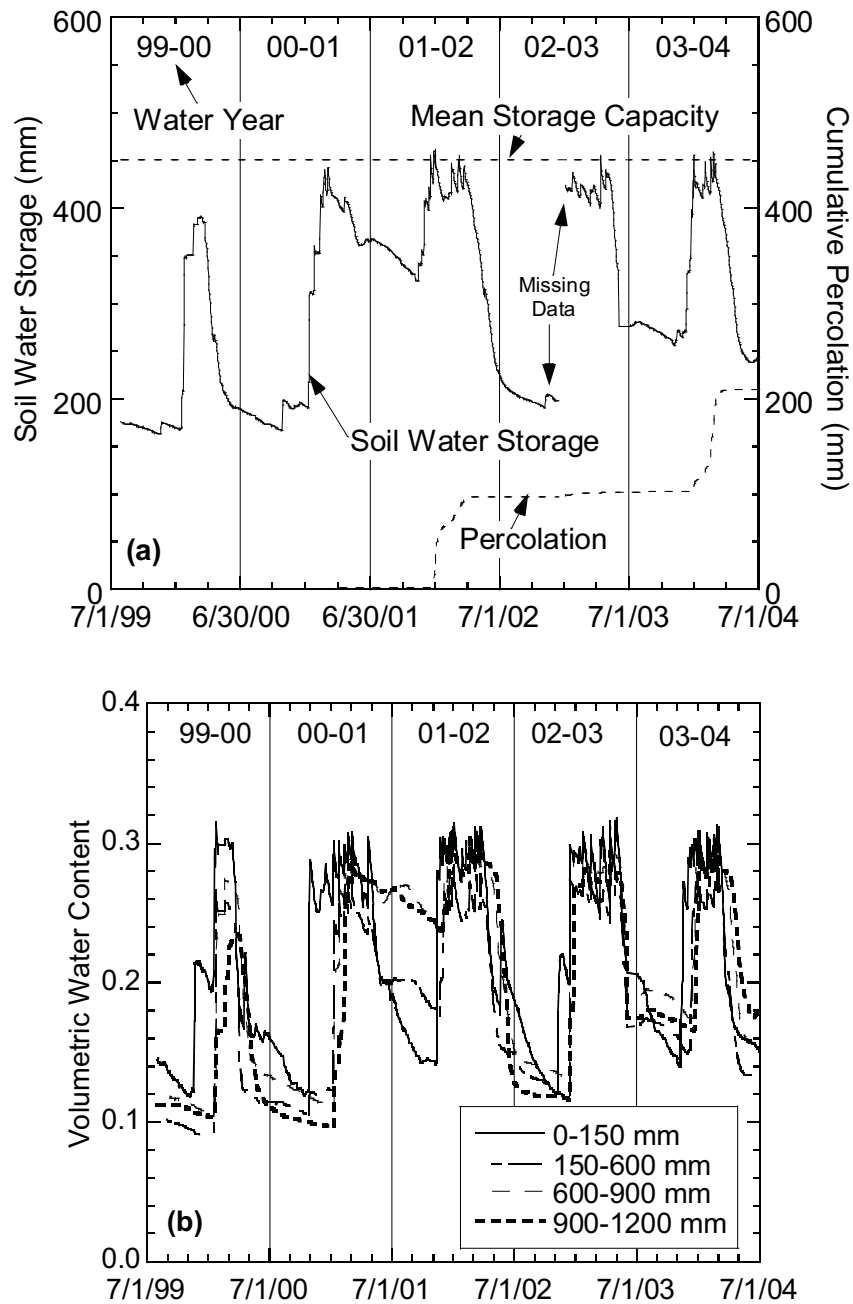


Fig. 10.3 Storage and percolation (a) and water contents at various depths (b) as a function of time for thin store-and-release cover evaluated by ACAP in Sacramento, CA.

10.3.3 Recommended Practice for Final Cover Monitoring

Given the important role that a final cover plays in long-term isolation of wastes and the changes in engineering properties that have been observed in cover materials, direct performance monitoring of final covers is prudent for facilities containing long-lived wastes (e.g., low-level radioactive wastes, mine wastes, etc.). At a minimum, at least one pan lysimeter having a minimum dimension of 10 m should be installed for performance monitoring. Given their extensive track record, ACAP-style pan lysimeters are recommended. Benson et al. (1999) describe how a pan lysimeter is installed.

If only one lysimeter is installed, the location should be selected to represent the most unfavorable condition at the site. In the northern hemisphere, north-facing locations on the top deck (mild slope) generally are the most unfavorable. However, site-specific conditions such as shading, prevailing wind direction, and snow accumulation may also affect the location for least favorable conditions. Thus, site-specific factors should be considered when selecting a location. If more than one lysimeter can be installed, the locations should be selected to evaluate top deck and side slopes as well as variations in the cover design in different parts of the facility.

The lysimeter should be supplemented with other performance and interpretive monitoring devices when practical. Spatial variability in flux can be evaluated by installing a distributed network of flux meters in the cover to assess the impact of microclimates induced by slopes oriented in different directions and top deck vs. slope. A flux meter can also be installed within or adjacent to the lysimeter to ascertain the bias between the percolation measurements made with both devices, thereby permitting assessment of data from flux meters in the context of data from large-scale lysimeters.

Sensors should also be installed to collect direct interpretive data, most importantly water content and temperature. At least one nest of sensors should be installed within the periphery of the lysimeter, with at least two sensors placed in each distinct layer (provided the layer is at least 300 mm thick) (Benson et al. 1999). An example of a sensor layout is shown in Fig. 10.4. Nests of sensors should also be placed at other locations in the cover to assess the variation in hydrologic conditions due to microclimates. If a network of flux meters is installed, a nest of water content and temperature sensors should be placed adjacent to each flux meter.

A wide range of sensors can be used to sense water content and temperature. Robust sensors that require little or no maintenance should be selected, and site-specific calibrations should be performed (Benson and Bosscher 1999). Because sensor technology is changing rapidly, specific sensors are not recommended in this report. However, the ACAP experience indicated that cost-effective and reliable monitoring of water content and temperature can be achieved with moderate frequency (MHz) time-domain reflectometry (TDR) sensors and sealed Type-T thermocouples (Fig. 10.5) (Albright et al. 2004, Albright and Benson 2009). Methods to calibrate these sensors are described in Kim and Benson (2002) and Benson and Wang (2006).

Experience with ACAP installations has shown that replication of lysimeters or sensors generally is not necessary except to provide redundancy to account for instrument failure, which was rare in ACAP (Albright et al. 2004). For example, two ACAP-style

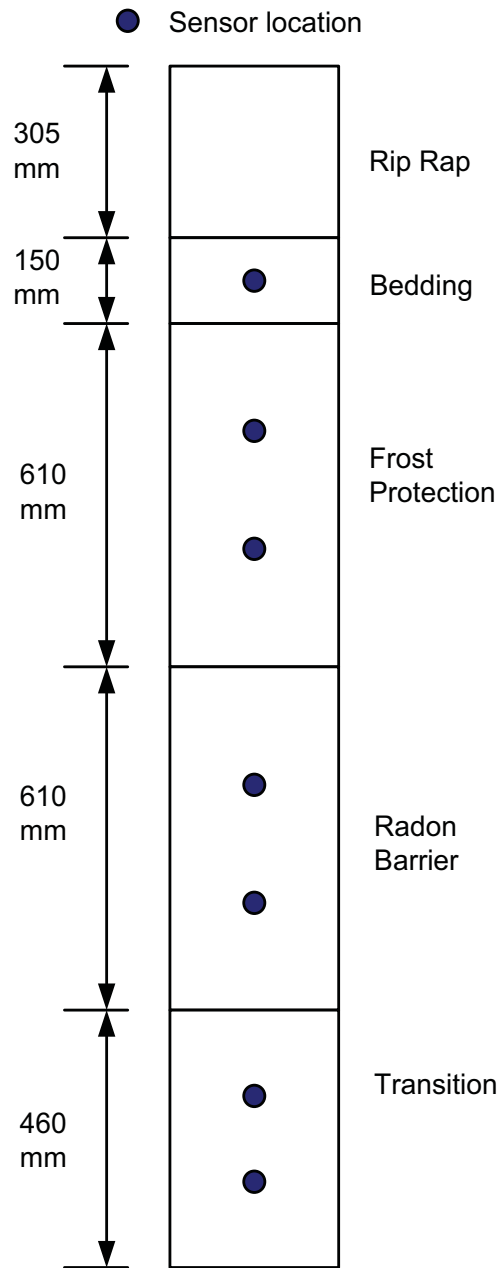


Fig. 10.4. Typical profile of a sensor nest used for interpretive data (adapted from Benson et al. 2009). Labels to right of profile describe layers in cover profile. No sensors were placed in rip rap layer due to the large particle sizes and the negligible storage anticipated in this layer.



Fig. 10.5. Moderate frequency TDR sensor ready to be pushed into cover profile. Type-T thermocouple (blue wire) is taped to head (white block) of TDR sensor.

lysimeters (Test Sections A and B) installed side-by-side at a field site near Grand Junction, CO are being used to evaluate the same cover profile. Water balance records from these lysimeters are shown in Fig. 10.6, and the water balance data are summarized in Table 10.1 (Benson et al. 2009). Nearly identical records were observed in both test sections (Fig. 10.6). Over the entire record, the cumulative percolation differs by no more than 1.0 mm between test sections and, after construction water ceased draining towards the end of 2008, the percolation differed no more than 0.1 mm between test sections (Table 10.1).

Water content records from the test sections near Grand Junction, CO are shown in Figs. 10.7 and 10.8. The records in Fig. 10.7 show data from up slope and down slope sensors in Test Section A located in two different layers. Nearly identical water content records were obtained from these replicate sensors. The data in Fig. 10.8 are from four sensors located at the same depth and in the same layer, but in two different test sections as well as up slope and down slope. The water contents differ by no more than 0.03 throughout the entire record, and are nearly identical for most of the record. Similar reproducibility was observed at other sites in ACAP (Albright et al. 2004). These comparisons suggest that sensor nests installed to evaluate large-scale spatial variations in cover hydrology are more useful than replicate nests used to check reproducibility.

Periodic vegetation and reconnaissance surveys should also be conducted, particularly for store-and-release covers that rely strongly on vegetation to manage the water balance. Vegetation surveys should evaluate the relative distribution of plant species on the cover as well as the percent coverage to ensure that a diverse and desirable plant community has been established and that succession towards a complex plant community is occurring. Surveys conducted in undistributed reference areas can be used as natural analogs to assess whether the plant community is on a trajectory commensurate with surrounding ecological conditions. Reconnaissance can be conducted concurrently to detect potential problems due to erosion or subsidence. Such surveys should be conducted annually for the initial 5 yr, when major changes in hydrologic performance can occur (Albright et al. 2004). Less frequent surveys can be conducted thereafter, depending on the trends that have been observed.

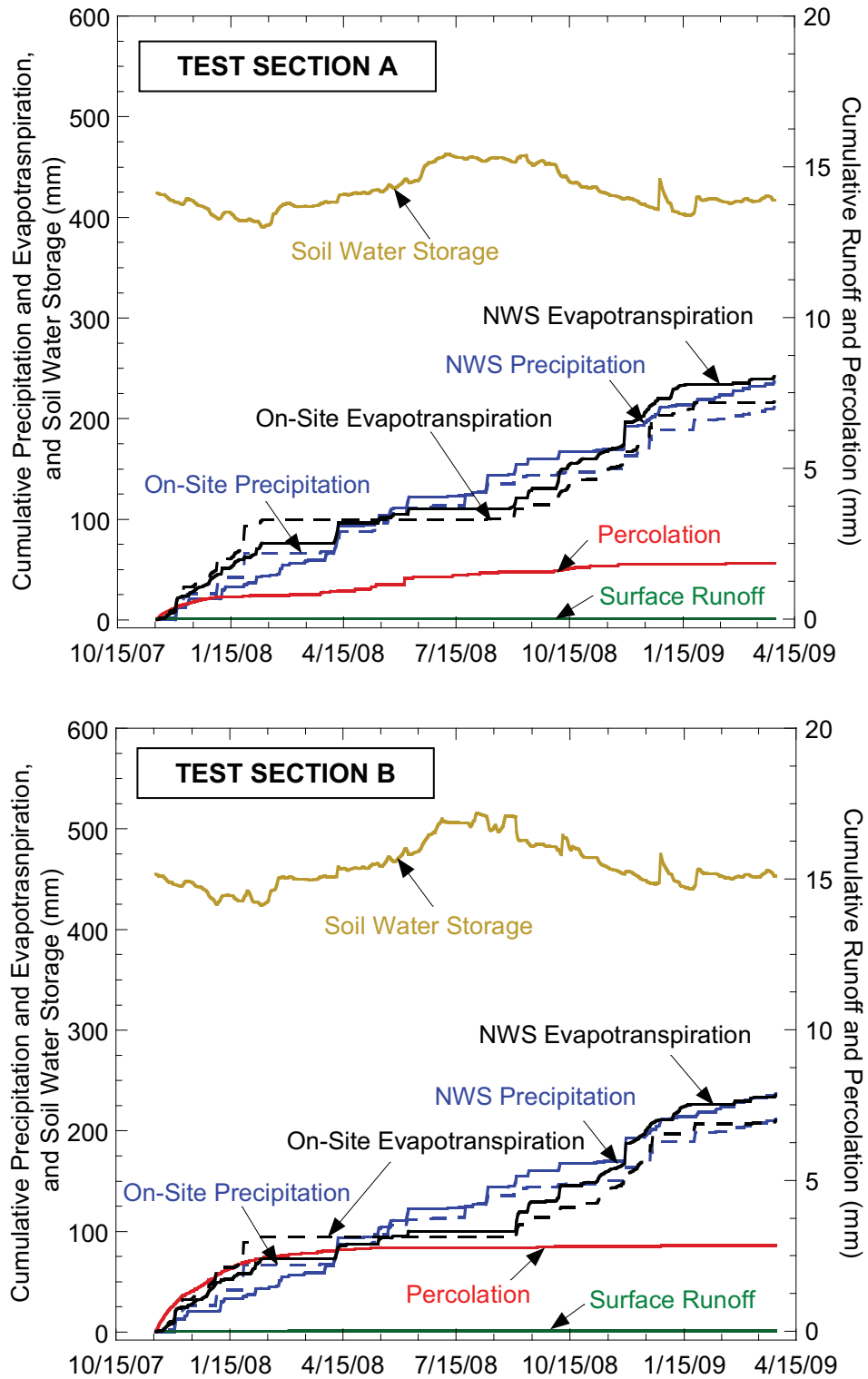


Fig. 10.6 Water balance quantities for ACAP test sections near Grand Junction, CO (from Benson et al. 2009).

Table 10.1. Water balance quantities for two ACAP test sections near Grand Junction, CO (from Benson et al. 2009).

Test Section	Period	Water Balance Quantities (mm)				
		Precipitation	Runoff	Evapotran- spiration	Δ Storage	Percolation
A	11/15/07- 11/15/08	169.2 (150.4)	0.0 (0.0%)	168.7 (99.7%)	-1.3	1.8 (1.0%)
	11/16/08- 03/29/09	67.6 (61.2)	0.0 (0.0%)	73.4 (108.6%)	-5.9	0.1 (0.1%)
B	11/15/07- 11/15/08	169.2 (150.4)	0.0 (0.0%)	160.9 (95.1%)	5.5	2.8 (1.7%)
	11/16/08- 03/29/09	67.6 (61.2)	0.0 (0.0%)	74.8 (110.7%)	-7.2	0.0 (0.1%)

Precipitation measured on-site is shown in parentheses in the precipitation column. Percentage of NWS precipitation is shown in parentheses in the columns of other water balance quantities.

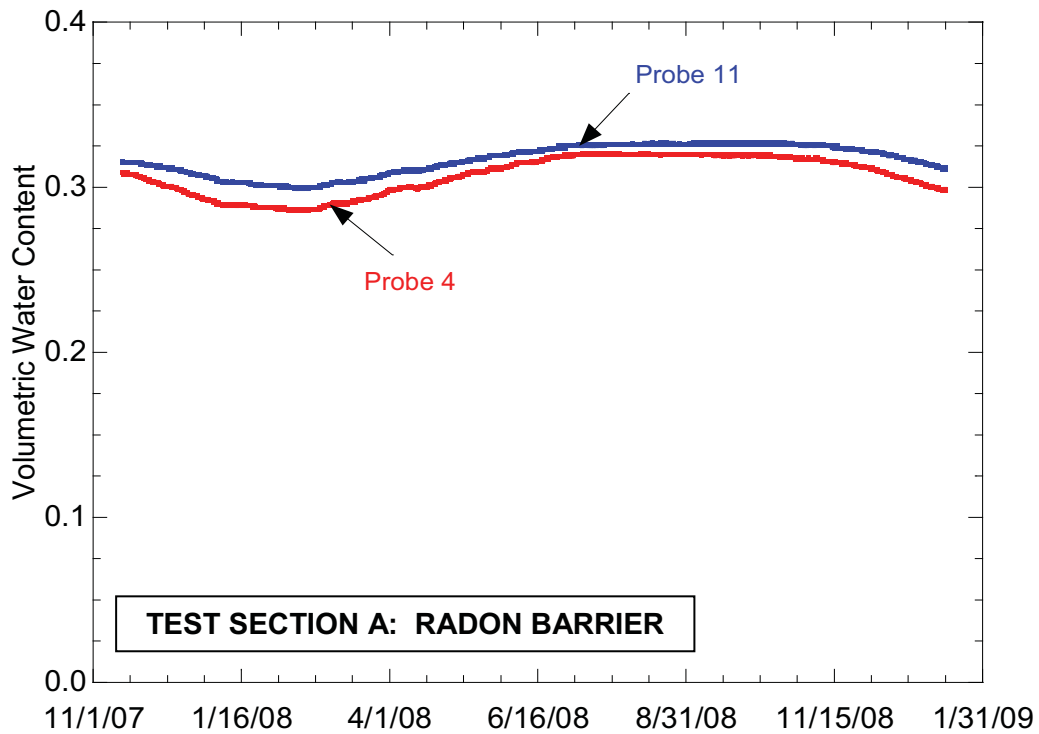
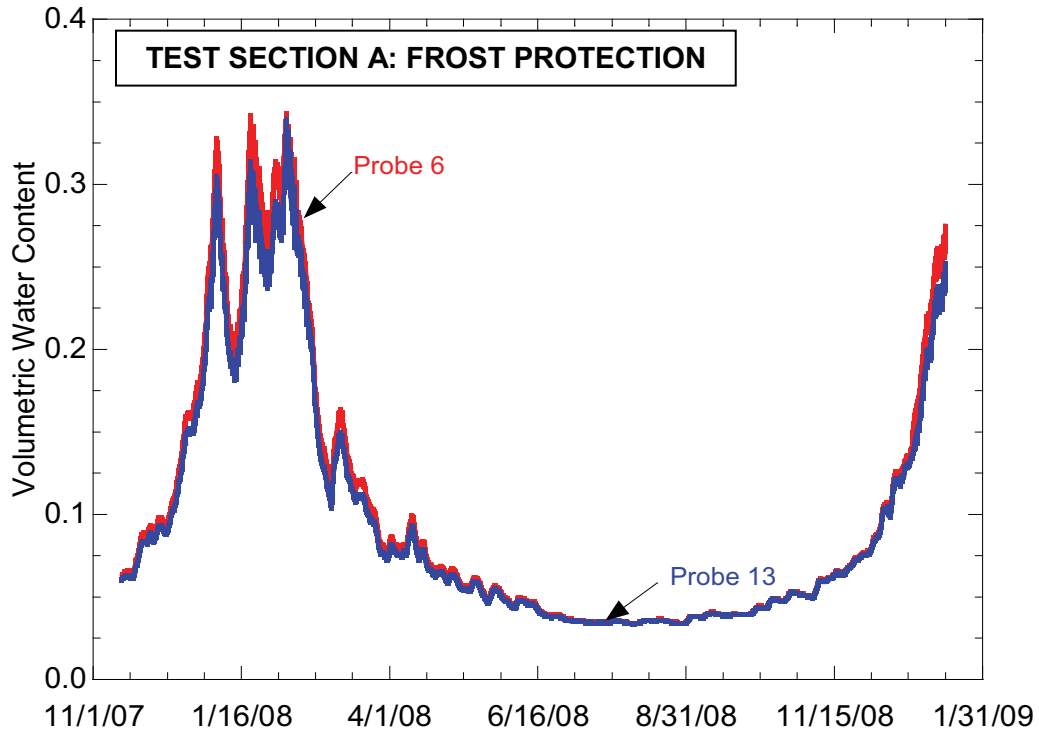


Fig. 10.7. Water contents in frost protection layer and radon barrier measured at same depth in up slope and down slope nests of Test Section A (adapted from Benson et al. 2009).

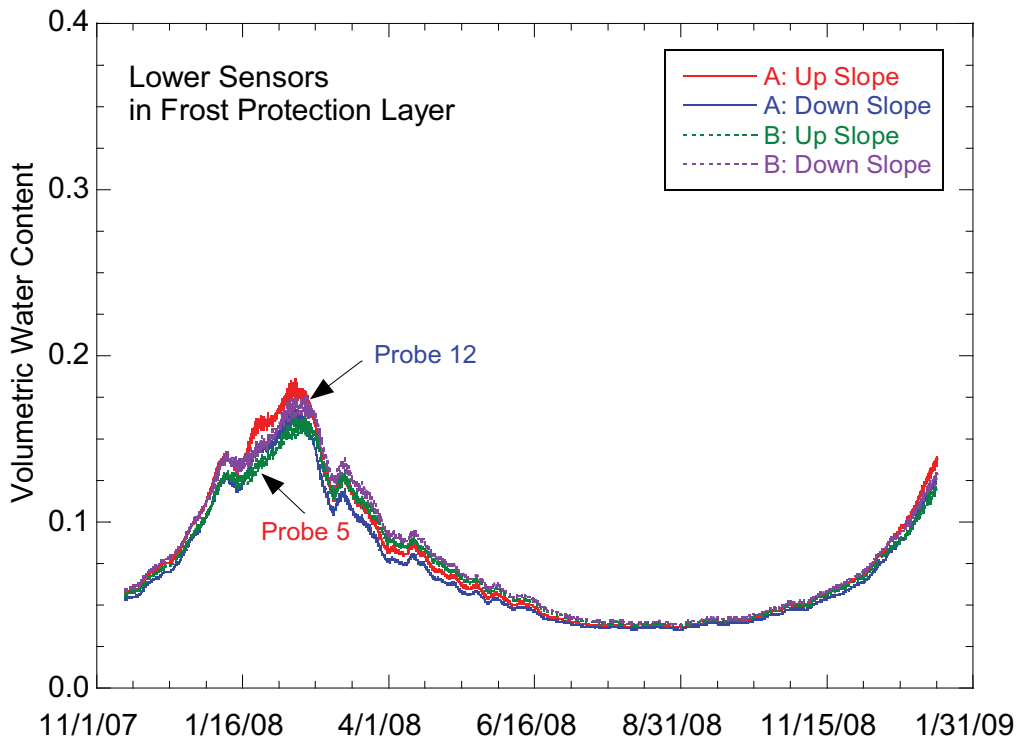


Fig. 10.8. Comparison of water contents in frost protection layer in upslope (Probe 5) and down slope (Probe 12) interpretive monitoring nests in duplicate test sections (Test Sections A and B).

11. CONCLUSIONS AND RECOMMENDATIONS

This study was conducted to evaluate how the engineering properties of materials used in final covers change while in service. This information is needed to realistically and reliably assess the performance of a containment facility and its impact on the surrounding environment. Final covers at test facilities and operating waste containment facilities were exhumed to evaluate how the properties of the cover materials changed approximately 5 to 10 yr after installation. Field tests were conducted, samples were collected, laboratory testing was performed, and data analyses were conducted.

Changes in hydraulic properties occurred in all cover soils that were evaluated due to the formation of soil structure, regardless of climate, cover design, or service life. The saturated hydraulic conductivity and the α parameter for the soil water characteristic curve (SWCC) increased, which reflects the formation of larger pores due to pedogenic processes such as wet-dry and freeze-thaw cycling. Larger changes were observed for soils with lower as-built saturated hydraulic conductivity and soils with a greater proportion of clay particles in the fines fraction. Hydraulic properties of the cover soils were similar when exhumed, regardless of the as-built condition. The saturated hydraulic conductivity at field scale ranged between 2.5×10^{-8} and 6.0×10^{-6} m/s, the saturated volumetric water content ranged between 0.35 and 0.45, van Genuchten's α parameter at field scale ranged between 0.01 and 0.33 kPa^{-1} , and van Genuchten's n parameter ranged between 1.1 and 1.5. Test scale had a significant effect on the hydraulic properties, with conditions near field-scale obtained using 0.3-m test specimens.

Substantial changes were also observed in some of the geosynthetic clay liners (GCLs). Analysis showed that GCLs have very low saturated hydraulic conductivity ($< 5 \times 10^{-11}$ m/s) when placed on a moist subgrade (gravimetric water content $> 10\%$) and covered with a geomembrane and cover soil soon after installation. GCLs installed on drier subgrades or not covered with a geomembrane and cover soil can be much more permeable. Changes in hydraulic conductivity or sensitivity to the permeant water were characteristic of GCLs that had undergone only modest hydration combined with partial to complete replacement of the native Na by Ca and/or Mg. GCLs that underwent complete hydration with osmotic swell maintained low hydraulic conductivity even when the native Na was replaced by Ca and Mg.

Changes in geomembranes and geosynthetic drainage layers were modest or small. Greater reductions in transmissivity and permittivity were observed for drainage layers covered with soils having higher fines content. However, this effect was modest, and all of the drainage layers functioned as anticipated. Analysis of antioxidants in the geomembranes showed that antioxidant depletion was consistent with expectations based on first-order kinetics and laboratory-measured depletion rates. Based on these rates, the minimum service life of geomembranes is on the order of 50-125 yrs. Actual service lives are likely to be longer, but are difficult to estimate. Methods to estimate actual service life are in Koerner et al. (2005) and Rowe et al. (2009). Geosynthetic materials in covers may need to be inspected and/or replaced periodically during the service life of the facility, especially in facilities containing wastes with very long life spans (100s to 1000s yr).

These findings have demonstrated that changes in the engineering properties of cover soils generally occur while in service and that long-term engineering properties should be used as input to models employed for long-term performance assessments. Recommendations for appropriate input have been made based on the data that were collected (Section 10). Because covers change over time, they should be monitored to ensure that they are functioning as intended. Monitoring using pan lysimeters combined with secondary measurements collected for interpretive purposes (water content, temperature, vegetation surveys, etc.) is recommended (Section 10).

This study represents a snap shot in the evolution of final covers approximately 5 to 10 yr after construction. Many of the properties coalesced into similar ranges during this period, which suggests that an equilibrium condition had been reached. Thus, these ranges are a good first estimate of long-term properties. However, these properties may not be representative of true long-term conditions corresponding to 100s or 1000s of years. Additional research investments are needed to more accurately and completely define these very long-term properties of earthen and geosynthetic cover materials. These research activities should include analog studies of natural environments where earthen and natural polymeric materials exist as well as accelerated laboratory experiments that can be used to develop predictive degradation models. A long-term national monitoring site should also be established where the durability and effectiveness of barrier components can be evaluated over decades and possibly centuries.

Research investments are also needed in remote monitoring methods that will permit long-term and low-cost reconnaissance from remote locations. These technologies likely would employ surface and airborne remote sensing methods to scan the condition of the cover non-intrusively. While some of these technologies exist today, they have not been coupled to cover performance. Research investments should explore appropriate remote sensing technologies and to develop relationships between remotely sensed information and direct performance data for final covers.

12. REFERENCES

- Albrecht, B. and Benson, C. (2001). Effect of desiccation on compacted natural clays. *Journal of Geotechnical and Geoenvironmental Engineering*, 127(1), 67-75.
- Albrecht, B. and Benson, C. (2002). Closure to discussions of "Effect of desiccation on compacted natural clays," *Journal of Geotechnical and Geoenvironmental Engineering*, 128(4), 356-360.
- Albright, W., Benson, C., and Waugh, W. (2010), *Water Balance Covers for Waste Containment: Principles and Practice*, ASCE Press, Reston, VA, 158 p.
- Albright, W., Benson, C., Gee, G., Abichou, T., McDonald, E., Tyler, S., and Rock, S. (2006). Field Performance of a compacted clay landfill final cover at a humid site. *Journal of Geotechnical and Geoenvironmental Engineering*, 132(11), 1393-1403.
- Albright, W., Benson, C., Gee, G., Roesler, A., Abichou, T., Apiwantragoon, P., Lyles, B., and Rock, S. (2004), Field Water Balance of Landfill Final Covers. *J. Environmental Quality*, 33(6), 2317-2332.
- Albright, W., Benson, C., Gee, G., Abichou, T., Tyler, S., and Rock, S. (2006). Field performance of three compacted clay landfill covers. *Vadose Zone Journal*, 5(4), 1157-1171.
- Annan, P. (2005). "Ground Penetrating Radar". In *Near Surface Geophysics*. D. Butler, ed., Society of Exploration Geophysics. 357-438.
- Benson, C. (1991), Predicting Excursions beyond Regulatory Thresholds of Hydraulic Conductivity Using Quality Control Measurements, *Proc. of the First Canadian Conference on Environmental Geotechnics*, Montreal, May 14-17, 447-454. 
- Benson, C. (1993). Probability distributions for hydraulic conductivity of compacted soil liners. *Journal of Geotechnical and Geoenvironmental Engineering*, 119(3), 471-486
- Benson, C., Abichou, T., Albright, W.H., Gee, G.W., and Roesler, A.C. (2001). Field evaluation of alternative earthen final covers, *International Journal of Phytoremediation*, 3(1), 1-21.
- Benson, C., Abichou, T., Olson, M., and Bosscher, P. (1995). Winter effects on the hydraulic conductivity of a compacted clay. *Journal of Geotechnical and Geoenvironmental Engineering*, 121(1), 69-79
- Benson, C., Abichou, T., Wang, X., Gee, G.W., Albright, W. (1999). Test section installation instructions, assessment program. Geo Engineering Report No. 99-3, University of Wisconsin-Madison. Madison, WI, USA.
- Benson, C. and Bosscher, P. (1999). Time-domain reflectometry (TDR) in geotechnics: a review, *Nondestructive and Automated Testing for Soil and Rock Properties*, STP 1350, ASTM, W. Marr and C. Fairhurst, eds., 113-136.

- Benson, C., Bosscher, P., Lane, D., and Pliska, R. (1994), Monitoring System for Hydrologic Evaluation of Landfill Final Covers, *Geotech. Testing J.*, 17(2), 138-149.
- Benson, C. and Daniel, D. (1990). Influence of clods on hydraulic conductivity of compacted clay. *Journal of Geotechnical and Geoenvironmental Engineering*, 116(8), 1231-1248.
- Benson, C. and Othman, M. (1993). Hydraulic conductivity of compacted clay frozen and thawed in situ. *Journal of Geotechnical and Geoenvironmental Engineering*, 119(2), 276-294.
- Benson, C., Hardianto, F., and Motan, E. (1994) Representative size for hydraulic conductivity assessment of compacted soil liners. *Hydraulic Conductivity and Waste Contaminant Transport in Soil*, STP 1142, ASTM, West Conshohocken, PA, 3-29.
- Benson, C., Lee, S., Wang, X., Albright, W., and Waugh, W. (2008), Hydraulic Properties and Geomorphology of the Hydraulic Properties and Geomorphology of the Earthen Component of the Final Cover at the Monticello Uranium Mill Tailings Repository, Geo Engineering Report No. 08-04, University of Wisconsin, Madison, WI, USA.
- Benson, C. and Meer, S. (2009), Relative abundance of monovalent and divalent cations and the impact of desiccation on geosynthetic clay liner, *Journal of Geotechnical and Geoenvironmental Engineering*, 133(5), 814-827.
- Benson, C., Sawangsuriya, A., Trzebiatowski, B., and Albright, W. (2007), Post-construction changes in the hydraulic properties of water balance cover soils. *Journal of Geotechnical and Geoenvironmental Engineering*, 133(4), 349-359.
- Benson, C., Thorstad, P., Jo, H., and Rock, S. (2007). Hydraulic performance of geosynthetic clay liners in a landfill final cover, *Journal of Geotechnical and Geoenvironmental Engineering*, 133(7), 814-827.
- Benson, C. and Wang, X. (2006), Temperature-Compensating Calibration Procedure for Water Content Reflectometers, *Proceedings TDR 2006: 3rd International Symposium and Workshop on Time Domain Reflectometry for Innovative Soils Applications*, Purdue University, West Lafayette, IN, USA, 50-1 - 5-16.
- Benson, C., Waugh, W., Albright, W., and Smith, G. (2009), The RECAP Test Sections at the Grand Junction Disposal Site: Construction Documentation and Instrument Calibration, Geo Engineering Report No. 09-12, University of Wisconsin, Madison, WI.
- Beven, K. and Germann, P. (1982). Macropores and water flow in soils. *Water Resources Research*, 18, 1311-1325.
- Black, P. and Holtz, R. (1999). Performance of geotextile separators five years after installation, *Journal of Geotechnical and Geoenvironmental Engineering*, 125(5), 404-412.
- Bolen, M., Roesler, A., Benson, C., and Albright, W. (2001). Alternative Cover Assessment Program: Phase II report. Geo-Engineering Report No. 01-10, University of Wisconsin, Madison, WI.

- Bonaparte, R., Daniel, D. and Koerner, R. (2002). Assessment and Recommendations for Improving the Performance of Waste Containment Systems, US Environmental Protection Agency, 600/R-02/099, Washington, DC.
- Bradshaw, S. (2008), Effect of cation exchange during subgrade hydration and leachate permeation, MS Thesis, University of Wisconsin, Madison, WI.
- Campbell, G. and Anderson, R. (1998). Evaluation of simple transmission line oscillators for soil moisture measurement, *Computers and Electronics Agric.*, 20, 31-44.
- Chaisson, P. (2005). Method of interpretation of borehole falling-head tests performed in compacted clay liners. *Canadian Geotechnical Journal*, 42, 79-90.
- Chamberlain, E. and Gow, A. (1979). Effect of freezing and thawing on permeability and structure of soils. *Engineering Geology*, 13, 73-92.
- Chamberlain, E., Iskander, I., and Hunsicker, S. (1990), Effect of Freeze-Thaw Cycles on the Permeability and Macrostructure of Soils, *Proc. International Symposium on Frozen Soil Impacts on Agricultural, Range, and Forest Lands*, Special Report No. 90-1, US Army Cold Regions Research and Engineering Laboratory, Hanover, NH.
- Corser, P. and Cranston, M. (1991). Observations on the performance of composite clay liners and covers. *Proceedings, Geosynthetic Design and Performance*, Vancouver Geotechnical Society, Vancouver, British Columbia, 16.
- Daniel, D. (1989). In situ hydraulic conductivity tests for compacted clay. *Journal of Geotechnical and Geoenvironmental Engineering*, 115(9), 1205-1226.
- Daniel, D. (1993). Clay liners. *Geotechnical Practice for Waste Disposal*. Chapter 7. Chapman and Hall, London, 137-163.
- Darilek, G. and Miller, L., (1998). Comparison of dye testing and electrical leak location testing of a solid waste liner system, *Proceedings Sixth International Conference on Geosynthetics*, Atlanta, Georgia, USA., 1998.
- Dwyer, S. (2001). Finding a better cover. *Civil Engineering* pp. 59-63.
- Egloffstein, T. (2001). Natural bentonites-influence of the ion exchange and partial desiccation on permeability and self-healing capacity of bentonites used in GCLs. *Geotextiles and Geomembranes*, 19, 427-444.
- Egloffstein, T. (2002). Bentonite as sealing material in geosynthetic clay liners-influence of the electrolytic concentration, the ion exchange and ion exchange with simultaneous partial desiccation on permeability. *Clay geosynthetic barriers*, H. Zanzinger, R. Koerner, and E. Gartung, eds., Swets and Zeitlinger, Lesse, 141-153.
- Eigenbrod, K. (2003). Self-healing in fractured fine-grained soils. *Canadian Geotechnical Journal*, 40, 435-449.

- Eith, A. and Koerner, G. (1997). Assessment of HDPE geomembrane performance in a municipal waste landfill double liner system after eight years of service, *Geotextiles and Geomembranes*, 15, 277-289.
- Frangos, W. (1997). Electrical detection of leaks in lined waste disposal ponds, *Geophysics*, 62(6), 1737-1744.
- Gee, G., Campbell, M., Campbell, G., and Campbell, J. (1992). Rapid measurement of low soil potentials using a water activity meter. *Soil Science Society of America Journal*, 56, 1068-1070.
- Gee, G. and Hillel, D. (1988), Gee, G. and Hillel, D. (1988), Groundwater Recharge in Arid Regions: Review and Critique of Estimation Methods, *Hydrological Processes*, 2, 255-266.
- Gheshlaghi, F. and Santamarina, J.. (1998). Data pre-processing in cross-hole geotomography. *Journal of Environmental and Engineering Geophysics* 3: 41-48
- Giroud, J. and Bonaparte, R. (1989). Leakage through liners constructed with geomembranes - Parts I and II, *Geotextiles and Geomembranes*, 8, 71-111.
- Gleason, M., Daniel, D.E., Eykholt, G.R., (1997). Calcium and sodium bentonite for hydraulic containment applications. *Journal of Geotechnical Engineering* 118(5), 438-445.
- Grassie, N. and Scott, G. (1985). *Polymer Degradation and Stabilization*, Cambridge University Press, Cambridge, UK.
- Gulec, S., Edil, T., and Benson, C. (2004), Effect of Acidic Mine Drainage (AMD) on the Polymer Properties of an HDPE Geomembrane, *Geosynthetics International*, 11(2), 60-72.
- Gurdal, T., Benson, C., and W. Albright. (2003). Hydrologic properties of final cover soils from the Alternative Cover Assessment Program, Geo Engineering Report 03-02, University of Wisconsin, Madison, WI, USA.
- Hanafy, S. and al Hagrey, S.. (2006). Ground-penetrating radar tomography for soil-moisture heterogeneity. *Geophysics*. 71(1): K9-K18
- Hills, E. (ed.) (1996), *Arid Lands: A Geographical Appraisal*, UNESCO, London.
- Hsuan, Y. and Koerner, R. (1998), Antioxidant depletion lifetime in HDPE geomembranes, *Journal of Geotechnical and Geoenvironmental Engineering*, 124(6), 532-541.
- Hvorslev, M. (1949). *Time Lag and Soil Permeability in Ground-Water Observation*, US Army Corps of Engineers, Waterways Experiment Station, Vicksburg, MS.
- Hytiris, N. and Berkhout, H. (1996). An assessment of geocomposite drain performance after long-term site use, *Geosynthetics: Applications, Design and Construction*, 299-306.

- Jackson, M. and Tweeton, D. (1996). 3DTOM, Three-dimensional geophysical tomography, USBM Report of Investigation 9617, 52 p.
- Jo, H., Benson, C., Lee, J., Shackelford, C., and Edil, T. (2005). Long-term hydraulic conductivity of a non-prehydrated geosynthetic clay liner permeated with inorganic salt solutions, *Journal of Geotechnical and Geoenvironmental Engineering*, 131(4), 405-417.
- Jo, H., Katsumi, T., Benson, C., and Edil, T. (2001). Hydraulic conductivity and swelling of nonprehydrated GCLs permeated with single-species salt solutions. *Journal of Geotechnical and Geoenvironmental Engineering*, 127(7), 557-567.
- Kelln, C., Barbour, L., and Qualizza, C. (2009). Fracture-dominated subsurface flow and transport in a sloping reclamation cover. *Vadose Zone Journal*, 8, 96-107.
- Khire, M., Benson, C., and Bosscher, P. (1997). Water balance modeling of earthen landfill covers. *Journal of Geotechnical and Geoenvironmental Engineering*, 123(8), 744-754.
- Khire, M., Benson, C., and Bosscher, P. (2000). Capillary barriers: Design variables and water balance. *Journal of Geotechnical and Geoenvironmental Engineering*, 126(8), 695-708.
- Kim, K.. and Benson, C.. (2002). Water content calibrations for final cover soils, Geo Engineering Report 02-12, University of Wisconsin, Madison, WI, USA.
- Kleppe, J. and Olson, R. (1985). Desiccation cracking of soil barriers. *Hydraulic Barriers in Soil and Rock*, STP 874, ASTM, West Conshohocken, PA, 263-275.
- Koerner, R. (2005). *Designing with Geosynthetics*, 5th Ed., Prentice–Hall, Upper Saddle River, NJ.
- Koerner, R., Hsuan, Y., and Koerner, G. (2005), Geomembrane Lifetime Prediction: Unexposed and Exposed Conditions, GRI White Paper No. 6, Geosynthetic Institute, Folsom, PA.
- Kolstad, D., Benson, C., and Edil, T. (2004). Hydraulic conductivity and swell of nonprehydrated GCLs permeated with multi-species inorganic solutions, *Journal of Geotechnical and Geoenvironmental Engineering*, 130(12), 1236-1249.
- Lee, J. and Shackelford, C. (2005), Concentration dependency on the prehydration effect for a geosynthetic clay liner, *Soils and Foundations*, 45(4), 27-41.
- Lin, L. and Benson, C. (2000). Effect of wet-dry cycling on swelling and hydraulic conductivity of GCLs, *Journal of Geotechnical and Geoenvironmental Engineering*, 126(1), 40-49.
- Malusis, M. and Benson, C. (2006), Lysimeters versus Water-Content Sensors for Performance Monitoring of Alternative Earthen Final Covers, *Unsaturated Soils 2006*, ASCE Geotechnical Special Publication No. 147, 1, 741-752.

- Mannsbart, G. and Christopher, B. (1997). R., Long-term performance of non-woven geotextile filters in five coastal and bank protection projects, *Geotextiles and Geomembranes*, 15, 207-222.
- Martin, R. (1960). Adsorbed water on clay: a re- view. *Proceedings 9th National Conference on Clays and Clay Minerals*, Clay Minerals Society, Lafayette, IN.
- McBride, M. (1994). *Environmental chemistry of soils*. Oxford University Press, New York, NY.
- McNeal, B. and Coleman, N. (1966) Effect of solution composition on soil hydraulic conductivity. *Soil Science Society of America Proceedings*, Vol. 30, 308-312.
- Mesri, G., and Olson, R. (1971). Mechanisms controlling the permeability of clays. *Clays Clay Minerals*, 19, 151-158.
- Meer, S. (2004). In-service hydraulic conductivity of GCLs in landfill covers, MS Thesis, University of Wisconsin, Madison, WI.
- Meer, S. and Benson, C. (2007). Hydraulic conductivity of geosynthetic clay liners exhumed from landfill final covers, *Journal of Geotechnical and Geoenvironmental Engineering*, 133(5), 550-563.
- Melchior, S. (1997). In-situ studies of the performance of landfill caps (compacted soil liners, geomembranes, geosynthetic clay liners, capillary barriers). *Land Contamination and Reclamation*, 5, 209-216.
- Melchior, S. (2002). Field studies and excavations of geosynthetic clay barriers in landfill covers, *Clay Geosynthetic Barriers*, H. Zanzinger, R. M. Koerner, and E. Gartung, (eds.), Swets and Zeitlinger, Lisse, 321-330.
- Miller, C., Mi, H., and Yesiller, N. (1998), Experimental analysis of desiccation crack propagation in clay liners. *Journal of the American Water Resources Association*, 34(3), 677-686.
- Mitchell, J. (1993), *Fundamentals of Soil Behavior*, 2nd Ed., John Wiley and Sons, Inc., New York, NY.
- Mooney, R., Keenan, A., and Wood, L. (1952). Adsorption of water vapor by montmorillonite. II. Effect of exchangeable ions and lattice swelling as measured by X-Ray diffraction, *Journal of the American Chemical Society*, 74(6), 1371-1374.
- National Research Council (2007). *Assessment of the Performance of Engineered Waste Containment Barriers*, The National Academies Press, Washington, D.C.
- Norrish, K., and Quirk, J. (1954). Crystalline swelling of montmorillonite, use of electrolytes to control swelling, *Nature*, 173, 255-257.
- Parra, J. (1988). Electrical response of a leak in a geomembrane liner. *Geophysics*. 53(11): 1445-1452.

- Peterson, J., (2001). Pre-inversion corrections and analysis of radar tomographic data. *Journal of Environmental and Engineering Geophysics*, 6, 1-18
- Petrov, R. and Rowe, R. (1997). Geosynthetic clay liner (GCL) – chemical compatibility by hydraulic conductivity testing and factors impacting its performance, *Canadian Geotechnical Journal*, 34, 863-885.
- Phene, C., Clark, D., Cardon, G., and Mead, R. (1992), Soil matric potential sensor research and applications, *Advances in Measurement of Soil Physical Properties: Bringing Theory into Practice*, G. Topp, D. Reynolds, and R. Green, eds., Soil Science Society of America, Madison, WI, USA, 263-280.
- Podgorney, R. and Bennett, J. (2006), Evaluating the long-term performance of geosynthetic clay liners exposed to freeze-thaw, *Journal of Geotechnical and Geoenvironmental Engineering*, 132(2), 265–268.
- Reitz, L. and Holtz, R. (1997). Performance of geotextiles in landfill covers, *Geosynthetics '97*, Industrial Fabrics Association International, St. Paul, MN.
- Roesler, A., Benson, C., and Albright, W. (2002). Field hydrology and model predictions for final covers in the Alternative Cover Assessment Program – (2002). Geo Engineering Report 02-08, University of Wisconsin, Madison, WI, USA.
- Rowe, R., Islam, M., Brachman, R., Arneppalli, D., and Ewais, A. (2010), Antioxidant Depletion from a High Density Polyethylene Geomembrane under Simulated Landfill Conditions, *Journal of Geotechnical and Geoenvironmental Engineering*, 136(7), 930–939.
- Rowe, R., Rimal, S., and Sangam, H. (2009), Aging of HDPE geomembrane exposed to air, water, and leachate at different temperatures, *Geotextiles and Geomembranes*, 27, 137-151.
- Rowe, R., Sangam., H. and Lake, C. (2003). Evaluation of an HDPE geomembrane after 14 years as a leachate lagoon liner, *Canadian Geotechnical Journal*, 40, 536-550.
- Russo, D., and Bouton, M. (1992). Statistical analysis of spatial variability in unsaturated flow parameters. *Water Resources Research*, 28(7), 1911-1925.
- Sangam, H. and Rowe, R. (2002). Effects of exposure conditions on the depletion of antioxidants from HDPE geomembranes. *Canadian Geotechnical Journal*, 39, 1221–1230.
- Santamarina, J. and Fratta, D. (2005). *Discrete Signals and Inverse Problems: an Introduction for Engineers and Scientists*, John Wiley and Sons, Chichester, UK.
- Scalia, J. (2009), Hydraulic and Chemical Properties of Geosynthetic Clay Liners Overlain by Geomembranes in Landfill Final Covers, MS Thesis, University of Wisconsin, Madison, WI.

- Scanlon, B., Christman, M., Reedy, R., Porro, I., Simunek, J., Flerchinger, G., (2002). Intercode comparisons for simulating water balance of surficial sediments in semiarid regions. *Water Resources Research*, 38 (12).
- Schmalholz, J., Stoffregen, H., Kemna, A., and Yaramanci, U. (2004). Imaging of Water Content Distributions inside a Lysimeter using GPR Tomography. *Vadose Zone Journal* 3, 1106–1115.
- Shackelford, C., Benson, C., Katsumi, T., Edil, T., and Lin, L. (2000). Evaluating the hydraulic conductivity of GCLs permeated with non-standard liquids, *Geotextiles and Geomembranes*, 18, 133-162.
- Shan, H. and Daniel, D. (1991). Results of laboratory tests on a geotextile/bentonite liner material. *Proc. Geosynthetic '91*, Industrial Fabrics Association International, St. Paul, MN, 517-535.
- Shang, J., Lo, K., Quigley, R., (1994). Quantitative determination of potential distribution in Stern-Guoy double-layer mode. *Canadian Geotechnical Journal*, 31, 624-636.
- Smesrud, J., Benson, C., Albright, W., Richards, J., Wright, S., Israel, T., and Goodrich, K. (2012), Using Pilot Test Data to Refine an Alternative Cover Design in Northern California, *International J. Phytoremediation*, in press.
- Stark, T., Williamson, T. and Eid, H. (1996). HDPE geomembrane/geotextile interface shear strength, *Journal of Geotechnical Engineering*, 122(3), 197-203.
- Suter, G., Luxmoore, R., and Smith, E. (1993). Compacted soil barriers at abandoned landfill sites are likely to fail in the long term. *Journal of Environmental Quality*, 22(2), 217-226.
- Thiel, R., and Criley, K. (2005). Hydraulic conductivity of partially prehydrated GCLs under high effective confining stress for three real leachates. *Waste Containment and Remediation, GSP 142*, ASCE, Reston, VA.
- Trast, J. and Benson, C. (1995). Estimating field hydraulic conductivity of compacted clay, *Journal of Geotechnical and Geoenvironmental Engineering*, 121(10), 736-739.
- UNESCO. (1979). Map of the world distribution of arid regions. MAB technical notes no. 7, UNESCO, Paris.
- USEPA (1996). Hydration of GCLs adjacent to soil layers. Report on 1995 Workshop on Geosynthetic Clay Liners. Report No. 600/R-96 /149, US Environmental Protection Agency Office of Research and Development, Washington, DC.
- Van, G., Park, S., and Hamilton, P. (1991). Monitoring leaks from storage ponds using resistivity methods, *Geophysics*. 56(8), 1267-1270.
- van Genuchten, M. (1980). A closed-form equation for predicting the hydraulic conductivity of unsaturated soils. *Soil Science Society of America Journal*, 44, 892-898.

Wang, X. and Benson, C. (2004). Leak-free pressure plate extractor for measuring the soil water characteristic curve. *Geotechnical Testing Journal*, 27(2), 1-10.

Zimmie, T. and LaPlante, C. (1990), The effect of freeze/thaw cycles on the Permeability of a fine-drained soil, *Proc. 22nd Midatlantic Industrial Waste Conference*, Technomic Publishers, Lancaster, PA.

BIBLIOGRAPHIC DATA SHEET

(See instructions on the reverse)

NUREG/CR-7028
Volume 1

2. TITLE AND SUBTITLE

Engineered Covers for Waste Containment: Changes in Engineering Properties and Implications for Long-Term Performance Assessment

3. DATE REPORT PUBLISHED

MONTH	YEAR
12	2011

4. FIN OR GRANT NUMBER

N 6366

5. AUTHOR(S)

C.H. Benson*, W.M. Albright**, D.O. Fratta*, J.M. Tinjum*, E. Kucukkirca*, S.H. Lee*, J. Scalia*, P.D. Schlicht*, and X. Wang*

6. TYPE OF REPORT

Technical

7. PERIOD COVERED (Inclusive Dates)

August 2006 - May 2009

8. PERFORMING ORGANIZATION - NAME AND ADDRESS (If NRC, provide Division, Office or Region, U.S. Nuclear Regulatory Commission, and mailing address; if contractor, provide name and mailing address.)

*Geological Engineering University of Wisconsin-Madison 1415 Engineering Drive Madison, WI 53706	**Desert Research Institute 2215 Raggio Parkway Reno, NV 89512
---	--

9. SPONSORING ORGANIZATION - NAME AND ADDRESS (If NRC, type "Same as above", if contractor, provide NRC Division, Office or Region, U.S. Nuclear Regulatory Commission, and mailing address.)

Division of Risk Analysis
Office of Nuclear Regulatory Research
U.S. Nuclear Regulatory Commission
Washington, DC 20555-0001

10. SUPPLEMENTARY NOTES

Jacob Philip, Project Manager

11. ABSTRACT (200 words or less)

This study demonstrates that engineering properties of cover soils change while in service and that long-term engineering properties should be used as input to models employed for performance assessments. Recommendations for appropriate input are made based on the data that were collected. Increases in the saturated hydraulic conductivity, saturated volumetric water content, and the air entry suction (as characterized by van Genuchten's alpha parameter) occurred due to formation of soil structure, regardless of climate, cover design, or service life. Substantial changes in hydraulic conductivity were observed in some geosynthetic clay liners (GCLs) that did not hydrate completely and underwent cation exchange. Changes in geomembranes and geosynthetic drainage layers were modest or small, and computations based on antioxidant depletion rates suggest that the minimum service life of geomembranes is in the order of 50-125 years (the actual service life will be longer). The findings indicate that covers should be monitored to ensure that they are functioning as intended. Monitoring using pan lysimeters combined with secondary measurements collected for interpretive purposes is recommended. Future research investments should include an evaluation of remote sensing technologies for cover monitoring and analog studies to estimate properties of earthen and geosynthetic cover materials corresponding to service lives of 100s to 1000s of years.

12. KEY WORDS/DESCRIPTORS (List words or phrases that will assist researchers in locating the report.)

alternative cover assessment program (ACAP)
changes in engineering properties of soils
engineered barriers
geomembrane (GM)
geosynthetic clay liner (GCL)
geosynthetics
long-term performance assessments
pan lysimeters
waste containment

13. AVAILABILITY STATEMENT

unlimited

14. SECURITY CLASSIFICATION

(This Page)

unclassified

(This Report)

unclassified

15. NUMBER OF PAGES

16. PRICE



Federal Recycling Program



**UNITED STATES
NUCLEAR REGULATORY COMMISSION**
WASHINGTON, DC 20555-0001

OFFICIAL BUSINESS

**NUREG/CR-7028, Vol. 1 Engineered Covers for Waste Containment: Changes in Engineering Properties
and Implications for Long-Term Performance Assessment**

December 2011